College de France lecture 2013: Optical traps and optical lattices

Jean Dalibard

Optical traps and optical lattices

Jean Dalibard
Collège de France, chair *Atoms and Radiation*

2012-13 lectures

Translated from French by Raphaël Saint-Jalm

Contents

Introduction

Laser cooling and laser trapping of particles are arguably two of the major advances in atomic physics and quantum optics over the last three decades. In particular, laser light can be used to create "potential landscapes", thereby controlling the motion of already cooled atoms. These atoms can remain trapped in such light cages for long periods of time and undergo a large variety of dynamical process, depending on the nature of the designed landscape.

A particularly interesting type of trap is obtained with a standing light wave, which realizes a periodic potential called an "optical lattice". The motion of atoms in an optical lattice has a deep analogy with the motion of electrons in a crystal, which makes it an important tool for quantum simulations of condensed matter phenomena using cold atoms.

This year's lecture series is devoted to the presentation of the basic principles governing the motion of atoms in these optical lattices. We will also describe several recent experiments exploiting this very particular dynamics. We will encounter aspects related to metrology as well as illustrations of condensed matter phenomena. The lecture series will be composed of the following six chapters:

Chapter 1. The dipolar potential. We will show how to describe the force $F(\boldsymbol{r})$ created by a monochromatic light beam in terms of its intensity profile $I(\boldsymbol{r})$. We will first evaluate this *dipole force* with the simple model of a two-level atom, then for a more realistic model of an atomic transition. We will show that this force derives from a potential $V(\boldsymbol{r})$, called dipole (or dipolar) potential, which is proportional to $I(\boldsymbol{r})$ in the limit of low intensities. We will finally evaluate the role of spontaneous emission processes, which can lead to undesired heating on the trapped atoms.

Chapter 2. Optical lattices: the basic principles. We will focus on the case of the periodic dipolar potential created by a 1D standing wave, $V(x) = V_0 \sin^2(kx)$, where k is the wave number of the light beam creating the standing wave. We will see that such a problem can be handled with the tools and concepts developed in solid state physics to study the motion of electrons in the periodic potential of a crystal lattice. We will see that the natural energy scale is given by the *recoil energy* $E_\mathrm{r} = \hbar^2 k^2/(2m)$ where m is the mass of the atom. We will present Bloch's theorem, the notion of Brillouin zone and we will describe the shallow lattice limit $V_0 \ll E_\mathrm{r}$, which is used in particular in many Bragg diffraction experiments.

Chapter 3. Optical lattices in the tight-binding regime. In this lecture, we will continue to transfer concepts from solid state physics to optical lattices, this time focusing on the tight-binding limit $V_0 \gg E_\mathrm{r}$ and introducing the concept of Wannier functions. In this tight-binding limit, the tunnelling of a low-energy atom from one site to another is only possible if these two sites are contiguous. The dynamics of the particles in the lattice can then be described by a very simple Hamiltonian, whose main properties will be described. We will discuss the role played by interactions in a lattice by looking at the stabilization of dimers occupying the same site, even if the atoms composing this dimer repel each other.

Chapter 4. Time-dependent lattices. The possibility to vary in time the parameters of the laser creating the standing wave opens many perspectives. For example, we can realize moving lattices $V(x,t) = V_0 \sin^2[k(x - x_0(t))]$, where $x_0(t)$ is a controlled function of time. In this course, we will establish the equivalence of several Hamiltonians that can describe this problem by using unitary transformations, each Hamiltonian being useful

to address a given phenomenon. We will focus on the phenomenon of dynamic localization, obtained by periodically modulating the position $x_0(t)$. We will see that this modulation can have spectacular consequences, such as the almost complete suppression of the tunnelling effect. We will describe the experimental demonstration and the use of this effect for lattices in one and two dimensions.

Chapter 5. Bloch oscillations in an optical lattice. When a constant force is added to the periodic force created by a lattice, a surprising phenomenon appears: the particles oscillate. Cold atoms trapped in optical lattices have allowed to study this phenomenon in great detail and we will present several experimental demonstrations. We will also discuss the metrological interest of these Bloch oscillations, both to determine fundamental constants such as the ratio $\hbar/m$ and to measure forces such as gravity.

Chapter 6. Topology in a lattice : the example of Dirac points. Optical lattices allow the realization of more complex potentials than sinusoidal $\sin^2(kx)$ potentials. In particular, one can produce two-dimensional lattices analogous to graphene, for which some singular points of the Brillouin zone, called *Dirac points*, appear. In the vicinity of these points, the behaviour of the particles is similar to that of ultra-relativistic particles, with a quasi-linear dispersion relation. We will see how the control of the lattice parameters allows one to move the Dirac points inside the Brillouin zone, or even to make them disappear. We will describe a recent experiment which allowed to reveal these points and to exploit the control one can have on the topology of the Brillouin zone.

Due to time limitations, these lectures only partially cover the current and extremely intense research activity on optical lattices. Thus, we will address the effects of interactions between particles only a few times, saving for the lectures of an upcoming year important phenomena such as the transition between the superfluid state and the Mott insulator. We will not deal with artificial magnetism in lattices this year either: it will also be the subject of a future series of lectures. Nevertheless, we hope that the tools provided in the following chapters and the description of the experiments will allow the interested reader to approach more easily the numerous research topics related to these "crystals made with light".

Chapter I

The dipolar potential

The starting point of this year's lectures is the fact that light can create a potential $V(\boldsymbol{r})$ on atoms. We will restrict ourselves here to monochromatic light of angular frequency ω and we will show that, in a perturbative limit to be defined, this potential is proportional to the light intensity. The ability to shape the light intensity profile $I(\boldsymbol{r})$ thus allows one to realize a fully controllable potential landscape.

The goal of this first lecture is to establish the relation between $V(\boldsymbol{r})$ and $I(\boldsymbol{r})$. We will start our study with a simple semi-classical approach before going to a quantum treatment. For a review of the dipole force and optical traps, one can refer to the very detailed article by Grimm, Weidemüller, et al. (2000).

To describe the action of light on an atom, we will start by considering a hypothetical atomic species that would have only one valence electron (as the alkali atoms), this electron having no spin (there will thus be no atomic fine structure), and the spin of the atomic nucleus being zero. Moreover, we will start by considering the case where only one atomic transition is involved, linking the ground state of zero angular momentum to an excited state of angular momentum 1. We will then gradually enrich this description of the atom to reach the case where the ground state has a non-zero spin (electronic and/or nuclear), and where the potential $V(\boldsymbol{r})$ depends on the spin of the occupied state.

1 The Optical Bloch equations

1-1 The two-level atom approximation

Our starting point in this paragraph is as stated in the introduction

- A laser wave with linear polarization $\boldsymbol{\epsilon}$, whose electric field is written

$$\mathcal{E}(\boldsymbol{r},t) = \boldsymbol{\epsilon}\, \mathcal{E}(\boldsymbol{r}) \cos\left[\omega t - \varphi(\boldsymbol{r})\right]. \tag{1}$$

  The amplitude $\mathcal{E}$ of the field and its phase φ both depend, a priori, on the position.

- An atomic transition that we model by a ground state of zero angular momentum $|g\rangle$ and an excited level of unit angular momentum, with its basis $\{|e,m_z\rangle,\ m_z=-1,0,+1\}$, where we have chosen the quantization axis for the angular momentum basis parallel to $\boldsymbol{\epsilon}$. The energy difference between $|g\rangle$ and $|e\rangle$ is denoted by $\hbar\omega_0$.

The interaction between the atom and the electromagnetic wave is treated within the electric dipole approximation, from which follows that the $|g\rangle$ state is coupled to the $|e,m=0\rangle$ state, that will be written more simply as $|e\rangle$ in the following. This electric dipole coupling has the form

$$\begin{aligned}\hat{V}_{\mathrm{e.d.}}(\hat{\boldsymbol{r}},t) &= -\hat{\boldsymbol{D}}\cdot\boldsymbol{\mathcal{E}}(\hat{\boldsymbol{r}},t)\\ &= -d_0\mathcal{E}(\hat{\boldsymbol{r}})\,(\hat{\sigma}_+ + \hat{\sigma}_-)\cos\left[\omega t - \varphi(\hat{\boldsymbol{r}})\right]\end{aligned} \tag{2}$$

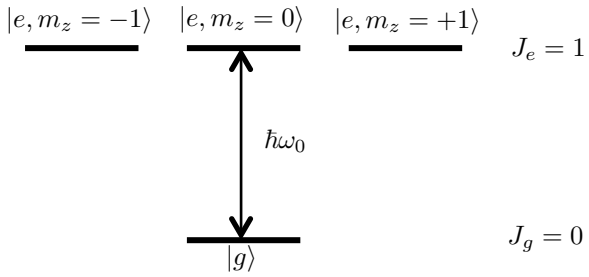

Figure 1. *Transition modelling a two-level atom: the ground state of zero angular momentum is coupled to an excited level of unit angular momentum. The electromagnetic field is assumed to be linearly polarized and the quantization axis of the angular momentum is chosen to be parallel to this polarization. The atom-field coupling then only involves the $|g\rangle \leftrightarrow |e, m_z = 0\rangle$ transition.*

where d_0 is the reduced atomic dipole, characteristic of the considered atomic transition, where $\hat{\boldsymbol{r}}$ represents the operator associated to the *position of the center-of-mass of the atom*, and where we have introduced the raising and lowering operators:

$$\hat{\sigma}_+ = |e\rangle\langle g|, \qquad \hat{\sigma}_- = |g\rangle\langle e|. \tag{3}$$

Note that the possibility to restrict the problem to a two-level transition remains valid if the polarization of the light wave is arbitrary. One should then define $|e\rangle$ as the linear combination of the three states $|e, m\rangle$ that is coupled to $|g\rangle$. For example, if the wave is circularly polarized, we will take for $|e\rangle$ one of the two states $|e, m = \pm 1\rangle$.

We also define the force operator

$$\begin{aligned} \hat{\boldsymbol{F}} &= -\boldsymbol{\nabla}_{\boldsymbol{r}} \hat{V}_{\text{e.d.}}(\hat{\boldsymbol{r}}, t) \\ &= d_0 \left(\hat{\sigma}_+ + \hat{\sigma}_-\right) \boldsymbol{\nabla}_{\boldsymbol{r}} \left\{\mathcal{E}(\hat{\boldsymbol{r}}) \cos\left[\omega t - \varphi(\hat{\boldsymbol{r}})\right]\right\} \end{aligned} \tag{4}$$

which involves both the gradients of the amplitude $\mathcal{E}$ and the phase φ of the electromagnetic field.

1-2 The semi-classical approach

The semi-classical approach consists in describing in a classical way the motion of the center-of-mass of the atom, while taking into account the quantum nature of its internal dynamics. For a static atom at position $\boldsymbol{r}$, we can then evaluate the average force acting on the atom from the steady-state value of the following matrix elements of the density operator $\hat{\rho}$ of the atom:

$$\rho_{eg} = \text{Tr}\left(\hat{\sigma}_- \hat{\rho}\right), \qquad \rho_{ge} = \text{Tr}\left(\hat{\sigma}_+ \hat{\rho}\right). \tag{5}$$

This steady-state value is calculated with the optical Bloch equations, which are the superposition of the semi-classical Hamiltonian evolution of the density operator

$$\frac{\mathrm{d}\hat{\rho}}{\mathrm{d}t} = \frac{1}{\mathrm{i}\hbar}[\hat{H}_{\text{s.c.}}, \hat{\rho}] \tag{6}$$

and irreversible evolution due to spontaneous emission processes, including

$$\left.\frac{\mathrm{d}\rho_{eg}}{\mathrm{d}t}\right|_{\text{sp.}} = -\frac{\Gamma}{2}\rho_{eg}, \qquad \left.\frac{\mathrm{d}\rho_{ge}}{\mathrm{d}t}\right|_{\text{sp.}} = -\frac{\Gamma}{2}\rho_{ge}. \tag{7}$$

In (6), the semi-classical Hamiltonian $\hat{H}_{\text{s.c.}}$ is the sum of the electric dipole coupling and of the Hamiltonian for the internal variables of an isolated atom:

$$\hat{H}_{\text{s.c.}} = \hat{V}_{\text{e.d.}} + \hbar\omega_0 |e\rangle\langle e|. \tag{8}$$

In (7), the coefficient Γ represents the natural linewidth of the excited state $|e\rangle$, whose lifetime is thus Γ^{-1}. In the framework of this two-level model, the coefficient Γ is expressed as a function of the reduced dipole d_0

$$\Gamma = \frac{d_0^2 \omega_0^3}{3\pi\epsilon_0 \hbar c^3}. \tag{9}$$

1-3 Dipole force and dipole potential

The evolution equation for ρ_{eg} can be explicitly written from the optical Bloch equations (Cohen-Tannoudji, Dupont-Roc, et al. 1992):

$$\frac{\mathrm{d}\rho_{eg}}{\mathrm{d}t} = -\left(\mathrm{i}\omega_0 + \frac{\Gamma}{2}\right)\rho_{eg} - \mathrm{i}\Omega\cos(\omega t - \varphi)\left(\rho_{gg} - \rho_{ee}\right), \tag{10}$$

where we have introduced the *Rabi frequency* Ω:

$$\hbar\Omega(\boldsymbol{r}) = -d_0\mathcal{E}(\boldsymbol{r}). \tag{11}$$

In most laser trapping experiments, one chooses a combination of laser intensity and detuning from the atomic resonance $\omega-\omega_0$ so that the steady-state population of the excited state is very small compared to 1, the atom thus essentially occupy the ground state. We can then approximate $\rho_{gg} \approx 1$, $\rho_{ee} \approx 0$ in (10), which provides the driven steady-state solution

$$\rho_{eg}(t) = \frac{\Omega}{2}\left[\frac{\mathrm{e}^{-\mathrm{i}(\omega t-\varphi)}}{\omega-\omega_0+\mathrm{i}\Gamma/2} - \frac{\mathrm{e}^{\mathrm{i}(\omega t-\varphi)}}{\omega+\omega_0-\mathrm{i}\Gamma/2}\right], \tag{12}$$

and the value for ρ_{ge} is deduced by complex conjugation. In all the applications that we will consider in the following, the detuning

$$\Delta = \omega - \omega_0 \tag{13}$$

is very large (in absolute value) compared to the natural width Γ (and a fortiori we have $\omega+\omega_0 \gg \Gamma$). One can thus take at the lowest order of the calculation

$$\rho_{eg}(t) = \frac{\Omega}{2}\left[\frac{\mathrm{e}^{-\mathrm{i}(\omega t-\varphi)}}{\omega-\omega_0} - \frac{\mathrm{e}^{\mathrm{i}(\omega t-\varphi)}}{\omega+\omega_0}\right]. \tag{14}$$

We deduce the average atomic dipole in the steady state

$$\boldsymbol{d}(t) = \mathrm{Tr}\left[\hat{\boldsymbol{D}}\,\hat{\rho}(t)\right] = \boldsymbol{\epsilon} d_0 \frac{\Omega}{\bar{\Delta}}\cos(\omega t-\varphi) = -\frac{d_0^2}{\hbar\bar{\Delta}}\boldsymbol{\mathcal{E}}(\boldsymbol{r},t), \tag{15}$$

where we have defined

$$\frac{1}{\bar{\Delta}} = \frac{1}{\omega-\omega_0} - \frac{1}{\omega+\omega_0}. \tag{16}$$

Depending on the sign of $\bar{\Delta}$, which is itself given by the sign of the detuning Δ, the dipole is in phase (if $\Delta<0$) or out-of-phase (if $\Delta>0$) with the electric field.

It is then simple to calculate the average value $\boldsymbol{f}$ of the force operator $\hat{\boldsymbol{F}}$ defined in (4):

$$\boldsymbol{f} = (\boldsymbol{\epsilon}\cdot\boldsymbol{d})\,\boldsymbol{\nabla}\left[\mathcal{E}\cos(\omega t-\varphi)\right]. \tag{17}$$

Using the expression (15) for the mean dipole, we can immediately see that two types of terms will appear: time-independent terms and terms oscillating as $\mathrm{e}^{\pm 2\mathrm{i}\omega t}$. The frequency ω being very large (optical frequency), the micro-motion of the center-of-mass of the atom induced by these oscillating terms is negligible and we can limit ourselves to the time-independent terms. We can then notice that the term related to the phase gradient $\boldsymbol{\nabla}\varphi$ has a zero contribution, and only the term in $\boldsymbol{\nabla}\mathcal{E}$, related to the intensity gradient of the light wave, remains.

We thus find the expression of the dipole force $\boldsymbol{f}_{\mathrm{dip}}$, deriving from the potential V:

$$\boldsymbol{f}_{\mathrm{dip}} = -\boldsymbol{\nabla}V \qquad \text{with} \qquad V(\boldsymbol{r}) = \frac{\hbar\Omega^2(\boldsymbol{r})}{4\bar{\Delta}} = \frac{d_0^2\mathcal{E}^2(\boldsymbol{r})}{4\hbar\bar{\Delta}}. \tag{18}$$

In the approach we have taken here, the physical interpretation of this potential is very simple. The light beam illuminating the atom induces a dipole $\boldsymbol{d} = \alpha(\omega)\,\boldsymbol{\mathcal{E}}$, where the polarizability $\alpha(\omega)$ can be deduced from (15):

$$\alpha(\omega) = -\frac{d_0^2}{\hbar\bar{\Delta}}. \tag{19}$$

The induced dipole then interacts with the incoming field and the corresponding interaction energy is written[1] $-(1/2)\boldsymbol{d}\cdot\boldsymbol{\mathcal{E}}$, whose time-average gives back (18). Note that our perturbative treatment leading to the expression

$$V(\boldsymbol{r}) = -\frac{\alpha(\omega)}{4}\mathcal{E}^2(\boldsymbol{r}) \tag{20}$$

for the dipole potential can be effortlessly generalized to the case where several excited levels $e_1, e_2, \ldots$ have a non-negligible contribution. The total polarizability is obtained by summing over these levels the different terms d_i^2, $i=1,2\ldots$, with the energy denominators chosen as $\omega\pm\omega_i$.

The crucial point that can be read on (18) or (20) is the following: the light creates on the atoms a potential $V(\boldsymbol{r})$ proportional to the local light intensity $I(\boldsymbol{r}) \propto \mathcal{E}^2(\boldsymbol{r})$. Depending on the sign of the detuning $\omega-\omega_0$, this potential attracts ($\omega<\omega_0$, red detuning) or repels ($\omega>\omega_0$, blue detuning) the atoms in/from the regions of high light intensity. In the case of an optical lattice, on which we will focus in the following lectures, we will

[1] Don't forget the $1/2$ factor due to the fact that this dipole is *induced*!

choose a periodically-varying Rabi frequency by taking for example in one dimension

$$\Omega(x) = \Omega_0 \sin(kx). \tag{21}$$

This variation is obtained by creating a standing light wave. The atoms will then accumulate in the vicinity of the nodes ($\Delta > 0$) or of the antinodes ($\Delta < 0$) of the wave.

What about the radiation pressure force? We do not find any force related to the gradient of the phase at this order of the calculation. Thus, if the laser wave is a travelling plane wave, $\mathcal{E}(\boldsymbol{r}) = \mathcal{E}_0$, $\varphi(\boldsymbol{r}) = \boldsymbol{k}\cdot\boldsymbol{r}$, we find no force acting on the atom while we would expect to find a non-zero radiation pressure. This is related to the approximation made between (12) and (14) which imposes that the induced dipole is exactly in-phase or out-of-phase with the electric field. In this case, the term related to the phase gradient in the expression (17) of the average force

$$\text{Radiation pressure:} \qquad \boldsymbol{f}_{\text{r.p.}} = -(\boldsymbol{\epsilon}\cdot\boldsymbol{d})\,\mathcal{E}\boldsymbol{\nabla}\varphi\,\sin(\omega t-\varphi) \tag{22}$$

has a zero time-average. To find a non-zero mean value for this term, one must (at least) push the calculation one step further in powers of Γ/Δ and approximate (12) by:

$$\frac{1}{\omega-\omega_0+\mathrm{i}\Gamma/2} \approx \frac{1}{\omega-\omega_0} - \mathrm{i}\frac{\Gamma/2}{(\omega-\omega_0)^2}. \tag{23}$$

The mean dipole then acquires a component in quadrature [$\sin(\omega t-\varphi)$] with the incident field, which leads to a non-zero time average of (22). In practice, we will not need to look at these correction terms in the present lectures.

1-4 Rotating wave approximation.

Note that our treatment does not resort to the rotating wave approximation (RWA). This approximation requires the additional assumption (Cohen-Tannoudji, Dupont-Roc, et al. 1992)

$$\text{rotating wave approximation:} \qquad |\Delta| \ll \omega_0, \qquad \bar{\Delta} \approx \Delta. \tag{24}$$

The main interest of this approximation is to allow analytical calculations with Bloch's equations even if the laser excitation is non-perturbative, i.e. even if we cannot make the approximation $\rho_{gg} \approx 1$, $\rho_{ee} \approx 0$ in (10). It simplifies the calculations from the start by replacing the electric dipole coupling by

$$\hat{V}_{\text{e.d.}}^{\text{rwa}} = \frac{\hbar\Omega}{2}\left[\hat{\sigma}_+ \mathrm{e}^{-\mathrm{i}(\omega t-\varphi)} + \hat{\sigma}_- \mathrm{e}^{+\mathrm{i}(\omega t-\varphi)}\right]. \tag{25}$$

However, this approximation can be *marginal* in some cold atom trapping experiments. For example, if rubidium atoms, with $\lambda_0 = 780\,\text{nm}$, are manipulated with a laser at $\lambda = 1064\,\text{nm}$, the non-resonant term increases the dipole potential by 15%. On the contrary, for a laser detuned on the blue side of the resonance at a typical value of $\lambda = 532\,\text{nm}$, the non-resonant term reduces the RWA potential by 19%.

2 The dressed atom picture

The dressed atom picture is a convenient alternative to the calculation of the dipole potential from the optical Bloch equations that we have performed above (Dalibard & Cohen-Tannoudji 1985). It is particularly simple in the case where the rotating wave approximation is valid. This point of view consists in studying the energy levels of the system *atom + laser mode*. We start from a basis of this system without a coupling $\{|g,N\rangle, |e,N\rangle,\ N\in\mathbb{N}\}$, where N represents the number of photons present in the laser mode. We immediately see that if $|\Delta| \ll \omega_0$, these levels group by multiplicities of dimension 2 (cf. figure 2):

$$|g,N\rangle \ : \text{energy } N\hbar\omega, \qquad |e,N-1\rangle \ : \text{energy } (N-1)\hbar\omega+\hbar\omega_0, \tag{26}$$

the difference between these two levels being $\hbar|\Delta|$. In the RWA approximation, the atom-laser interaction (25) is written in this picture

$$\hat{V}_{\text{e.d.}}^{\text{rwa}} = \frac{\hbar\Omega_1(\boldsymbol{r})}{2}\ \left[\hat{\sigma}_+\hat{a} + \hat{\sigma}_-\hat{a}^\dagger\right] \tag{27}$$

where $\hat{a}$ and $\hat{a}^\dagger$ destroy and create a photon in the laser mode, whose profile is described by $\Omega_1(\boldsymbol{r})$. This quantity Ω_1 can be understood as the Rabi

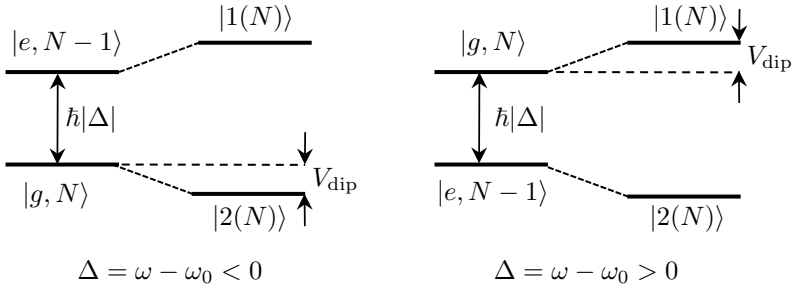

Figure 2. *Levels of the dressed atom, without and with a coupling between the atom and the electromagnetic field, and for the two possible signs of the detuning Δ. The dipole potential $V_{\rm dip}$ is interpreted as the light shift of the ground state $|g\rangle$. This shift occurs downwards or upwards, depending whether the detuning Δ is negative or positive.*

frequency at position $\boldsymbol{r}$ when there is only one photon in the considered mode to excite the atom.

The interaction (27) couples only the two levels of the same multiplicity of the dressed atom:

$$\langle e, N-1|\hat{V}_{\rm e.d.}^{\rm rwa}|g, N\rangle = \frac{\hbar\Omega_1(\boldsymbol{r})}{2}\sqrt{N}. \tag{28}$$

At this stage, the value of Ω_1 and the number of photons N are undetermined. When we consider a problem of cavity electrodynamics, the value of Ω_1 is imposed by the volume of the cavity itself. For an atom in free space, the only thing that matters is the value of the product $\Omega_1\sqrt{N}$ which is taken to be equal to the Rabi frequency Ω. To simplify the notations, we will assume that the phase of the laser $\varphi(\boldsymbol{r})$ is zero. This phase anyway does not appear in the expression of the energy of the dressed states [see for example (34)] and we will reinsert it in a natural way in the expression of the dressed states (38).

It is then very simple to find the eigenenergies for an atom located at position $\boldsymbol{r}$. The Hamiltonian for the multiplicity $\{|g, N\rangle, |e, N-1\rangle\}$ is written

$$\hat{H} = \frac{\hbar}{2}\begin{pmatrix}\Delta & \Omega \\ \Omega & -\Delta\end{pmatrix} + \epsilon_N \tag{29}$$

where we have set

$$\epsilon_N = \left(N - \frac{1}{2}\right)\hbar\omega + \frac{1}{2}\hbar\omega_0. \tag{30}$$

It is useful to introduce the mixing angle θ defined by

$$\cos[2\theta(\boldsymbol{r})] = \frac{\Delta}{\sqrt{\Delta^2 + \Omega^2(\boldsymbol{r})}}, \qquad \sin[2\theta(\boldsymbol{r})] = \frac{\Omega(\boldsymbol{r})}{\sqrt{\Delta^2 + \Omega^2(\boldsymbol{r})}}, \tag{31}$$

to write the Hamiltonian in the form:

$$\hat{H} = \frac{\hbar}{2}\sqrt{\Delta^2 + \Omega^2}\begin{pmatrix}\cos 2\theta & \sin 2\theta \\ \sin 2\theta & -\cos 2\theta\end{pmatrix} + \epsilon_N. \tag{32}$$

The eigenvectors are written

$$\begin{aligned} |1(N)\rangle &= \cos\theta\,|g, N\rangle + \sin\theta\,|e, N-1\rangle \\ |2(N)\rangle &= \sin\theta\,|g, N\rangle - \cos\theta\,|e, N-1\rangle \end{aligned} \tag{33}$$

and the corresponding energies are

$$E_{N,\pm} = \epsilon_N \pm \frac{\hbar}{2}\sqrt{\Delta^2 + \Omega^2}, \tag{34}$$

with sign $+$ for $|1(N)\rangle$ and $-$ for $|2(N)\rangle$.

In the perturbative limit that we are considering here, the inequality $|\Omega| \ll |\Delta|$ holds and we obtain the approximate expression for the energy levels that "repel each other" due to the coupling:

$$N\hbar\omega + \frac{\hbar\Omega^2}{4\Delta}, \qquad (N-1)\hbar\omega + \hbar\omega_0 - \frac{\hbar\Omega^2}{4\Delta}. \tag{35}$$

The first energy corresponds to the level stemming from $|g, N\rangle$, which is the populated level that interests us here. The second energy corresponds to the level from $|e, N-1\rangle$ which has a negligible population. The dipole potential $\hbar\Omega^2/4\Delta$ [cf. (18)] can therefore be interpreted as an energy shift of the state $|g, n\rangle$ due to the coupling with the laser. This shift can be downward or upward, depending whether the "repelling" level $|e, N-1\rangle$ is above or below $|g, N\rangle$ (cf. figure 2).

For $\Delta > 0$, the angle 2θ defined in (31) can be chosen close to 0, and the eigenstate linked to g is written

$$\Delta > 0 : \qquad \overline{|g,N\rangle} = |1(N)\rangle \approx |g,N\rangle + \frac{\Omega}{2\Delta}|e,N-1\rangle \tag{36}$$

For $\Delta < 0$, the angle 2θ can be chosen close to π, so that

$$\Delta < 0 : \qquad \overline{|g,N\rangle} = |2(N)\rangle \approx |g,N\rangle - \frac{\Omega}{2|\Delta|}|e,N-1\rangle. \tag{37}$$

In both cases we can reintroduce the explicit position dependence and reinsert, if relevant, the phase $\varphi(\boldsymbol{r})$ of the laser [cf. (25)], by defining:

$$\overline{|g,N\rangle}(\boldsymbol{r}) \approx |g,N\rangle + \frac{\Omega(\boldsymbol{r})}{2\Delta}\,\mathrm{e}^{\mathrm{i}\varphi(\boldsymbol{r})}\,|e,N-1\rangle. \tag{38}$$

The expression (38) is very convenient because it allows one to compute the steady-state values of the matrix elements of the density operator at order two in Ω. Indeed at this order, one can show that the steady-state population of the other dressed state of (33) is zero (it is at least of order 4 in Ω/Δ, see for example Dalibard & Cohen-Tannoudji (1985)). We can therefore deduce from (38) the matrix element ρ_{eg} already given in (14)

$$\rho_{eg} = \langle e,N-1|\left(\overline{|g,N\rangle}\,\overline{\langle g,N|}\right)|g,N\rangle = \frac{\Omega\,\mathrm{e}^{\mathrm{i}\varphi}}{2\Delta}, \tag{39}$$

the difference with (14) being due to the RWA approximation. In addition, the explicit time evolution $\mathrm{e}^{-\mathrm{i}\omega t}$ of (14) is here implicitly contained in the difference between the numbers of photons on the left and the right. We also deduce from (38) the population Π_e of the excited state at this order of the calculation

$$\Pi_e = \langle e,N-1|\left(\overline{|g,N\rangle}\,\overline{\langle g,N|}\right)|e,N-1\rangle = \frac{\Omega^2}{4\Delta^2}, \tag{40}$$

an expression that allows one to estimate the rate of spontaneous emission $\gamma = \Gamma\Pi_e$.

3 The case of alkali-metal atoms

The model of a $J_g = 0 \leftrightarrow J_e = 1$ transition applies well to alkaline earth atoms (at least if their nuclear spin is zero), but it cannot be used as such for alkali atoms. Because of their practical relevance, we will give some indications on how the previous results can be adapted. To simplify the notations, we will use here the rotating wave approximation.

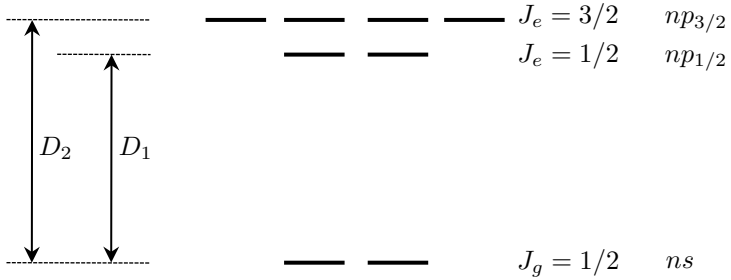

Figure 3. *Modelling the resonant transition of an alkali-metal atom. The effect of the hyperfine interaction with the nuclear spin and the degeneracy linked to this spin have been neglected.*

We first consider the case of a simplified alkali atom for which the nuclear spin is zero (figure 3). The ground state, a ns state, is then doubly degenerate because of the spin of the valence electron, and its angular momentum is $J_g = 1/2$. The resonant transition couples it to the np state which, due to the fine structure interaction, is split into two sublevels of angular momentum $1/2$ and $3/2$ noted $np_{1/2}$ and $np_{3/2}$. The two resonances $ns \leftrightarrow np_{1/2}$ and $ns \leftrightarrow np_{3/2}$ correspond to the D_1 and D_2 lines of angular frequency ω_1 and ω_2.

3-1 Linearly polarized light

If the polarization of the light beam is linear, the symmetry of the problem implies that the light shift of the two sublevels $|g, m_z = \pm 1/2\rangle$ are identical[2]. In this case, the light-shift operator is proportional to the identity in the subspace $|g, m = \pm 1/2\rangle$. Using the algebra of the angular momentum operators and the Clebsch–Gordan coefficients shown in figure 4, one can

[2]To see this easily, it is better to choose as before the quantization axis along the direction of the polarization.

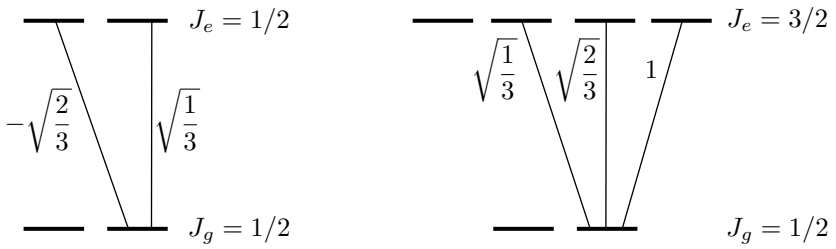

Figure 4. *Amplitude of the couplings for the two transitions D_1 and D_2 of the resonance line of an alkali-metal atom, starting from the ground state $m_z = +1/2$. The spin of the nucleus is assumed to be zero. The amplitudes of the couplings from the ground state $m_z = -1/2$ have values symmetrical to the ones shown here.*

prove that this light shift is

$$\hat{V} = \frac{\hbar\Omega^2}{4\Delta}\,\hat{1} \qquad \text{with} \qquad \frac{1}{\Delta} = \frac{1}{3}\left(\frac{1}{\Delta_1} + \frac{2}{\Delta_2}\right), \tag{41}$$

where $\Delta_1 = \omega - \omega_1$ and $\Delta_2 = \omega - \omega_2$ are the detunings of the laser with respect to the resonant D_1 and D_2 transitions. It is therefore sufficient to take a weighted average of the two detunings to recover the result of the $0 \leftrightarrow 1$ transition. This result remains valid when the hyperfine structure of the atom is taken into account, provided that the detunings Δ_1 and Δ_2 are large compared to the hyperfine structure of the excited levels $np_{1/2}$ and $np_{3/2}$, which will in practice always be the case during the rest of this lecture.

When $\Delta_{1,2}$ is large compared to the fine structure splitting $\omega_2 - \omega_1$, then $\Delta_1 \approx \Delta_2$ and the fine structure has no particular effect. On the other hand, when the detuning is on the same order as the fine structure splitting, the result is notably modified. In particular, we see that there is a particular value of Δ, such that $\Delta_2 = -2\Delta_1$ for which $\hat{V}$ cancels. For a rubidium atom, the wavelengths of the D_1 and D_2 lines are $\lambda_1 = 795\,\text{nm}$ and $\lambda_2 = 780\,\text{nm}$; this particular detuning is thus obtained by choosing a laser of wavelength $\lambda = 790\,\text{nm}$. For this value of λ, the dipole potential felt by the atoms is null; the atoms continue to see the light beam and to scatter photons (it is not a dark state), but they do not feel any dipole force.

3-2 Light with an arbitrary polarization

The situation becomes more complicated if the polarization of the laser is not linear, but elliptical or circular. In this case, the light-shift operator is no longer proportional to the identity in the subspace $|g, m = \pm 1/2\rangle$, which allows to generate potentials that depend on the spin $\boldsymbol{S}$ associated to this level. Let us write the laser field in the form

$$\boldsymbol{\mathcal{E}}(\boldsymbol{r}, t) = \frac{1}{2}\boldsymbol{\epsilon}\,\mathcal{E}(\boldsymbol{r})\,\mathrm{e}^{\mathrm{i}(\omega t - \varphi)} + \text{c.c.} \tag{42}$$

where the polarization vector $\boldsymbol{\epsilon}$ is now complex. Let us introduce the Rabi frequency vector $\boldsymbol{\Omega}$ whose three complex components Ω_α, $\alpha = x, y, z$ characterize the atom-laser coupling

$$\hbar\Omega_\alpha = -d_0\mathcal{E}(\boldsymbol{r})(\boldsymbol{\epsilon}\cdot\boldsymbol{u}_\alpha) \tag{43}$$

in the Cartesian basis $\boldsymbol{u}_\alpha$. We can also introduce the coordinates of the vector $\boldsymbol{\Omega}$ in the standard basis

$$\Omega_\pm = \frac{1}{\sqrt{2}}\left(\mp\Omega_x + \mathrm{i}\Omega_y\right), \qquad \Omega_0 = \Omega_z. \tag{44}$$

From this vector $\boldsymbol{\Omega}$, we can write the light-shift operator in the form

$$\hat{V} = \frac{\hbar|\boldsymbol{\Omega}|^2}{4\Delta}\hat{1} + \boldsymbol{B}\cdot\hat{\boldsymbol{S}}, \tag{45}$$

where the effective magnetic field is

$$\boldsymbol{B} = \frac{\mathrm{i}}{6}\left(\frac{1}{\Delta_2} - \frac{1}{\Delta_1}\right)\boldsymbol{\Omega}\times\boldsymbol{\Omega}^*. \tag{46}$$

The light-shift operator (45) thus involves both a scalar part and a vector part.

The origin of this result is clear; let us consider for example a circular light polarization σ_- close to the D_1 transition (we here forget the D_2 transition). One can immediately see on figure 4 (left) that the ground state $|g, m_z = -1/2\rangle$ is not coupled to the light, while the level $|g, m_z = +1/2\rangle$ is coupled to the light with a Clebsch–Gordan coefficient equal to $-\sqrt{2/3}$. The differential light shift between these two levels is described by this effective magnetic field $\boldsymbol{B}$. More precisely, the combination of the scalar term

and the vector term of (45) accounts for the fact that $|g, m_z = -1/2\rangle$ feels no potential while $|g, m_z = +1/2\rangle$ is displaced twice as much as if the light had a linear polarization of the same intensity.

The vector part of the light shift (Cohen-Tannoudji & Dupont-Roc 1972; Deutsch & Jessen 1998), proportional to $\boldsymbol{B}$, is comparable to, and possibly larger than the scalar part if the detuning is chosen of the same order as the fine structure. In particular, this vector part remains non-zero when we choose the detuning $\Delta_2 = -2\Delta_1$ that cancels the scalar part. On the other hand, this vector part decreases as $1/\Delta^2$ if we choose the detuning to be large compared to the fine structure. In this case, it is thus negligible compared to the scalar part, which only decreases as $1/\Delta$. This last point makes sense: if the detuning is large compared to the fine structure, the latter is negligible during the characteristic time Δ^{-1} associated to the atom-light interaction. If we can neglect the fine structure, we recover the $J_g = 0 \leftrightarrow J_e = 1$ transition that we have studied in the first part, since the electronic spin plays no role in the coupling Hamiltonian between the atom and the light. The degeneracy between the two spin sublevels $\pm 1/2$ therefore cannot be lifted by the atom-light interaction.

Let us look at two special cases of the general expression (46):

- For a linear polarization, for example $\boldsymbol{\Omega} = \Omega \boldsymbol{u}_z$, then the cross product $\boldsymbol{u}_z \times \boldsymbol{u}_z$ is zero, as is the effective magnetic field. The vector part of the light-shift operator vanishes, as mentioned above.

- For a circular polarization, for example a light beam propagating along the z axis such that $\boldsymbol{\Omega} = \Omega(\boldsymbol{u}_x + \mathrm{i}\boldsymbol{u}_y)/\sqrt{2}$, then the vector product $(\boldsymbol{u}_x + \mathrm{i}\boldsymbol{u}_y) \times (\boldsymbol{u}_x - \mathrm{i}\boldsymbol{u}_y) = -2\mathrm{i}\boldsymbol{u}_z$ and the effective magnetic field is aligned along z:

$$\boldsymbol{B} = \frac{|\Omega|^2}{6}\left(\frac{1}{\Delta_2} - \frac{1}{\Delta_1}\right)\boldsymbol{u}_z. \tag{47}$$

Note that unlike a magnetic field generated with external coils, this effective $\boldsymbol{B}$ can have spatial variations on the scale of the optical wavelength: this happens for example for a standing wave resulting from the overlap of two running waves with opposite directions and non-parallel linear polarizations.

We now only need to add the effect of the hyperfine structure of the ground state. If the nucleus has a spin I, this manifold is split into two sublevels of angular momentum $F = I \pm 1/2$. The Wigner-Eckart theorem indicates that the light-shift operator can be written in this case

$$\hat{V} = \frac{\hbar|\boldsymbol{\Omega}|^2}{4\Delta}\hat{1} + \boldsymbol{B}' \cdot \hat{\boldsymbol{F}}, \tag{48}$$

with, for the level $F = I \pm 1/2$:

$$\boldsymbol{B}' = \pm\frac{\boldsymbol{B}}{2I+1}. \tag{49}$$

The effective magnetic fields are thus opposite for the two hyperfine levels. The previous remarks on the relative values of the scalar and vector components of this light-shift operator are unchanged.

4 Quantum approach

The semi-classical approach has provided us with the value of the dipole potential, but it is useful to validate this result with an approach that treats the motion of the atom in a quantum manner. Most applications of optical lattices concerns aspects that are directly related to the quantum nature of this motion: energy bands, geometric phases, topological states of matter, ... Fortunately, the structure of the semi-classical treatment that has allowed us to compute the dipole potential can be transposed almost word for word; we will only have to add a few elements to obtain the fully quantum Hamiltonian describing the motion of the center-of-mass. In order to minimize the technical aspects of this study, we will restrict ourselves to the case of a two-level atom, as considered in § 1-1. The case of a multilevel atom is treated in detail by Gerbier & Dalibard (2010).

4-1 Slow and fast variables

The problem we deal with consists in eliminating fast variables to obtain the dynamics of slow ones. The fast variables relate to the internal dynamics of the atom, the slow variables to the center-of-mass motion. The

evolution of all these variables is described by the Hamiltonian

$$\hat{H} = \frac{\hat{\boldsymbol{p}}^2}{2m} + \hat{V}_{\rm e.d.} + \hbar\omega_0 |e\rangle\langle e|, \tag{50}$$

where the atom-light coupling in the electric dipole approximation was given in (2). We have to add to the reversible evolution described by this Hamiltonian the irreversible evolution due to spontaneous emission processes. This evolution has been given in (7) for the matrix elements of the density operator between $|g\rangle$ and $|e\rangle$. We will not need here the explicit expression for the terms describing the evolution of $\hat{\rho}_{ee}$ and $\hat{\rho}_{gg}$; they are given in Gerbier & Dalibard (2010).

Let us consider the evolution of the total density operator of the atom $\hat{\rho}$, which contains both the internal and external degrees of freedom. Let us first consider the evolution of $\hat{\rho}_{eg} = \langle e|\hat{\rho}|g\rangle$ which is an operator with respect to the external variables only. The corresponding evolution equation is deduced from the one written in the semi-classical picture (10):

$$\frac{{\rm d}\hat{\rho}_{eg}}{{\rm d}t} = \frac{1}{{\rm i}\hbar}\left[\frac{\hat{\boldsymbol{p}}^2}{2m}, \hat{\rho}_{eg}\right] - ({\rm i}\omega_0 + \frac{\Gamma}{2})\hat{\rho}_{eg} - {\rm i}\Omega\cos(\omega t - \varphi)\,(\hat{\rho}_{gg} - \hat{\rho}_{ee}). \tag{51}$$

We will make two approximations at this stage, similar to what we did in the semi-classical case. On the one hand we will neglect the fraction of atoms in the excited state, and thus omit the $\hat{\rho}_{ee}$ term in the above equation. On the other hand we will assume that the evolution of $\hat{\rho}_{eg}$ due to internal variables, with characteristic frequencies Δ and Γ, is much faster than the one due to external variables, coming for example from the kinetic energy Hamiltonian $\hat{\boldsymbol{p}}^2/2m$. Under these conditions, one can (i) omit the first commutator of the right-hand side of (51), (ii) neglect the variation of $\hat{\rho}_{gg}$ over a time $\sim \Gamma^{-1}$, (iii) formally integrate (51) in the limit $|\Delta| \gg \Gamma$ to finally obtain, in a very similar way to (14) :

$$\hat{\rho}_{eg}(t) = \frac{\Omega}{2}\left[\frac{{\rm e}^{-{\rm i}(\omega t-\varphi)}}{\omega - \omega_0} - \frac{{\rm e}^{{\rm i}(\omega t-\varphi)}}{\omega + \omega_0}\right]\hat{\rho}_{gg}(t). \tag{52}$$

This result means that the density operators corresponding to the "optical coherences" ρ_{eg} and ρ_{ge} follow adiabatically the much slower evolution of the density operator restricted to the ground state $|g\rangle$.

4-2 Effective Hamiltonian for the center-of-mass

The result (52) is then transferred into the evolution equation of $\hat{\rho}_{gg}$ to obtain:

$$\begin{aligned}\frac{{\rm d}\hat{\rho}_{gg}}{{\rm d}t} &= \left.\frac{{\rm d}\hat{\rho}_{gg}}{{\rm d}t}\right|_{\rm sp.} + \frac{1}{{\rm i}\hbar}\left[\frac{\hat{\boldsymbol{p}}^2}{2m}, \hat{\rho}_{gg}\right] \pm {\rm i}\Omega\cos(\omega t - \varphi)\,(\hat{\rho}_{eg} - \hat{\rho}_{ge})\,, \\ &\approx \frac{1}{{\rm i}\hbar}\left[\frac{\hat{\boldsymbol{p}}^2}{2m} + V(\hat{\boldsymbol{r}}), \hat{\rho}_{gg}\right]. \end{aligned} \tag{53}$$

Note that we restricted here to the lowest non-zero order in $1/\Delta$ and omitted the terms oscillating as ${\rm e}^{\pm 2{\rm i}\omega t}$, as we did in the semi-classical approximation. Note also that the term describing the evolution of ρ_{gg} due to spontaneous emission is $\propto \Gamma\rho_{ee}$; it does not contribute at this order of the calculation and is only relevant at a higher order in Γ/Δ [see e.g. Gerbier & Dalibard (2010)].

The result (53) corresponds to what we are looking for. This Hamiltonian evolution equation describes the motion of a particle of mass m without internal structure in the dipole potential $V(\boldsymbol{r})$ given in (18). The Hamiltonian

$$\hat{H} = \frac{\hat{\boldsymbol{p}}^2}{2m} + V(\hat{\boldsymbol{r}}) \tag{54}$$

will serve as a starting point for the following lectures, possibly with the modifications related to electronic and nuclear spins mentioned in 3.

5 Red vs. blue lattices

5-1 The "paradox" of Gordon & Ashkin (1980)

In this set of lectures, we will consider traps made of light, in particular periodic optical lattices, in a regime where spontaneous emission phenomena are negligible. In this context, spontaneous emission is indeed a nuisance[3]: its random character is a source of heating for the atoms, which must be

[3] The situation is very different for the original use of optical lattices, where optimal ways to cool an assembly of atoms were investigated.

reduced as much as possible. This non-dissipative regime is obtained by minimizing the excited state population (40):

$$\Pi_e = \frac{\Omega^2}{4\Delta^2}, \tag{55}$$

for a given value of the optical potential

$$V = \frac{\hbar\Omega^2}{4\Delta}. \tag{56}$$

This leads to the choice of the largest possible detuning and intensity: when keeping Ω^2/Δ constant, the quantity $\Omega^2/\Delta^2 \to 0$ if Ω, Δ become very large.

More precisely, consider an optical lattice generated by a one-dimensional standing wave, $\Omega(x) = \Omega_0 \sin(kx)$, leading to the potential

$$V(x) = V_0 \sin^2 kx, \qquad V_0 = \frac{\hbar\Omega_0^2}{4\Delta}. \tag{57}$$

The spontaneous emission rate can be minimized by a proper choice of the sign of the detuning Δ, for a given lattice depth V_0. For $\Delta > 0$ (blue), the atoms are trapped in the vicinity of the nodes of the standing wave that forms the lattice. On the contrary, for $\Delta < 0$ (red), the potential is minimal at the antinodes of the standing wave. One could naively think that, regarding the heating due to spontaneous emission phenomena, the situation is more favorable for a blue detuning than for a red one, since the intensity is smaller at the location of the atoms.

This naive reasoning was invalidated by Gordon & Ashkin (1980), who calculated the momentum diffusion coefficient of an atom in a standing wave. They showed that at a given V_0, this diffusion coefficient is the same at all points of the standing wave and does not depend on the sign of Δ. However, they did not give any physical interpretation of this result which thus remained somewhat mysterious. It has been analyzed by Cohen-Tannoudji (1992), then taken up recently in a more general framework by Gerbier & Dalibard (2010). The transposition of this problem to the case of atoms in cavities has been studied by Murr, Maunz, et al. (2006).

In the appendix of this chapter, we summarize the original argument of Gordon & Ashkin (1980) and its transposition to the formalism developed in paragraph 4, including in particular the approach of Gerbier & Dalibard (2010). In the following, we explain the surprising result of Gordon & Ashkin (1980) by using the dressed atom formalism.

5-2 Raman transitions in a deep lattice

To explain the paradoxical result of Gordon & Ashkin (1980), we consider a lattice with a large depth V_0 so that the motion of an atom is restricted to the bottom of a potential well; the tunnelling to neighbouring wells is assumed to be negligible.

In the case of a blue-detuned lattice, we take as in (57) a 1D lattice with a Rabi frequency $\Omega(x) = \Omega_0 \sin(kx)$ and we assume that the extent of the spatial motion of the atom is small compared to $k^{-1} = \lambda/(2\pi)$ so that we can approximate $\sin(kx) \approx kx$. The atom then undergoes a harmonic motion in the potential

$$V(x) \approx \frac{\hbar\Omega_0^2 k^2}{4\Delta} x^2 = \frac{1}{2} m\omega^2 x^2, \qquad \text{with} \quad \omega = \sqrt{\frac{\hbar\Omega_0^2 k^2}{2m\Delta}}. \tag{58}$$

The eigenstates describing the motion in this potential are the Hermite functions $H_n(x/a_{\rm ho})$, where the characteristic size of the ground state is

$$a_{\rm ho} = \sqrt{\hbar/m\omega}, \tag{59}$$

and the corresponding energies are $(n + 1/2)\hbar\omega$.

In the case of a red-detuned lattice, we will take $\Omega = \Omega_0 \cos(kx)$ to keep a well centered on $x = 0$. The expressions for the frequency ω at the bottom of the well, the size of the ground state $a_{\rm ho}$ and the energy spectrum $(n + 1/2)\hbar\omega$ are unchanged (up to the change $\Delta \to -\Delta$).

Spontaneous emission phenomena will cause transitions between the energy levels of this well by inducing Raman transitions (figure 5): the atom, initially in the electronic ground state g and a vibrational state n for its center-of-mass, can be transfered to an excited electronic state e by absorbing a photon from the laser beam creating the standing wave, and then fall back into the electronic ground state by emitting a fluorescence photon. During this second step, the atom can reach another vibrational state n': the Raman scattering thus induces a random walk for the state of the center-of-mass, which corresponds to heating.

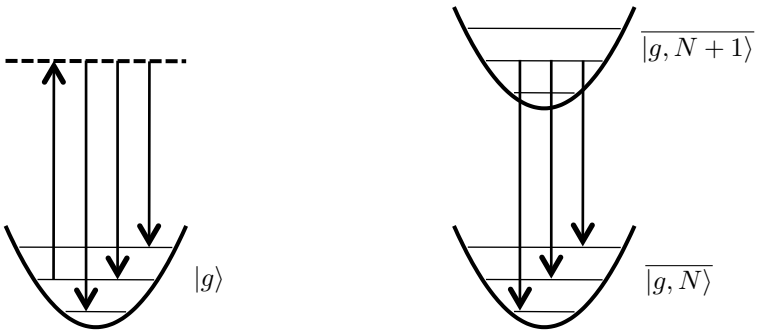

Figure 5. *Left: Raman transition that can cause a change in the vibrational state n of the atom. Right: the same transitions in the dressed atom picture correspond to a "radiative cascade".*

The formalism of the dressed atom is very convenient to visualize this random walk. The Raman transition we have just described corresponds to a transition from the $\{|g, N+1\rangle, |e, N\rangle\}$ multiplicity to the next lower multiplicity $\{|g, N\rangle, |e, N-1\rangle\}$ (figure 5). More precisely, at the lowest non-zero order in Ω, the only significant transition is

$$\overline{|g, N+1\rangle} \longrightarrow \overline{|g, N\rangle}. \tag{60}$$

The state $\overline{|g, N+1\rangle}$ has a non-zero (weak) overlap with $|e, N\rangle$ and is therefore unstable from the point of view of spontaneous emission. When de-exciting, it emits a photon and falls to the state $\overline{|g, N\rangle}$, which itself has a non-zero (strong) overlap with $|g, N\rangle$.

5-3 The transition rates $n \to n'$

We now evaluate the rates of $n \to n'$ transitions using the Fermi Golden Rule (FGR). The coupling $\hat{V}_{\rm vac}$ between the atom and the empty modes of the electromagnetic field (here considered in a 1D model) responsible for the spontaneous emission is written

$$\hat{V}_{\rm vac} = \sum_{k'} \mathcal{V}_{k'}\, \mathrm{e}^{\mathrm{i}k'x}\, \hat{a}^\dagger_{k'}\, \hat{\sigma}_- \quad + \text{h.c.} \tag{61}$$

where $\hat{a}^\dagger_{k'}$ creates a photon of wave vector k' along the x axis. The natural width of the excited atomic state $|e\rangle$ is in this model

$$\Gamma = \frac{2\pi}{\hbar} \left| \langle g\ ;\ k' | \hat{V}_{\rm vac} | e\ ;\ \text{vac} \rangle \right|^2\ \rho(\hbar c k' = \hbar\omega_{\rm A}), \tag{62}$$

where $\rho(E)$ represents the density of states for a final energy $\hbar c\,|k'|$ equal to the initial energy of an excited atom $\hbar\omega_{\rm A}$ (i.e. $k' = \pm\omega_{\rm A}/c$).

The initial state corresponds to the vacuum state of the radiation and the atom in the state $|\Psi_n^{(N+1)}\rangle$, which represents the n-th vibrational level, and the internal dressed state $\overline{|g, N+1\rangle}$:

$$\langle x | \Psi_n^{(N+1)} \rangle = H_n(x)\ \{\cos[\theta(x)]\,|g, N+1\rangle\ +\ \sin[\theta(x)]\,|e, N\rangle\}\,. \tag{63}$$

The final state corresponds to an emitted photon k' and the atomic state $|\Psi_{n'}^{(N)}\rangle$. The rate $\gamma_{n\to n'}$ we are looking for is then written using the FGR

$$\begin{aligned} \gamma_{nn'}(k') &\propto |\langle \Psi_{n'}^{(N)}\ ;\ k' | \mathrm{e}^{\mathrm{i}k'x}\, \hat{a}^\dagger_{k'}\, \hat{\sigma}_- | \Psi_n^{(N+1)}\ ; \text{vac} \rangle|^2 \\ &\propto |\langle \Psi_{n'}^{(N)} | \mathrm{e}^{\mathrm{i}k'x}\, \hat{\sigma}_- | \Psi_n^{(N+1)} \rangle|^2 \end{aligned} \tag{64}$$

By transferring the expression (63) in the matrix element to be calculated, we get to

$$\begin{aligned} \gamma_{n\to n'}(k') &\propto \left| \int H_{n'}(x)\ H_n(x)\ \mathrm{e}^{\mathrm{i}k'x}\ \sin[\theta(x)]\ \cos[\theta(x)]\,\mathrm{d}x \right|^2 \\ &\propto \left| \frac{1}{2\Delta} \int H_{n'}(x)\ H_n(x)\ \mathrm{e}^{\mathrm{i}k'x}\ \Omega(x)\ \mathrm{d}x \right|^2, \end{aligned} \tag{65}$$

where we have used the approximation $\sin(2\theta) \approx \Omega/\Delta$ [cf. (31)]. With this result, we are now able to compare what happens for an atom trapped at the vicinity of a node (blue lattice) or an antinode (red lattice) of the standing wave.

Blue lattice. Assuming a spatial extension of the atom wavefunction small compared to $1/k$, we can make the approximation $\Omega(x) \approx \Omega_0\, kx$, $\mathrm{e}^{\mathrm{i}k'x} \approx 1$ in the integral (65). The latter then simply reduced to

$$\gamma_{n\to n'} \propto \frac{\Omega_0^2}{4\Delta^2} \left| \langle H_{n'} | k\hat{x} | H_n \rangle \right|^2, \tag{66}$$

or, by restoring the so-far-omitted proportionality coefficients:

$$\gamma_{n\to n'} = \frac{\gamma_0}{2}\,(ka_{\rm ho})^2\,[(n+1)\,\delta_{n',n+1} + n\,\delta_{n',n-1}]\,, \tag{67}$$

where we have introduced the "typical" diffusion rate γ_0 for a Rabi frequency Ω_0:

$$\gamma_0 = \Gamma\frac{\Omega_0^2}{4\Delta^2}. \tag{68}$$

The expression (67) calls for two important remarks.

- The localization of the atom in the vicinity of a node of the standing wave leads to a strong reduction of the photon emission rate compared to the typical rate γ_0, by a factor $(ka_{\rm ho})^2 = \hbar k^2/(m\omega) \ll 1$ for the lowest vibrational level $n = 0$. This effect logically follows the fact that the atom experiences a reduced light intensity along the extent of its wave function, which is on the order of $a_{\rm ho}$.
- We see on (67) that the emission of a photon is necessarily accompanied by a level change of one unit, with a rate $\propto (n+1)$ for the transition $n \to n+1$, corresponding to the energy gain $\hbar\omega$, and a rate $\propto n$ for the transition $n \to n-1$, corresponding to the energy loss $\hbar\omega$ (figure 6). The energy gain per unit of time for an atom prepared in the n-th band is thus:

$$\frac{{\rm d}\bar{E}}{{\rm d}t} = \frac{\gamma_0}{2}\,(ka_{\rm ho})^2\,[(n+1)\hbar\omega - n\hbar\omega] = \gamma_0 E_{\rm r} \tag{69}$$

  where we have introduced the recoil energy

$$E_{\rm r} = \frac{\hbar^2k^2}{2m}. \tag{70}$$

Red lattice. In this case, to evaluate the integral (65), we can make the approximation that the Rabi frequency is constant along the extent of the atomic wave function: $\Omega(x) = \Omega_0\cos(kx) \approx \Omega_0$. We develop the exponential ${\rm e}^{{\rm i}k'x}$ at first order in x and we obtain

$$\gamma_{n\to n'}(k') \propto \frac{\Omega_0^2}{4\Delta^2}\,|\langle H_{n'}|1 + {\rm i}k'\hat{x}|H_n\rangle|^2 \tag{71}$$

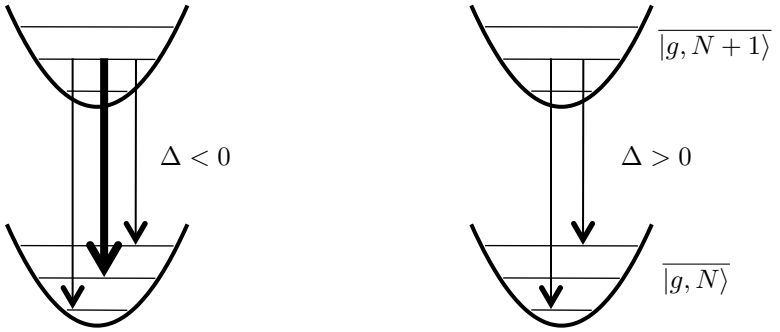

Figure 6. *The main transitions in the dressed atom picture (Lamb–Dicke regime). For a laser detuned on the red side of the atomic transition ($\Delta < 0$), the fluorescence rate is high: most of the photons are emitted on the recoil-less line $n \to n$ and the rest corresponds to $n \to n \pm 1$ transitions. For a blue-detuned beam ($\Delta > 0$), the photons are only emitted on the $n \to n \pm 1$ lines. The heating rate is the same in both cases, for fixed Ω_0 and $|\Delta|$.*

leading to

$$\gamma_{n\to n'} = \gamma_0\left\{\delta_{n,n'} + \frac{(ka_{\rm ho})^2}{2}\,[(n+1)\,\delta_{n',n+1} + n\,\delta_{n',n-1}]\right\} \tag{72}$$

where we have taken $k' \approx k$. The dominant term is this time $\gamma_0\,\delta_{n,n'}$, i.e. a spontaneous emission of photons without change of vibration level (figure 6). The corresponding rate is high, as expected at the antinodes of a standing wave, but this process does not correspond to a change in the energy of the atom: this photon emission without a recoil is the equivalent of the Mossbauer effect in nuclear physics, and is frequently encountered in trapped ion physics (Lamb-Dicke effect). The energy change comes from the second term of (72) which involves jumps from a vibrational state n to a neighboring state $n \pm 1$. These jumps are much rarer than the previous ones, and they lead to an energy gain per unit time identical to the one found for a blue lattice [equation (69)].

To conclude, we recover with this simple analysis the result of Gordon & Ashkin (1980): the heating rate is indeed the same at the nodes and at the antinodes of a standing wave. However, the mechanisms leading

to this rate are very different. For a blue lattice and atoms located at the nodes, the photon scattering rate is very small but each photon emission is accompanied by an energy change $\hbar\omega$. For a red lattice and atoms localized at the antinodes, the spontaneous emission rate is much higher, but the average energy gained during a spontaneous emission process is much lower because most of the emissions are recoil-free.

Here, we limited ourselves to the case where the tunnelling effect between the different wells of the lattice is negligible. When this tunnelling becomes significant, the discrete vibrational levels n are replaced by energy bands and a significant difference between the blue and red lattices may appear. In addition, one should consider the decoherence associated to the spontaneous emission processes: each process localizes the atom with a resolution of λ. A wave packet initially extending over several sites will thus lose its coherence much faster in the case of a red lattice than in the case of a blue lattice, even if the heating rates $\mathrm{d}\bar{E}/\mathrm{d}t$ are similar. This difference is studied in detail by Gerbier & Dalibard (2010).

6 Appendix: the Gordon-Ashkin paradox

We start with the Hamiltonian of a two-level atom with a resonance frequency $\omega_{\mathrm{A}} = (E_e - E_g)/\hbar$, illuminated by a monochromatic laser field of frequency ω_{L}, the strength of the coupling being characterized by the (possibly complex) Rabi frequency $\Omega(x)$. In the framework of the rotating wave approximation, this Hamiltonian is written

$$\hat{H}_{\mathrm{AL}} = \frac{\hat{p}^2}{2m} - \hbar\Delta\hat{\mathcal{P}}_e + \frac{\hbar\Omega(\hat{x})}{2}\hat{\sigma}_+ + \frac{\hbar\Omega^*(\hat{x})}{2}\hat{\sigma}_- \tag{73}$$

where $\hat{\mathcal{P}}_\alpha$ denotes the projector on the state $|\alpha\rangle$ ($\alpha = |g\rangle, |e\rangle$), and where $\hat{\sigma}_\pm$ are defined in (3). In addition to the Hamiltonian dynamics described by $\hat{H}$, we take into account the irreversible evolution due to spontaneous emission phenomena, characterized by the natural width Γ of the excited state $|e\rangle$.

The reasoning of Gordon & Ashkin (1980) starts from the limit of an infinite mass m, so that the atom has zero velocity and remains stationary at position x. The momentum can however be non-zero, and we define the average force $f(x)$ as

$$f(x) = \langle \hat{F}(x) \rangle \tag{74}$$

and the diffusion coefficient in momentum space $D_p(x)$

$$D_p(x) = \int_0^\infty \left[\frac{1}{2}\langle \hat{F}(x,0)\hat{F}(x,t) + \hat{F}(x,t)\hat{F}(x,0)\rangle - \Big(\langle \hat{F}(x)\rangle\Big)^2 \right]. \tag{75}$$

We have introduced here the force operator:

$$\hat{F}(x) = -\frac{\mathrm{d}\hat{H}}{\mathrm{d}x} = -\frac{\mathrm{d}}{\mathrm{d}x}\left(\frac{\hbar\Omega(x)}{2}\right)\hat{\sigma}_+ + \text{c.c.} \tag{76}$$

The average values of (74-75) are calculated assuming steady state for the internal variables of the atom, taking into account the dissipation induced by the spontaneous emission phenomena. In the definition (75), the quantity $F(\hat{x}, t)$ represents the force operator in the Heisenberg representation.

The explicit calculation of the diffusion coefficient is rather technical, and requires the use of the quantum regression theorem. We will only give here the result of Gordon & Ashkin (1980), which we will derive in the next paragraph with a slightly easier method. Let us concentrate on the case of a standing wave

$$\Omega(x) = \Omega_0 \sin(kx), \quad \Omega_0 \text{ real positive}, \tag{77}$$

and on the limit of large detunings

$$\Omega_0 \ll |\Delta|. \tag{78}$$

The average force is the dipole force

$$f(x) = -\frac{\mathrm{d}V(x)}{\mathrm{d}x}, \quad V(x) = -\frac{\Omega_0^2}{4\Delta}\sin^2(kx). \tag{79}$$

As for the diffusion coefficient, it is expressed as[4]

$$D_p = \hbar^2 k^2 \Gamma \frac{\Omega_0^2}{8\Delta^2}. \tag{80}$$

[4]We have slightly adapted the result of Gordon & Ashkin (1980) to the case where the photons emitted spontaneously by the atom propagate along the x axis.

This diffusion coefficient is independent of the position x considered: no matter whether the atom is placed around a node of the standing wave ($x = 0$, mod π) or around an antinode ($x = \pi/2$, mod π), the momentum diffusion and thus the heating related to the spontaneous emission processes are the same!

We now switch to a quantum description of the center-of-mass motion and we follow the approach proposed by Gerbier & Dalibard (2010) to recover the result of Gordon & Ashkin (1980). We found in § 4 that, when the heating related to spontaneous emission processes can be neglected, the dynamics of the atom is described by the Hamiltonian

$$\hat{H} = \frac{\hat{p}^2}{2m} + V(\hat{x}), \quad V(x) = V_0 \, \sin^2(kx), \quad V_0 = \frac{\Omega_0^2}{4\Delta}. \tag{81}$$

We now calculate the time evolution of the average energy

$$\bar{E}(t) = \langle H \rangle_t = \mathrm{Tr}(\hat{H}\rho(t)), \tag{82}$$

where $\hat{\rho}(t)$ represents the density operator of the atom, acting in the space of both internal and external variables. In the absence of spontaneous emission phenomena, this mean value would be constant, but this is not the case if these phenomena are taken into account.

We start with the equation of motion for $\hat{\rho}$:

$$\frac{\mathrm{d}\hat{\rho}}{\mathrm{d}t} = \left.\frac{\mathrm{d}\hat{\rho}}{\mathrm{d}t}\right|_{\mathrm{sp.}} + \frac{1}{\mathrm{i}\hbar}[\hat{H}_{\mathrm{AL}}, \hat{\rho}], \tag{83}$$

where the first term of this *master equation* describes the evolution due to the spontaneous emission. From this we obtain

$$\frac{\mathrm{d}\bar{E}(t)}{\mathrm{d}t} = \mathrm{Tr}\left(\hat{H} \left.\frac{\mathrm{d}\hat{\rho}}{\mathrm{d}t}\right|_{\mathrm{sp.}}\right) + \frac{1}{\mathrm{i}\hbar}\langle[\hat{H}, \hat{H}_{\mathrm{AL}}]\rangle_t. \tag{84}$$

Evolution due to spontaneous emission. In (83) the evolution term related to spontaneous emission is written as

$$\begin{aligned} \left.\frac{\mathrm{d}\hat{\rho}}{\mathrm{d}t}\right|_{\mathrm{sp.}} &= -\frac{\Gamma}{2}\left(\hat{\mathcal{P}}_e\hat{\rho} + \hat{\rho}\hat{\mathcal{P}}_e\right) \\ &\quad +\Gamma\int \mathcal{N}(k')\hat{\sigma}_-\mathrm{e}^{\mathrm{i}k'\hat{x}}\hat{\rho}\,\mathrm{e}^{-\mathrm{i}k'\hat{x}}\hat{\sigma}_+ \,\mathrm{d}k'. \end{aligned} \tag{85}$$

The first line of this equation gives the decay of the matrix elements of $\hat{\rho}$ that involve the excited state:

$$\left.\frac{\mathrm{d}\hat{\rho}_{ee}}{\mathrm{d}t}\right|_{\mathrm{sp.}} = -\Gamma\hat{\rho}_{ee}, \quad \left.\frac{\hat{\rho}_{\mathrm{eg}}}{\mathrm{d}t}\right|_{\mathrm{sp.}} = -\frac{\Gamma}{2}\rho_{eg}, \quad \left.\frac{\mathrm{d}\hat{\rho}_{ge}}{\mathrm{d}t}\right|_{\mathrm{sp.}} = -\frac{\Gamma}{2}\hat{\rho}_{ge}, \tag{86}$$

and the second line describes the population growth of the ground state $\hat{\rho}_{gg}$ due to the decay of the excited state. Note that these matrix elements $\hat{\rho}_{\alpha\beta}$ (with $\alpha, \beta = e, g$) remain operators with respect to the external variables x and p describing the motion of the center-of-mass of the atom. The function $\mathcal{N}(k')$ describes the distribution of the projection on the x axis of the wave vector of the spontaneously emitted photon. Since we take here a 1D model, we assume that these photons propagate along the x axis, with an equal probability to be emitted in the positive and in the negative direction, which amounts to take

$$\mathcal{N}(k') = \frac{1}{2}\left[\delta(k - k') + \delta(k + k')\right]. \tag{87}$$

Let us now evaluate the contribution of the first term of (84). The Hamiltonian $\hat{H}$ which intervenes in this term has itself two contributions, $\hat{p}^2/2m$ and $V(\hat{x})$. Let us start with $\hat{p}^2/2m$ and write

$$\mathrm{Tr}\left(\frac{\hat{p}^2}{2m}\left.\frac{\mathrm{d}\hat{\rho}}{\mathrm{d}t}\right|_{\mathrm{sp.}}\right) = \int \frac{p^2}{2m}\left(\langle p|\left.\frac{\mathrm{d}\hat{\rho}_{ee}}{\mathrm{d}t}\right|_{\mathrm{sp.}}|p\rangle + \langle p|\left.\frac{\mathrm{d}\hat{\rho}_{gg}}{\mathrm{d}t}\right|_{\mathrm{sp.}}|p\rangle\right)\mathrm{d}p. \tag{88}$$

We use (85- 87) and obtain

$$\langle p|\left.\frac{\mathrm{d}\hat{\rho}_{gg}}{\mathrm{d}t}\right|_{\mathrm{sp.}}|p\rangle = \frac{\Gamma}{2}\left(\langle p + \hbar k|\hat{\rho}_{ee}|p + \hbar k\rangle + \langle p - \hbar k|\hat{\rho}_{ee}|p - \hbar k\rangle\right). \tag{89}$$

By transferring this result into (88), we get to

$$\begin{aligned} \mathrm{Tr}\left(\frac{\hat{p}^2}{2m}\left.\frac{\mathrm{d}\hat{\rho}}{\mathrm{d}t}\right|_{\mathrm{sp.}}\right) &= -\frac{\Gamma}{2m}\int p^2\langle p|\hat{\rho}_{ee}|p\rangle\mathrm{d}p \\ &\quad +\frac{\Gamma}{4m}\int\left[(p + \hbar k)^2 + (p - \hbar k)^2\right]\langle p|\rho_{ee}|p\rangle\,\mathrm{d}p \\ &= \Gamma\Pi_e\,\frac{\hbar^2k^2}{2m}, \end{aligned} \tag{90}$$

where Π_e represents the total population of the excited state:

$$\Pi_e = \int \langle p|\hat{\rho}_{ee}|p\rangle \, \mathrm{d}p. \tag{91}$$

One can check with a similar calculation that the contribution of $V(x)$ (via $\hat{H}$) to the first term of (84) is null. We thus arrive at

$$\mathrm{Tr}\left(\hat{H}\left.\frac{\mathrm{d}\hat{\rho}}{\mathrm{d}t}\right|_{\mathrm{sp.}}\right) = \Gamma\Pi_e E_{\mathrm{r}}, \tag{92}$$

an expression that can easily be interpreted: $\Gamma\Pi_e$ corresponds to the photon scattering rate by the atom. Each spontaneously emitted photon gives a random kick of $\pm\hbar k$ to the atom, thus an average energy increase $E_{\mathrm{r}} = \hbar^2k^2/2m$. At order two in Rabi frequency, the value of Π_e is [*cf.* (40)]

$$\Pi_e \approx \frac{\langle\Omega^*(\hat{x})\Omega(\hat{x})\rangle}{4\Delta^2}, \tag{93}$$

which gives for the standing wave

$$\mathrm{Tr}\left(\hat{H}\left.\frac{\mathrm{d}\hat{\rho}}{\mathrm{d}t}\right|_{\mathrm{sp.}}\right) = \Gamma E_{\mathrm{r}}\frac{\Omega_0^2}{4\Delta^2}\,\langle\sin^2(kx)\rangle. \tag{94}$$

For an atom located at the vicinity of a node of the standing wave, $\sin^2(kx)$ goes to 0, the photon scattering rate also goes to 0, as does the corresponding energy increase.

Second term of (84). The commutator $[\hat{H}, \hat{H}_{\mathrm{AL}}]$ is easily calculated:

$$\begin{aligned}\frac{1}{\mathrm{i}\hbar}[\hat{H}, \hat{H}_{\mathrm{AL}}] = \; &- \; \frac{\hbar k\Omega_0}{4m}\left(\hat{\sigma}_+ + \hat{\sigma}_-\right)\left(\hat{p}\cos(k\hat{x}) + \cos(k\hat{x})\hat{p}\right)\\ &+ \; \frac{\hbar k\Omega_0^2}{8m\Delta}\left(\hat{p}\sin(2k\hat{x}) + \sin(2k\hat{x})\hat{p}\right).\end{aligned} \tag{95}$$

We are looking for a result at order 2 in Ω_0/Δ. We then start by evaluating the matrix elements of $\hat{\sigma}_\pm\hat{\rho}$ at the desired order to get the average value of the first row of (95). The master equation (83) gives

$$\frac{\mathrm{d}\hat{\rho}_{eg}}{\mathrm{d}t} \approx \left(\mathrm{i}\Delta - \frac{\Gamma}{2}\right)\hat{\rho}_{eg} - \mathrm{i}\frac{\Omega(\hat{x})}{2}\hat{\rho}_{gg}, \tag{96}$$

where we have neglected the contribution of $\hat{\rho}_{ee}$. In the (realistic) hypothesis where the characteristic time of evolution of the external variables is long compared to Γ^{-1}, we can consider that the internal dynamics of the atom follows adiabatically the external dynamics and solve (10) as[5]

$$\hat{\rho}_{eg} = \frac{\Omega(\hat{x})}{2\Delta + \mathrm{i}\Gamma}\hat{\rho}_{gg}, \quad \text{and similarly } \hat{\rho}_{ge} = \hat{\rho}_{gg}\frac{\Omega^*(\hat{x})}{2\Delta - \mathrm{i}\Gamma}. \tag{99}$$

To evaluate the first line of (95), we start by taking the trace on the internal variables. At the desired order in Ω_0/Δ, we find:

$$\begin{aligned}\mathrm{Tr}_{\mathrm{int}}\left[(\hat{\sigma}_+ + \hat{\sigma}_-)\hat{\rho}\right] = \; &\frac{\Omega_0}{2\Delta}\left[\sin(k\hat{x})\hat{\rho}_{gg} + \hat{\rho}_{gg}\sin(k\hat{x})\right]\\ + \; &\mathrm{i}\,\frac{\Gamma\Omega_0}{4\,\Delta^2}\left[\hat{\rho}_{gg}\sin(k\hat{x}) - \sin(k\hat{x})\hat{\rho}_{gg}\right].\end{aligned} \tag{100}$$

Let us finally transfer this result into the trace of (95). We see that the contribution of the second line of (95) exactly cancels the one coming from the first line of (100). Finally, there remains only the contribution coming from the second line of (100) which after a simple calculation gives

$$\frac{1}{\mathrm{i}\hbar}\langle[\hat{H}, \hat{H}_{\mathrm{AL}}]\rangle_t = \Gamma E_{\mathrm{r}}\frac{\Omega_0^2}{4\Delta^2}\langle\cos^2(kx)\rangle. \tag{101}$$

This term is all the more important as the atom is located at the vicinity of the nodes of the standing wave.

In total, when we sum the two contributions (94) and (101), we get the result

$$\frac{\mathrm{d}\bar{E}}{\mathrm{d}t} = \Gamma E_{\mathrm{r}}\frac{\Omega_0^2}{4\Delta^2}, \tag{102}$$

which is independent of the spatial state of the atom in the standing wave and also independent of the sign of the detuning of this wave: this is the result initially found by Gordon & Ashkin (1980).

[5] We can then push the calculation one step further to obtain the expression of $\hat{\rho}_{ee}$ at the lowest order. Starting from

$$\frac{\mathrm{d}\hat{\rho}_{ee}}{\mathrm{d}t} = -\Gamma\hat{\rho}_{ee} + \frac{\mathrm{i}}{2}\hat{\rho}_{eg}\Omega^*(\hat{x}) - \frac{\mathrm{i}}{2}\Omega(\hat{x})\hat{\rho}_{ge}, \tag{97}$$

and using (99), we obtain the "steady-state" value for the internal variables

$$\hat{\rho}_{ee} = \frac{1}{4\Delta^2}\Omega(\hat{x})\,\hat{\rho}_{gg}\,\Omega^*(\hat{x}), \tag{98}$$

which allows in particular to recover (93).

Chapter II

The basics of optical lattices

The goal of this chapter is to present the basic concepts of optical lattice physics. We start by recalling Bloch's theorem, which is the central tool to address the motion of individual particles in a periodic potential $V(\boldsymbol{r})$. We explain how the fundamental concepts of Bloch functions and energy bands emerge, and present a series of explicit results for these functions and bands in the case of a 1D sinusoidal lattice, $V(x) = V_0 \sin^2(kx)$. We then focus on the quantities one can access by ramping up and down the potential $V(\boldsymbol{r})$, an operation which is impossible in a real crystal, but easy with optical lattices. We end this chapter with a first approach to the propagation of wave packets in the lattice, and the notion of effective mass and group velocity.

1 How to generate an optical lattice

1-1 One-dimensional lattices

In its simplest version, an optical lattice consists of a one-dimensional standing light wave along an axis x (Figure 1). This wave is formed by two propagating waves of the same amplitude $\mathcal{E}_0$ travelling in opposite directions (we neglect here the influence of polarization):

$$\mathcal{E}_0 \sin(kx - \omega t + \phi_1), \qquad \mathcal{E}_0 \sin(kx + \omega t - \phi_2). \tag{1}$$

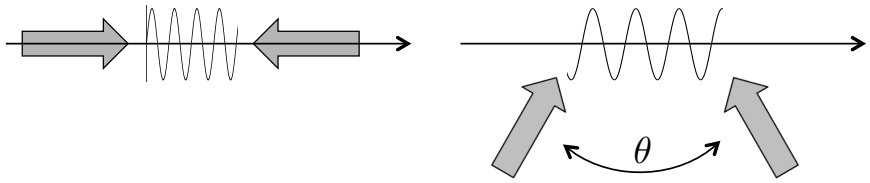

Figure 1. *1D optical lattice formed by a standing laser wave. Left: period $\lambda/2$; right: period $\lambda/[2\sin(\theta/2)]$.*

The resulting field is written as $\mathcal{E}(x,t) = \mathcal{E}(x)\,\cos(\omega t - \varphi)$ with $\varphi = (\phi_1 + \phi_2)/2$ and

$$\mathcal{E}(x) = 2\mathcal{E}_0 \sin(kx - \Phi), \qquad \Phi = (\phi_2 - \phi_1)/2. \tag{2}$$

In this chapter, we will choose the origin of coordinates $x = 0$ such that $\Phi = 0$, which corresponds to choosing this origin at a node of the standing wave. The atoms therefore sit in the periodic potential

$$V(x) = V_0 \sin^2(kx), \qquad V_0 = \frac{d_0^2 \mathcal{E}_0^2}{\hbar \tilde{\Delta}}, \tag{3}$$

where the sign of V_0 can be adjusted by changing the detuning of the laser with respect to the resonant transition of the atom.

If the standing wave is obtained by superimposing two plane waves of light that have opposite directions, k is equal to the wave vector of the

light k_L and the spatial period of the lattice is $a = \lambda/2 = \pi/k_\mathrm{L}$, where $\lambda = 2\pi/k_\mathrm{L}$ is the wavelength of the light. If the waves each have an angle $\theta/2$ with respect to the perpendicular to the x axis, $k = k_\mathrm{L}\sin(\theta/2)$, the spatial period is then increased: $a = \lambda/[2\sin(\theta/2)]$. We will see later that we can also choose in (1) a time-depending relative phase $\Phi = \phi_2 - \phi_1$, which allows to displace the periodic potential in the reference frame of the laboratory with the speed $\dot{\Phi}/(2k)$.

1-2 Multi-dimensional lattices

To create a periodic potential in several directions in space, the easiest and most robust technique is to overlap standing waves of different frequencies in the desired directions. For example, to make a square array in the xy plane, we can overlap

$$\mathcal{E}(\boldsymbol{r}) = 2\mathcal{E}_1\sin(k_1 x)\cos(\omega_1 t - \varphi_1) + 2\mathcal{E}_2\sin(k_2 y)\cos(\omega_2 t - \varphi_2). \qquad (4)$$

If the frequency difference $\omega_1 - \omega_2$ between the waves is large compared to the other frequencies involved in the motion of the center of mass of the atom, we can neglect the interference between these two standing waves and consider that the dipole potential

$$V(\boldsymbol{r}) = V_1\sin^2(k_1 x) + V_2\sin^2(k_2 y) \qquad (5)$$

acts on the atom. In practice, it is enough to take $(\omega_1 - \omega_2)/2\pi$ on the order of a few MHz (i.e. a relative difference of 10^{-8}) for this approximation to be valid.

We can also choose the same frequency for all the waves. In this case, if we want to use the superposition of two standing waves in the xy plane as in (4), we must control the relative phase $\varphi_1 - \varphi_2$ of these waves (Hemmerich & Hänsch 1993). This phase control can be used to vary the lattice topology, as we will see later for the detection of Dirac points in a hexagonal lattice (Tarruell, Greif, et al. 2012).

Note that there is an important exception to this requirement of a phase control: Grynberg, Lounis, et al. (1993) showed that if we restrict the number of beams to its minimum value (2 beams for a 1D lattice, 3 beams in 2D, 4 beams in 3D), then the interference pattern giving rise to the potential $V(\boldsymbol{r})$ is independent of the phases of the beams. A variation of these phases only translates the interference pattern, without changing its shape[1]. One can refer to the review article of Grynberg & Robilliard (2001) to have a complete panorama of the lattice forms that are accessible in the monochromatic case. Let us also mention that, in this case, one can go beyond the framework of periodic lattices and build quasi-periodic potentials analogous to those which appear in quasi-crystals (Guidoni, Triché, et al. 1997).

1-3 Back to 1D: Mathieu's equation

The study of the quantum motion of an atom of mass m in the periodic potential of the lattice requires the search for the eigenstates $|\psi\rangle$ (or $\psi(x) = \langle x|\psi\rangle$) of the Hamiltonian

$$\hat{H} = \frac{\hat{p}^2}{2m} + V_0\sin^2(k\hat{x}). \qquad (6)$$

The wave number k provides a natural energy scale, which we will call the *recoil energy*

$$E_\mathrm{r} = \frac{\hbar^2 k^2}{2m}, \qquad (7)$$

which allows to write the eigenvalue equation $\hat{H}\psi = E\,\psi$ in a dimensionless form

$$-\psi''(\tilde{x}) + \frac{\tilde{V}_0}{2}\left[1 - \cos(2\tilde{x})\right]\psi(\tilde{x}) = \tilde{E}\,\psi(\tilde{x}), \qquad (8)$$

where we have set $\tilde{x} = kx$, $\tilde{V}_0 = V_0/E_\mathrm{r}$ and $\tilde{E} = E/E_\mathrm{r}$. Note that the name *recoil energy* for E_r is a bit improper; the recoil energy (7) is usually defined as a characteristic quantity of the atom, where k is the wave number associated to the resonant transition. Here, the laser may have a different wave number k_L than the resonant value, and the wave number of the lattice may additionally differ from the wave number of the laser if one chooses a configuration with a $\theta \neq \pi$ angle.

Equation (8) is called *Mathieu's equation*[2] and is found in many physical problems, such as the motion of a classical particle driven by an oscillating force ($\tilde{x}$ is then the time variable), for example a Paul trap for charged

[1] This result is clearly seen in 1D on the expression (2).

[2] Émile Léonard Mathieu (1835-1890), a French mathematician, wrote this equation in 1865 while studying the vibrations of an elliptical membrane

particles. For a given initial condition in $\tilde{x} = 0$ and according to the value of the pair $(\tilde{V}_0, \tilde{E})$, the solutions remain bounded or on the contrary diverge in $\tilde{x} = \pm\infty$. In the case of a particle in a Paul trap, the bounded and divergent solutions correspond respectively to the stability and instability zones of the trap. For the quantum motion of an atom in an optical lattice, these solutions correspond to an energy E located in an "allowed" or "forbidden" (gap) zone.

Since the existence of these allowed or forbidden zones is not restricted to the case of a sinusoidal potential, but appears for any periodic potential, we will momentarily leave Mathieu's equation to address the general problem of the motion of a particle in a spatially periodic potential. However, we will later use some specific results related to this Mathieu equation, such as the asymptotic value of the bandwidths in the limit $V_0 \gg E_\mathrm{r}$.

2 Bloch's theorem

In the following, we consider the motion of a point-like, spinless particle in a periodic potential $V(\boldsymbol{r})$ without any other force (in particular no magnetic field). More precisely, we suppose that this potential is invariant when we make the substitution $\boldsymbol{r} \to \boldsymbol{r} + \boldsymbol{r}_j$, where $\boldsymbol{r}_j$ is one of the nodes of the lattice

$$\mathcal{B} = \{\boldsymbol{r}_j = j_1\boldsymbol{a}_1 + j_2\boldsymbol{a}_2 + j_3\boldsymbol{a}_3,\ j_1,\ j_2,\ j_3 \in \mathbb{Z}\}. \tag{9}$$

Such a lattice, which is stable under addition and subtraction, is called *a Bravais lattice*. We have written here the 3D version of the lattice, the vectors $\boldsymbol{a}_i$ being independent. In one dimension, we will use the simpler notation for the spatial period $a_1 \equiv a$. We are interested in finding the eigenstates of the Hamiltonian

$$\hat{H} = \frac{\hat{\boldsymbol{p}}^2}{2m} + V(\hat{\boldsymbol{r}}) \tag{10}$$

that describes the motion of the particle. Bloch's theorem[3] takes advantage of the discrete translation symmetry of the problem to search for a basis of eigenfunctions in a particularly convenient form.

[3] Felix Bloch proved this theorem while studying the motion of an electron in a periodic potential (Bloch 1929). The same mathematical result had been previously obtained in other contexts, including by Floquet (1883).

2-1 Statement of the theorem

Let us start with the following two points:

- the translation operators $\hat{T}_{\boldsymbol{a}}$ defined by
$$\hat{T}_{\boldsymbol{a}}\,\psi(\boldsymbol{r}) = \psi(\boldsymbol{r} - \boldsymbol{a}) \quad \text{i.e.} \quad \hat{T}_{\boldsymbol{a}} = \mathrm{e}^{-\mathrm{i}\boldsymbol{a}\cdot\hat{\boldsymbol{p}}/\hbar}\,, \tag{11}$$
commute one with the other,
- the translational symmetry of $V(\boldsymbol{r})$ entails that the translation operators $\hat{T}_{\boldsymbol{a}_i}$ commute with the Hamiltonian.

We can therefore look for a basis of eigenfunctions common to $\hat{H}$ and the $\hat{T}_{\boldsymbol{a}_i}$ operators. Now the diagonalization of an operator $\hat{T}_{\boldsymbol{a}}$ is easy; in particular, since $\hat{T}_{\boldsymbol{a}}$ is a unitary operator ($\hat{T}_{\boldsymbol{a}}^{-1} = \hat{T}_{-\boldsymbol{a}} = \hat{T}_{\boldsymbol{a}}^\dagger$), its eigenvalues λ are complex numbers of modulus 1 which can always be written under the form $\lambda = \mathrm{e}^{-\mathrm{i}\theta}$.

Let us now consider an eigenfunction $\psi_{\theta_1,\theta_2,\theta_3}$ of the Hamiltonian $\hat{H}$ and of each of the translation operators $\hat{T}_{\boldsymbol{a}_j}$, with the eigenvalue $\mathrm{e}^{-\mathrm{i}\theta_j}$ for $\hat{T}_{a_j}$. To express the triplet θ_j in a compact way, it is convenient to introduce the reciprocal lattice (another Bravais lattice) defined by:

$$\mathcal{B}' = \{\boldsymbol{Q}_{\boldsymbol{j}} = j_1\boldsymbol{b}_1 + j_2\boldsymbol{b}_2 + j_3\boldsymbol{b}_3,\ j_1,\ j_2,\ j_3 \in \mathbb{Z}\} \tag{12}$$

where the vectors $\boldsymbol{b}_i$ are defined by the identity[4]

$$\boldsymbol{a}_{i'} \cdot \boldsymbol{b}_i = 2\pi\,\delta_{i,i'}. \tag{13}$$

Let us now pose

$$\boldsymbol{q} = \frac{1}{2\pi}\sum_{j=1,2,3}\theta_j\boldsymbol{b}_j, \tag{14}$$

which leads to $\boldsymbol{a}_i \cdot \boldsymbol{q} = \theta_i$. The eigenfunction $\psi_{\theta_1,\theta_2,\theta_3}$, which can be noted in a more compact way $\psi_{\boldsymbol{q}}$, thus verifies

$$\psi_{\boldsymbol{q}}(\boldsymbol{r} - \boldsymbol{a}_j) = \mathrm{e}^{-\mathrm{i}\boldsymbol{a}_j\cdot\boldsymbol{q}}\psi_{\boldsymbol{q}}(\boldsymbol{r}), \quad j = 1, 2, 3\,. \tag{15}$$

[4] We have explicitly
$$\boldsymbol{b}_1 = 2\pi\frac{\boldsymbol{a}_2 \times \boldsymbol{a}_3}{\boldsymbol{a}_1 \cdot (\boldsymbol{a}_2 \times \boldsymbol{a}_3)}$$
and the two other relations are deduced by circular permutations of the indices.

Let us finally set

$$\psi_{\boldsymbol{q}}(\boldsymbol{r}) = \mathrm{e}^{\mathrm{i}\boldsymbol{r}\cdot\boldsymbol{q}}\, u_{\boldsymbol{q}}(\boldsymbol{r}). \tag{16}$$

By using this relation in (15), it is immediate to check that the function $u_{\boldsymbol{q}}(\boldsymbol{r})$ is periodic on the Bravais lattice $\mathcal{B}$:

$$u_{\boldsymbol{q}}(\boldsymbol{r}-\boldsymbol{a}_j) = u_{\boldsymbol{q}}(\boldsymbol{r}), \quad j=1,2,3. \tag{17}$$

Bloch's theorem can be stated as follows (Ashcroft & Mermin 1976; Kittel 1987): the eigenstates of a Hamiltonian corresponding to a spatially periodic potential $V(\boldsymbol{r})$ on the lattice $\mathcal{B}$ can be searched under the form of Bloch waves $\psi_{\boldsymbol{q}}(\boldsymbol{r})$, which are products of a plane wave [$\mathrm{e}^{\mathrm{i}\boldsymbol{r}\cdot\boldsymbol{q}}$] with a periodic function on $\mathcal{B}$ [$u_{\boldsymbol{q}}(\boldsymbol{r})$].

In all that follows, we will assume the periodic potential $V(\boldsymbol{r})$ to be sufficiently regular so that the function $u_{\boldsymbol{q}}(\boldsymbol{r})$ can be expanded in Fourier series. We will thus choose in 1D:

$$u_q(x) = \sum_{j\in\mathbb{Z}} C_j(q)\, \mathrm{e}^{2\mathrm{i}\pi j x/a}, \tag{18}$$

$$\text{that is} \quad \psi_q(x) = \sum_{j\in\mathbb{Z}} C_j(q)\, \mathrm{e}^{\mathrm{i}x(q+2\pi j/a)}. \tag{19}$$

The form (19) shows that Bloch waves are combs of plane waves with momenta $p=\hbar(q+2\pi j/a)$, with j integer.

Note that in the following, we will apply on the variable $\boldsymbol{q}$ all the usual operations for continuous variables: derivation (or gradient) with respect to q, integration over q, etc. Writing this variable $\boldsymbol{q}$ as a subscript of $\psi_{\boldsymbol{q}}(\boldsymbol{r})$ or $u_{\boldsymbol{q}}(\boldsymbol{r})$ is a usual convention, but one could also have written these functions as $\psi(\boldsymbol{r},\boldsymbol{q})$ or $u(\boldsymbol{r},\boldsymbol{q})$.

Also note that the angles θ_j characterizing the eigenvalues $\mathrm{e}^{-\mathrm{i}\theta_j}$ of the translation operators $\hat{T}_{a_j}$ are defined modulo 2π. When we write the arbitrariness of this phase in the definition (14), we see that the quasi-momentum $\boldsymbol{q}$ and the quasi-momentum $\boldsymbol{q}+\boldsymbol{Q}$, where $\boldsymbol{Q}$ is a vector of the reciprocal lattice $\mathcal{B}'$, lead to the same triplet of eigenvalues for $\hat{T}_{\boldsymbol{a}_j}$; we obtain in this case the same eigenvalue equation for the Hamiltonian $\hat{H}$ and the periodic part $u_{\boldsymbol{q}}$. In order to get rid of this phase arbitrariness, we will set in all the following

$$\psi_{\boldsymbol{q}+\boldsymbol{Q}}(\boldsymbol{r}) = \psi_{\boldsymbol{q}}(\boldsymbol{r}), \quad \boldsymbol{Q}\in\mathcal{B}'. \tag{20}$$

2-2 Searching for the eigenstates and the energy bands

In this paragraph, we stay in one dimension to simplify the notations. The explicit search for the eigenstates ψ_q of $\hat{H}$ is done by injecting (16) into the eigenvalue equation in order to derive an equation for the periodic part u_q of the Bloch function:

$$\hat{H}_{\mathrm{per}}(q) u_q(x) = E(q)\, u_q(x) \tag{21}$$

where $\hat{H}_{\mathrm{per}}(q)$ is a Hamiltonian that depends on the parameter q.

$$\hat{H}_{\mathrm{per}}(q) = \frac{(\hat{p}+\hbar q)^2}{2m} + V(\hat{x}). \tag{22}$$

The function $u_q(x)$ satisfies the boundary conditions

$$u_q(0) = u_q(a), \quad u_q'(0) = u_q'(a). \tag{23}$$

For a given value of q, the solutions of (21-23) can be identified by an index $n=0,1,2,\ldots$, the eigenvalues $E_n(q)$ being ordered by increasing values. To the energy $E_n(q)$ corresponds the solution $u_{n,q}(x)$, associated to the Bloch wave $\psi_{n,q}(x)$:

$$\hat{H}\psi_{n,q}(x) = E_n(q)\ \psi_{n,q}(x), \quad \psi_{n,q}(x) = \mathrm{e}^{\mathrm{i}qx} u_{n,q}(x). \tag{24}$$

We have already mentioned in (20) the invariance of the definition of the eigenfunctions $\psi_{n,q}(x)$ in the substitution $q \to q+2\pi/a$. The same is true for the eigenvalues[5]

$$E_n(q+2\pi/a) = E_n(q)\ . \tag{26}$$

Thanks to the spectral theorem, we know that we can form a basis with the eigenstates of the Hamiltonian. To choose this basis, it is important not to double count eigenstates, i.e. to take each eigenfunction once and only

[5] We also deduce from (16-20) that

$$u_{q+2\pi/a}(x) = \mathrm{e}^{-2\pi x/a} u_q(x), \tag{25}$$

which amounts to taking $C_j(q+2\pi/a) = C_{j+1}(q)$ in the expansion (18). The relation (25) plays an important role in the study of the topology of energy bands associated to a given potential (Zak 1989).

once. Thanks to the relation (20), we see that we have to restrict the domain of q to an interval of length $2\pi/a$, choosing for example the

$$\text{1st Brillouin zone :} \quad -\pi/a < q \leq \pi/a. \tag{27}$$

Note that it is often useful to treat q as a variable that can take any value between $-\infty$ and $+\infty$. There is no problem with this, as long as one remembers the periodicity of the states and their associated energies (20-26).

When q varies continuously in an interval of length $2\pi/a$, for example (27), each energy $E_n(q)$ obviously takes a value contained in the interval $I_n = [\min_q E_n(q), \max_q E_n(q)]$, which is called the *allowed energy band*. For the basic 1D lattice that we will consider most of the time, $V(x) = V_0 \sin^2(kx)$, $V_0 \neq 0$, the intervals I_n are disjoint [$\max_q E_n(q) < \min_q E_{n+1}(q)$].

In the multi-dimensional case, determining the Brillouin zone is not always as simple as in one dimension. We will see an example for the hexagonal lattice of graphene later. For the square or cubic lattices that we will consider in the meantime, the first Brillouin zone is immediately deduced from (27):

$$\text{1st Brillouin zone:} \quad \boldsymbol{q} = (q_1, q_2, q_3) \quad \text{with} - \pi/a_j < q_j \leq \pi/a_j. \tag{28}$$

2-3 Role of the symmetries of the Hamiltonian

Time reversal symmetry. For a spinless particle, the time-reversal transformation is described by the anti-unitary operator $\hat{K}_0$ defined by (Messiah 2003)

$$\hat{K}_0 \psi(\boldsymbol{r}) = \psi^*(\boldsymbol{r}). \tag{29}$$

This operator leaves $\boldsymbol{r}$ invariant and changes $\boldsymbol{p}$ to $-\boldsymbol{p}$. The Hamiltonian we consider here is quadratic in $\boldsymbol{p}$, since there is no magnetic field and therefore no linear term for the momentum of type $-\boldsymbol{p} \cdot \boldsymbol{A}$. This Hamiltonian is time-reversal invariant and commutes with $\hat{K}_0$.

This means that if $\psi_{\boldsymbol{q}}(\boldsymbol{r}) = \mathrm{e}^{\mathrm{i}\boldsymbol{r}\cdot\boldsymbol{q}}\, u_{\boldsymbol{q}}(\boldsymbol{r})$ is an eigenstate of $\hat{H}$ with eigenvalue E, then $\hat{K}_0 \psi_{\boldsymbol{q}}(x) = \mathrm{e}^{-\mathrm{i}\boldsymbol{r}\cdot\boldsymbol{q}}\, u^*_{\boldsymbol{q}}(\boldsymbol{r})$ is also an eigenstate of $\hat{H}$ with the same eigenvalue E. Now the function $\mathrm{e}^{-\mathrm{i}\boldsymbol{r}\cdot\boldsymbol{q}}\, u^*_{\boldsymbol{q}}(\boldsymbol{r})$ verifies all the properties of a Bloch function associated to the quasi-momentum $-\boldsymbol{q}$. We deduce that if we know how to solve the eigenvalue problem for the Hamiltonian for a quasi-momentum $\boldsymbol{q}$, we also know the solutions for the quasi-momentum $-\boldsymbol{q}$ by posing:

$$\psi_{-\boldsymbol{q}}(\boldsymbol{r}) \propto \psi^*_{\boldsymbol{q}}(\boldsymbol{r}), \qquad E(\boldsymbol{q}) = E(-\boldsymbol{q}). \tag{30}$$

Even in one dimension, each energy eigenvalue is therefore (at least) doubly degenerate, since the functions $\psi_{n,q}$ and $\psi_{n,-q}$ are independent. This result generalizes the one for the free particle, where $\mathrm{e}^{\mathrm{i}px/\hbar}$ and $\mathrm{e}^{-\mathrm{i}px/\hbar}$ are two eigenstates associated to the same energy $E_p = p^2/2m$. There are two exceptions to this double degeneracy[6], the cases $q = 0$ and $q = \pi/a$, for which $\psi_{n,q}$ and $\psi_{n,-q}$ are identical [*cf.* (20)].

Parity of the potential $V(\boldsymbol{r})$. For a spinless particle, the (Hermitian) parity operator $\hat{P}$ is defined by

$$\hat{P}\psi(\boldsymbol{r}) = \psi(-\boldsymbol{r}). \tag{31}$$

If $V(\boldsymbol{r})$ is symmetric about $\boldsymbol{r} = 0$, then the Hamiltonian commutes with $\hat{P}$. We deduce that if $\psi_{\boldsymbol{q}}(\boldsymbol{r})$ is an eigenstate of $\hat{H}$ with eigenvalue $E(\boldsymbol{q})$, then $\hat{P}\psi_{\boldsymbol{q}}(\boldsymbol{r})$ is also an eigenstate of $\hat{H}$ with the same eigenvalue. But $\hat{P}\psi_{\boldsymbol{q}}(\boldsymbol{r}) = \mathrm{e}^{-\mathrm{i}\boldsymbol{r}\cdot\boldsymbol{q}} u_{\boldsymbol{q}}(-\boldsymbol{r})$ verifies all the properties of a Bloch function associated to the quasi-momentum $-\boldsymbol{q}$. If we have been able to solve the eigenvalue problem for the Hamiltonian for the quasi-momentum $-\boldsymbol{q}$, we can deduce the solution for the quasi-momentum $-\boldsymbol{q}$:

$$\psi_{-\boldsymbol{q}}(-\boldsymbol{r}) \propto \psi_{-\boldsymbol{q}}(-\boldsymbol{r}), \qquad E(-\boldsymbol{q}) = E(\boldsymbol{q}),\ . \tag{32}$$

The equality between $E(\boldsymbol{q})$ and $E(-\boldsymbol{q})$ had already been obtained from the time-reversal invariance in (30), without assuming the parity of the potential. On the other hand, the relation between $\psi_{-\boldsymbol{q}}(\boldsymbol{r})$ and $\psi_{\boldsymbol{q}}(-\boldsymbol{r})$, valid only for an even potential, enriches the result (30).

[6] In the particular case $V = 0$, there is still a degeneracy for $q = \pi/a$, because two consecutive bands touch each other at this point (see § 3-1).

3 Energy bands for a sinusoidal potential

Let us now return to the 1D case of the potential $V(x) = V_0 \sin^2(kx)$, for which the eigenvalue equation is the Mathieu equation (8). We first consider the case $V_0 = 0$ for which we know the eigenstates, $\phi_p(x) = \mathrm{e}^{\mathrm{i}px/\hbar}$ and the associated energies $E_p = p^2/2m$. The use of Bloch's theorem to treat this problem is obviously a complicated way to address an already-known case, but it has the merit to give explicitly the energies $E_n(q)$ and the associated functions $u_{n,q}(x)$. The result will then be used as a guide to treat the case of non-zero potentials.

3-1 The case of zero potential, $V_0 = 0$

For the zero potential, any period a will do. Let us take $a = \pi/k$ to make the link with the case where $V_0 \neq 0$. A "plane wave" state $\phi_p(x) = \mathrm{e}^{\mathrm{i}px/\hbar}$ can be written as a Bloch wave

$$\phi_p(x) = \mathrm{e}^{\mathrm{i}qx}\mathrm{e}^{2\mathrm{i}jkx} \quad \text{with} \quad \frac{p}{\hbar} = 2jk + q, \tag{33}$$

where j is the closest integer to $p/(2\hbar k)$, and where q belongs to the first Brillouin zone $(-k, k]$. We have for the lowest band $n = 0$:

$$E_0(q) = \frac{\hbar^2 q^2}{2m}, \quad u_{0,q}(x) = 1, \tag{34}$$

and for the first excited band $n = 1$:

$$E_1(q) = \frac{\hbar^2}{2m}(q \pm 2k)^2, \quad u_{1,q}(x) = \mathrm{e}^{\pm 2\mathrm{i}kx}, \tag{35}$$

with sign $-$ (resp. $+$) when $q \geq 0$ (resp. < 0). In this very peculiar case, the functions $u_{n,q}(x)$ are thus independent of q, except for the change of sign of the exponent in (35) at $q = 0$. The plot of the functions $E_n(q)$ as a function of q is given in figure 2; it simply gives back the parabola $E(p) = p^2/2m$ folded on itself since the abscissa q, linearly related to p by (33), must remain in the first Brillouin zone.

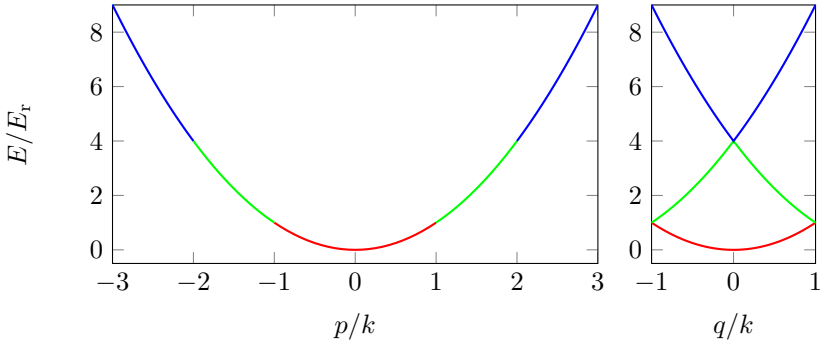

Figure 2. *Left: the dispersion relation for a free particle $E = p^2/2m$. Right: the folded parabola, giving the energy bands for the same free particle in the Bloch wave formalism.*

3-2 The central equation

We now consider the potential $V(x) = V_0 \sin^2(kx)$, with $V_0 > 0$. This potential has a period $a = \pi/k$ and we look for the eigenfunctions (Bloch waves) under the form [cf. (16)-(18)]

$$\psi_q(x) = \sum_{j\in\mathbb{Z}} C_j(q)\, \mathrm{e}^{\mathrm{i}(2jk+q)x}, \quad -k < q \leq k. \tag{36}$$

It amounts to the eigenvalue equation for a real symmetric tri-diagonal (and infinite) matrix, often called *central equation*:

$$\left[\left(2j + \frac{q}{k}\right)^2 + \frac{V_0}{2E_\mathrm{r}}\right] C_j - \frac{V_0}{4E_\mathrm{r}}(C_{j-1} + C_{j+1}) = \frac{E}{E_\mathrm{r}} C_j, \tag{37}$$

which can be solved numerically with standard algorithms for a given pair $(q/k, V_0/E_\mathrm{r})$. In practice, in order to determine for example the width of the lowest band with a relative precision of 10^{-6}, one can limit the sum (36) to $|j| \leq 20$ if the amplitude of the potential does not itself exceed $V_0/E_\mathrm{r} = 50$. The coefficients C_j are represented on figure 3 for three values of V_0 and for the lowest energy bands. We see that these coefficients take significant values only for relatively small values of j, which justifies the truncation of the system (37) at $|j| \leq 20$.

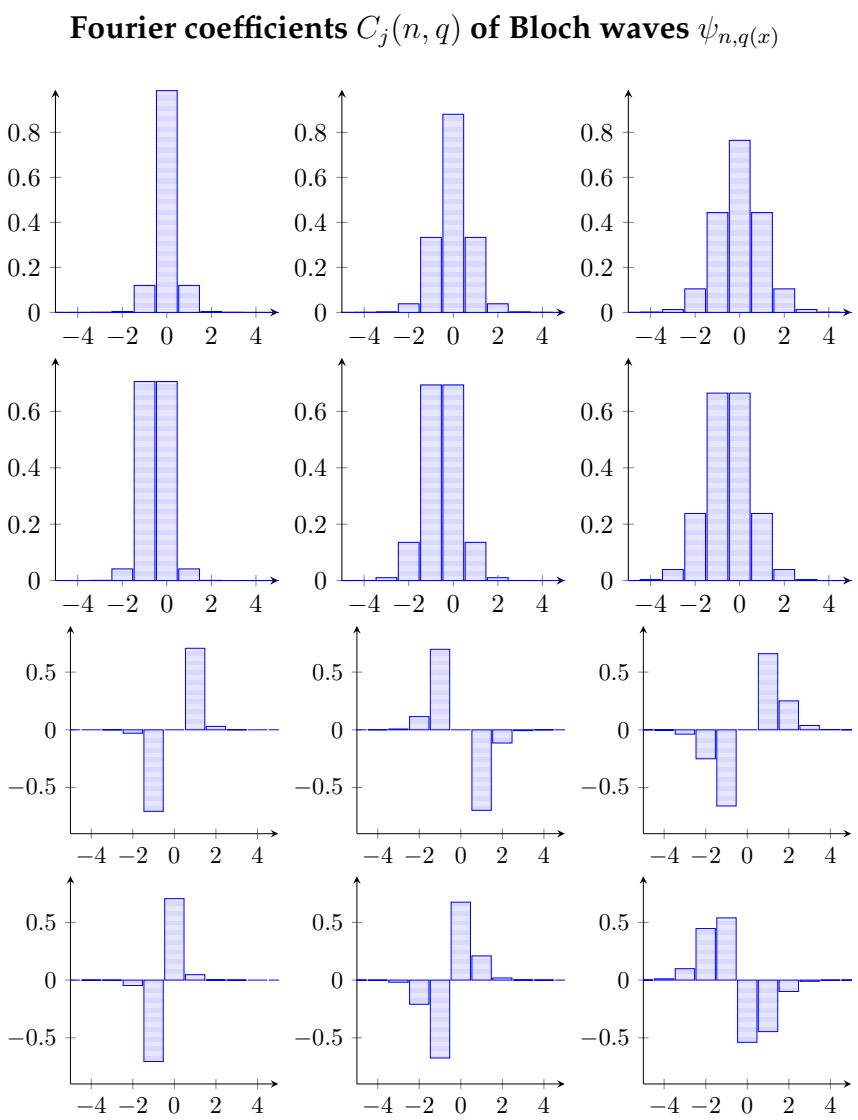

Figure 3. *Fourier coefficients $C_j(n,q)$ as a function of their index j. These coefficients are solutions of the central equation (37) for $V_0/E_r = 2$ (left column), $V_0/E_r = 8$ (middle column), $V_0/E_r = 20$ (right column). The rows correspond from top to bottom to $(n = 0, q = 0)$, $(n = 0, q = \pi/a)$, $(n = 1, q = 0)$, $(n = 1, q = \pi/a)$.*

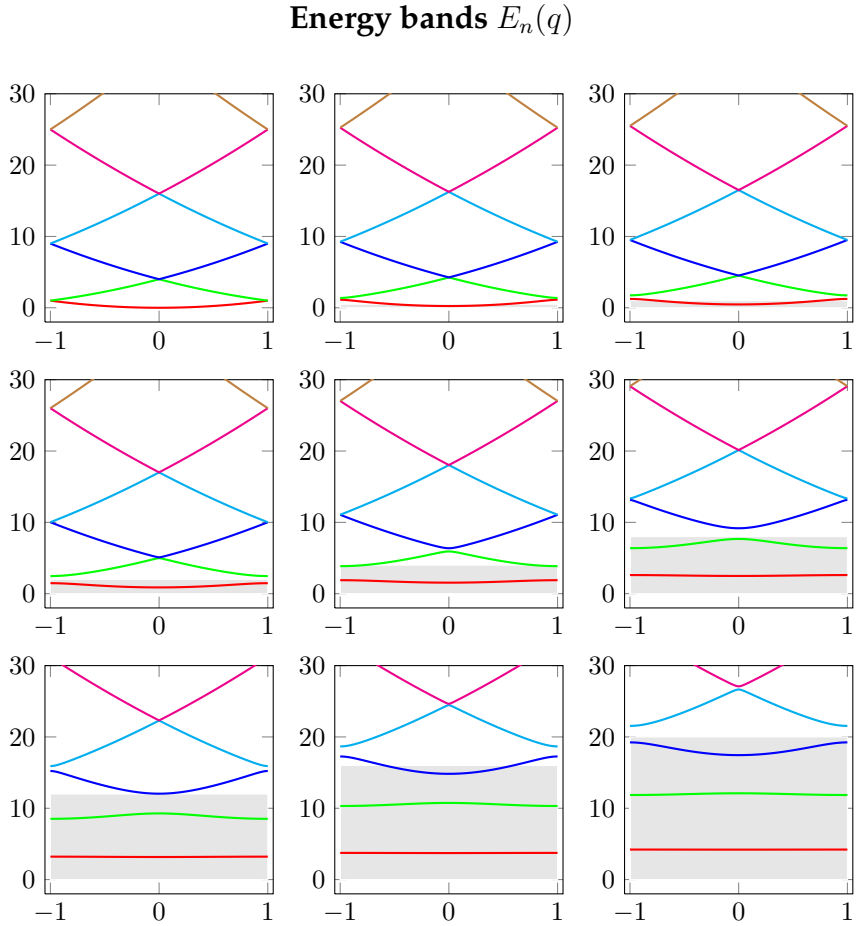

Figure 4. *Lowest energy bands $E_n(q)$ (in units of $E_r = \hbar^2k^2/2m$), as a function of q/k for a potential $V(x) = V_0 \sin^2(kx)$. From left to right, and from top to bottom: V_0/E_r =(0, 0.5, 1); (2, 4, 8); (12,16,20). The shaded rectangle represents the energy zone below the height of the potential V_0.*

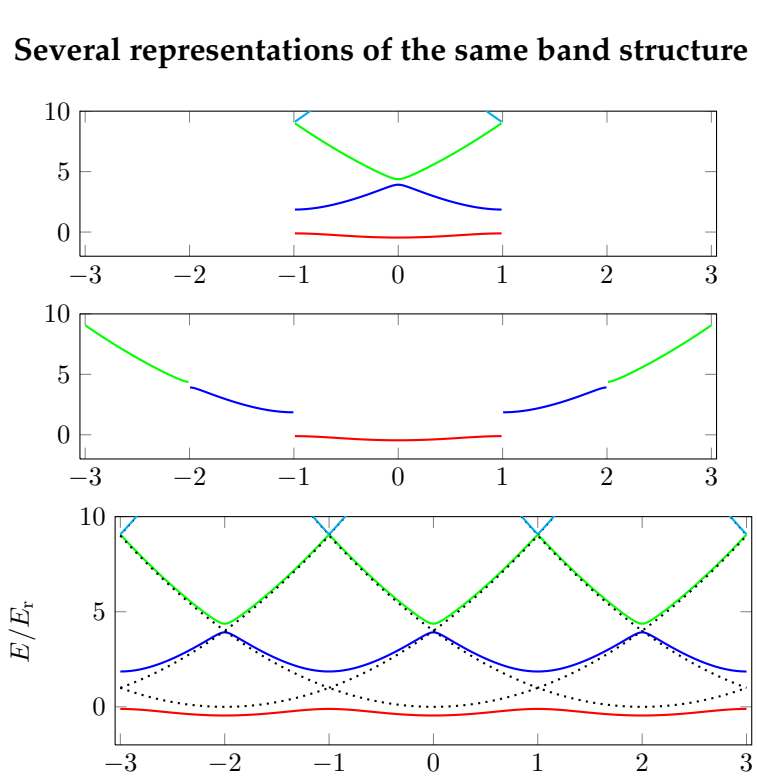

Figure 5. *Three possible representations of the band structure. On top, the usual diagram (folded band). In the middle, the unfolded band picture, which allows to make the link with the case of a free particle. At the bottom, the repeated zone picture, where each eigenstate $\psi_{n,q}$ is represented several times; this last representation is useful for the study of Bloch oscillations. The plots are drawn for $V_0 = 4\,E_r$, and we have subtracted here the mean value $V_0/2$ of the potential to facilitate the comparison with the case $V_0 = 0$. This case is represented with black dotted lines.*

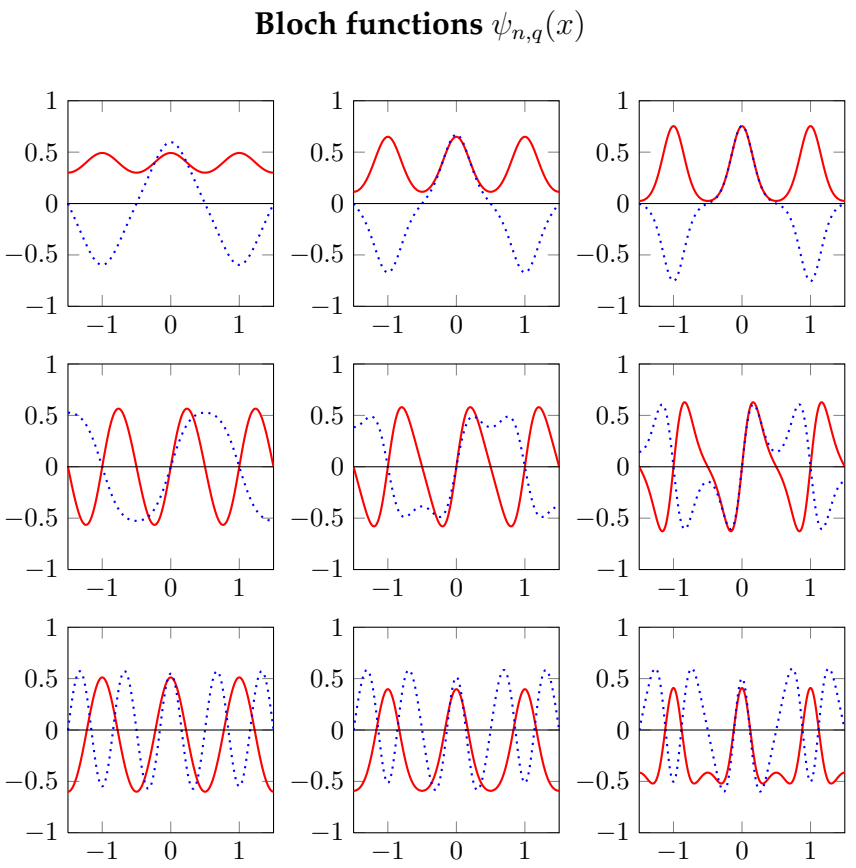

Figure 6. *Bloch functions $\psi_{n,q}(x)$ as a function of x/a for $V_0/E_r = 2$ (left column), $V_0/E_r = 8$ (middle column) and $V_0/E_r = 20$ (right column). The rows correspond to the band $n = 0$ (top), $n = 1$ (middle), $n = 2$ (bottom). On each graph, we have represented the quasi-momenta $q = 0$ (red continuous line) and $q = \pi/a$ (blue dotted line).*

The solutions of (37) are sorted as indicated above by increasing energy and they are labelled with the index $n = 0, 1, 2, \ldots$ The lowest energy bands $E_n(q)$ are plotted on figure 4 for several values of V_0/E_r. This plot shows the transition from the folded parabola obtained for $V_0 = 0$ to increasingly flat bands for potentials with $V_0 \gg E_\mathrm{r}$. This flattening corresponds to the situation where the amplitude of the tunnelling from one potential minimum to the next minimum becomes negligible, the energy levels then become close to those of a particle at the bottom of a single potential well, $V(x) \approx V_0 k^2 x^2$ for the central well for example. We will come back to this *tight-binding limit* in the next lecture.

Note that the folded representation in Figure 4 is not the only one possible. We have plotted two other representations in Figure 5 that may be useful, the unfolded representation and the repeated representation.

We have plotted on figure 6 some of the Bloch functions $\psi_{n,q}(x)$ for three values of V_0/E_r. These plots have been made by fixing the (arbitrary) phase of the Bloch function as follows:

- For even bands ($n = 0, 2, \ldots$), $\psi_{n,q}(x = 0)$ is real positive.
- For the odd bands ($n = 1, 3, \ldots$), $\frac{\mathrm{d}\psi_{n,q}}{\mathrm{d}x}(x = 0)$ is real positive.

With this convention, the Bloch functions for the quasi-momenta $q = 0$ and $q = \pi/a$ (the values used for the plots in figure 6) are real.

3-3 The case of the weak lattice

Let us now discuss the case $V_0 \lesssim E_\mathrm{r}$ that will be the starting point of the description of Bragg diffraction later on. In this case, we can treat perturbatively the effect of the potential $V(x) = V_0 \sin^2(kx) = (V_0/2) - (V_0/4)\left(\mathrm{e}^{2\mathrm{i}kx} + \mathrm{e}^{-2\mathrm{i}kx}\right)$, the dominant term of the Hamiltonian being the kinetic energy $\hat{H}_0 = \hat{p}^2/2m$. We have already given the expression of the eigenstates of $\hat{H}_0$ in the form of Bloch waves [cf. (33)], and we have plotted the eigenenergies $E_n(q)$ in the form of the folded parabola of figure 4a. Let us now look at the matrix elements of $V(x)$ between the eigenstates of $\hat{H}_0$. The constant term $V_0/2$ of the potential plays no role other than an overall translation of the energies. The terms in $(V_0/4)\mathrm{e}^{\pm 2\mathrm{i}kx}$ couple the plane

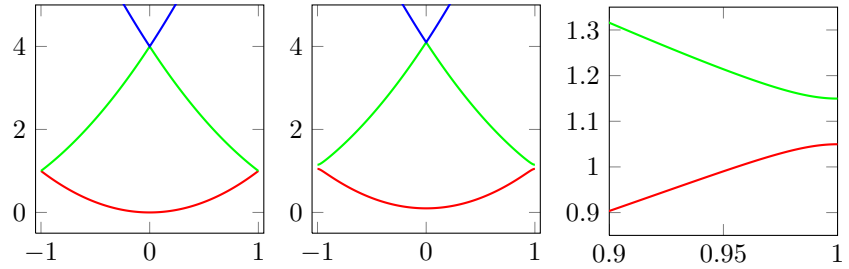

Figure 7. *The energy bands $E_n(q)$ (unit of E_r) as a function of q/k, for a potential $V_0 \ll E_\mathrm{r}$: (a): $V_0 = 0$ (same thing as in figure 4); (b): $V_0 = 0.2\,E_\mathrm{r}$; (c): a zoom on the band edge $q \approx k$ for the case $V_0 = 0.2\,E_\mathrm{r}$. We see that a gap of width $\approx V_0/2$ is opening.*

wave of momentum p to the plane waves $p \pm 2\hbar k$:

$$\hat{V}(x)\ \phi_p(x) = \frac{V_0}{2}\phi_p(x) - \frac{V_0}{4}\phi_{p-2\hbar k}(x) - \frac{V_0}{4}\phi_{p+2\hbar k}(x), \tag{38}$$

i.e. $\langle \phi_{p\pm 2\hbar k}|\hat{V}|\phi_p\rangle = -V_0/4$. In practice, this coupling is important only if the energy associated to the wave ϕ_p for the Hamiltonian H_0 is close to the energy of $\phi_{p-2\hbar k}$ or $\phi_{p+2\hbar k}$:

$$\frac{p^2}{2m} \approx \frac{(p \pm 2\hbar k)^2}{2m} \quad \Rightarrow \quad p \approx \mp \hbar k. \tag{39}$$

For the two lowest energy bands, this occurs only at the edge of the first Brillouin zone, i.e. where the bands touch in the case $V_0 = 0$.

Let us therefore consider the basis formed by the two plane-wave states $\{|p = -\hbar k\rangle, |p = +\hbar k\rangle\}$ of kinetic energy E_r. These two states are coupled by $V(x)$, and, at order 1 in V_0, the energy of the two eigenstates of $\hat{H}$ is obtained by diagonalizing the restriction of the Hamiltonian to this basis:

$$\hat{H} = \begin{pmatrix} E_\mathrm{r} + V_0/2 & -V_0/4 \\ -V_0/4 & E_\mathrm{r} + V_0/2 \end{pmatrix} \tag{40}$$

The eigenvalues of this matrix are (for $V_0 > 0$)

$$E = E_\mathrm{r} + \frac{V_0}{2} \pm \frac{V_0}{4} \quad \Rightarrow \quad E_0(k) = E_\mathrm{r} + \frac{V_0}{4}, \quad E_1(k) = E_\mathrm{r} + \frac{3V_0}{4}, \tag{41}$$

and the corresponding eigenstates are

$$\psi_{0,k}(x) \propto \cos(kx), \qquad \psi_{1,k}(x) \propto \sin(kx). \tag{42}$$

This result is easily understood: the low energy state $\psi_{0,k}$ is modulated so that the probability density $\propto \cos^2(kx)$ is minimal in the zones with a high potential [$V(x) = V_0 \sin^2(kx)$]. On the contrary the high energy state corresponds to a probability density "in phase" with the modulation of the potential. At this order of the calculation, the effect of the potential $V(x)$ is to open a gap of width $V_0/2$ between the two first bands. The opening of the gaps between the upper bands involves higher powers of V_0.

4 Ramping up and ramping down a lattice

4-1 Extension of Bloch's theorem

In the following chapters, we will frequently encounter problems which keep their spatial periodicity, but which depend explicitly on time. In this paragraph, we consider the Hamiltonian

$$\hat{H}(t) = \frac{\hat{\boldsymbol{p}}^2}{2m} + f_t\, V(\hat{\boldsymbol{r}}), \tag{43}$$

where V is spatially periodic on a lattice $\mathcal{B}$ and the function f_t describes how the lattice is ramped up or down. One can also take for f_t a function of the type $f_0 + f_1 \cos(\Omega t)$ where the modulated part, proportional to f_1 ($\ll f_0$), allows to make a spectroscopic study of the states in the lattice [see for example the articles by Denschlag, Simsarian, et al. (2002) and Kollath, Iucci, et al. (2006)].

Let us suppose that the wave function of the particle has initially the form of a Bloch wave

$$\phi(\boldsymbol{r}, t=0) = \mathrm{e}^{\mathrm{i}\boldsymbol{r}\cdot\boldsymbol{q}}\, u(\boldsymbol{r}, t=0), \tag{44}$$

where $u(\boldsymbol{r}, 0)$ is periodic on $\mathcal{B}$. We can then show that at a later time t, this Bloch waveform is preserved, with the same quasi-momentum $\boldsymbol{q}$:

$$\phi(\boldsymbol{r}, t) = \mathrm{e}^{\mathrm{i}\boldsymbol{r}\cdot\boldsymbol{q}}\, u(\boldsymbol{r}, t), \tag{45}$$

where $u(\boldsymbol{r}, t)$ is also periodic. The proof is simple: the function $\phi(\boldsymbol{r}, t)$ is obtained by making the evolution operator $\hat{U}(t)$ act on the initial state $\phi(\boldsymbol{r}, 0)$. Since $[\hat{H}(t), \hat{T}_{\boldsymbol{a}_j}] = 0$ at any time t, we deduce that $[\hat{U}(t), \hat{T}_{\boldsymbol{a}_j}] = 0$ and thus

$$\hat{T}_{\boldsymbol{a}_j}\hat{U}\phi(\boldsymbol{r},0) = \hat{U}\hat{T}_{\boldsymbol{a}_j}\phi(\boldsymbol{r},0) \;\Rightarrow\; \hat{T}_{\boldsymbol{a}_j}\left[\hat{U}\phi(\boldsymbol{r},0)\right] = \mathrm{e}^{\mathrm{i}\boldsymbol{a}_j\cdot\boldsymbol{q}}\left[\hat{U}\phi(\boldsymbol{r},0)\right]. \tag{46}$$

It follows that $\phi(\boldsymbol{r}, t) = \hat{U}\phi(\boldsymbol{r}, 0)$ is an eigenstate of $\hat{T}_{\boldsymbol{a}_j}$ with the same eigenvalue $\mathrm{e}^{\mathrm{i}\boldsymbol{a}_j\cdot\boldsymbol{q}}$ as $\phi(\boldsymbol{r}, 0)$, hence the writing under the form of a Bloch wave (45): the quasi-momentum $\boldsymbol{q}$ is conserved during the evolution.

In the context of optical lattices, this conservation of the quasi-momentum q when the intensity of an optical lattice is varied in time has a simple interpretation: the interaction of the atom with light occurs via processes involving the absorption of a photon from one wave and the stimulated emission of a photon in the other wave. Such a process changes the momentum of the atom by $\pm 2\,\hbar k$: an isolated atom initially prepared in a state of momentum p will later be in a superposition of states $p + 2n\hbar k$, where n is an integer. All these states correspond to the same quasi-momentum q of the Brillouin zone, q being defined by $q = p/\hbar$ modulo $2\pi/a$. Two elements can limit the scope of this reasoning:

- If the beam is not a plane wave, but has an intensity gradient along the x axis, then the momentum associated with a light beam is not exactly equal to $\hbar k$. This means that the intensity gradient causes a dipolar force on a spatial scale *a priori* larger than the period $\lambda/2$ of the lattice, a force which can modify the atomic momentum by an amount different from $2\hbar k$.

- If we set a lattice in motion by changing the frequency of one travelling wave with respect to the other, the two wave numbers $k_\pm$ associated to the two travelling waves are not strictly equal and the change of momentum $\hbar(k_+ + k_-)$ is not strictly equal to $2\hbar k$. In other words, the spatial period of the lattice changes with time, which invalidates Bloch's theorem. In practice, for the lattice velocities that are used, these deviations are very small.

4-2 Adiabatic ramp-up and ramp-down

We consider the 1D case to simplify the notations. In the previous paragraph, we have deduced the conservation of the quasi-momentum q from the translation invariance. We will now place ourselves in the situation where the initial state corresponds to one of the eigenstates of the Hamiltonian for the initial value of the potential $f_0\,V(x)$, that is $u(x,0) = u_{n,q}(x)$. We will investigate what can be said about the periodic part $u(x,t)$ at a later time if the coefficient f_t varies "slowly".

The spatially-periodic function $u(x,t)$ is determined by solving the differential equation obtained from the time-dependent Schrödinger equation:

$$\mathrm{i}\hbar\frac{\partial|u(t)\rangle}{\partial t} = \hat{H}_{\mathrm{per.}}[q,f_t]|u(t)\rangle \tag{47}$$

where $\hat{H}_{\mathrm{per.}}[q,f]$ is defined by (cf. 22)

$$\hat{H}_{\mathrm{per.}}[q,f] = \frac{(\hat{p}+\hbar q)^2}{2m} + fV(\hat{x}). \tag{48}$$

For each value of q and f, we know the eigenstates $|u^{(f)}_{n,q}\rangle$ of this Hamiltonian. We assume that the initial state $|u(0)\rangle$ is one of these eigenstates ($|u(0)\rangle = |u^{(f_0)}_{n,q}\rangle$) and we have to determine under which condition the state $|u(t)\rangle$ will be close to $|u^{(f_t)}_{n,q}\rangle$ at time t.

We start by recalling the general criterion necessary the adiabatic approximation to be valid (Messiah 2003). We consider a Hamiltonian $\hat{H}(\lambda)$ that depends on a parameter λ, for which we assume that we have solved the eigenvalue equation. We suppose for simplicity that the energies $\epsilon_n(\lambda)$ are non-degenerate and form a discrete set. The associated eigenvectors are denoted by $|\phi_n(\lambda)\rangle$. We are interested in a situation where the parameter λ depends on time. We suppose that the system is prepared at time $t = 0$ in an eigenstate $|\phi_n[\lambda(0)]\rangle$ and we search for the condition under which the system will be in the state $|\phi_n[\lambda(t)]\rangle$ at time t with a probability close to 1. We can show that this will be the case if the inequality

$$\hbar\left|\langle\phi_{n'}|\frac{\mathrm{d}}{\mathrm{d}t}|\phi_n\rangle\right| \ll |E_{n'} - E_n|\,, \quad \forall n' \neq n, \tag{49}$$

is satisfied at each time.

To concretely apply this criterion to our situation where a lattice is ramped up and down, let us assume that the atoms are initially prepared in the zero momentum state $|p=0\rangle$, with the lattice turned off. This state is identified with $|\psi_{n=0,q=0}\rangle$. When we ramp up the lattice, we know that the quasi-momentum will remain $q = 0$ and the question is to know whether we leave or not the lowest band $n = 0$. Let us restrict ourselves to the case of relatively weak lattices, $f_t V_0 \lesssim E_{\mathrm{r}}$, for which we can perturbatively determine the eigenstates $|\psi_{n,q=0}\rangle$ (Dahan 1997). At order 1 in V_0, the ground state $|\psi_{n=0,q=0}\rangle$ is obtained by mixing the zero momentum state $|p=0\rangle$ and the two states $|p=\pm 2\hbar k\rangle$. The gap between the unperturbed levels is $4E_{\mathrm{r}}$ and the perturbation $fV_0\sin^2(kx) = -(fV_0/4)\left(\mathrm{e}^{2\mathrm{i}kx} + \mathrm{e}^{-2\mathrm{i}kx}\right) + fV_0/2$ gives a matrix element $-fV_0/4$, which provides

$$|\psi_{n=0,q=0}\rangle \approx |p=0\rangle + \frac{fV_0}{16E_{\mathrm{r}}}\left(|p=2\hbar k\rangle + |p=-2\hbar k\rangle\right). \tag{50}$$

The non-adiabatic coupling will essentially induce a transition to the state

$$|\psi_{n',q=0}\rangle \approx \frac{1}{\sqrt{2}}\left(|p=2\hbar k\rangle + |p=-2\hbar k\rangle\right). \tag{51}$$

The matrix element at play in the left-hand side of (49) is then written

$$\langle\psi_{n',q=0}|\frac{\mathrm{d}}{\mathrm{d}t}|\phi_{n=0,q=0}\rangle = \frac{\dot{f}V_0}{16E_{\mathrm{r}}}\sqrt{2} \tag{52}$$

and the energy gap of the right-hand side is $4E_{\mathrm{r}}$. The adiabaticity criterion is written in this case:

$$\dot{f} \ll 32\sqrt{2}\,\frac{E_{\mathrm{r}}^2}{\hbar V_0}. \tag{53}$$

Let us take the case where we ramp a potential up to the value $V_0 = E_{\mathrm{r}}$ linearly in time, during a duration τ. The above criterion becomes

$$\tau \gg \frac{1}{32\sqrt{2}}\frac{\hbar}{E_{\mathrm{r}}}. \tag{54}$$

For sodium atoms illuminated near their resonance wavelength (589 nm), the time $\hbar/E_{\mathrm{r}} \approx 6\,\mu$s, so that the above condition is written $\tau \gg 0.15\,\mu$s. We have shown in figure 8 a result obtained by the NIST group to test this adiabatic ramping. Note that the maximum value reached, $V_0 = 14\,E_{\mathrm{r}}$, is outside the scope of our perturbative theory.

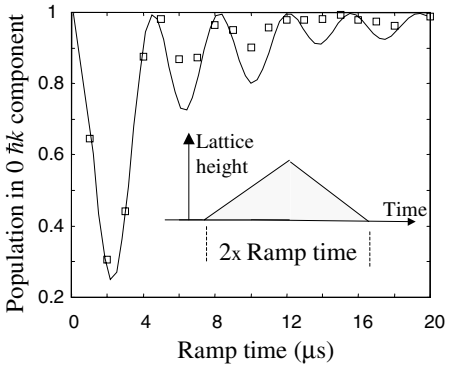

Figure 8. *Test for adiabaticity of the loading of atoms in a lattice. Sodium atoms are initially prepared at ≈ zero momentum. A lattice is ramped up, reaching a maximum depth of $V_0 = 14\,E_\mathrm{r}$, and then ramped down. The fraction of atoms in the zero momentum state is measured at the end of the process. The continuous curve is obtained by a direct integration of the Schrödinger equation. This figure is extracted from the article of Denschlag, Simsarian, et al. (2002).*

Note 1. We have considered here the lowest band at $q = 0$, which is a favorable case to ramp up a lattice. There are other situations where it is impossible to guarantee adiabaticity. This is for example the case if we start from $|\psi_{n=1,q=0}\rangle$ which has the same energy as $|\psi_{n=2,q=0}\rangle$ when the lattice is switched off. This is also the case if we start from the band edge $q = \pm k$. This last case is interesting because it gives rise to Bragg diffraction, which is used a lot in practice as an atomic beam splitter (see paragraph below).

Note 2. We are interested here in the adiabaticity criterion for a single particle. In the case where we start from a state with inter-particle correlations, the time scales needed to maintain adiabaticity can be very different, as the energy gaps between the different N-body states accessible can be much smaller.

4-3 Bragg diffraction

Bragg diffraction consists in taking advantage of the periodicity of the lattice to efficiently diffract a wave in a given direction. In the case of an atom interacting with an optical lattice, we want to create momentum-selective coherent transitions

$$\boldsymbol{p} \longrightarrow \boldsymbol{p} + 2n\hbar\boldsymbol{k} \tag{55}$$

where n is an integer. In what follows, we will restrict ourselves to the case of a weak potential ($V_0 \lesssim E_\mathrm{r}$), which guarantees that we populate significantly only one class of momentum $\boldsymbol{p} + 2n\hbar\boldsymbol{k}$ and not a comb with many components.

Let us consider here a one-dimensional lattice and atoms prepared in a given momentum state p, which will interact with the lattice during a time t_int. Since $V_0 \lesssim E_\mathrm{r}$, only atoms with a quasi-momentum q such that two energy bands $E_n(q)$ and $E_{n'}(q)$ are close to each other will be affected by the potential and can be efficiently coupled :

- As we have seen in §3-3, this coupling occurs at order 1 in V_0 for $q \approx \pm k$ between the bands $n = 0$ and $n = 1$: an atom with initial momentum $p = +\hbar k$ can be resonantly transferred to the momentum state $-\hbar k$, in a process where a photon is absorbed in one of the two traveling waves forming the standing wave, and a photon is stimulatedly emitted in the other wave (figure 9).
- More generally, one can directly see on figure 7 that one can also observe Bragg diffraction at higher orders: (i) at $q \approx \pm k$ between a band $2n$ and a band $2n+1$ (coupling term in V_0^{2n+1}); (ii) at $q \approx 0$ between a band $2n+1$ and a band $2n+2$ (coupling term in V_0^{2n+2}).

In what follows, we will focus on the coupling at order 1 between the bands $n = 0$ and $n = 1$, using the Bloch state formalism developed above. The use of this formalism to treat Bragg diffraction was initiated by Champenois, Buchner, et al. (2001) [for earlier approaches based on a different approach, one can refer to Keller, Schmiedmayer, et al. (1999) and Horne, Jex, et al. (1999)].

Let us consider the simple situation where the function f_t is a square pulse, equal to 1 for t between 0 and t_int and zero elsewhere. Before switch-

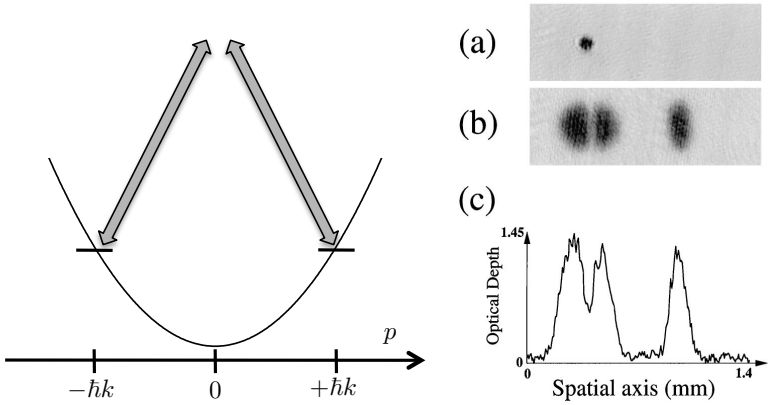

Figure 9. *Left: Bragg diffraction seen in terms of a two-photon transition. The two states $p = \pm\hbar k$ are coupled in a resonant way by a process with an absorption in a running wave and a stimulated emission in the other running wave. Right: Observation of a Bragg transition with atoms of a sodium condensate (figure extracted from Kozuma, Deng, et al. (1999)). (a) Image before the Bragg pulse. (b) Image after the Bragg pulse and a time of flight of 10 ms; only a narrow slice of the velocity distribution has undergone the diffraction phenomenon and has gained the momentum $2\hbar k$. (c) Density profile associated with the image (b).*

ing on the lattice, the atom is in the state $|p\rangle$. At time $t = 0$, when the potential is switched on, we assume that the state of the atom remains $|p\rangle$: this is the "sudden approximation", valid if the actual ramping time is short compared to the inverse of all the characteristic frequencies of the problem. Let us decompose this state on the eigenstates of the Hamiltonian with the lattice. Since $V_0 \lesssim E_\mathrm{r}$, only the eigenstates of the two lower bands $|\psi_{n=0,q}\rangle$ and $|\psi_{n=1,q}\rangle$ with $q = p/\hbar$ are significantly populated:

$$|\Psi(t=0)\rangle = |p\rangle \approx \cos(\theta/2)\,|\psi_{n=0,q}\rangle - \sin(\theta/2)\,|\psi_{n=1,q}\rangle. \tag{56}$$

We have already determined in (42) the relation between $|p\rangle$ and the eigenstates $|\psi_{n=0/1,q}\rangle$ in the particular case $p = \hbar k$. In the more general case where p is not strictly equal to $\hbar k$, the calculation is a bit longer. We have to take into account in the Hamiltonian (40) the difference in kinetic energy between the two ground states, $p^2/2m$ for the first one, $(p - 2\hbar k)^2/2m$ for the other. After a few lines of calculation, we find the value of the mixing angle θ involved in (56):

$$\mathrm{cotan}\,\theta = [1 - p/(\hbar k)]\,\frac{8E_\mathrm{r}}{V_0}. \tag{57}$$

The subsequent evolution in the presence of the lattice is a simple Rabi oscillation and the probability of finding the atom in the momentum state $p - 2\hbar k$ when the lattice is switched off is written

$$\mathcal{P}_{p\to p-2\hbar k}(t) = \sin^2\theta\ \sin^2(\Omega t/2). \tag{58}$$

This oscillation is sometimes called *Pendellösung*, a term initially introduced to describe the diffraction of X-rays by a crystal. Its frequency is $\Omega \approx V_0/(2\hbar)$ since the energy difference between the two levels is $\approx V_0/2$ [cf. (41)] . The prefactor

$$\sin^2\theta = \frac{(V_0/8E_\mathrm{r})^2}{[p/(\hbar k) - 1]^2 + (V_0/8E_\mathrm{r})^2} \tag{59}$$

fixes the selectivity in momentum of the Bragg diffraction phenomenon. For $p = \hbar k$, the oscillation occurs with an amplitude of 100%; by choosing $\Omega t_\mathrm{int} = \pi/2$, one realizes a 50%–50% beam splitter, and one obtains a perfect Bragg mirror for $\Omega t_\mathrm{int} = \pi$. For $V_0 \ll E_\mathrm{r}$, the modulation amplitude drops rapidly when we deviate from the condition $p = \hbar k$, the full width at half-maximum of the resonance curve being

$$\frac{\Delta p_{1/2}}{\hbar k} = \frac{V_0}{4\,E_\mathrm{r}}. \tag{60}$$

A comparison between the prediction of this two-level model and the one obtained by a complete numerical solution that takes into account a large number of eigenstates of the Hamiltonian can be found in Champenois, Buchner, et al. (2001). The differences between the results of the two approaches are negligible for $V_0 \lesssim E_\mathrm{r}$.

Bragg diffraction was first observed in the group of D. Pritchard (Martin, Oldaker, et al. 1988). In recent years, it has become an essential tool in matter-wave interferometry and cold atom physics:

- By successively imposing three Bragg diffractions corresponding to $\Omega t = \pi/2, \pi, \pi/2$, one realizes a two-path Mach-Zender interferometer

(see for example Lepoutre, Gauguet, et al. (2012)). A variant of this Bragg diffraction is often used, in which the $2\hbar k$ momentum transfer is accompanied by a change of internal state [Raman transitions between hyperfine levels (Kasevich & Chu 1991)]. Interferometers using Raman transitions can also operate in the $\pi/2$–π–$\pi/2$ mode or in the Ramsey-Bordé scheme, with four interaction zones (see for example Durfee, Shaham, et al. (2006) and Gauguet, Canuel, et al. (2009)). It is also possible to sweep in time the frequency of one of the two travelling waves that form the standing wave, in order to induce multiple Bragg diffraction processes and increase in this way the transferred momentum. This brings us closer to the problem of Bloch oscillations, which we will discuss at length in following chapters. An example of a $\pi/2$–π–$\pi/2$ interferometer working with $10\,\hbar k$ splitters thanks to an optimized f_t function can be found in Kovachy, Chiow, et al. (2012).

- One can take advantage of the selectivity in velocity (60) to measure the momentum distribution of a gas of free atoms (Kozuma, Deng, et al. 1999; Stenger, Inouye, et al. 1999). In practice, to probe the population of a class of velocity v, one uses a moving optical lattice formed by two progressive waves of frequency $\omega_L \pm k(v - v_\mathrm{r})$ where $v_\mathrm{r} = \hbar k/m$ is the recoil velocity. One can choose for example $\Omega t = \pi$ and measure the population transferred in the velocity class $v - 2v_\mathrm{r}$ (see for example figure 9 extracted from Kozuma, Deng, et al. (1999)). More generally, Bragg diffraction is also used to probe systems of interacting particles. One can send two laser beams with frequencies ω_j and wave vectors $\boldsymbol{k}_j$, $j = 1, 2$, and study the probability that the system undergoes an absorption-emission transition, which changes its energy by $\hbar\omega = \hbar(\omega_1 - \omega_2)$ and its momentum by $\boldsymbol{k} = \boldsymbol{k}_1 - \boldsymbol{k}_2$. By varying the frequency of the lasers and their relative angle, one can then reconstruct the dynamical structure factor $S(\boldsymbol{k}, \omega)$ of this system. This method was used for example by Steinhauer, Ozeri, et al. (2002) to measure the dispersion relation of Bogoliubov excitations in an interacting condensate.

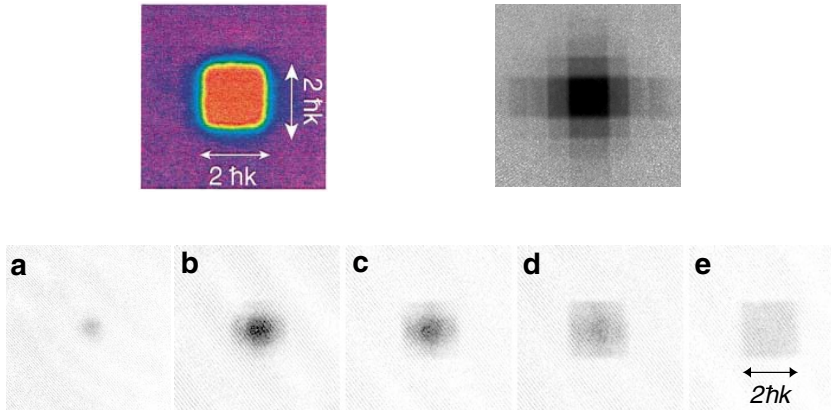

Figure 10. *Upper row: figure extracted from Greiner, Bloch, et al. (2001), obtained with ^{87}Rb bosonic atoms placed in a two-dimensional square lattice. Lower row: figure extracted from Köhl, Moritz, et al. (2005), obtained with ^{40}K fermionic atoms (without interaction) placed in a 3D cubic lattice.*

4-4 How to observe the band structure?

The notion of adiabatically ramping a lattice also finds an important application in the technique of *band mapping*, where one transfers the contents of different energy bands in the presence of the lattice to well-defined momentum states in the absence of the lattice. This requires an adiabatic ramp to switch off the lattice so that an atom initially in the state of band n and quasi-momentum q ends up in the momentum state $p = \hbar(q \pm 2n\hbar k)$. The simplest way, at least in 1D, to unambiguously link the initial state $\psi_{n,q}$ to the final momentum p is to use the unfolded band diagram shown in figure 5 (middle row).

The pictures shown in figure 10, obtained by the Munich group, constitute one of the first demonstrations of the visualization of the Brillouin zone allowed by this technique. For the picture on the left, we start from a deep 2D lattice ($12\,E_\mathrm{r}$) for which the width of the lowest band ($W_0 \sim E_\mathrm{r}/20$) is very small compared to the gap between the band $n = 0$ and the first excited band $n = 1$ ($\Delta_0 \sim 5\,E_\mathrm{r}$). A gas of bosons (^{87}Rb) is prepared in the lattice, with a temperature which is intermediate between

these two energy scales: $W_0 \ll k_B T \ll \Delta_0$. The gas uniformly fills the states $|\psi_{0,q}\rangle$ of the lowest band, but the population of excited bands is negligible. After an adiabatic ramp-down of the potential, the atoms are free and their momentum distribution is a square function with non-zero values only between $-\hbar k$ and $\hbar k$. To observe this momentum distribution, one can make a time of flight of duration t_{flight} sufficiently long so that the cloud spreads out by a large distance compared to its initial size: we obtain a segment of atoms (a square in two dimensions, a cube in three dimensions) of length $2\hbar k t_{\text{flight}}/m$.

In the right-hand photo of Figure 10, the upper bands were deliberately populated by applying an additional pair of laser beams that create a Raman transition between band n and band $n+1$. The time of flight then reveals the population transferred in these upper bands, with a near-uniform distribution within each band.

We show on the bottom row of the figure a result obtained for non-interacting fermions (^{40}K) in a 3D cubic lattice by T. Esslinger's group (Köhl, Moritz, et al. 2005). Because of the Pauli principle, these (polarized) fermions gradually fill up all the states of the lowest band when their number increase (from left to right). On the image "e", the band is full (a band insulator has been realized) and the square structure of the Brillouin zone is perfectly visible.

5 Propagation of wave packets

An essential characteristic of an optical lattice is the dispersion relation $E_n(q)$ associated to each band. In this paragraph, we show how to extract two important physical quantities related to this relation: the group velocity of a wave packet and the effective mass. We end this paragraph by giving some indications on how the interactions between atoms are modified when they are placed in the lattice.

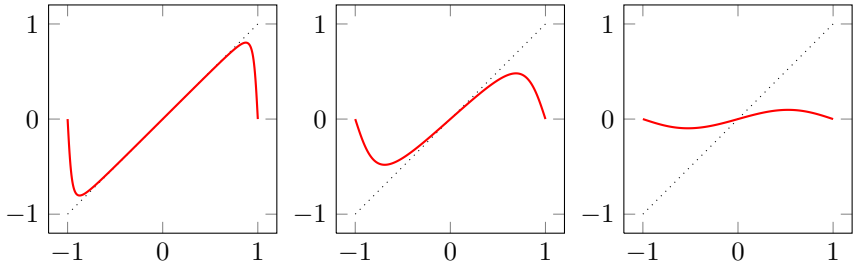

Figure 11. *Group velocity $v_g(q)$ (in units of the recoil velocity $v_r = \hbar k/m$) in the lattice $V(x) = V_0 \sin^2(kx)$ for $V_0/E_r = 0.4, 2, 8$, as a function of q/k. The dotted line corresponds to the result in the absence of a lattice: $mv_g = \hbar q$.*

5-1 The group velocity in an optical lattice

Let us suppose that we have prepared a particle in an initial state $\psi(x,0)$ superposition of Bloch states $\psi_{n,q}(x)$ all belonging to the same band n:

$$\psi(x,0) = \int c(q)\, \psi_{n,q}(x)\, \mathrm{d}q. \tag{61}$$

Let q_0 be the center of the distribution $c(q)$ and let us also assume that its width Δq around q_0 is much smaller than the width $2k$ of the Brillouin zone. This assumption allows the expansion

$$E_n(q) = E_n(q_0) + (q - q_0)\, \frac{\mathrm{d}E_n}{\mathrm{d}q}\bigg|_{q=q_0}. \tag{62}$$

Note that the assumption $\Delta q \ll k$ leads to the wave packet extending over several sites, typically $k/\Delta q$. We now define

$$v_{g,n}(q_0) = \frac{1}{\hbar}\, \frac{\mathrm{d}E_n}{\mathrm{d}q}\bigg|_{q=q_0}, \tag{63}$$

a quantity which has the dimension of a velocity and we will show that it can be interpreted as the group velocity for the band n around the quasi-momentum q_0.

At time t, the wave function of the particle is

$$\psi(x,t) = \int c(q)\, \psi_{n,q}(x)\, \mathrm{e}^{-\mathrm{i}E_n(q)t/\hbar}\, \mathrm{d}q, \tag{64}$$

which can also be written using the expansion (62)

$$\psi(x,t) \approx \mathrm{e}^{-\mathrm{i}\omega_0 t} \int c(q)\, \psi_{n,q}(x)\, \mathrm{e}^{-\mathrm{i}qv_{\mathrm{g},n}t}\mathrm{d}q, \tag{65}$$

where we have introduced the frequency

$$\omega_0 = E_n(q_0)/\hbar \; - \; q_0 v_{\mathrm{g},n}. \tag{66}$$

Let us choose the time t such that $v_{\mathrm{g},n}t = a$. Using the fact that $\psi_{n,q}(x-a) = \mathrm{e}^{-\mathrm{i}qa}\psi_{n,q}(x)$, we deduce that

$$\begin{aligned} \psi(x, t = a/v_{\mathrm{g},n}) &\approx \mathrm{e}^{-\mathrm{i}\omega_0 t} \int c(q)\, \psi_{n,q}(x-a)\mathrm{d}q \\ &= \mathrm{e}^{-\mathrm{i}\omega_0 t}\, \psi(x-a,0). \end{aligned} \tag{67}$$

We see that the wave packet periodically reforms without deformation (at this order of the calculation) with successive position shifts of a at all the instants separated by $a/v_{\mathrm{g},n}$, which corresponds to a propagation with the group velocity $v_{\mathrm{g},n}$.

5-2 The notion of effective mass

In the study we conducted for the sinusoidal potential, we found that the bands $E_n(q)$ are extremal at the points $q = 0$ and $q = \pm k$. At these points, the group velocity cancels and the band is characterized by its curvature, from which we define the effective mass m^* by

$$\frac{1}{m^*} = \frac{1}{\hbar^2}\frac{\mathrm{d}^2 E_n}{\mathrm{d}q^2}, \tag{68}$$

a quantity that can be positive or negative. This effective mass at the bottom of the lowest band is plotted on figure 12. Its value is $m^* \approx m$ for shallow lattices and it increases indefinitely as V_0 increases.

Let us consider a particle prepared in the lowest band, with a distribution of quasi-momenta centered on $\bar{q}$ and of width Δq, such that $|\bar{q}|, \Delta q \ll k$. We can then write the energy of each Bloch state in the form

$$E(q) = \frac{\hbar^2 q^2}{2m^*} + \text{constant}. \tag{69}$$

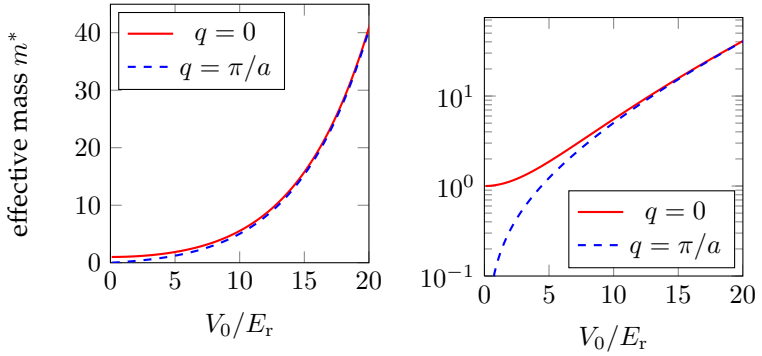

Figure 12. *Effective mass m^*/m [cf. (68)] as a function of V_0/E_r for the lowest band $n = 0$ and for the two values $q = 0$ and $q = \pi/a$ of the quasi-momentum. Note that the sign of m^* is negative for $q = \pi/a$ and that we have therefore plotted $|m^*|/m$ in this case (left: linear coordinates, right: logarithmic coordinates).*

We have determined above the velocity $\mathrm{d}\bar{x}/\mathrm{d}t$ of the center of a wave packet that we build by superposing states of this type:

$$\frac{\mathrm{d}\bar{x}}{\mathrm{d}t} = \frac{1}{\hbar}\left.\frac{\mathrm{d}E_n}{\mathrm{d}q}\right|_{q=\bar{q}} = \frac{\hbar\bar{q}}{m^*}. \tag{70}$$

Let us complete this result by another point that we will prove later in this lecture: if we apply to a particle placed in a periodic potential a force F that is uniform at the scale of the wave packet, then the evolution of the quasi-momentum is given by

$$\hbar\frac{\mathrm{d}\bar{q}}{\mathrm{d}t} = F. \tag{71}$$

The combination of the two equations (70-71) corresponds to the motion of a fictitious particle of mass m^* in the force field coming from F. The only effect of the lattice on this isolated particle is the renormalization of the mass $m \to m^*$.

5-3 Interactions in the lattice, a first overview

The study of interactions in an optical lattice is a very vast subject that we will only briefly mention here. The point we want to show is that a lattice provides a fairly simple way to increase the effects of interactions between particles, by localizing their wave function at the vicinity of the potential minima.

We consider in this paragraph bosonic particles moving along the x axis. To simplify the notations, we take a system of size L, with periodic boundary conditions (L is a multiple of the period a of the lattice: $L = Na$). Under these conditions, the quasi-momentum is quantized:

$$q = \frac{2\pi}{L} j = k \frac{2j}{N}, \quad j \text{ integer } \in \{-\frac{N}{2}+1, \ldots, 0, \ldots, \frac{N}{2}\}. \tag{72}$$

We assume that these particles interact with a contact interaction $g\,\delta(x)$. Without a lattice potential, the Hamiltonian in second quantization is written

$$\hat{H} = \sum_p \frac{p^2}{2m} \hat{a}_p^\dagger \hat{a}_p + \frac{g}{2L} \sum_{p_1,p_2,p_3} \hat{a}_{p_1-p_3}^\dagger \hat{a}_{p_2+p_3}^\dagger \hat{a}_{p_2} \hat{a}_{p_1} \tag{73}$$

where $\hat{a}_p^\dagger$ creates an atom in the plane wave of momentum p, $\psi_p = \mathrm{e}^{\mathrm{i}px/\hbar}/\sqrt{L}$.

In the presence of a lattice, we write the Hamiltonian in second quantization in the basis of Bloch waves. To simplify the notations, we restrict to the case where only the lowest band $n = 0$ is populated and we denote as $\hat{b}_q^\dagger$ the operator creating an atom in the state $\psi_{0,q}$. We find

$$\hat{H} = \sum_q E_0(q)\, \hat{b}_q^\dagger \hat{b}_q + \frac{g}{2} \sum_{q_1,q_2,q_1',q_2'} C(q_1,q_2,q_1',q_2')\, b_{q_1'}^\dagger b_{q_2'}^\dagger b_{q_2} b_{q_1} \tag{74}$$

with

$$C(q_1,q_2,q_1',q_2') = \int_0^L \psi_{0,q_1'}^*(x)\, \psi_{0,q_2'}^*(x)\, \psi_{0,q_1}(x)\, \psi_{0,q_2}(x)\, \mathrm{d}x. \tag{75}$$

In the discretized version we have chosen here for the Brillouin zone, a convenient form for the Bloch waves is

$$\psi_{0,q}(x) = \frac{1}{\sqrt{N}}\, \mathrm{e}^{\mathrm{i}qx}\, u_{0,q}(x), \tag{76}$$

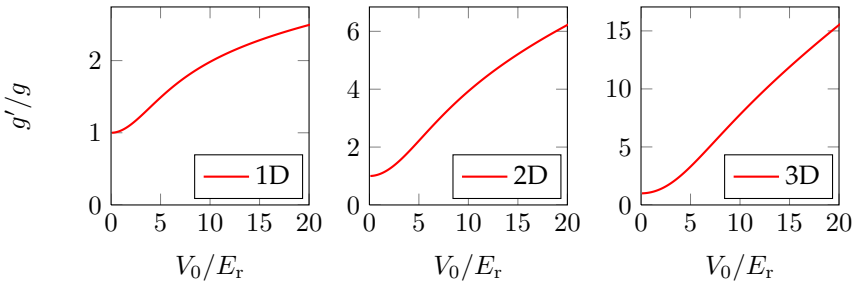

Figure 13. *"Amplification factor" g'/g of contact interactions as a function of V_0/E_r [cf. (80)]. This increase is due to the localization of the Bloch functions at the vicinity of the minima of the potential V. The 2D and 3D values are simply the square and cube of the 1D value.*

where $\psi_{n,q}$ is normalized on the segment of length L and the periodic part $u_{n,q}$ is normalized on the unit cell of length a:

$$\int_0^L |\psi_{n,q}(x)|^2\, \mathrm{d}x = 1, \qquad \int_0^a |u_{n,q}(x)|^2\, \mathrm{d}x = 1. \tag{77}$$

The Bloch form immediately imposes the relation (conservation of the momentum):

$$q_1' + q_2' = q_1 + q_2 \quad (\text{modulo } 2\pi/a). \tag{78}$$

Let us assume for simplicity that only the states at the bottom of the band $n = 0$ are populated ($|q| \ll k$). We can then approximate the Hamiltonian (74) by

$$\hat{H} \approx \sum_q \frac{\hbar^2 q^2}{2m^*}\, \hat{b}_q^\dagger \hat{b}_q + \frac{g'}{2L} \sum_{q_1,q_2,q_3} b_{q_1-q_3}^\dagger b_{q_2+q_3}^\dagger b_{q_2} b_{q_1} \tag{79}$$

where the "renormalized" interaction coefficient g' is given by

$$\frac{g'}{g} = a \int_0^a |u_{0,0}(x)|^4\, \mathrm{d}x. \tag{80}$$

Without a lattice, the periodic part of the Bloch function $u_{0,0}(x)$ is constant and equal to $1/\sqrt{a}$, so that $g'/g = 1$. With the lattice, the function $u_{0,0}$

is modulated while remaining normalized ($\int_0^a |u_{0,0}(x)|^2 \, \mathrm{d}x = 1$), which leads to $g' > g$: localizing the atoms in some regions of space increases their interactions. The ratio g'/g is plotted as a function of the lattice depth on figure 13. If we go to 2D or 3D with a square or cubic lattice (potential in $V(x) + V(y) + V(z)$), we must take the square or the cube of this ratio to evaluate the change of the coupling g (see figure 13).

In summary, adding a lattice has two consequences regarding the dynamics at the bottom of the band $n = 0$:

- It increases the effective mass and thus *decreases* the contribution of the kinetic energy.
- It increases the coefficient g and thus *increases* the contribution of the interaction energy.

These two effects go in the same direction by favoring the appearance of strongly correlated states at the expense of mean-field states, like a Bose-Einstein condensate. The culmination of this effect is the superfluid-Mott insulator transition. However, before reaching this point, we go through a domain, for relatively strong lattices, where all the states of the lowest band acquire a significant population. The Hamiltonian (79) is then no longer relevant and one has to go back to (74) to describe the dynamics of the problem. We will present in the next chapter an approach that is easier to handle in the case of these strong lattices, using the Wannier function basis.

Chapter III

Optical lattices in the tight-binding regime

The Bloch waves described in the previous chapter are to the motion in a periodic potential what plane waves are to the motion of a free particle. Since they are eigenstates of the Hamiltonian and of the translation operator, they are delocalized in the entire space. They form an orthogonal basis of the one-particle Hilbert space, and they can be normalized in the usual sense of continuous bases by imposing

$$\int_{-\infty}^{+\infty} \psi^*_{n,q}(x)\, \psi_{n',q'}(x)\, \mathrm{d}x = \delta_{n,n'}\, \delta(q-q'), \tag{1}$$

where the first δ, referring to the band index n, is a Kronecker symbol and the second δ, referring to the quasi-momentum q, is a Dirac distribution. We have chosen here a one dimension approach to simplify the notation, but the extension to higher dimensions is immediate.

For many problems, it is useful to introduce a second basis of the Hilbert space, also orthonormal and consisting of functions localized at the vicinity of the local minima of the lattice ("sites"), called *Wannier functions* (Wannier 1937). The one-particle Hamiltonian written in the basis of the Wannier functions is very intuitive: it corresponds to hopping terms between sites, whose amplitude depends on the height of the potential barriers between the wells.

In the tight-binding limit which, for a sinusoidal potential $V_0 \sin^2(kx)$, corresponds to the situation where V_0 is large compared to the recoil energy E_r, we can limit ourselves to hopping between neighbouring sites. We will study this limit, in the case where only one energy band, the lowest band for example, contributes significantly to the dynamics. When on-site interactions are taken into account, we obtain in this way the *Hubbard Hamiltonian*, which allows to illustrate many physical phenomena. We will also give some examples of interesting energy band shapes that appear for lattices with more complex patterns than the simple sinusoidal case.

1 The Wannier functions

1-1 A new basis

To define the basis of Wannier functions, we start with a series of equidistant points x_j, $j \in \mathbb{Z}$, distant from each other by a. In the following, we will choose these points at the minima of the potential $V(x)$: $x_j = ja = j\lambda/2$. We then define the Wannier function $w_{j,n}$ for the band n by:

$$w_{n,j}(x) = \left(\frac{a}{2\pi}\right)^{1/2} \int_{-\pi/a}^{+\pi/a} \psi_{n,q}(x)\, \mathrm{e}^{-\mathrm{i}jaq}\, \mathrm{d}q. \tag{2}$$

It is immediate to show from the definition (2) that the Wannier functions $w_{n,j}$ can be deduced (for a fixed n) one from the other by translations:

$$w_{n,0}(x-ja) = w_{n,j}(x). \tag{3}$$

It is therefore sufficient to characterize the Wannier functions $w_{n,0}(x)$ to know them all. The definition (2) can be inverted to give [1]

$$\psi_{n,q}(x) = \left(\frac{a}{2\pi}\right)^{1/2} \sum_{j\in\mathbb{Z}} w_{n,0}(x-ja)\, \mathrm{e}^{\mathrm{i}jaq}, \tag{5}$$

and, for the periodic part $u_{n,q}$ of Bloch waves:

$$u_{n,q}(x) = \left(\frac{a}{2\pi}\right)^{1/2} \sum_{j\in\mathbb{Z}} w_{n,0}(x-ja)\, \mathrm{e}^{-\mathrm{i}q(x-ja)}. \tag{6}$$

The definition of the Wannier functions depends on the phase given to each Bloch wave, this phase being arbitrary at this stage. For a potential with a mirror symmetry [$V(x) = V(-x)$] and for disjoint energy bands I_n, Kohn (1959) showed that there is a unique choice for this phase which guarantees that the Wannier function (i) is real, (ii) is even or odd with respect to $x = 0$ or $x = a/2$, (iii) decays exponentially fast at infinity. For the lattice $\sin^2(kx)$, a relevant choice of phase is to take $\psi_{n,q}(0)$ real positive for all q if n is even, and $\mathrm{d}\psi_{n,q}/\mathrm{d}x|_{x=0}$ real positive if n is odd. This leads to

$$\psi_{n,q}(-x) = \psi^*_{n,q}(x) = \psi_{n,-q}(x). \tag{7}$$

We then check from the definition (2) that the Wannier function $w_{0,0}(x)$ is even with respect to $x = 0$. The Wannier functions associated with site $j = 0$ for several values of the potential V_0 are plotted on figure 1. For a zero potential, this Wannier function is proportional[2] to $\mathrm{sinc}(kx)$.

Using the fact that the Bloch functions constitute an orthonormal basis of the space of square-integrable functions of the variable x, we can easily verify using (2-5) that the set of Wannier functions also forms an orthonormal basis of the space of functions:

$$\int w_{n,j}(x)\, w_{n',j'}(x)\, \mathrm{d}x = \delta_{n,n'}\, \delta_{j,j'}. \tag{8}$$

[1] For the functions considered here, we use the relation

$$\sum_{j\in\mathbb{Z}} \mathrm{e}^{\mathrm{i}qja} = (2\pi/a)\, \delta(q). \tag{4}$$

where the distribution $\delta(q)$ is defined up to an element of the reciprocal lattice (the multiples of $2\pi/a$ in 1D).

[2] It does not decrease exponentially at infinity because W. Kohn's assumption of disjoint energy bands is not verified in this case.

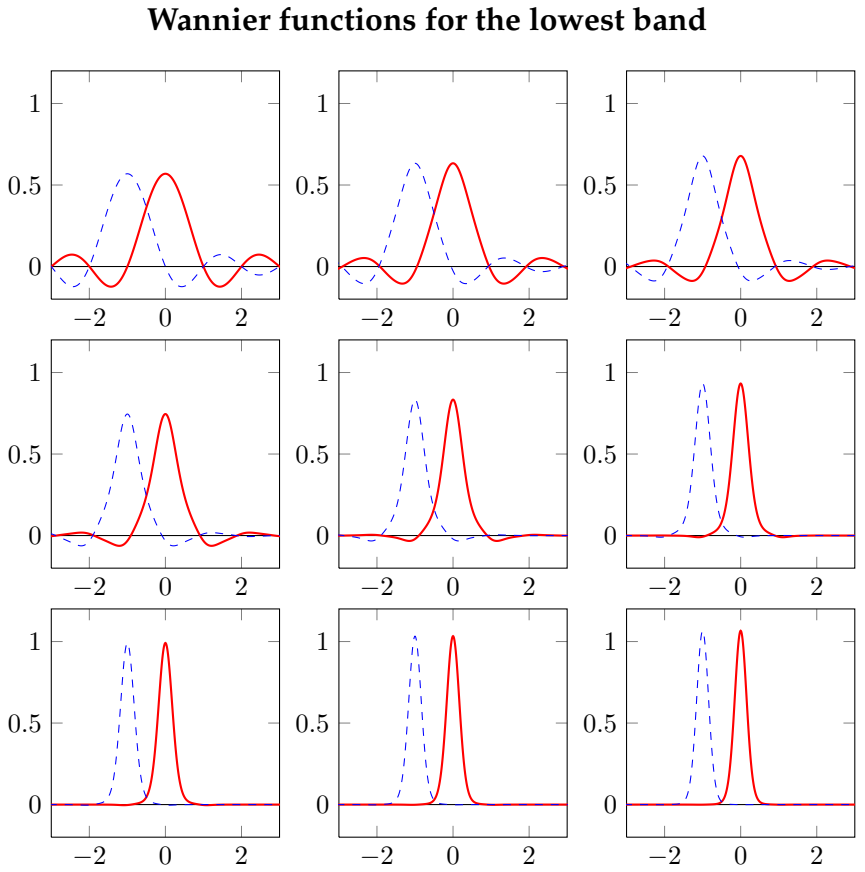

Figure 1. *Wannier functions $w_{0,0}(x)$ as a function of kx/π for the periodic potential $V(x) = V_0 \sin^2(kx)$. From left to right, and from top to bottom: V_0/E_r =(0, 0.5, 1); (2, 4, 8); (12,16,20). The dotted lines indicate the Wannier function shifted by one site ($w_{0,-1}(x)$).*

Note that each Wannier function $w_{n,j}(x)$ must necessarily take positive and negative values, to ensure the orthogonality between itself and the Wannier function shifted by a distance a, $w_{n,j\pm1}(x)$.

1-2 Wannier functions in the reciprocal space

Let us define the Fourier transform $\tilde{w}_n(\kappa)$ of the central Wannier function $w_{n,0}(x)$:

$$\tilde{w}_n(\kappa) = \frac{1}{\sqrt{2\pi}} \int_{-\infty}^{+\infty} w_{n,0}(x)\, \mathrm{e}^{-\mathrm{i}x\kappa}\, \mathrm{d}x. \tag{9}$$

It is then quite simple to show that this function is directly related to the expansion of the Bloch function on the plane wave basis. More precisely, we have

$$\psi_{n,q}(x) = \frac{1}{\sqrt{a}} \sum_{j\in\mathbb{Z}} \tilde{w}_n(q + 2\pi j/a)\, \mathrm{e}^{\mathrm{i}x(q+2\pi j/a)}. \tag{10}$$

We can prove this result either by using the definition (2) in the Fourier transform (9), or by using the Poisson summation formula.

This formula gives a new insight into the Wannier functions: the modulus square of their Fourier transform gives the weight of the different components of the momentum comb that forms each Bloch function. Note that without a lattice, the Bloch functions are known to be plane waves: only one tooth of the comb is non-zero; for example, for the lowest band, $\psi_{0,q}(x) \propto \mathrm{e}^{\mathrm{i}xq}$ for q in the interval $]-\pi/a, +\pi/a]$ corresponding to the Brillouin zone. The Fourier transform $\tilde{w}_0(\kappa)$ is then a square function, constant on this interval [equal to $(a/2\pi)^{1/2}$] and null everywhere else.

1-3 The Hamiltonian in terms of Wannier functions

In the Bloch function basis, the Hamiltonian describing the motion of a particle is by definition diagonal

$$H = \sum_n \int_{-\pi/a}^{+\pi/a} \mathrm{d}q\; E_n(q)\, |\psi_{n,q}\rangle\langle\psi_{n,q}| = \sum_n \int \mathrm{d}q\; E_n(q)\, \hat{a}^\dagger_{n,q}\hat{a}_{n,q}, \tag{11}$$

where we have adopted a second quantization notation in the right-hand side, which is more convenient to later treat problems with interaction between particles. In this notation, the operator $\hat{a}_{n,q}$ destroys a particle in the Bloch wave $\psi_{n,q}$.

The change of basis (5), which is written in second quantization

$$\hat{a}_{n,q} = \left(\frac{a}{2\pi}\right)^{1/2} \sum_j \mathrm{e}^{\mathrm{i}jaq}\, \hat{b}_{n,j}, \tag{12}$$

where $\hat{b}_{n,j}$ destroys a particle in the Wannier function $w_{n,j}$, leads to the following expression for the Hamiltonian:

$$\hat{H} = \sum_n \sum_{j,j'} J_n(j-j')\, \hat{b}^\dagger_{n,j}\hat{b}_{n,j'}. \tag{13}$$

The interpretation of this Hamiltonian is simple: it describes the jump of the particle from the site $x_{j'} = j'a$ to the site $x_j = ja$ with the amplitude $J_n(j-j')$ which depends on the band n considered and the distance between the two sites. By construction, $J_n(j-j')$ is equal to the matrix element of the Hamiltonian between two Wannier functions

$$J_n(j) = \int w^*_{n,j}(x)\, \left(\frac{\hat{p}^2}{2m} + V(x)\right)\, w_{n,0}(x)\, \mathrm{d}x, \tag{14}$$

and verifies the property

$$J_n(-j) = J^*_n(j), \tag{15}$$

which guarantees that $\hat{H}$ in (13) is Hermitian. If the Wannier functions can be chosen real, $J_n(j)$ is also real and $J_n(-j) = J_n(j)$.

The matrix element $J_n(j)$ is written in terms of the energies $E_n(q)$:

$$J_n(j) = \frac{a}{2\pi} \int_{-\pi/a}^{+\pi/a} \mathrm{d}q\; E_n(q)\, \mathrm{e}^{\mathrm{i}jaq}, \tag{16}$$

a relation that can be inverted to give

$$E_n(q) = \sum_{j\in\mathbb{Z}} J_n(j)\, \mathrm{e}^{-\mathrm{i}jaq}, \tag{17}$$

$$= 2\sum_{j=1}^{\infty} J_n(j)\cos(j\,aq), \tag{18}$$

where the second line is valid if the Wannier functions can be chosen real. The energy bands and the hopping amplitudes between (near or distant) neighbours are thus linked by Fourier-transform-like relations. The coefficient $J_n(0)$ simply corresponds to the uniform average of the energy $E_n(q)$ over the Brillouin zone.

1-4 The multi-dimensional case

Consider a particle moving in three dimensions placed in the periodic potential

$$V(\boldsymbol{r}) = V_0 \sin^2(kx) + V_0' \sin^2(ky) + V_0'' \sin^2(kz). \tag{19}$$

Since the Hamiltonian can be written as the sum $\hat{H}_x + \hat{H}_y + \hat{H}_z$, we can look for its eigenstates as products of Bloch waves along each direction:

$$\Psi_{\boldsymbol{n},\boldsymbol{q}}(\boldsymbol{r}) = \psi_{n_x,q_x}(x)\ \psi_{n_y,q_y}(y)\ \psi_{n_z,q_z}(z), \tag{20}$$

where the quasi-moment $\boldsymbol{q}$ is chosen in the first Brillouin zone, which is in this case a cube centered on 0 and of side $2\pi/a$.

As for the one-dimensional case, we can define Wannier functions associated to each site of the cubic lattice $\boldsymbol{j}a = (j_x, j_y, j_z)a$:

$$w_{\boldsymbol{n},\boldsymbol{j}}(\boldsymbol{r}) = \left(\frac{a}{2\pi}\right)^{3/2} \int_{\text{B.Z.}} \Psi_{\boldsymbol{n},\boldsymbol{q}}(\boldsymbol{r}) \mathrm{d}^3 q = w_{n_x,j_x}(x)\ w_{n_y,j_y}(y)\ w_{n_z,j_z}(z). \tag{21}$$

Similarly, we can define and calculate the matrix elements of the Hamiltonian for any pair of Wannier functions:

$$\langle w_{\boldsymbol{n},\boldsymbol{j}} | \hat{H} | w_{\boldsymbol{n}',\boldsymbol{j}'} \rangle = \int w_{\boldsymbol{n},\boldsymbol{j}}(\boldsymbol{r}) (\hat{H}_x + \hat{H}_y + \hat{H}_z) w_{\boldsymbol{n}',\boldsymbol{j}'}(\boldsymbol{r}) \mathrm{d}^3 r. \tag{22}$$

As in 1D, these coefficients are non-zero only if $\boldsymbol{n} = \boldsymbol{n}'$: the "hoppings" from one site to another can only occur within the same band, which is natural since these bands correspond to eigen-subspaces of the Hamiltonian. Another result, more surprising at first sight, appears when we evaluate (22): the hoppings can only be done along the axes of the lattice. Indeed, the matrix element (22) is written as the sum of three terms coming from the contributions of $\hat{H}_x$, $\hat{H}_y$, $\hat{H}_z$. The contribution of $\hat{H}_x$ for example reads:

$$\left(\int w_{n_x,j_x} \hat{H}_x w_{n_x,j_x'}\ \mathrm{d}x \right) \delta_{j_y,j_y'}\ \delta_{j_z,j_z'} = J_{n_x}(j_x - j_x')\ \delta_{j_y,j_y'}\ \delta_{j_z,j_z'}. \tag{23}$$

The hoppings along the diagonals of the lattice are of course present eventually in this description, but they result from combinations of hoppings along the x, y, z axes. This remark indicates that one should be careful of the apparently very intuitive character of Wannier functions: they are powerful computational tools, in particular in the case of the strongly-modulated potentials that we will study below, but they also have some confusing aspects; we will see another example later when we discuss the consequences of the phase arbitrariness of Bloch functions.

2 Strongly-modulated sinusoidal potential

Let us now turn to the practically important case of strongly-modulated potentials $V_0 \gg E_\mathrm{r}$. In this limit, the influence of the tunnelling effect, which allows a particle to jump from one well to a neighbouring well even if its energy is lower than V_0, is expected to become increasingly weak. If the tunnelling effect plays a negligible role, the energy levels are expected to be similar to those of each individual well, at least for energies $E \ll V_0$. The energy bands must therefore become thinner, to tend towards discrete energy levels.

2-1 Width of the allowed bands

The quantitative study of the eigenstates and the corresponding energies confirms this scenario. Let us start by looking at how the width W_n of the bands varies with V_0. This variation is plotted on figure 2 for the first four energy bands and we see a rapid decrease of W_n with V_0. In the limit of a large V_0, one can establish an approximate analytical expression for the width of the first few bands (Campbell 1955). In particular, we obtain for the lowest band an exponential decrease of the width with $(V_0/E_\mathrm{r})^{1/2}$:

$$\frac{W_0}{E_\mathrm{r}} \approx \frac{16}{\sqrt{\pi}} \left(\frac{V_0}{E_\mathrm{r}}\right)^{3/4} \exp\left[-2\left(\frac{V_0}{E_\mathrm{r}}\right)^{1/2}\right], \tag{24}$$

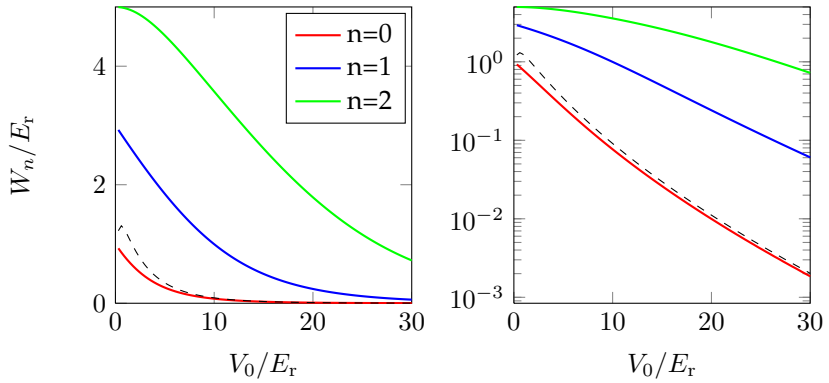

Figure 2. *Solid lines: width W_n of the first three energy bands of the sinusoidal potential as a function of V_0, in linear (left) and logarithmic (right) coordinates. The dashed curve is the asymptotic value (24) for the width of the lowest band.*

a prediction plotted as a dashed line in figure (2). The relative accuracy of this approximation is better than 20% as soon as $V_0 > 10E_r$.

2-2 Matrix elements of hopping between neighbours

This reduction in the width of the lowest bands is associated to an increasingly strong localization of the Wannier functions, that appears clearly on figure 1. This strong localization of the Wannier functions has itself a consequence on the hopping amplitudes $J_n(j)$ which characterize the Hamiltonian (13). If the Wannier functions $w_{n,0}(x)$ and $w_{n,j}(x)$ do not take significant values in the same regions of space, the hopping amplitude $J_n(j)$ given in (14) is negligible. More precisely, one can show that the amplitude $J_n(j)$ decreases exponentially with distance j, with the same characteristic distance as the Wannier function itself. As V_0/E_r increases, the amplitudes $J_n(j)$ ($j \geq 2$) for the "long-range" hoppings of length j therefore decrease faster than the amplitude $J_n(1)$ of the hoppings between nearest neighbours. We have plotted on figure 3 the variation of the matrix elements associated with the hoppings $J_0(j)$ as well as the ratios $J_0(j)/J_0(1)$ for the first values of j, limited to the lowest band $n = 0$. In particular we note that for $V_0 \gtrsim 10\,E_r$, all the matrix elements for "distant" hoppings, i.e. $j > 1$,

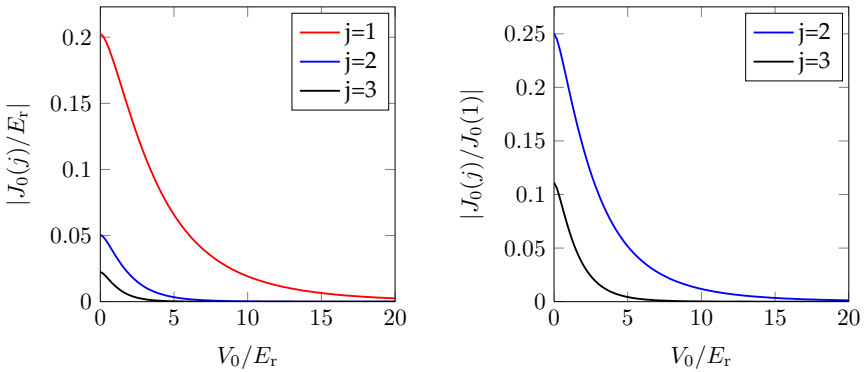

Figure 3. *Matrix elements associated with hoppings of length j, as a function of V_0.*

are less than 1% of the matrix element for a jump between nearest neighbours ($j = 1$). If we estimate that in this situation the amplitudes $J_0(j)$ ($j \geq 2$) can be neglected, then we realize the *tight-binding regime*, where the dynamics of the atoms in the lattice is governed almost exclusively by the jumps between nearest neighbours.

When the width of $w_{0,0}(x)$ becomes very small compared to the period a of the potential, at most one term of the sum (5) contributes at a given point x. We deduce that in this asymptotic case, the probability distribution $|\psi_{n,q}(x)|^2$ does not depend on q and is approximately equal to the sum of the probability distributions of the Wannier functions.

2-3 Tight-binding spectrum

Let us consider the limiting case of a very large V_0, for which the tunnelling effect between neighbouring sites becomes very weak, at least for the lowest energy bands. We can then study the spectrum of the motion of a particle by linearizing the trapping potential at the vicinity of the minimum of potential, which reads for the well centered at $x = 0$:

$$kx \ll 1 \quad \Rightarrow \quad V(x) \approx V_0 k^2 x^2. \tag{25}$$

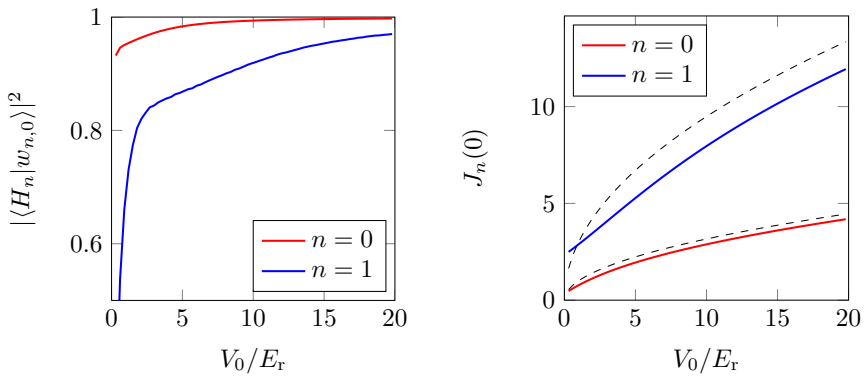

Figure 4. *Left: overlap $|\langle H_n|w_{n,0}\rangle|^2$ between the Wannier functions $w_{n,0}(x)$ and the Hermite functions $H_n(x)$. Right: average energies $\bar{E}_n = J_n(0)$, compared to the expected value for a harmonic well $(n+1/2)\hbar\omega$.*

In fact, for $|kx| = 1/2$, this harmonic approximation is valid with a precision of 10%. We then obtain a harmonic oscillator Hamiltonian of frequency ω such that

$$\hbar\omega = 2\sqrt{V_0 E_\mathrm{r}}, \tag{26}$$

with the spectrum $(n+1/2)\hbar\omega$. A necessary condition for this harmonic approximation to be valid for the first levels of the oscillator is that the extent of the ground state

$$a_\mathrm{ho} = (\hbar/m\omega)^{1/2} \tag{27}$$

verifies the hypothesis of (25), $ka_\mathrm{ho} \ll 1$, which can also be written as

$$ka_\mathrm{ho} = (E_\mathrm{r}/V_0)^{1/4} \ll 1. \tag{28}$$

We then have the inequalities:

$$E_\mathrm{r} \ll \hbar\omega \ll V_0. \tag{29}$$

The (arbitrary) criterion $ka_\mathrm{ho} \leq 1/2$ leads to $V_0/E_\mathrm{r} \geq 16$, or $\omega \geq 8\omega_r$. With this "minimal" constraint, we find two bound states ($E_0 \approx 4E_\mathrm{r}$, $E_1 \approx 12\,E_\mathrm{r}$) inside each potential well.

On figure 4 (left) we have plotted the modulus square of the scalar product between the Wannier function $w_{n,0}(x)$ and the expected state for a harmonic potential, the Hermite function $H_n(x)$ for $n = 1, 2$. For the lowest band, this overlap very quickly takes values close to 1 (> 0.97 for $V_0/E_\mathrm{r} > 3$). Figure 4 (right) compares the average energies of the first two bands $\bar{E}_n = J_n(0)$, with the prediction $(n+1/2)\hbar\omega$. The actual average energies are lower than the harmonic prediction (by an amount $\sim E_\mathrm{r}$), which is well explained by considering the first "sub-harmonic" correction in the potential $\sin^2(kx)$.

In the following, we will frequently use the approximate expression for the Wannier function of the lowest band $w_{0,0}(x) \approx H_0(x)$, which is explicitly written

$$w_{0,0}(x) \approx \frac{1}{(\pi a_\mathrm{ho}^2)^{1/4}}\, \mathrm{e}^{-x^2/(2\,a_\mathrm{ho}^2)}. \tag{30}$$

3 Hubbard Hamiltonian

In the case of a strongly-modulated potential, one can often limit oneself to considering the states of the lowest band. This considerably reduces the Hilbert space and allows to greatly simplify the notations and the calculations. We will detail here the main ingredients of this approach on the very simple case of the potential $V_0 \sin^2(kx)$ that we have considered until now. We will see how to introduce interactions in this formalism and we will illustrate their role on a remarkable experiment, the demonstration of bound pairs of atoms, although these atoms interact repulsively.

Note that the sinusoidal potential considered in this paragraph has the particularity of having only one site in its unit cell, which makes the treatment of the one-particle physics very simple. We will come back later to this Hubbard model in the slightly more complicated (and richer) case of two-site unit cells.

3-1 The one-particle Hamiltonian (no interaction)

Let us then place ourselves in this approximation and additionally assume that only the matrix elements $J_{n=0}(j=0)$ (on site) and $J_{n=0}(j=1)$ (between nearest neighbours) take significant values. The term $\bar{E}_0 = J_0(0)$ is a constant that represents the on-site energy, which we will shift from now on to $\bar{E}_0 = 0$. We define

$$J = -J_{n=0}(j=1), \quad J \text{ positive}, \tag{31}$$

and the Hamiltonian is then very simple

$$\hat{H} = -J\left(\hat{T} + \hat{T}^\dagger\right) \tag{32}$$

where $\hat{T}$ is the operator that translates the particle by one site to the right:

$$\hat{T} = \sum_{j\in\mathbb{Z}} |w_{j+1}\rangle\langle w_j|. \tag{33}$$

We have noted the Wannier functions $w_j \equiv w_{0,j}$ since we limit our state space to the band $n = 0$. We will also use the expression of the same Hamiltonian in second quantization:

$$\hat{H} = -J\sum_j \hat{b}^\dagger_{j+1}\hat{b}_j \ + \text{h.c.}, \tag{34}$$

where $\hat{b}^\dagger_j$ creates a particle at site j with wave function $w_j(x)$.

In this one-band Hubbard model, shown schematically in Figure 5, the only periodic function on the lattice is:

$$|u\rangle = \sum_j |w_j\rangle \tag{35}$$

and the Bloch states thus have the form

$$|\psi_q\rangle = \sum_j \mathrm{e}^{\mathrm{i}jaq}|w_j\rangle. \tag{36}$$

If we transfer this form into the eigenvalue equation for the Hamiltonian, we obtain the very simple equation

$$-J\left(\mathrm{e}^{\mathrm{i}aq} + \mathrm{e}^{-\mathrm{i}aq}\right) = E \tag{37}$$

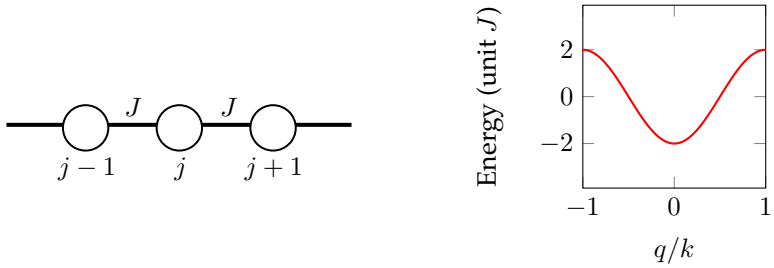

Figure 5. *Schematic representation of the 1D Hubbard model described by the Hamiltonian (34) on the left, and the corresponding spectrum on the right [cf. eq. (38)].*

i.e.

$$E(q) = -2J\cos(aq), \tag{38}$$

The spectrum $E_0(q) \equiv E(q)$ of the lowest band is sinusoidal in this case, which was to be expected since we keep only one of its Fourier components in (17).

The lowest band has width[3] $4J$. This width can be identified with the approximate expression (24) obtained in the limit $V_0 \gg E_\mathrm{r}$, which provides the approximate expression of J

$$\frac{J}{E_\mathrm{r}} \approx \frac{4}{\sqrt{\pi}}\left(\frac{V_0}{E_\mathrm{r}}\right)^{3/4} \exp\left[-2\left(\frac{V_0}{E_\mathrm{r}}\right)^{1/2}\right]. \tag{39}$$

3-2 The sign of the tunnelling coefficient

We have indicated in the definition of the tunnel matrix element J of the tight-binding model [*cf.* (31)] that this coefficient is always positive. This leads the Bloch state $|\psi_{q=0}\rangle$, of energy $-2J$, to be the ground state of the particle on the lattice. On the contrary, if J were negative, the ground state would be $|\psi_{q=k}\rangle$, of energy $+2J$.

[3] In the square case in 2D (cubic in 3D), each atom has 4 (6) nearest neighbours, and the width of this band becomes $8J$ ($12J$).

To prove this property, let us use the Sturm–Liouville theorem. Let us restrict ourselves to a lattice of finite size L (multiple of a). Since the potential $V(x)$ is regular, we know that we can classify the eigenstates of the Hamiltonian by increasing energy according to the number of their nodes: the ground state has no node, the first excited state has one node, etc. In a double well for example, the antisymmetric state is always above the symmetric state in energy. Now the function $\psi_k(x)$ at the edge of the band verifies

$$\psi_k(x) = \sum_j (-1)^j w_j(x) \quad \Rightarrow \quad \psi_k(x+a) = -\psi_k(x). \tag{40}$$

This function necessarily cancels between 0 and a. On the segment of length $L = Na$, it has at least N nodes and cannot be the ground state. J cannot therefore be negative. We will see later that this conclusion can be invalidated if we extend the class of available Hamiltonians by considering potentials that are explicitly time-dependent.

3-3 Interactions in the Hubbard model

Let us now describe how the interactions between particles are taken into account in this tight-binding model, when the dynamics is restricted to the lowest band. We will take the example of spinless bosons, but the formalism extends without difficulty to the case of a gas of non-polarized fermions.

The short-range interaction Hamiltonian (s-wave for bosons) reads, in the pseudo-potential approximation

$$\hat{H}_{\rm int} = \frac{g}{2} \int \hat{\Psi}^\dagger(x)\, \hat{\Psi}^\dagger(x)\, \hat{\Psi}(x)\, \hat{\Psi}(x) \mathrm{d}x, \tag{41}$$

where the field operator $\hat{\Psi}(x)$ destroys a particle at point x. This operator is written in terms of Wannier functions

$$\hat{\Psi}(x) = \sum_{n,j} w_{n,j}(x)\, \hat{b}_{n,j}. \tag{42}$$

When we use this expansion in (41), we obtain a complicated expression, involving terms that couple the different bands and sites of the lattice:

$$\begin{aligned} \hat{H}_{\rm int} &= \frac{g}{2} \sum_{n_1,j_1} \sum_{n_2,j_2} \sum_{n_3,j_3} \sum_{n_4,j_4} \hat{b}^\dagger_{n_3,j_3} \hat{b}^\dagger_{n_4,j_4} \hat{b}_{n_1,j_1} \hat{b}_{n_2,j_2} \\ &\times \int w_{n_1,j_1}(x)\, w_{n_2,j_2}(x)\, w_{n_3,j_3}(x)\, w_{n_4,j_4}(x)\, \mathrm{d}x\,. \end{aligned} \tag{43}$$

However, for a deep lattice ($V_0 \gg E_{\rm r}$) and if we exclude the vicinity of a Feshbach resonance, the interaction energy per atom remains small compared to the gap $\hbar\omega$ between the lowest band and the first excited band. This leads to two successive simplifications:

- We can restrict the development of $H_{\rm int}$ to the lowest band $n = 0$, as we did for the kinetic energy. The sum over n_1, n_2, n_3, n_4 disappears from (43) and we keep only the term $n_1 = n_2 = n_3 = n_4 = 0$.
- As soon as the depth of the lattice exceeds about ten $E_{\rm r}$, the overlap between two Wannier functions on two different sites, $w_{0,j}(x)$ and $w_{0,j'}(x)$, becomes very small (see figure 1). The integral on x appearing in (43) thus takes values significantly different from 0 only if all the indices j appearing there are equal to each other. The resulting integral
$$\int w^4_{0,j}(x)\, \mathrm{d}x \tag{44}$$
is then independent of j, since the function $w_{0,j}$ is simply the translation of $w_{0,0}$ by the distance ja.

The development of $\hat{H}_{\rm int}$ is then considerably simplified. Only the terms describing on-site interactions remain and the result is written:

$$\hat{H}_{\rm int} \approx \frac{U}{2} \sum_j \hat{n}_j\, (\hat{n}_j - 1)\,, \tag{45}$$

where we have introduced the particle number operator on site j, $\hat{n}_j = \hat{b}^\dagger_j \hat{b}_j$ and where we have used $\hat{b}^\dagger_j \hat{b}^\dagger_j \hat{b}_j \hat{b}_j = \hat{b}^\dagger_j \hat{b}_j \hat{b}^\dagger_j \hat{b}_j - \hat{b}^\dagger_j \hat{b}_j = \hat{n}^2_j - \hat{n}_j$. Note that we have omitted here to write the band index n since we restrict ourselves to $n = 0$. The energy U is the energy required to put two atoms on the same

site; it can be written explicitly as

$$U = g \int w_{0,0}^4(x)\, \mathrm{d}x \approx \frac{g}{\sqrt{2\pi}\, a_{\mathrm{ho}}}, \tag{46}$$

where we have used the Gaussian approximation (30) for the Wannier function of the lowest band.

As we have indicated, the formalism presented here concerns spinless bosons. Let us indicate without demonstration (it is simple to establish) how the expression (45) is modified for a gas of fermions with spin 1/2, still with short-range interactions:

$$\hat{H}_{\mathrm{int}} \approx U \sum_j \hat{n}_{j,\uparrow} \hat{n}_{j,\downarrow}. \tag{47}$$

The operators $\hat{n}_{j,\uparrow}$ and $\hat{n}_{j,\downarrow}$ have eigenvalues 0 and 1, since we cannot put more than one fermion in a given state, in this case the Wannier function w_j with a given spin state.

The above calculations have been carried out for a 1D lattice. They can directly be transposed to the 3D case for a cubic lattice and we obtain

$$U^{(3D)} = \frac{g^{(3\mathrm{D})}}{(\sqrt{2\pi}\, a_{\mathrm{ho}})^3}. \tag{48}$$

The coupling $g^{(3\mathrm{D})}$ is expressed in terms of the scattering length a_{sc} as

$$g^{(3\mathrm{D})} = \frac{4\pi\hbar^2 a_{\mathrm{sc}}}{m}, \tag{49}$$

and (48) is then written

$$\frac{U^{(3\mathrm{D})}}{E_{\mathrm{r}}} = \sqrt{\frac{8}{\pi}}\, k a_{\mathrm{sc}} \left(\frac{V_0}{E_{\mathrm{r}}}\right)^{3/4}. \tag{50}$$

Let us now discuss the value of this coefficient U. We will conduct this discussion in the 3D case since we have the explicit expression (50) at our disposal. Away from a Feshbach resonance, the scattering length is on the nanometer scale (3 nm for ^{23}Na, 5 nm for ^{87}Rb). Since the light used for the lattice has a micrometer wavelength λ, the product $k a_{\mathrm{sc}} = 2\pi a_{\mathrm{sc}}/\lambda$ is small, between 10^{-2} and 10^{-1}. The product V_0/E_{r} usually does not exceed a few tens: beyond this value, the tunnelling effect between sites becomes completely negligible and the lattice is only a collection of independent traps. The coefficient U is therefore in general smaller than the recoil energy. Recall that it is important that $U n_j(n_j-1)/2$ remains small compared to $\hbar\omega = 2\sqrt{V_0 E_{\mathrm{r}}}$ for the restriction to the lowest band to be valid.

Despite this relatively low value U, the interactions play a considerable role and cause the apparition of a strongly correlated ground state (Jaksch, Bruder, et al. 1998). To understand this point, one must compare the strength of these interactions, characterized by U, to the kinetic energy, characterized by the tunnelling coefficient J. The N-body effects become important when the interactions exceed the kinetic energy, and this can happen for relatively shallow lattices, because the coefficient J decreases exponentially with V_0/E_{r} [cf. eq. (39)].

In summary, the implementation of an optical lattice allows to cumulate two effects favouring N-body physics:

- It strongly reduces the kinetic energy term, thanks to the exponential decrease of J with V_0/E_{r} [cf. eq. (39)].
- It moderately increases the interaction term, thanks to the power-law growth of U with V_0/E_{r} [cf. eq. (50)].

3-4 Illustration : the repulsively bound pairs

This competition between kinetic energy and interaction energy has been demonstrated in optical lattices many times in the last ten years[4]. The most famous manifestation is probably the phase transition between the superfluid and the Mott insulator regimes at a critical value of the ratio U/J, for

[4] This competition also occurs in a uniform gas; for a fluid of density ρ, corresponding to an average distance between particles $\ell = \rho^{-1/3}$, we can evaluate a characteristic kinetic energy $\hbar^2/(m\ell^2)$. This energy must be compared to the interaction energy which is $\hbar^2 a_{\mathrm{sc}}\rho/m$, up to a multiplicative factor. The ratio between these two energies scales as $(\rho a_{\mathrm{sc}}^3)^{1/3}$. When this parameter is small compared to 1 (dilute gas), a description in terms of the mean-field Gross–Pitaevskii equation is a good approximation, whereas the fluid becomes strongly correlated when this parameter becomes of order unity.

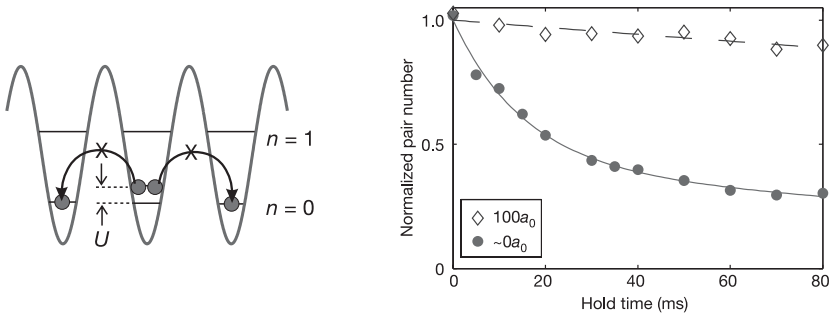

Figure 6. *Left: principle of the experiment of Winkler, Thalhammer, et al. (2006): atoms in repulsive interaction are prepared on the same site of a lattice. If the interaction is strong enough, the atoms remain together in spite of the repulsion. Right: evolution of the number of pairs in the presence of repulsion (scattering length of 5 nm, i.e.*$100\,a_0$*) and in the absence of repulsion (zero scattering length). Figures extracted from Winkler, Thalhammer, et al. (2006).*

a given filling of the lattice, for example one atom per site (Fisher, Weichman, et al. 1989; Jaksch, Bruder, et al. 1998; Greiner, Mandel, et al. 2002). We will describe this phenomenon in detail in a future lecture.

Here, we will illustrate this competition with a phenomenon that is simpler to describe theoretically, which concerns the existence of bound pairs in the presence of repulsive interactions (cf. figure 6). This phenomenon has been demonstrated and interpreted by the Innsbruck group (Winkler, Thalhammer, et al. 2006). We start with a gas of Rb_2 molecules, prepared at the vicinity of a Feshbach resonance (at $\sim 1000\,$G). These molecules are trapped at the minima of a high-intensity cubic optical lattice, with a relatively low filling (~ 0.3). At a given time, we lower the depth of the lattice along one direction to allow the tunnelling effect along this axis. At the same time the magnetic field is moved away from the Feshbach resonance, which has the effect of dissociating the pairs. The interaction between the two atoms that formed the pair becomes repulsive and is characterized by the scattering length $a_{\rm sc} = +5\,$nm (about 100 Bohr radii a_0). One would naively expect that the stronger the repulsion, the faster the pair of atoms would separate. This is not the case, as can be seen on figure 6. While the pairs separate quite quickly if the coefficient U is zero, a strong repulsion keeps them together!

The explanation of this phenomenon is simple, at least qualitatively. The bound pair has an energy U; if this energy is large compared to the bandwidth $4J$ (or rather $8J$ because each atom of the pair has access to a band of width $4J$), then this interaction energy cannot be converted into kinetic energy.

The exact expression of the corresponding bound state can be determined quite easily (Winkler, Thalhammer, et al. 2006). The Hubbard Hamiltonian of the two atoms (which we assume here to be distinguishable) in the lattice is written

$$\begin{aligned}\hat{H} &= -J\left(\hat{T}(1)+\hat{T}^\dagger(1)\right) - J\left(\hat{T}(2)+\hat{T}^\dagger(2)\right) \\ &\quad +U\sum_{j_1,j_2}\delta_{j_1,j_2}|w_{j_1},w_{j_2}\rangle\langle w_{j_1},w_{j_2}|, \end{aligned} \tag{51}$$

where we define $|w_{j_1},w_{j_2}\rangle$ as the state where atom 1 occupies site w_{j_1} and atom 2 occupies site w_{j_2}. The operator $\hat{T}(\alpha)$, already introduced above, shifts particle α by one site to the right.

As always in a two-body problem, it is useful to introduce the variables of the center of mass and the relative coordinate. Let us define

$$c = j_1 + j_2, \quad r = j_1 - j_2, \quad |c,r\rangle \equiv |w_{j_1},w_{j_2}\rangle, \tag{52}$$

so that the position of the center of mass is $ac/2$ (multiple or half-multiple of a). The Hamiltonian is rewritten in terms of these new variables:

$$\hat{H} = -J\,\left(\hat{T}(c)+\hat{T}^\dagger(c)\right)\otimes\left(\hat{T}(r)+\hat{T}^\dagger(r)\right) + U\,\hat{1}_c\otimes\hat{\mathcal{P}}_0. \tag{53}$$

where $\hat{T}(c)$ and $\hat{T}(r)$ are the jump operators by one site to the right, respectively for the center of mass and for the relative position, and where $\hat{\mathcal{P}}_0$ is the projector on the $|r=0\rangle$ state, corresponding to the case when both atoms are on the same site:

$$\hat{\mathcal{P}}_0 \;=\; |r=0\rangle\langle r=0|. \tag{54}$$

At a fixed r, the motion of the center of mass described by (53) is that of a free particle on a lattice and its eigenstates are Bloch waves

$$|\Psi_q\rangle = \sum_{c\in\mathbb{Z}} \mathrm{e}^{\mathrm{i}caq/2}|c\rangle. \tag{55}$$

We will therefore look for the eigenstates of $\hat{H}$ in the form

$$|\Psi_q\rangle \otimes |\Phi\rangle, \quad \text{with} \quad |\Phi\rangle = \sum_{r\in\mathbb{Z}} \alpha_r |r\rangle. \tag{56}$$

Let us specify the domain in which the quasi-moment q can be chosen for the motion of the center of mass. Looking at expression (55) in which c is an integer, the interval $-\pi < qa/2 \leq \pi$ (of length $4\pi/a$) would seem natural. In fact, we can reduce this interval by a factor of 2 by noticing that

$$|\Psi_q\rangle \otimes |\Phi\rangle = |\Psi_{q\pm 2\pi/a}\rangle \otimes |\tilde{\Phi}\rangle, \quad \text{with} \quad |\tilde{\Phi}\rangle = \sum_r (-1)^r \, \alpha_r \, |r\rangle, \tag{57}$$

this identity coming from $(-1)^c = (-1)^{j_1+j_2} = (-1)^{j_1-j_2} = (-1)^r$. To avoid any double counting, we will restrict the values of q to the interval

$$-\frac{\pi}{a} < q \leq \frac{\pi}{a}. \tag{58}$$

Let us now use the form (56) in the eigenvalue equation for the Hamiltonian (53). For a given value of q, we obtain:

$$-J_q \left(\hat{T}(r) + \hat{T}^\dagger(r)\right) |\Phi\rangle + U\hat{\mathcal{P}}_0|\Phi\rangle = E\,|\Phi\rangle, \tag{59}$$

where we have defined

$$J_q = 2J\cos(qa/2). \tag{60}$$

This equation is translated in terms of the coefficients α_j of the development of $|\Phi\rangle$:

$$\begin{aligned} j \neq 0 \quad & -J_q\,(\alpha_{j+1} + \alpha_{j-1}) = E\,\alpha_j \\ j = 0 \quad & -J_q\,(\alpha_1 + \alpha_{-1}) = (E-U)\,\alpha_0. \end{aligned} \tag{61}$$

This system admits two types of solutions: (i) scattering (unbound) states for which α_j is a trigonometric function of j, (ii) a bound state, for which α_j decreases exponentially with $|j|$. It is this second type of solution that interests us here. We can simply check that

$$\alpha_j = \alpha_0 \, \mathrm{e}^{-\beta|j|} \, (-1)^j \tag{62}$$

is solution of the system (61) if we take

$$E_q = \left[U^2 + 4J_q^2\right]^{1/2}, \qquad \beta_q = \ln\left[2J_q/(E_q - U)\right]. \tag{63}$$

For each value of the quasi-momentum q of the center of mass, there is therefore a bound state of the pair of atoms. The energy of this bound state is as expected on the order of U if we choose $U \gg J$. Since this bound state is an eigenstate of the Hamiltonian, a pair of particles prepared in this state will remain there indefinitely, even if its energy is higher than that of the continuum of scattering states (the energy band of width $4J$).

4 The case of a super-lattice

The simplicity of the definition of Wannier functions for the sinusoidal lattice is a bit misleading. For more complicated lattices, for example potentials with several local minima per period a, it is not always obvious to choose the "good" basis of Wannier functions, corresponding to the intuition of wave functions localized around these local minima.

We will not describe here the general principles to find these maximally localized Wannier functions. One can refer to the recent review article by Marzari, Mostofi, et al. (2012) on this subject. In the following, we will only state the nature of the problem and illustrate it on a simple example.

4-1 The arbitrariness of the phase

The required property for Bloch functions is to form a normalized eigenstate basis of the Hamiltonian and the translation operator. In the absence of degeneracy (at least in 1D), they are therefore defined up to a phase: one can multiply $\psi_{n,q}(x)$ by a phase factor $\mathrm{e}^{\mathrm{i}\theta_n(q)}$ while still satisfying this property[5].

While this phase arbitrariness has no effect on the spatial variation of Bloch functions, it can have a considerable influence on the shape of the

[5] We have indicated earlier that we required Bloch functions to be periodic in q, $\psi_{n,q+2\pi/a} = \psi_{n,q}$, which leads $\theta_n(q)$ to be also periodic in q.

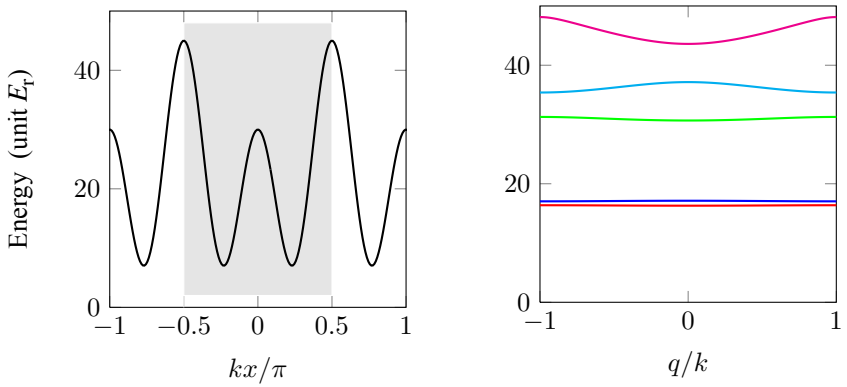

Figure 7. *Left: superlattice $V(x)/E_r = 15[\sin^2(kx) + 2\cos^2(2kx)]$. The shaded area represents the central unit cell, located between $kx/\pi = -1/2$ and $kx/\pi = 1/2$ (i.e. between $x = -a/2$ and $x = a/2$). Right: band spectrum for this superlattice. The two lowest bands, almost flat, are well separated from the rest of the spectrum.*

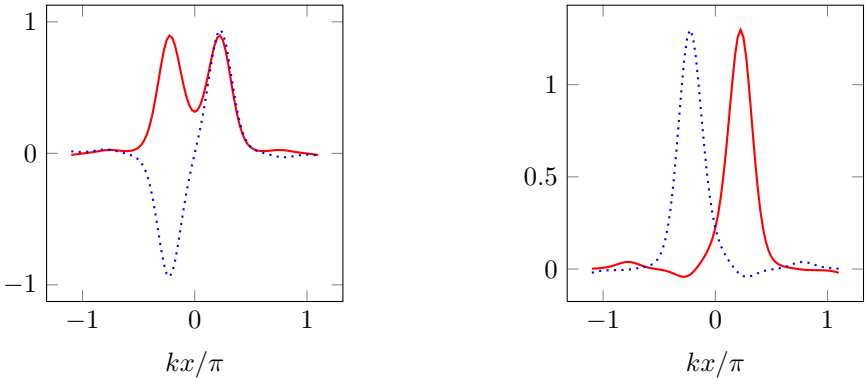

Figure 8. *Left: Wannier functions $w_0(x)$ (red solid line) and $w_1(x)$ (blue dashed line) associated with the two lowest bands of the superlattice in figure 7. Right: localized Wannier functions w_A and w_B, obtained by sum and difference of w_0 and w_1.*

Wannier function

$$w_{n,0}(x) = \left(\frac{a}{2\pi}\right)^{1/2} \int_{-\pi/a}^{+\pi/a} \psi_{n,q}(x)\, \mathrm{d}q. \tag{64}$$

We can therefore exploit this arbitrariness of phase to construct a basis of Wannier functions while optimizing a given criterion.

4-2 Mixing different bands

A second subtlety in the construction of the Wannier function basis appears when the spectrum of the Hamiltonian is composed of several energy bands close to one another, which are well separated from the rest of the spectrum. It is then interesting to mix the Wannier functions coming from these bands to build the best adapted functions for the considered problem.

Let us illustrate this point on the case of a superlattice, obtained by superimposing the sinusoidal potential $V_0 \sin^2(kx)$ with a potential of half periodicity $V_1 \cos^2(2kx)$. This potential, plotted on figure 7 with $V_1 = 2\,V_0$, presents two local minima in the period $a = \pi/k$. The band spectrum associated with this potential is plotted on figure 7 for $V_0 = 15\,E_r$. We can clearly see that the two lowest bands $n = 0$ and $n = 1$ form a narrow doublet, separated from the upper bands by a large gap.

If we follow the procedure described earlier in this chapter, in particular equation (64), we will construct a Wannier function for each band, in particular a Wannier function $w_0(x)$ for the band $n = 0$ and a Wannier function $w_1(x)$ for the band $n = 1$. These Wannier functions w_0 and w_1 are plotted in figure 8; they are respectively symmetric and antisymmetric, just like the well-known eigenstates for a single double-well.

In many cases, these symmetric and antisymmetric Wannier functions are not the best suited to model the problem. If we want to perform a Hubbard-type treatment for example, we prefer to have basis vectors corresponding to an atom located in the left (A) or right (B) well of the unit cell. For our example, the solution is simple: we can define the correspond-

ing Wannier functions from the mixture of the bands $n = 0$ and $n = 1$:

$$w_A(x) = \frac{1}{\sqrt{2}}\left(w_0(x) - w_1(x)\right), \quad \text{located on the left,} \tag{65}$$

$$w_B(x) = \frac{1}{\sqrt{2}}\left(w_0(x) + w_1(x)\right), \quad \text{located on the right.} \tag{66}$$

These two functions are plotted on the right side of figure 8.

In this particular case, the mixing of the bands is done in a natural way. In more complicated cases, one has to identify the proper minimizer that leads to the optimal hybridization regarding the localization of these Wannier functions (Marzari, Mostofi, et al. 2012).

4-3 The tight-binding Hamiltonian for the superlattice

Once the Wannier functions w_A and w_B have been identified, we can look for the eigenstates of the Hamiltonian in the tight-binding limit, now restricting ourselves to the two lowest bands. As above, we will consider in the following only jumps between nearest neighbours.

The Hamiltonian is thus written

$$\hat{H} = -J\sum_j |w_{B,j}\rangle\langle w_{A,j}| - J'\sum_j |w_{A,j+1}\rangle\langle w_{B,j}| + \text{h.c.} \tag{67}$$

The first term describes the tunnelling rate through the low barrier in figure 7, and the second term describes the rate through the high barrier. A schematic representation of this tight-binding model is given in figure 9.

The unit cell of this problem has two sites, A and B, and the relevant periodic functions therefore have the form

$$|u_q\rangle = \alpha_q\left(\sum_j |w_{A,j}\rangle\right) + \beta_q\left(\sum_j |w_{B,j}\rangle\right), \tag{68}$$

where α_q and β_q are for now arbitrary coefficients. Let us write that the Bloch function

$$|\psi_q\rangle = \sum_j \mathrm{e}^{\mathrm{i}jaq}\left(\alpha_q|w_{A,j}\rangle + \beta_q|w_{B,j}\rangle\right) \tag{69}$$

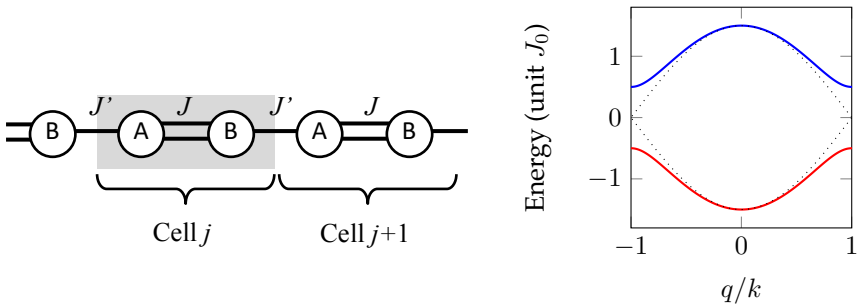

Figure 9. *Left: discretized version of the superlattice shown in figure 7. Right: band spectrum (71) obtained for $J = J_0$, $J' = J_0/2$. The dotted lines represent the result obtained for $J = J' = 3/4\, J_0$.*

is eigenstate of the Hamiltonian (67). We project the eigenvalue equation onto the two functions $|w_{A,j}\rangle$ and $|w_{B,j}\rangle$ of any site j, and we obtain an eigenvalue equation for a 2×2 Hermitian matrix $\hat{\mathcal{H}}(q)$ (Hamiltonian in reciprocal space)

$$\hat{\mathcal{H}}(q)\begin{pmatrix}\alpha_q\\ \beta_q\end{pmatrix} = E\begin{pmatrix}\alpha_q\\ \beta_q\end{pmatrix}, \qquad \hat{\mathcal{H}}(q) = -\begin{pmatrix}0 & J + J'\mathrm{e}^{-\mathrm{i}aq}\\ J + J'\mathrm{e}^{\mathrm{i}aq} & 0\end{pmatrix}. \tag{70}$$

The eigenvalues of $\hat{\mathcal{H}}(q)$ are

$$E(q) = \pm\left|J + J'\mathrm{e}^{\mathrm{i}aq}\right| = \pm\left(J^2 + J'^2 + 2JJ'\cos(aq)\right)^{1/2}. \tag{71}$$

Except for the case $J = J'$ where this model in fact corresponds to the tight-binding model with one site that we have studied in 3, we find two[6] subbands separated by a gap $2|J - J'|$. The opening of this gap is called *Peierls instability*: a 1D crystal with one electron per ion is unstable because its energy can be lowered by distorting it as in figure 9, so as to form both strong and weak bonds. This type of Hamiltonian obtained with a superlattice has been studied experimentally by several groups, in particular the Bloch group in Munich (Fölling, Trotzky, et al. 2007) [see figure 10] and the Porto group at NIST (Lee, Anderlini, et al. 2007).

[6] The number of subbands is equal to the dimension of the matrix $\hat{\mathcal{H}}(q)$, which is itself equal to the number of sites in the unit cell of the lattice.

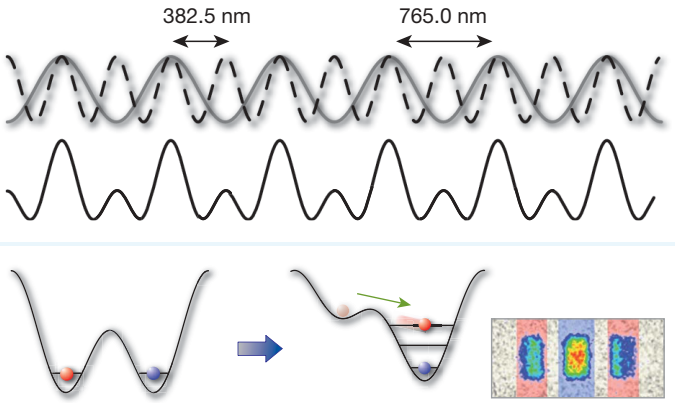

Figure 10. *Superlattice realized by the Munich group for rubidium atoms. By controlling the intensity and the relative phase of the two light waves creating the lattice, one can deform the superlattice into a regular lattice, with the atoms in the B wells ending up in the lowest band $n = 0$ of the final lattice, and the atoms in the A wells spilling out into the band $n = 2$. The band mapping technique seen in chapter 2 then allows the counting of the respective populations of these two types of wells. Figures extracted from Fölling, Trotzky, et al. (2007), see also Sebby-Strabley, Brown, et al. (2007) and Lee, Anderlini, et al. (2007).*

4-4 Flat bands

As an illustration, we describe here another remarkable aspect of this multi-site tight-binding model, which is the emergence of completely flat energy bands. We stay in one dimension and consider the sawtooth lattice shown in figure 11. This lattice is characterized by three different tunnelling coefficients J, J', J''. The unit cell still contains two sites, and the Hamiltonian in reciprocal space is written

$$\hat{\mathcal{H}}(q) = -\begin{pmatrix} 0 & J' + J''\mathrm{e}^{-\mathrm{i}aq} \\ J' + J''\mathrm{e}^{\mathrm{i}aq} & 2J\cos(aq) \end{pmatrix}. \tag{72}$$

The diagonalization of this matrix gives two subbands $E_\pm(q)$ which are roots of trigonometric functions of qa. Their expression simplifies considerably in the case

$$J' = J'' = \sqrt{2}\, J. \tag{73}$$

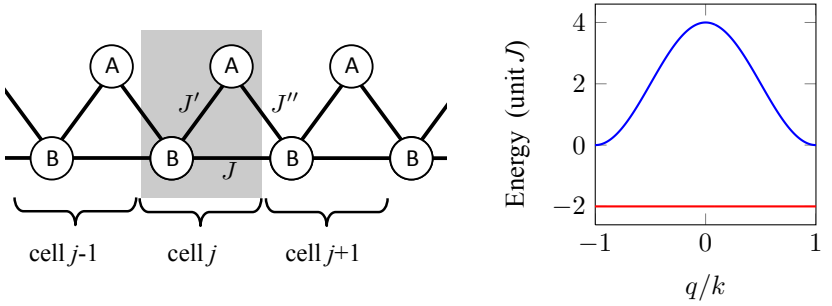

Figure 11. *A two-site array featuring a flat lowest band for $J' = J'' = \sqrt{2}\, J$. The energy bands are plotted for $J < 0$.*

and we find

$$E_+(q) = 2J, \qquad E_-(q) = -2J\,[1 + \cos(aq)]\,. \tag{74}$$

One of the energy bands is completely flat! The corresponding effective mass is therefore infinite, which means that an atom prepared in this band will remain indefinitely where it is, without its wave packet undergoing any spreading in real space. If we take the usual sign ($J > 0$) for the tunnelling coefficient, the flat band is the first excited band. We will see later that it is possible to change the sign of J by modulating the lattice temporally, which allows us to have this flat band as the lowest band.

The physical interpretation of these non-diffusive states is simple. One can explicitly write localized states which do not evolve, due to an interference phenomenon. There is such a state[7] for each lattice cell, and one of them is represented on figure 12 :

$$|\psi_j^{(\mathrm{loc})}\rangle = \frac{1}{2}\left(|w_{A,j-1}\rangle + |w_{A,j}\rangle - \sqrt{2}\,|w_{B,j}\rangle\right). \tag{75}$$

In order to spread out starting from such a "V-state", the particle should go on one of the two sites $|w_{B,j\pm1}\rangle$. But the signs in the expression of the state (75) and the ratio $\sqrt{2}$ chosen between the coefficients J and $J' = J''$ make the transition amplitude from $|\psi_j^{(\mathrm{loc})}\rangle$ to each of these two states vanish.

[7] The states (75) are not orthogonal to each other, but one can construct an orthogonal basis of Wannier functions for this problem [see Huber & Altman (2010)].

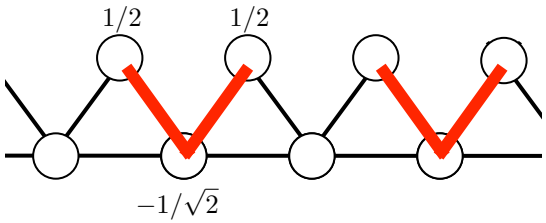

Figure 12. *Representation of the non-diffusive V-state given in (75). For a lattice with N sites* (i.e. *$N/2$ elementary cells), one can place $N/4$ atoms in these states without any spatial overlap between the various occupied states. For a higher filling and in the presence of interactions, the ground state is a Luttinger liquid (Huber & Altman 2010).*

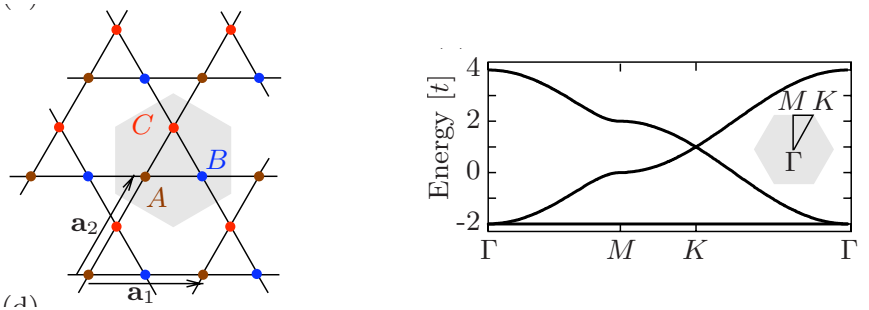

Figure 13. *Left: Kagome lattice. The unit cell contains 3 sites A, B, C. All tunnelling matrix elements between nearest neighbours are equal. The diagonalization of the Hamiltonian in the reciprocal space (77) shows that the lowest band (for a positive tunnel coefficient) is flat. The corresponding spectrum is shown on the right for $J < 0$, a choice for which the flat band is the lowest band. Figures taken from Huber & Altman (2010).*

In addition to the elegant character of this quantum interference effect, these flat bands are very interesting for the search of strongly correlated states. We indicated above that the interesting regime of the N-body problem appears when the interaction energy between particles becomes of the order of the kinetic energy. In the present model, the kinetic energy (given by the bandwidth) is zero. The ground state of the system is then governed only by the interactions, at least as long as the interaction energy remains smaller than the gap between the flat band and the first (dispersive) excited band.

A natural question is to determine the ground state of N bosons prepared in such a band. Without interactions, there is no condensation since all single-particle states have the same energy. With repulsive interactions, a transition occurs when the density becomes greater than $1/4$ atom per site, in which case there is necessarily an overlap between the V-states arranged on the lattice. The high density state is a *Luttinger liquid* phase, analyzed analytically and numerically in Huber & Altman (2010).

As an exercise, one can study a similar problem (from the point of view of single-particle physics) in two dimensions. A well suited configuration is the *Kagome lattice* represented in figure 13. It is obtained by tiling the plane with the translation of a unit cell according to a triangular lattice generated by the vectors

$$\boldsymbol{a}_1 = a\,\boldsymbol{u}_x, \qquad \boldsymbol{a}_2 = a\left(\frac{1}{2}\boldsymbol{u}_x + \frac{\sqrt{3}}{2}\boldsymbol{u}_y\right). \tag{76}$$

The unit cell has three sites noted A, B, C coupled by tunnelling. All matrix elements between nearest neighbours have the same value. The reciprocal lattice Hamiltonian is

$$\hat{\mathcal{H}}(\boldsymbol{q}) = -J\begin{pmatrix} 0 & 1+\mathrm{e}^{-\mathrm{i}Q_1} & 1+\mathrm{e}^{-\mathrm{i}Q_2} \\ 1+\mathrm{e}^{\mathrm{i}Q_1} & 0 & 1+\mathrm{e}^{-\mathrm{i}Q_3} \\ 1+\mathrm{e}^{\mathrm{i}Q_2} & 1+\mathrm{e}^{\mathrm{i}Q_3} & 0 \end{pmatrix}, \tag{77}$$

where we have defined $Q_j = \boldsymbol{q}\cdot\boldsymbol{a}_j$, $j = 1, 2$ and $Q_3 = Q_1 - Q_2$. The diagonalization of this 3×3 matrix gives a flat band of energy $2J$ and two dispersive bands. The analysis of N-body states that can appear at high density, namely a supersolid-type phase, is done in Huber & Altman (2010).

This lattice has been realized experimentally in the Berkeley group by superimposing two commensurate triangular lattices created with light beams at 532 and 1064 nm (see figure 14). The Kagome structure was iden-

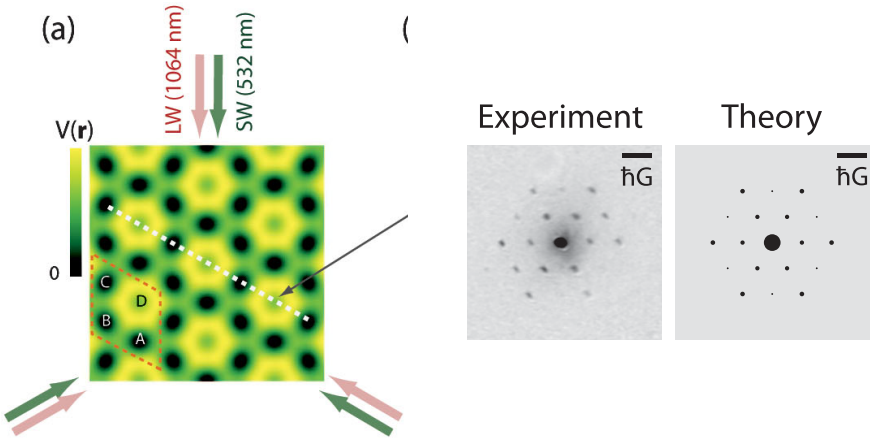

Figure 14. *Left: realization of a Kagome lattice from two triangular lattices. Right: time-of-flight pattern for a superfluid initially trapped in the Kagome lattice. Figures taken from Jo, Guzman, et al. (2012).*

tified by placing a superfluid in this lattice, abruptly switching off the lattice and observing the Bragg peaks after a time of flight. Note that in this experiment, the sign of the tunnelling coefficient was the usual sign ($-J$), and the flat band is the upper band of the three lowest sub-bands. In addition to the appearance of flat bands, this Kagome lattice is particularly interesting in magnetism, with a very rich phase diagram in the presence of antiferromagnetic interactions.

Chapter IV

Time-dependent lattices

Among the many possibilities offered by optical lattices, one of the most important is the control over time of the lattice parameters. We have already mentioned in Chapter 2 the consequences of a variation of the lattice amplitude and we have discussed the adiabatic and sudden limits for the ramping up or down of the periodic potential. In this chapter and the next one, we will be interested in another type of temporal variation: we will study the phenomena that appear when the position of the nodes of the lattice is varied in time, thus replacing the potential $V(x)$ (in 1D) by the potential $V[x - x_0(t)]$, where $x_0(t)$ is a controlled function of time.

In this chapter, we will first establish, via unitary transformations, the equivalence between several Hamiltonians that describe a moving lattice. We will then study the particular case of a periodic modulation of $x_0(t)$ and we will discuss the phenomenon of dynamical localization which can then appear. The next chapter will be devoted to Bloch oscillations, which occur when $x_0(t)$ corresponds to a uniformly accelerated motion. This situation is equivalent (by change of reference frame) to the case where we add a spatially-uniform time-independent force to the one created by the lattice.

We will not have enough time here to discuss other – and also very interesting – classes of phenomena related to the temporal variation of some lattice parameters. Let us mention the spectroscopy of the atoms in the lattice, which can be performed by time-modulating the amplitude V_0 of the periodic potential [see for example the article of Kollath, Iucci, et al. (2006) and its references]. Another example is the use of a pulsed lattice to study chaos or Anderson localization phenomena [see the recent article by Lopez, Clément, et al. (2012) and references therein].

1 Some relevant Hamiltonians

The studies that we will carry out in this chapter and the next one deal with time-dependent Hamiltonians that keep their spatially-periodic structure. In the 1D case which will interest us first, these Hamiltonians have the form

$$\hat{H}(t) = \frac{(\hat{p} - A(t))^2}{2m} + V(\hat{x}, t), \tag{1}$$

with

$$V(x + a, t) = V(x, t). \tag{2}$$

We will see later on how Bloch's theorem allows us to deduce general information about the evolution of systems governed by these Hamiltonians. In this first paragraph, we will start our study by identifying some Hamiltonians which can be reduced to the form (1) via a unitary transformation, even if the problem they describe is not spatially periodic.

1-1 Unitary transformations

Let us start by recalling the principle of a unitary transformation. We give ourselves a unitary operator $\hat{U}(t)$ that possibly depends on time, and we

consider a system described by a state $|\psi(t)\rangle$ evolving under the effect of the Hamiltonian $\hat{H}(t)$:

$$\mathrm{i}\hbar\frac{\mathrm{d}|\psi\rangle}{\mathrm{d}t} = \hat{H}(t)\,|\psi(t)\rangle. \tag{3}$$

We perform the transformation

$$|\tilde{\psi}(t)\rangle = \hat{U}(t)|\psi(t)\rangle. \tag{4}$$

The transformed state $|\tilde{\psi}\rangle$ still follows a hamiltonian evolution:

$$\mathrm{i}\hbar\frac{\mathrm{d}|\tilde{\psi}\rangle}{\mathrm{d}t} = \hat{\tilde{H}}(t)\,|\tilde{\psi}(t)\rangle \tag{5}$$

and the corresponding Hamiltonian is

$$\hat{\tilde{H}}(t) = \hat{U}(t)\hat{H}(t)\hat{U}^\dagger(t) + \mathrm{i}\hbar\frac{\mathrm{d}\hat{U}(t)}{\mathrm{d}t}\hat{U}^\dagger(t). \tag{6}$$

If some technical aspects (e.g. searching for eigenstates) are simpler for $\hat{\tilde{H}}$ than for $\hat{H}$, it is better to carry out the calculations in the *transformed* point of view and then come back to the initial point of view via the inverse transformation of (4).

In the following we will consider two classes of unitary transformations:

$$\hat{U}_1(t) = \mathrm{e}^{-\mathrm{i}\,\hat{x}\,p_0(t)/\hbar}, \quad \hat{U}_2(t) = \mathrm{e}^{-\mathrm{i}\,x_0(t)\,\hat{p}/\hbar}, \tag{7}$$

where $x_0(t)$ and $p_0(t)$ can be any functions of time that respectively have the dimension of a position and a momentum. The position and momentum operators[1] are transformed as follows:

$$\hat{U}_1\,\hat{x}\,\hat{U}_1^\dagger = \hat{x}, \quad \hat{U}_1\,\hat{p}\,\hat{U}_1^\dagger = \hat{p} + p_0, \tag{9}$$

and

$$\hat{U}_2\,\hat{x}\,\hat{U}_2^\dagger = \hat{x} - x_0, \quad \hat{U}_2\,\hat{p}\,\hat{U}_2^\dagger = \hat{p}. \tag{10}$$

Let us also indicate the value of the term $\mathrm{i}\hbar(\mathrm{d}\hat{U}/\mathrm{d}t)\hat{U}^\dagger$ appearing in the transformed Hamiltonian (6)

$$\mathrm{i}\hbar\frac{\mathrm{d}\hat{U}_1}{\mathrm{d}t}\hat{U}_1^\dagger = \hat{x}\,\dot{p}_0, \qquad \mathrm{i}\hbar\frac{\mathrm{d}\hat{U}_2}{\mathrm{d}t}\hat{U}_2^\dagger = \dot{x}_0\,\hat{p}. \tag{11}$$

1-2 Change of reference frames

Let us start with a system described by the Hamiltonian

$$\hat{H}_0(t) = \frac{[\hat{p} - A(t)]^2}{2m} + V(\hat{x}), \quad V(x+a) = V(x), \tag{12}$$

with a time-independent spatially-periodic potential $V(x)$ and a spatially uniform vector potential $A(t)$. We now look at how the evolution of this system transforms under the effect of $\hat{U}_1$ or $\hat{U}_2$ for well-chosen functions x_0 and p_0.

We start with $\hat{U}_1$ by taking

$$p_0(t) = A(t). \tag{13}$$

We obtain

$$\hat{H}_1(t) = \frac{\hat{p}^2}{2m} + V(\hat{x}) - F(t)\,\hat{x} \qquad \text{with} \quad F(t) = -\frac{\mathrm{d}A(t)}{\mathrm{d}t}. \tag{14}$$

The Hamiltonian (14) describes the motion of a particle in the superposition of the periodic potential $V(x)$ and a potential corresponding to a spatially constant force $F(t)$, that possibly depends on time. This is not a surprise: In electromagnetism, a time-dependent vector potential is associated with an electric field $\mathcal{E} = -\dot{A}$. The unitary transformation from $\hat{H}_0$ to $\hat{H}_1$ is exactly the same as the one used in electrodynamics to introduce the electric dipole Hamiltonian in the long-wavelength approximation (see the complement $\mathrm{A_{IV}}$ of Cohen-Tannoudji, Dupont-Roc, et al. 1989). Note that the problem (14) *which is not periodic*, can thus be reduced to the problem (12) *which is periodic*.

[1] In this chapter, the position and momentum operators are defined by their action on a function $\psi(x)$ in the usual way:

$$\hat{x}\,\psi(x) = x\,\psi(x), \quad \hat{p}\,\psi(x) = -\mathrm{i}\hbar\frac{\mathrm{d}\psi}{\mathrm{d}x}. \tag{8}$$

The link between these operators and the result of a position or velocity measurement depends on the unitary transformation that has been performed.

Let us now look at the action of $\hat{U}_2$ on the initial Hamiltonian (12), by choosing[2]

$$x_0(t) = \frac{1}{m}\int_0^t A(t')\,\mathrm{d}t'. \tag{15}$$

We find

$$\hat{\tilde{H}}_2(t) = \frac{\hat{p}^2}{2m} + V[\hat{x} - x_0(t)] + \frac{A^2(t)}{2m}. \tag{16}$$

The last term is an energy which is independent of x and p and which is added to the Hamiltonian. We can eliminate it by performing a last (and very simple) unitary transformation generated by

$$\hat{U}_3 = \exp\left(\frac{\mathrm{i}}{\hbar}\int_0^t \frac{A^2(t')}{2m}\,\mathrm{d}t'\right) \tag{17}$$

which leaves $\hat{x}$ and $\hat{p}$ unchanged. After this operation, we arrive at

$$\hat{H}_2(t) = \frac{\hat{p}^2}{2m} + V[\hat{x} - x_0(t)]. \tag{18}$$

This form indicates how to practically realize the situations discussed in this chapter: one must control the phase of the travelling waves forming the standing wave in order to move the position of its nodes and antinodes according to the law given by $x_0(t)$.

In conclusion, the three Hamiltonians (12)-(14)-(18), which are gathered in table IV.1, allow to describe the same physical situation and we can choose one or the other according to the aspects we want to emphasize. Note that there is a simple interpretation for the series of transformations generated by $\hat{U} = \hat{U}_1\hat{U}_2^\dagger\hat{U}_3^\dagger$, which makes us go from the Hamiltonian (18), describing a moving lattice, to the Hamiltonian (14), describing a stationary lattice superimposed on a uniform force $F(t)$. It is a change of reference frame, from the laboratory reference frame to the reference frame moving with the lattice, in which the inertial force $F(t) = -m\ddot{x}_0(t) = -\dot{A}(t)$ appears.

[2]This transformation is known as the Kramers–Henneberger transformation in quantum electrodynamics, see for example Cohen-Tannoudji, Dupont-Roc, et al. 1989, §IV.B.4.

2 The shaken lattice

The situation that we will discuss in the rest of this chapter is that of an infinite lattice whose position is periodically modulated by taking for example:

$$\hat{H}_2(t) = \frac{\hat{p}^2}{2m} + V[\hat{x} - x_0(t)], \qquad x_0(t) = \bar{x}_0\cos(\omega t). \tag{19}$$

This problem was studied theoretically by Dunlap & Kenkre (1986) and Holthaus (1992). The goal then was to understand the behaviour of electrons in crystals in the presence of the electric field of an electromagnetic wave. The phenomenon that appears is called *Dynamical localization*. The main conclusion is the existence of a value of the oscillating field for which the transport disappears: The spreading of an electron wave packet that would be observed in the absence of the field is completely blocked. In particular, Holthaus predicted a collapse of the mini-bands expected in a superlattice with a period of about ten nanometers, when it is illuminated with far-infrared light.

This question of a shaken lattice was therefore raised long ago, but the physics of cold atoms has brought it back to the forefront because the modulation of the lattice allows one to control the amplitude and the sign of the tunnel coefficient J, and even to make it complex. The control of the amplitude of the coefficient J can be used to vary the ratio between the kinetic energy and the interaction energy, which we pointed out in a previous chapter as being decisive for the emergence of N-body physics. Thus, Eckardt, Weiss, et al. (2005) proposed to use lattice modulation to induce the transition between a superfluid and a Mott insulator. The possibility to make the coefficient J complex is interesting when considering a two or three dimensional lattice. We can then realize a situation where the atom accumulates a non-zero phase when it performs a closed loop by tunnelling from one site to another. This is exactly what is needed to realize an artificial gauge field. We will not deal with these artificial gauge fields in this year's lecture, but we nevertheless give below some indications on this possible way of modifying J.

$\hat{H}_1$	$\hat{H}_0$	$\hat{H}_2$
$\dfrac{\hat{p}^2}{2m} + V(\hat{x}) - F(t)\,\hat{x}$	$\dfrac{[\hat{p} - A(t)]^2}{2m} + V(\hat{x})$	$\dfrac{\hat{p}^2}{2m} + V[\hat{x} - x_0(t)]$
$q(t) = q_{\rm in} + \dfrac{1}{\hbar}\displaystyle\int_0^t F(t')\,\mathrm{d}t'$	$q(t) = q_{\rm in}$	$q(t) = q_{\rm in}$
$-J\displaystyle\sum_j (\lvert w_{j+1}\rangle\langle w_j\rvert + \text{h.c.}) - \; a\,F(t)\sum_j j\lvert w_j\rangle\langle w_j\rvert$	$-J\displaystyle\sum_j \Big(\lvert w_{j+1}\rangle\langle w_j\rvert\, \mathrm{e}^{\mathrm{i}\,a\,A(t)/\hbar} + \text{h.c.}\Big)$	
$\overleftarrow{\hat{U}_1 = \exp(-\mathrm{i}\hat{x}\,p_0(t)/\hbar)}$		$\overrightarrow{\hat{U}_2 = \exp(-\mathrm{i}x_0(t)\,\hat{p}/\hbar)}$

Table IV.1. *The three Hamiltonians used in this chapter, the time evolution of the quasi-momentum and the tight-binding version of this Hamiltonian. We go from one to the other by the unitary transformations indicated on the last line, with $p_0(t) = A(t) = m\dot{x}_0(t)$ and $F(t) = -m\ddot{x}_0(t)$.*

2-1 Hamiltonian in the tight-binding approximation

On the theory side, our starting point will be the Hamiltonian of an atom in a "shaken" optical lattice

$$\hat{H}_2(t) = \frac{\hat{p}^2}{2m} + V[\hat{x} - x_0(t)], \tag{20}$$

where $x_0(t)$ is a time-periodic function of frequency ω. We will assume that the atoms are prepared in a given band of the lattice, the lowest band for example, and that they remain there during the evolution. We will therefore restrict the dynamics of the atoms to this band and omit the band index in the following. The necessary conditions for such an adiabatic following of the initially populated energy band will be discussed in detail in the next chapter in the context of Bloch oscillations.

Moreover, we will do most of our study in the tight-binding limit, where only jumps between nearest neighbours play a significant role. In order to write the corresponding Hamiltonian from (20), it is useful to first perform the unitary transformations $\hat{U}_1$ and $\hat{U}_2$ to get to the Hamiltonian $\hat{H}_1$

$$\hat{H}_1(t) = \frac{\hat{p}^2}{2m} + V(\hat{x}) - F(t)\,\hat{x}. \tag{21}$$

The expression of this Hamiltonian in the tight-binding model is simple. Its unmodulated part is the Hubbard Hamiltonian that we have already met:

$$\frac{\hat{p}^2}{2m} + V(\hat{x}) \quad \longrightarrow \quad -J\left(\hat{T}_1 + \hat{T}_1^\dagger\right) \tag{22}$$

where $\hat{T}_j$ shifts the particle by j sites to the right:

$$\hat{T}_j = \sum_{j' \in \mathbb{Z}} |w_{j+j'}\rangle\langle w_{j'}| \tag{23}$$

The term related to the inertial force is written as

$$-F(t)\,\hat{x} \quad \longrightarrow \quad -a\,F(t)\sum_j j\,|w_j\rangle\langle w_j| \tag{24}$$

where we have used the fact that the position operator is diagonal in the basis of the Wannier functions (see for example Eckardt, Holthaus, et al. (2009))

$$\langle w_j|\hat{x}|w_{j'}\rangle = ja\,\delta_{j,j'}. \tag{25}$$

The Hubbard Hamiltonian of a shaken lattice is therefore

$$\hat{H}_1 = -J\left(\hat{T}_1 + \hat{T}_1^\dagger\right) + \hbar\omega\,\xi(t)\sum_j j\,|w_j\rangle\langle w_j|, \tag{26}$$

where we have characterized the amplitude of the modulation by the dimensionless parameter $\xi(t)$

$$\xi(t) = -\frac{aF(t)}{\hbar\omega} = \frac{ma}{\hbar\omega}\ddot{x}_0(t). \tag{27}$$

This coefficient is defined (up to its sign) as the ratio between the work aF of the inertial force $F = -m\ddot{x}_0$ over a period of the lattice, and the energy quantum $\hbar\omega$ associated to the shaking.

For a sinusoidal modulation, we define

$$x_0(t) = \bar{x}_0\cos(\omega t), \quad F(t) = -m\ddot{x}_0(t) = m\omega^2\bar{x}_0\cos(\omega t), \tag{28}$$

which leads to

$$\xi(t) = \xi_0\cos(\omega t), \quad \xi_0 = -ma\omega\bar{x}_0/\hbar. \tag{29}$$

From the expression (26) of $\hat{H}_1$ in the tight-binding regime, we can go back to the "$\hat{H}_0$-version" of the problem. To do this, we have to use the discretized version of the unitary transformation $\hat{U}_1(t)$:

$$\hat{U}_1(t) = E^{-\mathrm{i}\,\hat{x}\,p_0(t)/\hbar} \qquad \longrightarrow \qquad \hat{U}_1(t)|w_j\rangle = \mathrm{e}^{-\mathrm{i}\,jap_0(t)/\hbar}|w_j\rangle \tag{30}$$

which leads to

$$\begin{aligned}\hat{H}_0(t) &= \hat{U}_1^\dagger(t)\hat{H}_1(t)\hat{U}_1(t) + \mathrm{i}\hbar\frac{\mathrm{d}\hat{U}_1^\dagger}{\mathrm{d}t}\hat{U}_1 \\ &= -J\left(\hat{T}_1\,\mathrm{e}^{\mathrm{i}\,ap_0(t)/\hbar} + \hat{T}_1^\dagger\,\mathrm{e}^{-\mathrm{i}\,ap_0(t)/\hbar}\right)\end{aligned} \tag{31}$$

with $p_0(t) = m\dot{x}_0(t)$. In this point of view, the shaking of the lattice is described by a periodic modulation of the tunnel coefficients, which become complex.

Note that, from (31), one can easily take into account hoppings between more distant neighbours. By noting $J(j)$ the matrix element for a hopping

of j sites (cf. chapter 3), the expression (31) is immediately generalized into

$$\hat{H}_0 = \sum_{j=1}^{+\infty} J(j) \left(\hat{T}_j \, \mathrm{e}^{\mathrm{i}\, j\, ap_0(t)/\hbar} + \hat{T}_j^\dagger \, \mathrm{e}^{-\mathrm{i}\, j\, ap_0(t)/\hbar} \right). \tag{32}$$

Recall that in all the above we chose $J(1) = -J$ with $J > 0$. Recall also that the tunnel matrix elements $J(j)$ are the Fourier components of the energy $E(q)$ of the considered band:

$$E(q) = 2 \sum_{j=1}^{+\infty} J(j) \, \cos(jaq). \tag{33}$$

2-2 The Pisa experience (Lignier, Sias, et al. 2007)

The first demonstration of the dynamical localization effect with cold atoms was made by Madison, Fischer, et al. (1998). The lattice was put in oscillating motion by phase modulating one of the beams that create the standing wave. By performing the spectroscopy of an energy band in the lattice, a spectacular narrowing of this band could be observed for a critical value of the amplitude of the oscillation of the lattice.

We show in figure 1 the results obtained by Lignier, Sias, et al. (2007) with a condensate of rubidium loaded in a shaken 1D optical lattice:

$$x_0(t) = \bar{x}_0 \cos(\omega t). \tag{34}$$

The lattice depths were chosen between 4 and 9 recoil energies E_r, which is a bit low for the tight-binding approximation of the previous paragraph to be accurate, but it nevertheless gives a good justification of the experimental results, as we will see in the following.

Lignier, Sias, et al. (2007) measured the time-spreading of the spatial distribution of the atoms in the lattice. To do this, they first trapped the particles in the vicinity of $x = 0$ using an additional dipole trap, then turned off this trap while leaving the lattice on. The results of this experiment are consistent with the idea that the shaken lattice is essentially equivalent to a fixed lattice, but with a modified tunnel coefficient J'.

The measurement of the tunnel coefficient J' has been done for several lattice depths V_0, several modulation frequencies ω and several modulation

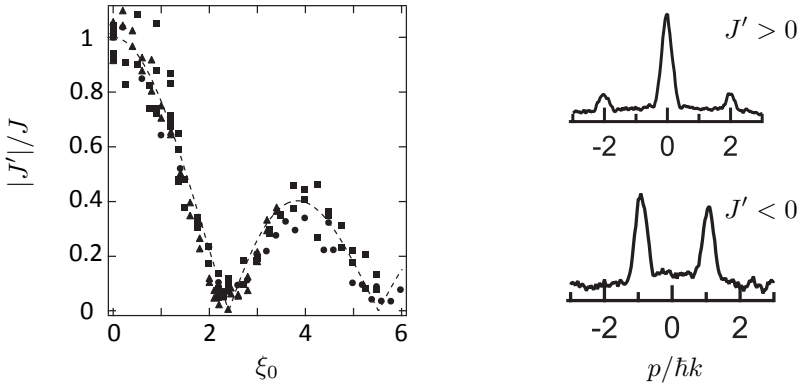

Figure 1. *Dynamical suppression of tunnelling in a shaken 1D lattice for a condensate of ^{87}Rb atoms. Left: The absolute value of the tunnel coefficient (normalized by its value in the absence of shaking) is obtained from the spreading of a wave packet in the lattice. This figure gathers points obtained for different lattice depths (4 to 9 E_r) and different shaking frequencies (0.5 and 1 kHz). The shaking amplitude $\bar{x}_0$ is at maximum on the order of $0.5\,a$ and the ratio $\hbar\omega/J$ varies between 0.3 and 30. Right: momentum distribution of atoms in the shaken lattice for $\xi_0 < 2.4$ (top) and for ξ_0 slightly larger than 2.4 (bottom). In the second case, the presence of two peaks at $p = \pm\hbar k$ indicates that the minimum of the band is located at the edge of the Brillouin zone, corresponding to an effective tunnel coefficient $J' < 0$. Figures extracted from Lignier, Sias, et al. (2007).*

amplitudes $\bar{x}_0$. The experimental results show a remarkable phenomenon: the ratio J'/J of the tunnel rates with and without modulation depends only on the parameter $\xi_0 = -ma\omega\bar{x}_0/\hbar$ introduced above (29). The dotted line is the absolute value of the Bessel function $\mathcal{J}_0(\xi_0)$, a result that we will justify later. In particular, one observes a cancellation of the tunnel coefficient (no spatial diffusion) for $\xi_0 \approx 2.4$ (the first zero of the Bessel function is at 2.405).

The study of spatial diffusion does not provide the sign of J'. One can access it with a time-of-flight experiment, where the momentum distribution of the atoms is measured. For $\xi_0 < 2.4$, we find that this distribution is centered on $p = 0$, indicating that the minimum of the energy band is

located at $q = 0$, which means that $J' > 0$. On the other hand, for $\xi_0 > 2.4$, we find a momentum distribution with two peaks of comparable heights at $p = \pm\hbar k$, indicating that the minimum of the band has been shifted to $q = \pm k$, as expected for a tunnel coefficient $J' < 0$. In the following we will explain the essence of these results and refer the reader interested in more detailed theoretical analyses to the papers by Eckardt, Holthaus, et al. (2009) and Creffield, Sols, et al. (2010).

3 A simple approach to shaken lattices

3-1 Preliminary: a two-site system

To start with, we consider a simpler system than an infinite lattice, limiting ourselves to a double-well potential in which we identify two states $|w_j\rangle$, $j = \pm$, corresponding to a particle located on the right ($x = +a/2$) or on the left ($x = -a/2$) of the center. This problem has been studied theoretically by Grossmann, Dittrich, et al. (1991) and we refer to Grifoni & Hänggi (1998) for a review of possible theoretical treatments. We limit ourselves here to a simple mathematical approach, which nevertheless allows us to capture the core of the phenomenon.

For a two-site system, the Hamiltonian (26) is replaced by

$$\hat{H}(t) = -J\,(|w_+\rangle\langle w_-| \;+\; |w_-\rangle\langle w_+|) + \frac{1}{2}\hbar\omega\;\xi(t)\;\;(|w_+\rangle\langle w_+| - |w_-\rangle\langle w_-|) \tag{35}$$

which can be written

$$\hat{H} = -J\;\hat{\sigma}_x \;+\; \frac{1}{2}\hbar\omega\;\xi(t)\;\hat{\sigma}_z \tag{36}$$

where the $\hat{\sigma}_i$ are the Pauli matrices in the basis $\{|w_+\rangle, |w_-\rangle\}$. Let us write the state of the particle under the form

$$|\psi(t)\rangle = \sum_{j=\pm} \alpha_j(t)|w_j\rangle. \tag{37}$$

The evolution of the α_j's is then given by:

$$\mathrm{i}\,\dot{\alpha}_+ = \frac{\omega}{2}\,\xi(t)\,\alpha_+ - \frac{J}{\hbar}\alpha_-, \qquad \mathrm{i}\,\dot{\alpha}_- = -\frac{\omega}{2}\,\xi(t)\,\alpha_- - \frac{J}{\hbar}\alpha_+\,. \tag{38}$$

These two equations can be rewritten as

$$\mathrm{i}\hbar\,\dot{\tilde{\alpha}}_+ = -J\,\mathrm{e}^{\mathrm{i}\eta}\;\tilde{\alpha}_-, \qquad \mathrm{i}\hbar\,\dot{\tilde{\alpha}}_- = -J\,\mathrm{e}^{-\mathrm{i}\eta}\;\tilde{\alpha}_+\,, \tag{39}$$

where we have defined

$$\tilde{\alpha}_\pm = \alpha_\pm \exp(\pm\mathrm{i}\eta/2), \quad \eta(t) = \omega\int_0^t \xi(t')\;\mathrm{d}t'. \tag{40}$$

Consider the situation where the evolution due to the tunnelling between the two wells, of time scale $\hbar/J$, is much slower than the modulation frequency ω giving the evolution of the function $\xi(t)$. Let us take the time average[3] of equations (39) on a time period $T = 2\pi/\omega$ of the fast oscillation and write, at the lowest order in $J/\hbar\omega$:

$$\mathrm{i}\hbar\,\dot{\bar{\alpha}}_+ = -J'\bar{\alpha}_-, \qquad \mathrm{i}\hbar\,\dot{\bar{\alpha}}_- = -J'^{*}\bar{\alpha}_+, \tag{41}$$

where we have defined:

$$J' = J\;\langle\mathrm{e}^{\mathrm{i}\eta}\rangle. \tag{42}$$

These evolution equations for $\bar{\alpha}_\pm$ are the same as those for a double well without fast modulation, except for a renormalization of the tunnel coefficient: $J \to J'$.

Let us take the case of a sinusoidal modulation:

$$\xi(t) = \xi_0\cos(\omega t), \quad \eta(t) = \xi_0\sin(\omega t), \tag{43}$$

which leads to

$$J' = J\;\mathcal{J}_0(\xi_0), \tag{44}$$

where $\mathcal{J}_0$ is the Bessel function of the first kind defined by

$$\mathcal{J}_0(x) = \frac{1}{\pi}\int_0^\pi \cos[x\sin(\tau)]\;\mathrm{d}\tau. \tag{45}$$

Since this function takes positive and negative values according to its argument, we see that the fast modulation in $\xi(t)$ allows to reduce the tunnel coefficient, or even to cancel it and change its sign.

[3] We could justify this procedure by using a Fourier development for the known function $\eta(t)$ and the unknown functions $\tilde{\alpha}_\pm(t)$ and by solving perturbatively these equations in powers of the small parameter $J/\hbar\omega$. We will not do it here because this procedure is closely related to the Floquet approach which we will present later.

3-2 Analogy with a spin $1/2$ in an oscillating field

In the case of atoms in an optical potential that creates a double well, the experimental demonstration of the modification of the tunnel coefficient has been described by Kierig, Schnorrberger, et al. (2008). The situation we have studied here is mathematically equivalent to the modification of the Landé factor of an atom with a spin $1/2$ whose magnetic moment is coupled to a fast oscillating magnetic field:

$$\boldsymbol{B}(t) = B_0 \boldsymbol{u}_x + B_1(t)\boldsymbol{u}_z, \qquad B_1(t) = \bar{B}_1 \cos(\omega t). \tag{46}$$

This situation is indeed described by a Hamiltonian that is formally identical to (36):

$$\hat{H}(t) = \frac{\hbar\omega_0}{2}\hat{\sigma}_x + \frac{\hbar\bar{\omega}_1}{2}\cos(\omega t)\hat{\sigma}_z. \tag{47}$$

We have denoted here respectively as ω_0 and $\bar{\omega}_1$ the Larmor frequency for the fields B_0 and $\bar{B}_1$. In the limit $\omega_0 \ll \bar{\omega}_1$, the equivalent of the modification of the tunnel coefficient J is a modification of the Larmor frequency ω_0 which becomes

$$\omega_0' = \omega_0 \, \mathcal{J}_0(\bar{\omega}_1/\omega). \tag{48}$$

This change in ω_0, which can be interpreted as a change in the Landé factor caused by the fast oscillating field, has been observed by Haroche, Cohen-Tannoudji, et al. (1970). The main result is shown in figure 2: in particular we observe a cancellation, then a change of sign of the Landé factor, in good agreement with the prediction (48).

Note that the theoretical study of this modification of the Landé factor becomes much simpler to carry out if we consider a square-wave modulation of the field $B_1(t)$ rather than a sinusoidal modulation. For a field $\boldsymbol{B}_1(t) = \bar{B}_1\boldsymbol{u}_z$ during one half-period π/ω and $\boldsymbol{B}_1(t) = -\bar{B}_1\boldsymbol{u}_z$ during the other half-period, one can explicitly compute the evolution of the spin $1/2$ at order 1 in $B_0/\bar{B}_1$, by considering the following points:

- The Larmor frequency is independent of time and is $\omega_L = (\omega_0^2 + \bar{\omega}_1^2)^{1/2} \approx \bar{\omega}_1$.
- The direction of the magnetic field oscillates between the two directions $\boldsymbol{n} = \pm\cos\theta\ \boldsymbol{u}_z + \sin\theta\ \boldsymbol{u}_x$, with $\tan\theta = B_0/\bar{B}_1 \ll 1$.

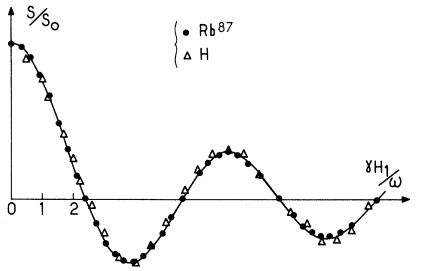

Figure 2. *Modification of the Landé factor of rubidium and hydrogen atoms, when they are illuminated by a radiofrequency field H_1 with frequency $\omega/2\pi$ of a few kHz. Figure extracted from Haroche, Cohen-Tannoudji, et al. (1970).*

- The evolution operator during a time t for which the magnetic field keeps a fixed direction $\boldsymbol{n}$ is

$$\hat{U}(t) = \mathrm{e}^{-\mathrm{i}\hat{H}t/\hbar} = \hat{1}\cos(\bar{\omega}_1 t/2) - \mathrm{i}(\boldsymbol{n}\cdot\hat{\boldsymbol{\sigma}})\sin(\bar{\omega}_1 t/2) \tag{49}$$

We can then calculate the product of the evolution operators on the two segments[4] that constitute one oscillation period $T = 2\pi/\omega$ and we arrive at:

$$\hat{U}(T) \approx \hat{1} - \mathrm{i}\hat{\sigma}_x \, \frac{\omega_0 T}{2} \, \mathrm{sinc}\left(\frac{\pi}{2}\,\frac{\bar{\omega}_1}{\omega}\right), \tag{50}$$

which, for $\omega_0 T \ll 1$, corresponds to the modification of the Larmor frequency

$$\omega_0' = \omega_0 \, \mathrm{sinc}\left(\frac{\pi}{2}\,\frac{\bar{\omega}_1}{\omega}\right) \tag{51}$$

where the Bessel function of (48) has been replaced by a sinc function.

The cancellation of the Landé factor is particularly simple in this point of view: it occurs for $\bar{\omega}_1 T/2 = 2\pi$, which means that the spin makes a

[4] We can take for example $B_1(t) = \bar{B}_1$ between 0 and $T/4$, then $B_1(t) = -\bar{B}_1$ between $T/4$ and $3T/4$, and finally $B_1(t) = \bar{B}_1$ between $3T/4$ and T, to calculate the evolution operator between 0 and T. This choice of phase, which is the equivalent for a square lattice of $\bar{B}_1\cos(\omega t)$ for a sinusoidal modulation, will be made in all this chapter. One can consult the article by Eckardt, Holthaus, et al. (2009) for a discussion on the spurious effects that can appear with other choices for the phase.

complete turn during each half-period for which the field B_1 keeps a constant direction. It is clear that the spin does not evolve "on average", which corresponds to a zero Landé factor with respect to the B_0 field.

3-3 The shaken lattice (simple approach)

Our approach is implemented for a lattice in almost the same way as for the double well. We write the state vector of a particle under the form

$$|\phi(t)\rangle = \sum_j \alpha_j(t)\,|w_j\rangle, \tag{52}$$

we obtain the evolution of the coefficients α_j for the tight-binding Hamiltonian $H_1(t)$ given in (26)

$$\mathrm{i}\,\dot{\alpha}_j = j\,\omega\,\xi(t)\alpha_j - \frac{J}{\hbar}(\alpha_{j-1} + \alpha_{j+1}). \tag{53}$$

We introduce the variables

$$\tilde{\alpha}_j = \alpha_j \exp(\mathrm{i}\,j\eta) \tag{54}$$

where η is defined as in (40) by $\eta = \omega \int_0^t \xi(t')\,\mathrm{d}t'$, and we obtain[5]

$$\mathrm{i}\hbar\dot{\tilde{\alpha}}_j = -J\left(\mathrm{e}^{\mathrm{i}\eta}\,\tilde{\alpha}_{j-1} + \mathrm{e}^{-\mathrm{i}\eta}\,\tilde{\alpha}_{j+1}\right). \tag{55}$$

After averaging over one period of the fast oscillation, this equation of motion is identical to that of a lattice without modulation and a renormalized tunnel coefficient $J\langle \mathrm{e}^{\pm\mathrm{i}\eta}\rangle$, where the sign $+$ (resp. $-$) corresponds to hoppings to the right (resp. left). For a sinusoidal modulation, the time average is expressed in terms of the Bessel function of the first kind

$$J' = J\mathcal{J}_0(\xi_0), \tag{56}$$

a result identical to that of the double well. In particular, we find that we can cancel the tunnel effect by choosing ξ_0 equal to the first zero of the Bessel function (≈ 2.405) or change the sign of J by choosing ξ_0 slightly higher than this value. This simple approximation thus explains the experimental results described in the previous paragraph.

[5] Note that we could have written this system of equations directly starting from the Hamiltonian $\hat{H}_0$ (31) instead of $\hat{H}_1$, and using $ap_0(t)/\hbar = \eta(t)$.

4 Bloch approach for a shaken lattice

We now go beyond the simple approach developed in the previous section and study in a more rigorous way the evolution of a wave packet in a shaken lattice. The essential tool is once again Bloch's theorem, which puts strong constraints on the possible form of the solutions of the Schrödinger equation. These constraints are such that the exact solution of the problem can be written explicitly if we limit the dynamics of the atoms to a single band. In the case where several bands are simultaneously populated, we have to resort to the Floquet method, whose broad lines will be presented.

4-1 Bloch theorem in the time-dependent case

The Bloch theorem encountered in chapter 2 provides the eigenstates of a time-independent Hamiltonian with a spatially periodic potential $V(x)$

$$\hat{H} = \frac{\hat{p}^2}{2m} + V(\hat{x}), \quad V(x+a) = V(x). \tag{57}$$

Bloch theorem indicates that one can search for an eigenstate basis of this Hamiltonian in the form of Bloch waves $\psi_q(x) = \mathrm{e}^{\mathrm{i}xq}u_q(x)$, where $u_q(x)$ is also spatially periodic and where q is the quasi-momentum chosen by convention in the first Brillouin zone $]-\pi/a, \pi/a]$. Recall that the defining property of these Bloch waves is the fact that they are eigenstates of the spatial translation operator $\hat{T}_a$ with eigenvalue $\mathrm{e}^{-\mathrm{i}aq}$.

We also mentioned in chapter 2 the case of spatially periodic and time-dependent Hamiltonians, and we indicated that the Bloch waveform is then preserved during the evolution. Let us briefly prove again this point by considering for example the Hamiltonian

$$\hat{H}(t) = \frac{(\hat{p} - A(t))^2}{2m} + V(\hat{x}, t), \tag{58}$$

with

$$V(x+a, t) = V(x, t). \tag{59}$$

This Hamiltonian commutes at each time with the spatial translation operator $\hat{T}_a$, and this property also holds for the evolution operator between an

initial time t_0 and a final time t_1. We deduce that if the initial state $\psi(x,t_0)$ is an eigenstate of $\hat{T}_a$ with eigenvalue $\mathrm{e}^{-\mathrm{i}aq}$ [i.e. $\psi(x,t_0)=\mathrm{e}^{\mathrm{i}xq}u_q(x,t_0)$], it will also be the case for the final state $\psi(x,t_1)$, with the same eigenvalue [i.e. $\psi(x,t_1)=\mathrm{e}^{\mathrm{i}xq}u_q(x,t_1)$].

4-2 Evolution of the quasi-momentum $q(t)$

Since a Hamiltonian of the form (58) preserves the form of Bloch functions, an initial state $\mathrm{e}^{\mathrm{i}xq_{\mathrm{in}}}\,u(x,0)$ with $u(x,0)$ which is spatially periodic keeps this form during the evolution, with the same quasi-momentum q_{in}. This property applies to the two Hamiltonians $\hat{H}_0(t)$ and $\hat{H}_2(t)$ which indeed have the form (58), but it does not apply to the Hamiltonian $\hat{H}_1(t)$

$$\hat{H}_1(t)=\frac{\hat{p}^2}{2m}+V(\hat{x})-F(t)\,\hat{x} \tag{60}$$

that describes the motion of the particle in the presence of the spatially uniform force $F(t)$, in addition to the periodic potential $V(x)$.

However, the solutions of the Schrödinger equation for $\hat{H}_1(t)$ are also very simple. If $\phi_0(x,t)=\mathrm{e}^{\mathrm{i}xq_{\mathrm{in}}}\,u(x,t)$ is the solution of the Schrödinger equation for the Hamiltonian $\hat{H}_0$, then the unitary transformation $\hat{U}_1$ gives the solution $\phi(x,t)$ for the Hamiltonian $\hat{H}_1$:

$$\phi(x,t)=\hat{U}_1\phi_0(x,t)=\mathrm{e}^{\mathrm{i}x\,q(t)/\hbar}\,u(x,t) \tag{61}$$

with

$$q(t)=q_{\mathrm{in}}-A(t)/\hbar=q_{\mathrm{in}}+\frac{1}{\hbar}\int_0^t F(t')\,\mathrm{d}t'. \tag{62}$$

The Hamiltonian $\hat{H}_1(t)$ thus preserves the Bloch waveform, but with a quasi-momentum that depends on time by "integrating" the force $F(t)$.

Finally, we need to determine the evolution of the periodic part $u(x,t)$, no matter if we choose to work with $\hat{H}_0(t)$, $\hat{H}_1(t)$ or $\hat{H}_2(t)$. We already encountered this kind of questions while studying the ramping of a lattice. We explained that if the lattice parameters vary slowly, the particle initially prepared in a Bloch function of the n-th band, associated with the periodic state $|u_{n,q}\rangle$, follows adiabatically this state $|u_{n,q}\rangle$. In what follows, we will again make this adiabatic assumption. As we have already mentioned, we will detail in the next chapter the conditions that need to be satisfied for this approximation to be valid when we study Bloch oscillations.

4-3 Localization in the lowest band

To solve the problem of the evolution of a particle in a shaken lattice when this evolution is restricted to the lowest band, we will use the point of view of the Hamiltonian $\hat{H}_0$, for which the calculations are the simplest. We therefore start from the tight-binding Hamiltonian

$$\hat{H}_0(t)=-J\left(\hat{T}_1\,\mathrm{e}^{\mathrm{i}ap_0(t)/\hbar}+\hat{T}_1^\dagger\,\mathrm{e}^{-\mathrm{i}ap_0(t)/\hbar}\right), \tag{63}$$

or its more complete version that includes the hoppings between distant neighbors, but still restricted to the lowest band [with $J(1)=-J$]:

$$\hat{H}_0(t)=\sum_{j'=1}^{+\infty}J(j')\left(\hat{T}_{j'}\,\mathrm{e}^{\mathrm{i}j'ap_0(t)/\hbar}+\hat{T}_{j'}^\dagger\,\mathrm{e}^{-\mathrm{i}j'ap_0(t)/\hbar}\right). \tag{64}$$

We assume that the system is initially prepared in a Bloch function ψ_q (we forget the band index since we restrict ourselves to $n=0$). Because of the single-band approximation, this Bloch function is unique and is written, up to a global phase:

$$|\psi(0)\rangle\propto|\psi_q\rangle=\sum_{j\in\mathbb{Z}}\mathrm{e}^{\mathrm{i}jaq}|w_j\rangle. \tag{65}$$

The periodic function $|u_q\rangle$ associated to $|\psi_q\rangle$ is also unique in this single-band approximation and it is in fact independent of q:

$$|u\rangle=\sum_{j\in\mathbb{Z}}|w_j\rangle. \tag{66}$$

Let us look for the evolution of $|\psi(t)\rangle$ under the effect of the Hamiltonian $\hat{H}_0(t)$. Since this Hamiltonian is spatially periodic, we know that the Bloch form will be preserved and the quasi-momentum q will not change over time. Since we assume that the system remains in the lowest band, the state vector at time t is necessarily proportional to the state $|\psi_q\rangle$, since this

is the only Bloch state available for this quasi-momentum. The state $|\psi(t)\rangle$ can only differ from $|\psi_q\rangle$ by a phase factor and is therefore written

$$|\psi(t)\rangle = \mathrm{e}^{-\mathrm{i}\Phi_q(t)}\ |\psi_q\rangle. \tag{67}$$

The determination of the global phase $\Phi_q(t)$ is simple. We only need to use the expression (67) for $|\psi(t)\rangle$ in the time-dependent Schrödinger equation. By construction, the state $|\psi_q\rangle$ is an eigenstate of the translational operators $\hat{T}_{j'}$ with eigenvalues $\mathrm{e}^{-\mathrm{i}j'aq}$. It is therefore an eigenstate of the Hamiltonian $\hat{H}_0(t)$ at any time t.

$$\hat{H}_0(t)|\psi_q\rangle = E[q - p_0(t)/\hbar]|\psi_q\rangle, \tag{68}$$

where we have used the expression of the energy of the lowest band of the Hamiltonian (63):

$$E(q) = -2J\cos(aq) \tag{69}$$

and

$$E(q) = 2\sum_{j'=1}^{+\infty} J(j')\cos(j'aq) \tag{70}$$

for the Hamiltonian (64) including distant hoppings.

The equation to determine the global phase $\Phi_q(t)$ is therefore

$$\hbar\dot{\Phi}_q = E[q - p_0(t)/\hbar], \tag{71}$$

which is formally integrated to give

$$\Phi_q(t) = \Phi_q(0) + \frac{1}{\hbar}\int_0^t E[q - p_0(t')/\hbar]\ \mathrm{d}t'. \tag{72}$$

Let us consider the instants $0, T, 2T, \ldots, nT, \ldots$, where $T = 2\pi/\omega$ is the shaking period of the lattice. Because of the temporal periodicity of $p_0(t')$, one can immediately show from (72) that

$$\Phi_q(nT) - \Phi_q(0) = n\ [\Phi_q(T) - \Phi_q(0)] \tag{73}$$

where n is an integer: the accumulated phase $\Delta\Phi_q$ is proportional to the elapsed time nT. This evolution is very similar to the one we would find for a time-independent problem, at least if we limit ourselves to a "stroboscopic" observation of this state by looking at its value at integer multiples nT of the oscillation period T.

To formalize this analogy, let us introduce the *quasi-energy*

$$\epsilon(q) = \frac{\hbar}{T}\left[\Phi_q(T) - \Phi_q(0)\right] = \frac{1}{T}\int_0^T E[q - p_0(t)/\hbar]\ \mathrm{d}t. \tag{74}$$

We can then rewrite the previous result in the form

$$|\psi(nT)\rangle = \mathrm{e}^{-\mathrm{i}\epsilon(q)nT/\hbar}|\psi(0)\rangle, \tag{75}$$

which is very similar to the evolution we would have in a time-independent lattice for a Bloch wave:

$$|\psi(t)\rangle = \mathrm{e}^{-\mathrm{i}E(q)t/\hbar}|\psi(0)\rangle. \tag{76}$$

In other words, if we limit ourselves to a stroboscopic observation at times which are multiples of T, the evolution of a Bloch wave (or more generally of a wave packet formed by Bloch waves of the considered band), is identical to the case of an unmodulated lattice provided that we make the substitution

$$E(q) \quad \rightarrow \quad \epsilon(q) = \frac{1}{T}\int_0^T E[q - p_0(t)/\hbar]\ \mathrm{d}t. \tag{77}$$

We will see in the next paragraph that this conclusion is a special case of the consequences of Floquet's approach, which allows to deal with time-periodic Hamiltonians. The treatment presented here is particularly simple because we have limited ourselves to a single band. As soon as we want to take several bands into account, the Floquet method requires a numerical treatment. Indeed, the modulation can induce interband transitions (at a given q), which makes the problem much more complex.

Since we have the explicit expression of the energy $E(q)$ as a function of the tunnel coefficients $J(j')$, we can evaluate precisely the integral (74). Let us consider the sinusoidal motion

$$x_0(t) = \bar{x}_0\cos(\omega t), \quad p_0(t) = -m\omega\bar{x}_0\sin(\omega t), \tag{78}$$

for which the equation (74) providing the quasi-energy ϵ_q becomes:

$$\epsilon(q) = \frac{2}{T} \sum_{j'=1}^{\infty} J(j') \int_0^T \cos\left\{j'[aq + \xi_0 \sin(\omega t')]\right\} \, \mathrm{d}t', \tag{79}$$

where we have defined as previously

$$\xi(t) = \frac{ma}{\hbar\omega} \ddot{x}_0(t) = \xi_0 \cos(\omega t), \qquad \xi_0 = -ma\omega\bar{x}_0/\hbar. \tag{80}$$

This integral is easily calculated:

$$\epsilon(q) = 2 \sum_{j'=1}^{\infty} J(j') \, \cos(j'aq) \, \mathcal{J}_0(j'\xi_0), \tag{81}$$

to be compared to the energies without the modulation ($\xi_0 = 0$)

$$E(q) = 2 \sum_{j'=1}^{\infty} J(j') \, \cos(j'aq). \tag{82}$$

The expression (81) for quasi-energies allows to describe the phenomenon of dynamical localization in a very simple way. Let us consider the tight-binding limit where only the hoppings between nearest neighbours, described by the parameter $J = -J(1)$, are significant. We then have:

$$E(q) = -2J\cos(aq) \quad \rightarrow \quad \epsilon(q) \approx -2J\cos(aq)\,\mathcal{J}_0(\xi_0), \tag{83}$$

where we find the renormalization of the tunnel coefficient $J \rightarrow J'$ determined in (56). More precisely, the quasi-energies form a band with a width reduced with respect to the initial band, the reduction coefficient being $\mathcal{J}_0(\xi_0) < 1$. When the argument of this Bessel function is chosen to be equal to the first zero of this function (≈ 2.405), the band is infinitely narrow: all quasi-energies $\epsilon(q)$ are equal to each other (in this case zero). It is then immediate to show that the state of the particle will remain the same at all times 0, T, $2T$, etc. It is enough to consider the expansion of this state on the Bloch states

$$|\psi(0)\rangle = \int C(q)|\psi_q\rangle \, \mathrm{d}q \quad \rightarrow \quad |\psi(nT)\rangle = \int C(q) \, \mathrm{e}^{-\mathrm{i}\epsilon(q)nT/\hbar} \, |\psi_q\rangle \, \mathrm{d}q, \tag{84}$$

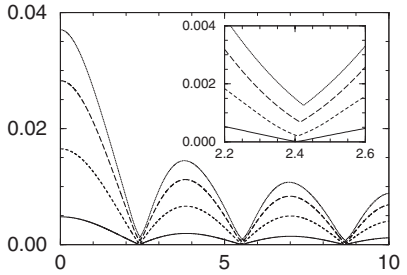

Figure 3. *Width of the quasi-band of lowest energy (in units of E_r) as a function of the modulation index ξ_0 for different depths of the lattice; from top to bottom: $V_0/E_\mathrm{r} = 2$, 3, 5, 10. The introduction of terms beyond $j = 1$ in the sum (81) results in the bandwidth not exactly cancelling when ξ_0 is equal to a zero of the Bessel function $\mathcal{J}_0$. Figure extracted from Eckardt, Holthaus, et al. (2009).*

and to use the fact that all quasi-energies $\epsilon(q)$ have the same value. The vector state $|\psi(nT)\rangle$ is then equal to $|\psi(0)\rangle$ and an initial wave packet does not spread over times that are large compared to T; more precisely, its evolution between nT and $(n+1)T$ is identical to its evolution between 0 and T.

If the hoppings between nearest neighbours are not sufficient to describe the dynamics in the lowest band, we must consider the next terms $J(2)$, $J(3)$ in the expansion (81). There is then no value of the modulation amplitude for which the quasi-band is infinitely narrow. This quasi-band is nevertheless strongly narrowed close to $\xi_0 = 2.405$. We show on figure 3 a result extracted from Eckardt, Holthaus, et al. (2009), which shows the width of the quasi-band for different values of the potential V_0. Even for a relatively small value of V_0 ($V_0 = 2E_\mathrm{r}$), the bandwidth in the vicinity of $\xi_0 = 2.4$ is reduced by more than a factor of 20 compared to its value without modulation.

Note: We have focused here on a sinusoidal modulation of the position of the lattice $x_0(t)$. Eckardt, Holthaus, et al. (2009) show that if one chooses a scheme such that the force $F(t)$ is a rectangular function (the lattice is accelerated uniformly to the left, then to the right), then the quasi-band can have a zero width even if one takes into account the couplings J_2, J_3,

etc. Indeed, the Bessel function of (81) is replaced, as for the case of spin 1/2 studied in (51), by a sinc function:

$$\mathcal{J}_0(j\xi_0) \quad \longrightarrow \quad \mathrm{sinc}(\pi j \xi_0/2) \tag{85}$$

and this coefficient cancels when ξ_0 is an even integer, fo any j.

4-4 The Floquet method

In the previous paragraph, we have been able to solve the problem of the shaken lattice thanks to the one-band approximation which allowed us to derive in a simple way the notion of quasi-energy. If we wish to go beyond this approximation, it is necessary to consider the evolution of a system under the effect of a time-periodic Hamiltonian in a more formal way. The theoretical method adapted to this problem was developed by Floquet. We will recall in the following the important points of this approach for the problem we are interested in, and we will draw the link with the results of the previous paragraph.

Floquet's approach is a general method for dealing with the evolution of a dynamical system governed by

$$\frac{\mathrm{d}}{\mathrm{d}t}\boldsymbol{X} = \hat{M}(t)\ \boldsymbol{X}, \tag{86}$$

where $\boldsymbol{X}$ is a column vector with d components (real or complex) and $\hat{M}(t)$ is a square matrix $d\times d$, explicitly time-dependent and periodic with period T:

$$\hat{M}(t+T) = \hat{M}(t). \tag{87}$$

This method is a transposition to the time domain of the Bloch function method, which exploits the translation invariance in the spatial domain.

Before presenting Floquet's method, let us first recall the known results for a time-independent Hamiltonian $\hat{H}$. Let us denote $\{|\phi_\alpha\rangle\}$ the eigenvectors of $\hat{H}$ and $\{E_\alpha\}$ the associated energies. The evolution operator from time 0 to time T, denoted $\hat{U}(T)$, is equal to $\exp(-\mathrm{i}\hat{H}T/\hbar)$. The states $|\phi_\alpha\rangle$ are eigenstates of this operator:

$$\hat{U}(T) = \mathrm{e}^{-\mathrm{i}\hat{H}T/\hbar}, \qquad \hat{U}(T)\,|\phi_\alpha\rangle = \mathrm{e}^{-\mathrm{i}E_\alpha T/\hbar}\,|\phi_\alpha\rangle. \tag{88}$$

Let us now turn to the case of a time-periodic Hamiltonian with the Floquet method. We are not going to use this method in all its details, but some of its general results will serve as a guide. Let us specify them here:

- The Schrödinger equation is of the type (86) and the evolution operator from time 0 to time nT, where n is an integer, verifies

$$\hat{U}(nT) = \left[\hat{U}(T)\right]^n. \tag{89}$$

- The operator $\hat{U}(T)$ is unitary and can be diagonalized, and its eigenvalues have a modulus 1. Let us note these eigenvalues $\mathrm{e}^{-\mathrm{i}\epsilon_\alpha T/\hbar}$, where the quantities ϵ_α are real and have the dimension of an energy. The ϵ_α are called *quasi-energies*, by analogy to the quasi-momentum q, and are defined modulo $2\pi\hbar/T$, just as the quasi-momentum q is defined modulo $2\pi/a$. Let us note $|\phi_\alpha\rangle$ the associated eigenvectors

$$\hat{U}(T)|\phi_\alpha\rangle = \mathrm{e}^{-\mathrm{i}\epsilon_\alpha T/\hbar}|\phi_\alpha\rangle. \tag{90}$$

  These vectors form an orthogonal basis of the Hilbert space and we find for any initial state $|\psi(0)\rangle$:

$$|\psi(nT)\rangle = \sum_\alpha C_\alpha\ \mathrm{e}^{-\mathrm{i}n\epsilon_\alpha T/\hbar}|\phi_\alpha\rangle \tag{91}$$

  where the coefficients C_α are given by $C_\alpha = \langle\phi_\alpha|\psi(0)\rangle$.

- Let us consider the state $|\psi_\alpha(t)\rangle$ obtained by starting from $|\phi_\alpha(t)\rangle$ at time $t=0$ and after an evolution under the effect of $\hat{H}(t)$:

$$|\psi_\alpha(t)\rangle = \hat{U}(t)\,|\phi_\alpha\rangle. \tag{92}$$

  Since $|\phi_\alpha\rangle$ is an eigenstate of $\hat{U}(T)$, it is clear that

$$|\psi_\alpha(T)\rangle = \mathrm{e}^{-\mathrm{i}\epsilon_\alpha T/\hbar}|\psi_\alpha(0)\rangle. \tag{93}$$

  Even if the evolution of $|\psi_\alpha(t)\rangle$ can be arbitrarily complicated between 0 and T, we see that this vector becomes equal to its initial value after a period T, up to the phase $\epsilon_\alpha T/\hbar$.

- To eliminate this remaining phase $\epsilon_\alpha T/\hbar$ in the evolution of $|\psi_\alpha(t)\rangle$, let us introduce the state vector $|u_\alpha(t)\rangle$ such that

$$|\psi_\alpha(t)\rangle = \mathrm{e}^{-\mathrm{i}\epsilon_\alpha t/\hbar}|u_\alpha(t)\rangle. \tag{94}$$

It is immediate that $|u_\alpha(t)\rangle$ is time-periodic with a period T, which allows to decompose it in Fourier series:

$$|u_\alpha(t)\rangle = \sum_{n\in\mathbb{Z}} \mathrm{e}^{\mathrm{i}n\omega t}|\chi_{\alpha,n}\rangle, \tag{95}$$

where the time-independent vectors $|\chi_{\alpha,n}\rangle$ are for now unknown.

- To simplify the notations, we will assume that $\hat{H}(t)$ can be written as[6].

$$\hat{H}(t) = \hat{H}_0 + \mathrm{e}^{\mathrm{i}\omega t}\,\hat{V}_+ + \mathrm{e}^{-\mathrm{i}\omega t}\,\hat{V}_-, \tag{96}$$

with $\hat{V}_- = \hat{V}_+^\dagger$. When we replace $|\psi_\alpha\rangle$ by its expression in terms of $|u_\alpha\rangle$ and we use the Fourier expansion of this vector, the Schrödinger equation $i\hbar|\dot{\psi}_\alpha\rangle = \hat{H}(t)|\psi_\alpha\rangle$ becomes

$$(\epsilon_\alpha - n\hbar\omega)|\chi_{\alpha,n}\rangle = \hat{H}_0|\chi_{\alpha,n}\rangle + \hat{V}_+|\chi_{\alpha,n-1}\rangle + \hat{V}_-|\chi_{\alpha,n+1}\rangle. \tag{97}$$

- The evolution under the periodic Hamiltonian $\hat{H}(t)$ will be completely solved once we have explicitly determined the states $|\chi_{\alpha,n}\rangle$ and the quasi-energies ϵ_α. For this, let us assume that we can restrict the relevant part of the Hilbert space to a subspace of dimension d. The operators $\hat{H}_0$, V_+, V_- are then $d\times d$ square matrices and the kets $|\chi_{\alpha,n}\rangle$ are vectors with d components. Let us then form the infinite dimension vector

$$|\Xi\rangle = {}^t(\ldots, |\chi_{\alpha,n-1}\rangle, |\chi_{\alpha,n}\rangle, |\chi_{\alpha,n+1}\rangle, \ldots) \tag{98}$$

obtained by putting all the vectors $|\chi_{\alpha,n}\rangle$ one below the other. The system (97) can be rewritten as an eigenvalue equation

$$\epsilon_\alpha\,|\Xi\rangle = \hat{\mathcal{H}}\,|\Xi\rangle \tag{99}$$

for the operator $\hat{\mathcal{H}}$ also of infinite dimension, obtained as a band matrix defined by $d\times d$ blocks:

$$\hat{\mathcal{H}} = \begin{pmatrix} \ddots & & & & & & & \\ \ldots & 0 & \hat{V}_+ & \hat{H}_0+(n-1)\hbar\omega & \hat{V}_- & 0 & & \\ & \ddots & 0 & \hat{V}_+ & \hat{H}_0+n\hbar\omega & \hat{V}_- & 0 & \ddots \\ & & \ddots & 0 & \hat{V}_+ & \hat{H}_0+(n+1)\hbar\omega & \hat{V}_- & \ldots \\ & & & \ddots & & & & \ddots \end{pmatrix}. \tag{100}$$

Due to the presence of the term $n\hbar\omega$ on the diagonal, we obtain a spectrum that extends periodically from $-\infty$ to $+\infty$. In a "Brillouin" zone of width $\hbar\omega$, we find d eigenvalues. In practice, we truncate this infinite matrix at $|n| < n_{\max}$ and diagonalize numerically the resulting square matrix.

Link with the results of the previous paragraph. In the one-band approximation, the conservation of the quasi-momentum implies that the Bloch waves are eigenstates of the evolution operator $\hat{U}(T)$. The most delicate step of Floquet's method, namely the search for these eigenstates, is thus immediately done ($|\psi_\alpha\rangle = |\psi_{n,q}\rangle$), and the quasi-energies $\epsilon_\alpha = \epsilon(q)$ are also known. One could extend Floquet's approach to determine the periodic functions $|u_\alpha(t)\rangle$ at any time t, which would allow to specify the evolution of any initial state between 0 and T. One could thus evaluate the breathing of a wave packet between 0 and T in the non-diffusive case obtained for $\mathcal{J}_0(\xi_0) = 0$.

5 Example of a shaken 2D lattice

The control of the tunnel coefficient by modulating the position of an optical lattice has been implemented in two dimensions in an experiment conducted in Hamburg. The lattice is formed by three quasi-planar waves propagating in the xy plane at 120 degrees from each other, with wave vectors

$$\boldsymbol{k}_1 = k\begin{pmatrix}1\\0\end{pmatrix}, \qquad \boldsymbol{k}_2 = \frac{k}{2}\begin{pmatrix}-1\\\sqrt{3}\end{pmatrix}, \qquad \boldsymbol{k}_3 = -\frac{k}{2}\begin{pmatrix}1\\\sqrt{3}\end{pmatrix}. \tag{101}$$

[6] It is not difficult to introduce more harmonics in the Hamiltonian $\hat{H}(t)$, but it complicates the equations a bit, by adding an extra index.

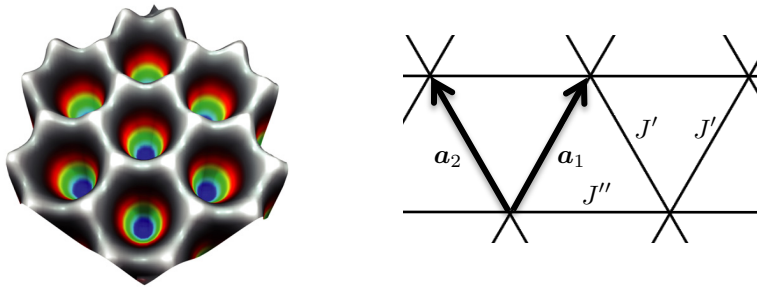

Figure 4. *(a) Intensity profile for a red-detuned lattice formed by three plane waves propagating at 120 degrees from each other in the xy plane. The three waves have the same intensity and are linearly polarized along Oz [Figure taken from Becker, Soltan-Panahi, et al. 2010]. (b) Triangular lattice with basis vectors $\boldsymbol{a}_1$ and $\boldsymbol{a}_2$, and tunnel coefficients J' and J'' that can be controlled independently by modulating the phases φ_2 and φ_3 of two of the laser beams forming the lattice.*

The three waves have the same intensity I_0 and are all polarized along the axis Oz, so that the intensity at a point xy is written

$$\begin{aligned} I(x,y) &= I_0 \left| \mathrm{e}^{\mathrm{i}kx} + \mathrm{e}^{-\mathrm{i}k(x-\sqrt{3}\,y)/2} + \mathrm{e}^{-\mathrm{i}k(x+\sqrt{3}\,y)/2} \right|^2 \\ &= I_0 \left| \mathrm{e}^{3\mathrm{i}kx/2} + 2\cos(\sqrt{3}\,ky/2) \right|^2 . \end{aligned} \tag{102}$$

We have chosen by convention that the three beams are in phase at position $x = y = 0$. The detuning is chosen negative (on the red side) so that the potential minima are located at the intensity maxima. These maxima, where $I = 9I_0$, are distributed according to a triangular lattice, at the vertices of the Bravais lattice formed by the union of the two sets

$$\begin{aligned} &(i) \qquad 3kx/2 = 0 \pmod{2\pi}, \quad \sqrt{3}\,ky/2 = 0 \pmod{2\pi}, \\ &(ii) \qquad 3kx/2 = \pi \pmod{2\pi}, \quad \sqrt{3}\,ky/2 = \pi \pmod{2\pi}. \end{aligned} \tag{103}$$

i.e.

$$\mathcal{B} = \{ j_1 \boldsymbol{a}_1 + j_2 \boldsymbol{a}_2,\ j_1, j_2 \in \mathbb{Z} \} \tag{104}$$

with

$$\boldsymbol{a}_1 = \frac{2\pi}{3k} \begin{pmatrix} 1 \\ \sqrt{3} \end{pmatrix}, \qquad \boldsymbol{a}_2 = \frac{2\pi}{3k} \begin{pmatrix} -1 \\ \sqrt{3} \end{pmatrix} \tag{105}$$

The intensity profile is shown in figure 4a. In the experiment of Struck, Oelschlaeger, et al. (2011), the intensity I_0 is large enough for the dynamics in the lowest band of the lattice to be well approximated by the tight-binding limit, with a depth of $5.6E_\mathrm{r}$ and a tunnel coefficient $J = 0.002E_\mathrm{r}$. The confinement along the z direction is much softer, and a triangular lattice of tubes is realized, each containing a few hundred atoms. The gas is sufficiently cold for each tube to be considered as a micro-condensate, with a well-defined phase.

If we change the phases φ_2 and φ_3 of the two waves that have wave vectors $\boldsymbol{k}_2$ and $\boldsymbol{k}_3$, it is easy to show that the intensity profile $I(x,y)$ is simply translated in the xy plane by the quantity

$$\Delta x = \frac{1}{3k}(\varphi_2 + \varphi_3), \qquad \Delta y = \frac{1}{\sqrt{3}k}(\varphi_2 - \varphi_3). \tag{106}$$

A sinusoidal time modulation of φ_2 and φ_3 thus induces a shaking of the lattice.

Struck, Oelschlaeger, et al. (2011) have chosen temporal variations of φ_2 and φ_3 such that $\Delta x = x_0 \cos(\omega t)$, $\Delta y = y_0 \sin(\omega t)$, which allows to modify in a different way the two tunnel coefficients J' and J'' indicated in figure 4; J' corresponds to transitions along $\boldsymbol{a}_1$ and $\boldsymbol{a}_2$, J'' to transitions along $\boldsymbol{a}_1 - \boldsymbol{a}_2$, parallel to the Ox axis. With arguments similar to those of the simple approach developed above for the case of a 1D lattice, the tunnel coefficients J' and J'' are written

$$J' = J\mathcal{J}(\xi_0'), \quad J'' = J\mathcal{J}(\xi_0''), \tag{107}$$

with

$$\xi_0' = \frac{m\omega^2 a}{2\hbar}\sqrt{x_0^2 + 3y_0^2}, \qquad \xi_0'' = \frac{m\omega^2 a}{\hbar} x_0. \tag{108}$$

By controlling separately the values of x_0 and y_0, one can thus adjust independently the magnitudes and signs of the coefficients J' and J''. In particular, one can choose modulations such that $J' > 0$, $J'' < 0$ (and vice versa), whereas without the modulation, we have $J' = J'' > 0$.

As in the 1D experiment in Pisa, the sign flip of one of the tunnel coefficients results in a shift of the minima of the lowest band in the space of quasi-momenta $\boldsymbol{q}$. These minima are observed directly by time of flight,

since they correspond to the macroscopically occupied states when a condensate is placed in the lattice. Two clearly different time-of-flight pictures are shown on figure 5, the one on the left being obtained for $J', J'' > 0$ and the one on the right for $J' < 0$, $J'' > 0$.

To account for this change in band structure, let us write the one-particle Hamiltonian as

$$\begin{aligned}\hat{H} &= -J' \sum_{j_1,j_2} \left(|w_{j_1+1,j_2}\rangle\langle w_{j_1,j_2}| + |w_{j_1,j_2+1}\rangle\langle w_{j_1,j_2}| + \text{h.c.}\right) \\ &\quad -J'' \sum_{j_1,j_2} \left(|w_{j_1+1,j_2-1}\rangle\langle w_{j_1,j_2}| + \text{h.c.}\right) \end{aligned} \tag{109}$$

where the first line corresponds to hoppings along the directions $\boldsymbol{a}_1$ and $\boldsymbol{a}_2$, and the second line to hoppings parallel to the Ox axis, along the vector $\boldsymbol{a}_1 - \boldsymbol{a}_2$. A Bloch state

$$|\psi_{\boldsymbol{q}}\rangle = \sum_{\boldsymbol{j}} \mathrm{e}^{\mathrm{i}\boldsymbol{r_j}\cdot\boldsymbol{q}} |w_{\boldsymbol{j}}\rangle \tag{110}$$

is eigenstate of $\hat{H}$ with eigenvalue

$$E(\boldsymbol{q}) = -2\left[J' \cos(\boldsymbol{a}_1 \cdot \boldsymbol{q}) + J' \cos(\boldsymbol{a}_2 \cdot \boldsymbol{q}) + J'' \cos((\boldsymbol{a}_1 - \boldsymbol{a}_2) \cdot \boldsymbol{q})\right]. \tag{111}$$

Let us first take $J', J'' > 0$. In this case, the ground state is obtained for $\boldsymbol{q} = 0$, with a corresponding energy $E = -4J' - 2J''$. This is indeed the most populated state on the left image of the figure 5. Let us now choose $J' < 0$, $J'' > 0$. The minimum is obtained by taking for example $\boldsymbol{a}_1 \cdot \boldsymbol{q} = \boldsymbol{a}_2 \cdot \boldsymbol{q} = \pi$, which corresponds to $\boldsymbol{q} = \boldsymbol{u}_y \sqrt{3}k/2$, with a corresponding energy $E = -4|J'| - 2J''$. This prediction[7] corresponds to the result visible on the right image of figure 5.

An original point of view on the physics of atoms in this triangular lattice is put forward by Struck, Oelschlaeger, et al. (2011); it highlights the use of the lattice to simulate the classical magnetism of a triangular lattice. By assigning a phase $\theta_{\boldsymbol{i}}$ to the micro-condensate trapped at the site $|w_i\rangle$ of the lattice, one can write the energy of a given configuration $\{\theta_i\}$ as

$$E\left(\{\theta_{\boldsymbol{i}}\}\right) = -N \sum_{\langle \boldsymbol{i},\boldsymbol{j}\rangle} J_{\boldsymbol{i},\boldsymbol{j}} \cos(\theta_{\boldsymbol{i}} - \theta_{\boldsymbol{j}}). \tag{112}$$

[7] We can also take $\boldsymbol{a}_1 \cdot \boldsymbol{q} = \pi$ and $\boldsymbol{a}_2 \cdot \boldsymbol{q} = -\pi$, which corresponds to $\boldsymbol{q} = \boldsymbol{u}_x(3k/2)$ also visible on the right image of figure 5.

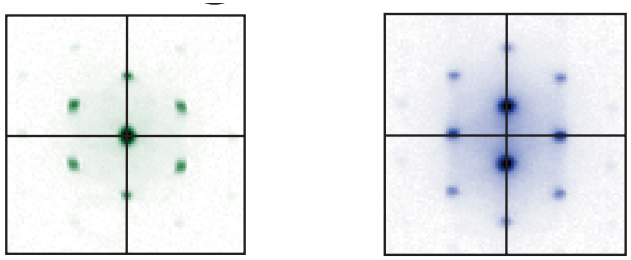

Figure 5. *Time-of-flight figures extracted from Struck, Oelschlaeger, et al. (2011). Left: figure obtained for $J', J'' > 0$. Right: figure obtained for $J' < 0$, $J'' > 0$.*

The sum runs over all pairs of nearest neighbours $\langle \boldsymbol{i}, \boldsymbol{j}\rangle$, and we have performed the substitution

$$|w_{\boldsymbol{i}}\rangle\langle w_{\boldsymbol{j}}| \longrightarrow \mathrm{e}^{\mathrm{i}(\theta_i - \theta_j)}. \tag{113}$$

This substitution is valid if we can describe the state of each micro-condensate by a classical field $\sqrt{N_{\boldsymbol{j}}}\,\mathrm{e}^{\mathrm{i}\theta_j}$ and assume that the numbers of atoms in all these micro-condensates are similar.

The energy functional (112) is formally identical to that of an assembly of spins $\boldsymbol{S_i} = [\cos(\theta_{\boldsymbol{i}}), \sin(\theta_{\boldsymbol{i}})]$ arranged on the nodes of the lattice $\mathcal{B}$, with interactions between nearest neighbours:

$$E\left(\{\theta_{\boldsymbol{i}}\}\right) = -\sum_{\langle \boldsymbol{i},\boldsymbol{j}\rangle} J_{\boldsymbol{i},\boldsymbol{j}} \boldsymbol{S_i} \cdot \boldsymbol{S_j}. \tag{114}$$

The different structures which appear in time of flight when we vary the amplitude and the sign of J' and J'' thus allow us to find the magnetic phases of this lattice of interacting spins. The two images shown on figure 5 correspond to the ferromagnetic phase (all the spins aligned, all the phases $\theta_{\boldsymbol{j}}$ equal, energy minimum in $\boldsymbol{q} = 0$) and to the rhombic phase (lines along the x axis with spins pointing in a given direction, alternating with lines of opposite spins).

We end this paragraph by mentioning that it is also possible to time-modulate the lattice in a way that gives a non-zero imaginary part to the tunnel coefficient (Struck, Ölschläger, et al. 2012). To do this, one can choose a function $\eta(t)$ such that $\langle \mathrm{e}^{\mathrm{i}\eta}\rangle$ has a non-zero imaginary part. This

allows to have a particle that travels along the edges of the unit cell of the lattice accumulating a non-zero phase, which is the basis for the generation of artificial magnetic fields. We will come back to this point in an upcoming lecture series.

Chapter V

Bloch oscillations in an optical lattice

In the previous chapter, we studied the dynamics of atoms placed in an optical lattice whose periodic potential $\mathcal{V}(x,t)$ depends on time. In the case where this dependence is limited to a displacement of the lattice

$$\mathcal{V}(x,t) = V(x - x_0(t)), \tag{1}$$

we have shown that we can, thanks to a unitary transformation, analyze the problem in the reference frame of the lattice. We then recover a problem with a static lattice $V(x)$ to which we superimpose the inertial force $F(t) = -m\ddot{x}_0(t)$.

It is therefore natural at this stage to look further into the question of the dynamics of a particle placed simultaneously in a periodic potential independent of time and with a spatially uniform force. The simplest case is the one of a time-independent force F, and we will consider this case during most of this chapter. Our Hamiltonian will therefore be

$$\hat{H} = \frac{\hat{p}^2}{2m} + V(\hat{x}) - F\,\hat{x}. \tag{2}$$

This problem was initially addressed by Zener to model the behavior of an electron in a crystal lattice, on which an external electric field is applied. The Hamiltonian (2) describes the motion of the particle in the reference frame of the laboratory. The same problem is encountered with cold atoms in a stationary lattice to which we add gravity or the force created by a magnetic field gradient, like in the Stern and Gerlach experiment.

Moreover, with the equivalence between a moving lattice (without additional force) and a fixed lattice with a force $F(t)$, we see that we can create this potential by starting from a periodic lattice in an uniformly accelerated motion in the reference frame of the laboratory: if we take $x_0(t) = -Ft^2/(2m)$ in the Hamiltonian

$$\hat{H}_2(t) = \frac{\hat{p}^2}{2m} + V(\hat{x} - x_0(t)), \tag{3}$$

we recover the Hamiltonian (2) in the uniformly accelerated reference frame in which the lattice is stationary, thanks to the unitary transformation given in the previous lecture.

Bloch oscillations of cold atoms in optical lattices have become a powerful tool in recent years and are used in many applications: gravity measurement, study of force fields near surfaces, beam splitting for atomic interferometry. Even if cold atoms are not the first physical system on which oscillations have been observed (see for example the review article of Mendez & Bastard (1993) for studies on solid superlattices), Bloch oscillations constitute an object of study with plentiful and diverse aspects for cold gases, thanks to the richness of their applications.

1 The principle of Bloch oscillations

1-1 The evolution of the quasi-momentum

In the previous chapter, we studied the evolution of a particle under the effect of a Hamiltonian of type

$$\hat{H} = \frac{\hat{p}^2}{2m} + V(\hat{x}) - F(t)\,\hat{x}. \tag{4}$$

where $V(x)$ is periodic with period a. In particular, we have shown that the Bloch form is preserved during the evolution. An initial state

$$\psi(x,0) = \mathrm{e}^{\mathrm{i}xq_{\mathrm{in}}}\,u(x,0) \tag{5}$$

will keep this form and be written at time t

$$\psi(x,t) = \mathrm{e}^{\mathrm{i}xq(t)}\,u(x,t). \tag{6}$$

The quasi-momentum $q(t)$ is given by

$$q(t) = q_{\mathrm{in}} + \frac{1}{\hbar}\int_0^t F(t')\,\mathrm{d}t'. \tag{7}$$

For the case that interests us here, the force F is independent of time and $q(t)$ evolves linearly in time

$$q(t) = q_{\mathrm{in}} + Ft/\hbar. \tag{8}$$

A time scale and an energy scale are therefore naturally introduced: the time

$$\tau_{\mathrm{B}} = 2\hbar k/F \tag{9}$$

represents the time necessary for $q(t)$ to go through the Brillouin zone, which has size $2k = 2\pi/a$. To this time is associated the angular frequency $\omega_{\mathrm{B}} = 2\pi/\tau_{\mathrm{B}}$ and the energy

$$\hbar\omega_{\mathrm{B}} = \pi F/k = Fa. \tag{10}$$

This energy represents the work of the force F over a period of the potential $V(x)$; it is therefore the decrease in energy between two successive local minima of the potential $V(x) - Fx$ (cf. figure 1).

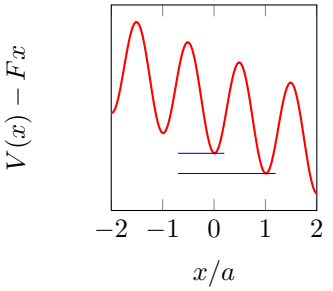

Figure 1. *Potential $V(x) - Fx$ giving rise to Bloch oscillations, with $V(x) = V_0 \sin^2(\pi x/a)$ and $\hbar\omega_{\mathrm{B}} \equiv Fa = V_0/5$. The energy difference between the two horizontal lines is equal to $\hbar\omega_{\mathrm{B}}$.*

At this point, we cannot yet say anything about the spatially-periodic function $u(x,t)$ which multiplies $\mathrm{e}^{\mathrm{i}xq(t)}$ in (6), except that it is a solution of

$$\mathrm{i}\hbar\frac{\mathrm{d}}{\mathrm{d}t}|u(t)\rangle = \hat{H}_{\mathrm{per}}[q(t)]\,|u(t)\rangle, \tag{11}$$

where $\hat{H}_{\mathrm{per}}[q]$ is the Hamiltonian for the periodic part of the Bloch functions:

$$\hat{H}_{\mathrm{per}}[q] = \frac{(\hat{p}+\hbar q)^2}{2m} + V(\hat{x}). \tag{12}$$

It is the adiabatic approximation which, as in the previous chapter in the case of a sinusoidal force, will allow us to progress.

1-2 The adiabatic approximation

From now on, we assume that the initial state $\mathrm{e}^{\mathrm{i}q_{\mathrm{in}}x}\,u(x,0)$ is a Bloch function, i.e. an eigenstate $\psi_{n,q_{\mathrm{in}}}(x)$ of the n-th energy band of the Hamiltonian

$$\hat{H}_0 = \frac{\hat{p}^2}{2m} + V(\hat{x}) \tag{13}$$

corresponding to the case $F = 0$. In other words, the function $u(x,0) = \langle x|u(t=0)\rangle$ coincides (up to a global phase) with the eigenstate $u_{n,q_{\mathrm{in}}}(x)$ of the Hamiltonian $\hat{H}_{\mathrm{per}}[q_{\mathrm{in}}]$ for the periodic part (12).

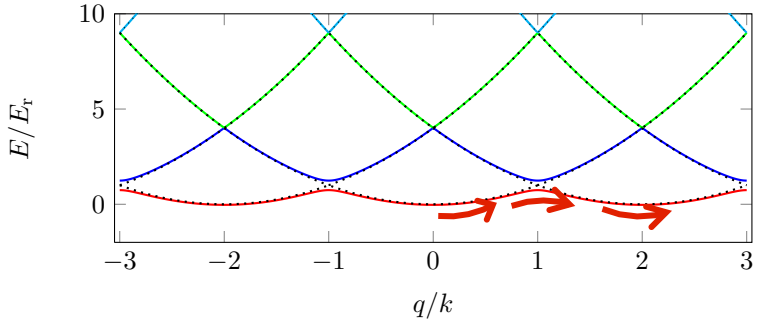

Figure 2. *The evolution of the quasi-momentum in the repeated band picture. The Bloch oscillation regime corresponds to the situation where the particle follows adiabatically the initial energy level (here the red curve) and does not go to another energy level (here the blue curve). The dangerous zone is located at the points where q/k is an odd integer, where the red and blue bands are the closest. This figure is plotted for $V_0 = E_r$.*

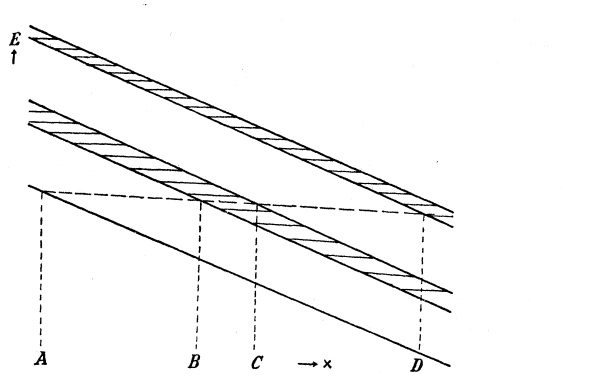

FIG. 1.—"Potential barrier" diagram. The shaded regions represent zones of forbidden energy in the presence of an electric field.

Figure 3. *Figure taken from the original paper by Zener (1934), representing the energy bands tilted by the potential $-Fx$.*

The adiabatic approximation consists in assuming that the state $|u(t)\rangle$ solution of (11) remains equal (up to a global phase) to $|u_{n,q(t)}\rangle$, that is

$$\psi(x,t) \propto \mathrm{e}^{\mathrm{i}xq(t)}\, u_{n,q(t)}(x). \tag{14}$$

Since the quasi-momentum $q(t)$ moves at uniform speed and spans the Brillouin zone in a time τ_B, the time-evolution of $\psi(x,t)$ is periodic (up to a global phase[1]), with this same period τ_B. This evolution is represented on figure 2 in the so-called *repeated zone* representation.

This periodic evolution of the state of the particle under the effect of a uniform force (in addition to the potential $V(x)$) is a remarkable phenomenon, which originates in the structure in energy bands of the spectrum of the unperturbed Hamiltonian. The name *Bloch oscillations* for this phenomenon is rather paradoxical. Indeed, this effect is not described in Bloch's seminal paper on the quantum physics of electrons in crystals. Its first public appearance seems to be in the paper of Zener (1934). Another paradox is that the oscillation is not what interested Zener. He was looking for the effect that an electric field could have on an insulator and it was therefore the interband transitions that we will see a little later in this lecture that motivated his study: the aim was to find a force F large enough so that the adiabatic following would not take place, while the oscillation itself was probably considered as trivial by Zener...

It is interesting to look at the first figure in Zener's paper of 1934, with which he interprets the oscillation phenomenon (see Figure 3). He makes a local approximation of the energy bands, by plotting these bands as a function of position after adding the potential energy $-Fx$. The forbidden bands are represented by the hatched areas. The horizontal line represents a possible energy for an electron. This electron starts from point A, is accelerated by the force F until it arrives at point B, and it can then (i) turn around, which constitutes the oscillation phenomenon, or (ii) go to point C by tunnelling, at the bottom of the next energy band, and thus contribute to the electric conduction. We deduce from this image the amplitude of the oscillations in real space, $x_B - x_A = \Delta E/F$, where ΔE is the width of the allowed band that is initially occupied.

The amplitude of the oscillations in real space can be found by considering a wave packet centered on $\bar{q}(t)$ in momentum space, and whose dispersion in q remains at each instant small compared to k. In real space,

[1] We will not consider the phase (Zak 1989) accumulated during an oscillation in this chapter, this will be the topic of a later lecture.

we note $\bar{x}(t)$ the center of this wave packet; the average velocity of the wave packet is given by the group velocity

$$\frac{\mathrm{d}\bar{x}}{\mathrm{d}t} = v_{\mathrm{g}}(t) = \frac{1}{\hbar}\left.\frac{\mathrm{d}E_{n,q}}{\mathrm{d}q}\right|_{q=\bar{q}(t)}, \tag{15}$$

which evolves periodically in time. This evolution equation is integrated to give

$$\bar{x}(t) - \bar{x}(0) = \frac{1}{\hbar}\int_0^t \frac{\mathrm{d}E_{n,q}}{\mathrm{d}q}\,\mathrm{d}t = \frac{1}{F}\int_{q_{\mathrm{in}}}^{q(t)} \frac{\mathrm{d}E_{n,q}}{\mathrm{d}q}\,\mathrm{d}q, \tag{16}$$

where we have used the relation $q = Ft/\hbar$. We finally arrive at

$$\bar{x}(t) - \bar{x}(0) = \frac{1}{F}\left(E_{n,\bar{q}(t)} - E_{n,q_{\mathrm{in}}}\right), \tag{17}$$

which corresponds to the intuitive relationship suggested by figure 3.

There are several ways to represent the Bloch oscillation phenomenon. We have so far chosen the one that uses the band structure of the energy diagram (with no force). Another very useful point of view, directly inspired by quantum optics, is represented on figure 4ab. This point of view, valid for small lattice depths, consists in treating perturbatively the effect of the lattice in the form of multi-photon transitions that can occur when a resonance condition is satisfied. First, we plot the dispersion relation without the lattice $E = p^2/2m$; the presence of the force F will force the atom to travel across the momentum space according to the law $\dot{p} = F$. When an atom, starting for example from $p = 0$ arrives at $p = \hbar k$, a resonant two-photon transition can transfer it to $p = -\hbar k$ (4a). This jump can also be seen as a total Bragg reflection of the atomic wave of wavelength $2\pi/k$ on the lattice of constant π/k. The acceleration starts again from the momentum $p = -\hbar k$ and we recover the periodic oscillation, of frequency $F/(2\hbar k) = \omega_{\mathrm{B}}/2\pi$, predicted above. This picture generalizes easily to the Bloch oscillations in the upper bands. Figure 4b represents for example the Bloch oscillation in the first excited band, $n = 1$, in terms of two multi-photon transitions, one with two photons, and the other with four photons.

The last point of view on these Bloch oscillations that we will mention here is based on the plane wave expansion of the Bloch functions, which is expressed in terms of the Fourier transform of the Wannier functions (see

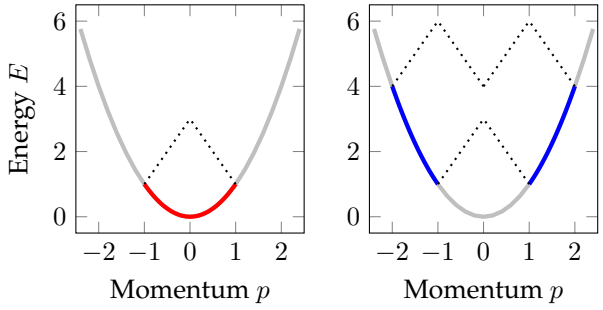

Figure 4. *Representation of Bloch oscillations in the lowest band ($n = 0$) on the left and in the first excited band ($n = 1$) on the right, in terms of multi-photon transitions. Under the effect of the constant force F, the momentum increases linearly with time ($\dot{p} = F$). When the momentum of the atom is such that a resonant multi-photon transition, represented by the black dotted lines, can occur ($p/\hbar k$ non-zero integer), a Bragg reflection occurs and the momentum of the atom switches from p to $-p$. The frequency of the oscillation, independent of the band, is $F/(2\hbar k) = \omega_{\mathrm{B}}/2\pi$.*

Chapter 3):

$$\psi_{n,q}(x) = \frac{1}{\sqrt{a}}\sum_{j\in\mathbb{Z}} \tilde{w}_n(q + 2\pi j/a)\,\mathrm{e}^{\mathrm{i}x(q+2\pi j/a)}. \tag{18}$$

During the oscillation, this comb of momenta runs at constant speed and the amplitude of the different components follows the envelope given by the function $\tilde{w}_n(\kappa)$, the Fourier transform of the Wannier function $w_{n,0}(x)$.

2 Experimental observations

2-1 First experiments with cold atoms

In quantum optics, the first Bloch oscillations have been observed in the groups of Christophe Salomon in Paris and Mark Raizen in Austin (Wilkinson, Bharucha, et al. 1996; Niu, Zhao, et al. 1996; Ben Dahan, Peik, et al.

1996; Peik, Ben Dahan, et al. 1997; Raizen, Salomon, et al. 1997). These observations were following a demonstration in solid samples, in particular in superlattices (Mendez & Bastard 1993). In Paris as well as in Austin, the force F was inertial, $F = -m\ddot{x}_0$, obtained thanks to an accelerated lattice

$$V(x,t) = V_0 \sin^2\left[k(x - x_0(t))\right] \tag{19}$$

with $x_0(t) = \gamma t^2/2$. Recall that such an acceleration is realized by varying in time the phases ϕ_1 and ϕ_2 of the two travelling waves $\mathrm{e}^{\mathrm{i}(kx-\omega t-\phi_1)}$ and $\mathrm{e}^{-\mathrm{i}(kx+\omega t+\phi_2)}$ forming the lattice. This acceleration a can for example be obtained by choosing

$$\phi_1(t) = k\gamma t^2/2, \qquad \phi_2(t) = -k\gamma t^2/2, \tag{20}$$

which corresponds to the "instantaneous frequencies"

$$\omega_1 = \omega + \frac{\mathrm{d}\phi_1}{\mathrm{d}t} = \omega + k\gamma t, \quad \omega_2 = \omega + \frac{\mathrm{d}\phi_2}{\mathrm{d}t} = \omega - k\gamma t. \tag{21}$$

The Paris experiment was conducted with cesium atoms ($m = 133$) while the Austin experiment used sodium atoms ($m = 23$). This significant factor on the masses, associated with an equally significant factor on the wavelengths of the used lattices, leads to important qualitative differences on the accelerations that are compatible with an adiabatic following (see for example the table V.1). In practice, the typical acceleration of the Paris experiments was between 1 and a few tens of ms^{-2}, while those used in Austin went up to several thousand ms^{-2}. In both cases, the lattice depth V_0 measured in units of E_r was of the order of a few units.

Some results illustrating these oscillations measured in the reference frame of the lattice (data extracted from Dahan:1996,Peik:1997) are shown in figure 6. We see in the left column the periodic evolution of the momentum distribution. In the right column, we have represented the evolution of the average velocity of the wave packet, in good agreement with the law (15). Note in particular the deformation of this curve when we go from small V_0/E_r (weak links, top) to large V_0/E_r (tight-binding, bottom):

- In the case of weak links, we have $E_{0,q} \approx \hbar^2 q^2/2m$ except at the edge of the zone, and the group velocity is therefore almost everywhere equal to $\hbar q/m$, i.e. a linear function of time since $q(t) = q_0 + Ft/\hbar$. The Bragg reflection at the edge of the zone corresponds to a fast variation of v, hence this sawtooth evolution.

- In the tight-binding limit, we saw in Lecture 3 that the lowest band is sinusoidal, $E_{0,q} \approx -2J\cos(aq)$, and the velocity therefore varies sinusoidally with time: $v(t) \propto \sin[aq(t)]$.

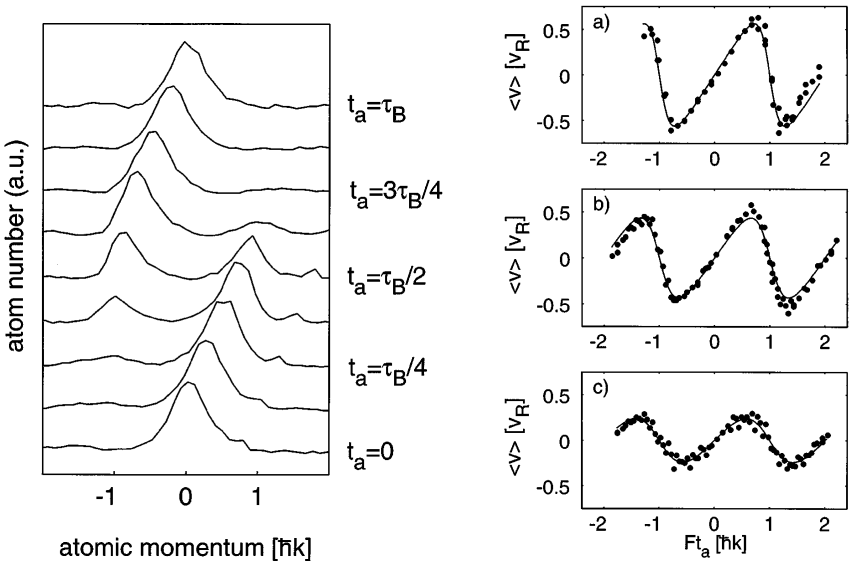

Figure 5. *Bloch oscillations observed in C. Salomon's group in 1996-97 in an accelerated optical lattice (Ben Dahan, Peik, et al. 1996; Peik, Ben Dahan, et al. 1997). The atomic velocities are measured in the reference frame in which the optical lattice is stationary. The atoms are initially prepared in the lowest band $n = 0$. Left: evolution of the velocity distribution for $V_0 = 2.3\,E_\mathrm{r}$ and $\gamma = 0.85\,ms^{-2}$. Right: evolution of the average velocity of the wave packet for different lattice depths: $V_0/E_\mathrm{r} = 1.4,\ 2.3,\ 4.4$.*

The distributions in figure 5 represent measurements of the velocities in the accelerated reference frame of the lattice. It is also interesting to represent these velocities in the reference frame of the laboratory, which is done in figure 6. We can see that for these parameters which correspond to a

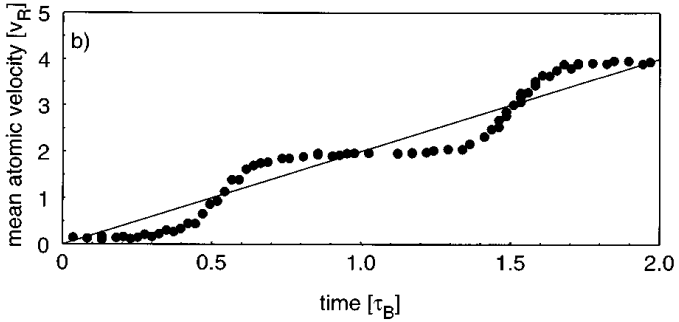

Figure 6. *Evolution of the average velocity of the atoms in the laboratory reference frame for the parameters of figure 5 (left). Figure extracted from Peik, Ben Dahan, et al. (1997).*

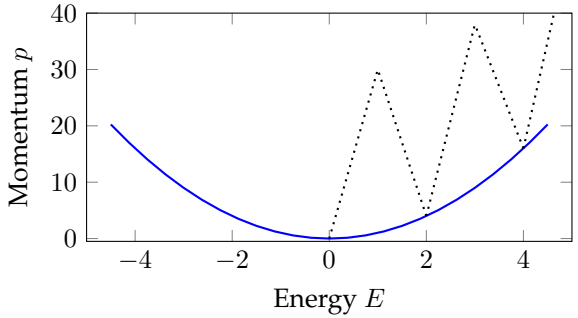

Figure 7. *Acceleration of atoms by successively resonant multiphoton transitions.*

limit of weak links, the atoms keep a constant speed most of the time, but periodically undergo a strong acceleration which increases their speed by $2\hbar k/m$. This dynamics has a simple interpretation in terms of two-photon transitions (cf. figure 7). These transitions are successively resonant at instants t_j such that the instantaneous frequencies of the laser waves forming the lattice verify

$$\hbar[\omega_1(t_j) - \omega_2(t_j)] = [(2j+2)^2 - (2j)^2]E_\mathrm{r} = (8j+4)E_\mathrm{r}, \tag{22}$$

for the transition $p = 2j\hbar k \to p = (2j+2)\hbar k$ (j is an integer). By taking the expression (21) of $\omega_{1,2}(t)$, we see that these accelerations occur for

$$t_j = \left(j + \frac{1}{2}\right)\,\tau_\mathrm{B}. \tag{23}$$

This accelerated lattice device is thus an efficient way to communicate a given momentum to the atoms. In practice, this momentum can reach several hundreds of $\hbar k$.

2-2 Note: momentum balance in an accelerated lattice

When we consider the point of view of the multi-photon transitions in figure 7, it is clear that the momentum gain of the atom during the acceleration of a lattice is a multiple of $2\,\hbar k$. This result is less obvious when the analysis is performed in the accelerated frame of reference; we propose to show it explicitly in the following paragraphs (see also Browaeys, Häffner, et al. (2005)).

Let us start with an atom that has a well-determined momentum p_in. Let us take $|p_\mathrm{in}| < \hbar k$, so that this momentum is in the first Brillouin zone[2]. Let us first adiabatically ramp up the stationary lattice. The state of the atom follows the Bloch function $\psi_{n=0,q_\mathrm{in}}$ with $q_\mathrm{in} = p_\mathrm{in}/\hbar$. Once the lattice has reached its full power, we put it in motion with an acceleration $\ddot{x}_0(t)$. In the reference frame of the lattice, the inertial force $F(t) = -m\ddot{x}_0(t)$ creates the running of the quasi-momentum

$$q(t) = q_\mathrm{in} + \frac{1}{\hbar}\int_0^t F(t')\,\mathrm{d}t' = q_\mathrm{in} - \frac{m}{\hbar}\dot{x}_0(t), \tag{24}$$

while the atom remains in the lowest band $n = 0$.

We then stop the acceleration of the lattice at time T, and then decrease its depth adiabatically until it is completely extinguished. In the reference frame of the lattice, this method of band-mapping will bring the atom into a well-defined momentum state $p_\mathrm{end}^{(\mathrm{lattice})}$, associated to the lowest band, thus between $-\hbar k$ and $\hbar k$. More precisely $p_\mathrm{end}^{(\mathrm{lattice})}$ is equal to $\hbar q(t)$, modulo

[2]The following reasoning is valid even if the momentum distribution is not a delta peak, the important assumption is that this distribution lies entirely in the Brillouin zone.

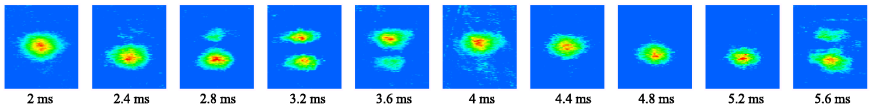

Figure 8. *Bloch oscillations of ^{40}K atoms (fermions) under gravity, observed with a potential $V_0 = 2\,E_r$, $\lambda = 873\,nm$ [figure taken from Roati, Mirandes, et al. (2004)]. The absence of interaction between the polarized fermions allows the observation of these oscillations with a good contrast for a long time (more than $100\,\tau_B$).*

a vector of the reciprocal lattice:

$$p_{\text{end}}^{(\text{lattice})} = \hbar q(T) + 2N\hbar k \tag{25}$$

where N is the integer closest to $-q(T)/(2k)$.

If we return to the reference frame of the laboratory at this time, the atomic momentum is

$$\begin{aligned} p_{\text{end}}^{(\text{lab})} &= p_{\text{end}}^{(\text{lattice})} + mv^{(\text{lattice})}(T) \\ &= p_{\text{end}}^{(\text{lattice})} + m\dot{x}_0(T) \\ &= \hbar q(T) + 2N\hbar k + m\dot{x}_0(T) \\ &= p_{\text{in}} + 2N\hbar k, \end{aligned} \tag{26}$$

which indeed corresponds to the expected result. The only case where this demonstration is not valid is when $p_{\text{end}}^{(\text{lattice})}$ is in the immediate vicinity of the band edge, i.e. $q(T) = k$ modulo $2k$, because the adiabatic ramping of the lattice is then not possible: the atom finds itself in a linear superposition of $q_{\text{in}} + 2N\hbar k$ and $q_{\text{in}} + (2N+2)\hbar k$; this case corresponds to an interruption of the acceleration at the precise instant when the two-photon transition sketched in figure 7 occurs.

2-3 Oscillations due to gravity

One of the main difficulties in observing Bloch oscillations lies in the necessity to prepare an assembly of atoms with an initial momentum dispersion small compared to $\hbar k$. This difficulty is almost automatically overcome if

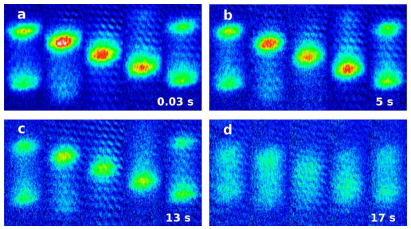

Figure 9. *Bloch oscillations of ^{88}Sr atoms (bosons) under the effect of gravity in a lattice of period $a = 266\,nm$ and depth $V_0 \approx 3\,E_r$ [figure extracted from Poli, Wang, et al. (2011)]. The Bloch period is $\omega_B/2\pi = 574\,Hz$ and the Bloch oscillations can be observed for nearly 20 seconds. The images correspond to the oscillation No. 1, 2900, 7500 and 9800. The extremely low value of the scattering length for ^{88}Sr atoms allows to minimize the phase shift of the oscillations due to interactions. From these oscillations, we can deduce the value of g within 6×10^{-6}. The accuracy of this measurement of g is significantly improved if one uses instead – on the same experimental setup – Wannier–Stark spectroscopy (see § 5).*

one has a Bose-Einstein condensate or a degenerate Fermi gas at hand. We cannot describe or even mention all the Bloch oscillation experiments that followed the arrival of these degenerate gases in the laboratories. Let us simply mention a class of experiments that are substantially different from those of Paris and Austin, in which the force F is not inertial, but exists in the reference frame of the laboratory. The simplest way is to choose gravity, by arranging the optical lattice along the vertical axis. We have reproduced on the figures 8 and 9 results obtained in the groups of M. Inguscio (Roati, Mirandes, et al. 2004) and G. Tino (Poli, Wang, et al. 2011) where atoms are "in suspension" in an optical lattice. The measurement of the oscillation frequency gives in principle a direct access to the value of gravity at the point where the atoms are. In fact, to optimize the determination of g with atoms confined in a lattice, it seems preferable to use the spectroscopy of Wannier–Stark states, which we will discuss later (Poli, Wang, et al. 2011; Pelle, Hilico, et al. 2013). Poli, Wang, et al. (2011) indeed indicate significantly larger fluctuations when directly observing Bloch oscillations, due to the residual instability of the initial position of the atoms and to a greater sensitivity to the timing of the experiment.

	Li	Na	K	Rb	Cs
mass (amu)	7	23	39	87	133
λ_0 (nm)	671	589	770	780	852
$E_\mathrm{r}/(2\pi\hbar)$ (kHz)	63.0	25.9	8.59	3.75	2.06
$\omega_\mathrm{B}/2\pi$ (kHz)	0.058	0.17	0.37	0.84	1.4
$\hbar\omega_\mathrm{B}/E_\mathrm{r}$	0.0009	0.0067	0.043	0.22	0.68
F_c/m for $V_0 = E_\mathrm{r}$ (ms^{-2})	3300	450	70	13.5	4.4

Table V.1. *Recoil energy and frequency of Bloch oscillations under the effect of gravity for alkali atoms ($F/m = 9.81\,ms^{-2}$). The optical lattice is assumed to be at the resonant frequency of the atom $\omega_0 = 2\pi c/\lambda_0$ and its spatial period is $a = \lambda_0/2$. The ratio $\hbar\omega_\mathrm{B}/E_\mathrm{r}$ is crucial to evaluate the adiabaticity of the motion in the band $n = 0$ (cf. figure 10). The last line gives the critical acceleration appearing in the Landau–Zener formula (38), for a lattice depth chosen equal to the recoil energy.*

3 The adiabatic approximation and beyond

3-1 Validity of the adiabatic approximation

We will now discuss the validity of the adiabatic approximation at the basis of the Bloch oscillation phenomenon. We have already given in a previous chapter the general criterion characterizing this approximation (Messiah 2003). Let us recall it briefly: We consider a Hamiltonian $\hat{H}(\lambda)$ that depends on a parameter λ, for which we have solved the eigenvalue equation. We assume for simplicity that the energies $\epsilon_n(\lambda)$ are non-degenerate and form a discrete set. The associated eigenvectors are denoted $|\phi_n(\lambda)\rangle$. We are interested in a problem where the parameter λ depends on time. We suppose that the system is prepared at time $t = 0$ in an eigenstate $|\phi_n[\lambda(0)]\rangle$ and we search for the condition under which the system will be at time t in the state $|\phi_n[\lambda(t)]\rangle$ with probability close to 1. We can show that this will be the case if the inequality

$$\hbar \left| \langle \phi_{n'} | \frac{\mathrm{d}}{\mathrm{d}t} | \phi_n \rangle \right| \ll |E_{n'} - E_n|\,, \quad \forall n' \neq n, \tag{27}$$

is satisfied at each time (the parameter $\lambda(t)$ is implicit).

For the case we are interested in here, the quasi-momentum q plays the role of the parameter λ and the quantum number n is the band index. The Hamiltonian is $\hat{H}_\mathrm{per}[q]$ given in (12), which determines the periodic part of the Bloch functions, and the states $|\phi_n(\lambda)\rangle$ are the periodic parts $|u_{n,q}\rangle$. Using the fact that $\dot{q} = F/\hbar$, the adiabaticity criterion is therefore

$$F\,|\langle u_{n',q}|\partial_q u_{n,q}\rangle| \ll |E_{n'}(q) - E_n(q)|\,, \tag{28}$$

where we have noted

$$|\partial_q u_{n,q}\rangle \equiv \frac{\mathrm{d}}{\mathrm{d}q}|u_{n,q}\rangle. \tag{29}$$

The scalar product $\langle u_{n',q}|\partial_q u_{n,q}\rangle$ can be rewritten in a convenient form, involving the matrix element of the momentum operator $\hat{p}$. This relation is established by differentiating with respect to q the eigenvalue equation for the Hamiltonian $\hat{H}_\mathrm{per}$, and projecting the resulting equation onto $|u_{n',q}\rangle$ (Ashcroft & Mermin 1976). We find

$$[E_n(q) - E_{n'}(q)]\,\langle u_{n',q}|\partial_q u_{n,q}\rangle = \frac{\hbar}{m}\langle u_{n',q}|\hat{p}|u_{n,q}\rangle, \tag{30}$$

which allows us to rewrite the adiabaticity condition in the form

$$\frac{F\hbar}{m}\,|\langle u_{n',q}|\hat{p}|u_{n,q}\rangle| \ll [E_n(q) - E_{n'}(q)]^2. \tag{31}$$

First, let us consider the weak-binding regime and apply this result to the most critical point for the adiabatic following, $q \approx k$, where the lowest band $n = 0$ is closest to the first excited band $n' = 1$. The gap between the levels is $V_0/2$ and the functions $u_{n,q}(x)$ are equal to $1 \pm \mathrm{e}^{\pm 2\mathrm{i}kx}$ (see Chapter 2). The matrix element of $\hat{p}$ is therefore $\sim \hbar k$ and the condition (31) becomes

$$\frac{F\hbar}{m}\hbar k \ll \frac{V_0^2}{4} \quad \Leftrightarrow \quad F \ll \frac{V_0^2}{8E_\mathrm{r}}k \quad \Leftrightarrow \quad \frac{\hbar\omega_\mathrm{B}}{E_\mathrm{r}} \ll \frac{\pi}{8}\left(\frac{V_0}{E_\mathrm{r}}\right)^2. \tag{32}$$

Let us now turn to the opposite tight-binding regime. One can find in the thesis of M.Dahan (1997) a (not very constraining) adiabaticity condition deduced from (31). We give here another one which consists in imposing that the energy shift $aF = \hbar\omega_\mathrm{B}$ between two successive wells (cf. fig. 1) remains lower than the energy difference $\hbar\omega \approx 2\sqrt{V_0 E_\mathrm{r}}$ between the

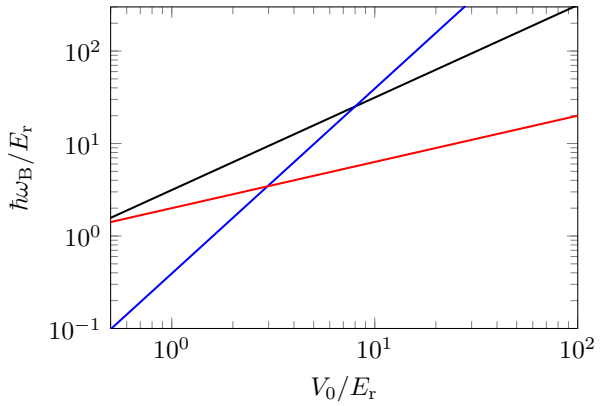

Figure 10. *Zones of validity of the adiabatic approximation (it is necessary to be located under the corresponding lines for the approximation to be valid). Blue: weak-binding case (32); red: tight-binding case (33). The black line gives the limit (34) for the force F, above which the potential $V(x) - Fx$ has no more local minimum.*

two lowest bands. This prevents a resonant tunnelling from the vibrational state $n = 0$ of the well located at ja to the vibrational state $n = 1$ of the well located at $(j + 1)a$. This condition is written in the limit $V_0 \gg E_r$:

$$\frac{\hbar\omega_B}{E_r} < 2\left(\frac{V_0}{E_r}\right)^{1/2}. \tag{33}$$

We have drawn in figure 10 the different zones of interest in the plane $(V_0, \hbar\omega_B)$. We have added the zone delimited by the condition

$$F < kV_0 \quad \Leftrightarrow \quad \frac{\hbar\omega_B}{E_r} < \pi\frac{V_0}{E_r}, \tag{34}$$

which corresponds to imposing that the tilted potential of figure 1 has local minima. The adiabaticity conditions given in (32-33) are well within this domain.

3-2 Landau–Zener transitions

The validity of the adiabatic approximation in the weak-binding case can be more quantitatively assessed by modelling the avoided crossing between the two lowest bands by a Landau–Zener type approach.

Let us first recall the main results of this approach. We consider a two-level system modelled by a spin 1/2 and we suppose that this spin evolves under the effect of the explicitly time-dependent Hamiltonian

$$\hat{H}(t) = \alpha t\,\hat{\sigma}_z + \beta\,\hat{\sigma}_x, \tag{35}$$

where the $\hat{\sigma}_i$ are the Pauli matrix. The instantaneous eigenvalues are $\pm\left(\alpha^2t^2 + \beta^2\right)^{1/2}$. Let us consider a spin prepared in the state $|+\rangle$ at a negative time t_i such that $|t_i| \gg \beta/\alpha$. At a time t_f positive and $\gg \beta/\alpha$, the spin will have followed adiabatically the corresponding energy level with a probability

$$\mathcal{P} = 1 - \mathrm{e}^{-\pi\beta^2/(\hbar\alpha)}. \tag{36}$$

In the case of interest, the intersecting energy levels are $E = \hbar^2q^2/2m$ and $E = \hbar^2(q - 2k)^2/2m$ at the quasi-momentum $q = k$. Since $\dot{q} = F/\hbar$, the coefficient α is $\alpha = \hbar kF/m$. The coefficient β, which characterizes the coupling between the two levels, is $\beta = V_0/4$. The probability of adiabatic following can be written as

$$\mathcal{P} = 1 - \mathrm{e}^{-F_c/F}, \tag{37}$$

where we introduced the critical force

$$F_c = \frac{\pi}{32}\frac{V_0^2}{E_r}k. \tag{38}$$

The condition of adiabatic following, $\mathcal{P} \approx 1$ and thus $F \ll F_c$, gives again the result found in (32).

The verification of this law for an atom in an optical lattice was performed during the first experiments in Paris and Austin in the years 1996-97. We show on figure 11 a more recent result obtained in Pisa (Zenesini, Lignier, et al. 2009) where we see the successive decreases of the band occupation $n = 0$ each time the atom's momentum passes at the edge of the Brillouin zone.

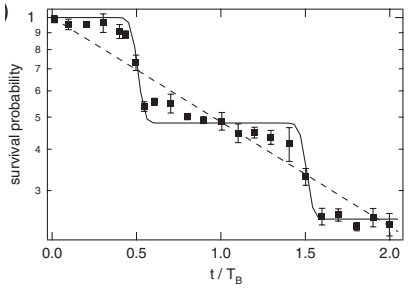

Figure 11. *Result from Zenesini, Lignier, et al. (2009), showing the decay of the occupation probability of the band $n = 0$ in a Bloch oscillation experiment conducted with rubidium atoms. The lattice has a depth $V_0 = E_\mathrm{r}$. The lattice, of period $a = 421\,nm$, is uniformly accelerated and provides an inertial force such that $\hbar\omega_B \approx 0.4E_\mathrm{r}$. The solid line corresponds to the numerical integration of the time-dependent Schrödinger equation, which essentially gives back the Landau–Zener prediction. The dashed curve corresponds to an exponential approximation.*

As we have stated above, this question of interband transitions was central to Zener's original paper in 1934. After deriving the transition probability at each edge of the Brillouin zone, Zener ends his analysis with a reasoning similar to the one of Gamow to determine the lifetime of a nucleus in a radioactive process α. The atom (or the electron for Zener) "takes its chance" $\omega_\mathrm{B}/2\pi$ times per unit of time, and each time it has the probability $\mathcal{P}$ to stay in the band $n = 0$. If we multiply these probabilities for the $j = t/\tau_\mathrm{B}$ trials which take place during a duration t, we deduce the probability $\Pi(t)$ for the particle to be still in the band $n = 0$ at the instant t

$$\Pi(t) \approx \mathcal{P}^j = \exp\left[j \ln\left(1 - \mathrm{e}^{-F_\mathrm{c}/F}\right)\right] \approx \exp(-t/\tau) \tag{39}$$

where the decay time τ is given by

$$\tau = \tau_\mathrm{B}\, \mathrm{e}^{F_\mathrm{c}/F}. \tag{40}$$

3-3 Beyond Landau–Zener

In the treatment that leads to the exponential rate law (40), one incoherently adds up the different probability amplitudes corresponding to the successive diabatic transitions when the atom passes over the edge of the Brillouin zone. In reality, these transitions are coherent processes and it is possible to observe significant deviations from the simple Landau–Zener law due to the interference between these processes. A first analysis, theoretical and experimental, of these deviations was made in Austin at the end of the 1990s (Wilkinson, Bharucha, et al. 1997; Niu & Raizen 1998). A detailed theoretical treatment is presented by Holthaus (2000). Recently, an experiment conducted in Pisa in the group of E. Arimondo has very convincingly demonstrated the *Stückelberg interference* between two successive Landau-Zener processes (Zenesini, Ciampini, et al. 2010). The principle of the experiment and its result are shown in figure 12. Similar results have been obtained in Bonn in the group of M. Weitz (Kling, Salger, et al. 2010).

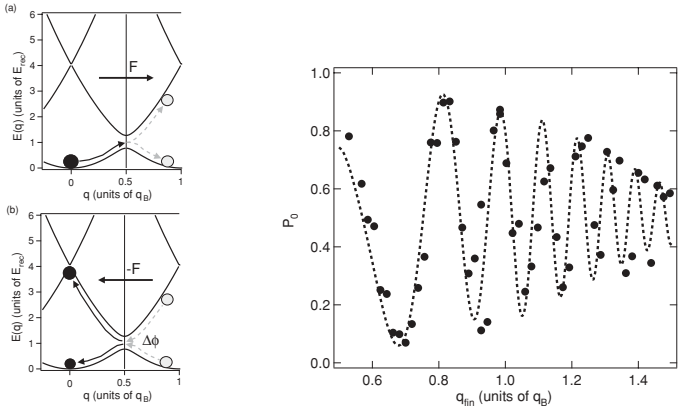

Figure 12. *Observation of Stückelberg oscillations, with an optical lattice for rubidium atoms, $V_0 = 1.4\,E_\mathrm{r}$ and $\hbar\omega_\mathrm{B} = 1.2\,E_\mathrm{r}$ ($a = 421\,nm$). The atoms are placed in the lowest band $n = 0$ at $q = 0$. They are accelerated to cross the edge of the first Brillouin zone and reach a momentum q_end such that $0.5 < q_\mathrm{end}/k < 1.5$. The force is then reversed to bring the atoms back to $q = 0$. Finally, one measures the population of the lowest band. The dashed line is a prediction made by assuming an initial momentum width $\Delta q/k = 0.03$ (figures taken from Zenesini, Ciampini, et al. (2010)).*

3-4 A beam splitter

Thanks to Bloch oscillations, it is possible to coherently transfer a controlled (and important) momentum to atoms by placing them in an accelerated lattice. The fact that the probability of transferring or not this momentum depends strongly on the band n occupied by the atoms allows to realize coherent beam splitters. The principle, implemented by Denschlag, Simsarian, et al. (2002), then taken up again by Cladé, Guellati-Khélifa, et al. (2009) and Müller, Chiow, et al. (2009) is simple:

- Starting from atoms of momentum p_0 such that $|p_0| < \hbar k$, we apply to these atoms a Bragg pulse which places each atom in a superposition of p_0 and $p_0 + 2\hbar k$, or even p_0 and $p_0 + 4\hbar k$ in the case of Denschlag, Simsarian, et al. (2002).

- An optical lattice is adiabatically ramped up to a depth V_0 so that the atoms are placed in a coherent superposition of states $|n = 0, q_0\rangle$ and $|n = 2, q_0\rangle$, where $q_0 = p_0/\hbar$. Note that it is better to choose $p_0 \neq 0$ to avoid being bothered by the quasi-degeneracy of the bands $n = 1$ and $n = 2$ when the lattice still has a very low intensity, which prevents a good adiabaticity .

  The optical lattice is accelerated. The pair *acceleration–depth* is chosen in order to (i) have an excellent adiabatic following for the $n = 0$ band, (ii) have almost no adiabatic following for the $n = 2$ band. Thanks to this choice, the component $|n = 0, q\rangle$ is accelerated with the lattice and acquires a large momentum in the laboratory reference frame. On the contrary, the component $|n = 2, q\rangle$ undergoes diabatic transitions, and the atom is transferred to the higher bands $n = 2 \to n = 3 \to \ldots$ in the accelerated reference frame. More simply, this means that for this part of the vector state, the atoms remain stationary in the reference frame of the laboratory. One can verify on the figure 13, extracted from the article of Cladé, Guellati-Khélifa, et al. (2009), that there is indeed an appreciable range of values of V_0 for which these two "antagonistic" conditions are simultaneously satisfied.

  At the end of this acceleration of duration t, $N = t/\tau_B$ Bloch oscillations have occurred and the atom is in the state

$$|n = 0, p_0 + 2N\hbar k\rangle + e^{i\phi}|n = 2, p_0 + 2\hbar k\rangle. \qquad (41)$$

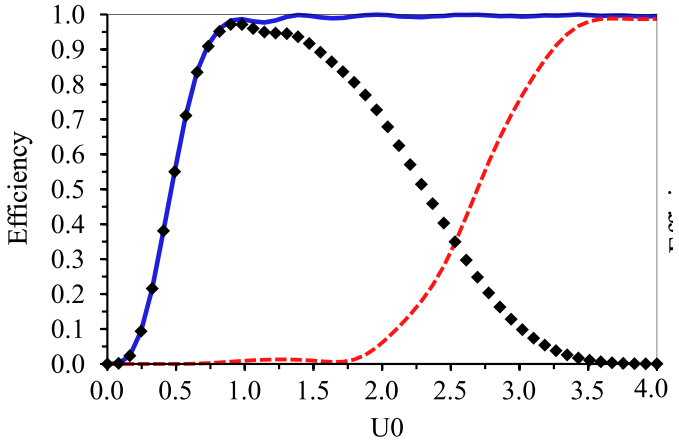

Figure 13. *Probability $\mathcal{P}_n$ to adiabatically follow the band n for ^{87}Rb atoms placed in an optical lattice accelerated at $\sim 100\,ms^{-2}$, as a function of the lattice depth $U_0 = V_0/(8\,E_r)$. The blue (resp. red) curve corresponds to $n = 0$ (resp. $n = 2$). The beam splitter will be efficient if $\mathcal{P}_0 \approx 1$ and $\mathcal{P}_2 \approx 0$. The black curve $\mathcal{P}_0(1 - \mathcal{P}_2)$ is a measure of the overall efficiency, which is optimal for $U_0 \approx 1$, so $V_0 \approx 8\,E_r$ (Figure taken from Cladé, Guellati-Khélifa, et al. (2009)).*

The coherence of this superposition can be tested by constructing a Mach-Zender type interferometer, where the two arms undergo this acceleration at different times (Denschlag, Simsarian, et al. 2002).

If one wants to use this beam splitter for atomic interferometry and precision measurements, an important difficulty comes from the differential light shift between the two arms. The part of the wave function corresponding to an accelerated atom (in the band $n = 0$) does not have the same spatial location in the lattice as the part of the wave function of a non-accelerated atom (in the band $n = 2$). For example, if the lattice is blue-detuned with respect to the atomic resonance, the atoms in the band $n = 0$ will remain localized in the vicinity of the nodes of the standing wave, whereas the atoms in the band $n = 2$ will successively explore the nodes and the anti-nodes of this standing wave. The light shift is therefore not the same in both cases, which leads to a phase shift between the two

arms that is difficult to control. More complicated interferometric schemes are needed to restore a sufficient symmetry between these arms [Cladé, Guellati-Khélifa, et al. (2009), Müller, Chiow, et al. (2009)].

4 Bloch oscillations in the tight-binding regime

Considering the practical importance of the Bloch oscillation phenomenon, it is useful to see it from several angles, in particular in the tight-binding regime. In this limit, we have simple analytical expressions for the different quantities involved, which are useful to get an intuition of the problem.

4-1 The oscillating wave function

In the tight-binding limit, we assume that the dynamics of the particle is restricted to the lowest band. We will therefore omit the band index $n = 0$ in this section. We only take into account the hopping between nearest neighbours, and write the initial Hamiltonian (2) as:

$$\hat{H} = -J\left(\hat{T} + \hat{T}^\dagger\right) - Fa\sum_j j|w_j\rangle\langle w_j|, \tag{42}$$

where $|w_j\rangle$ represents the state where the particle is localized at site j and $\hat{T}$ is the translation operator by one site to the right:

$$\hat{T} = \sum_j |w_{j+1}\rangle\langle w_j|. \tag{43}$$

Recall that the Bloch functions $|\psi_q\rangle$, their periodic part $|u_q\rangle$ and the associated energy $E(q)$ are written

$$|\psi_q\rangle = \sum_j \mathrm{e}^{\mathrm{i}jaq}|w_j\rangle, \quad |u_q\rangle = \sum_j |w_j\rangle, \quad E(q) = -2J\cos(aq), \tag{44}$$

and $|u_q\rangle$ is independent of q in this particular case.

We can already introduce a dimensionless number which will be useful to characterize the influence of the force F on the particle placed in the lattice. Consider the picture of Zener (Figure 3), which shows a characteristic length for the oscillation, $L = \Delta E/F$, where ΔE is the bandwidth. In the case of tight-binding, we simply have $\Delta E = 4\,J$. We denote by ν the number of sites that are located within this distance L

$$\nu = \frac{4J}{Fa} = \frac{\Delta E}{\hbar\omega_\mathrm{B}}. \tag{45}$$

We expect that this dimensionless number ν will play a role in the characterization of the amplitude of the oscillations.

We start with a particle prepared in the Bloch function $|\psi_{q_\mathrm{in}}\rangle$. The general results obtained in the previous chapter can be written in this limit

$$|\psi(t)\rangle = \mathrm{e}^{-\mathrm{i}\Phi(t)}\sum_j \mathrm{e}^{\mathrm{i}jaq(t)}|w_j\rangle, \tag{46}$$

where $q(t) = q_\mathrm{in} + Ft/\hbar$ as in (8) and where the phase Φ corresponds to the dynamic phase:

$$\Phi(t) = \Phi(0) + \frac{1}{\hbar}\int_0^t E[q(t')]\,\mathrm{d}t' = \frac{\nu}{2}\left\{\sin\left[aq(t)\right] - \sin[aq_\mathrm{in}]\right\}. \tag{47}$$

It is quite clear that in this tight-binding limit, we have neglected all the interband transitions studied above. The assumption of adiabatic following is therefore implicit in this section.

4-2 Evolution operator and oscillations in real space

In the tight-binding approximation, the form of the evolution operator is remarkably simple, both in the basis of Bloch functions and in the basis of Wannier functions. The calculations are detailed in the article of Hartmann, Keck, et al. (2004), and we simply give here the essential results.

In the Bloch functions basis, the evolution operator is immediately deduced from (46):

$$\langle\psi_{q'}|\hat{U}(t)|\psi_q\rangle = \delta(q' - q - Ft/\hbar)\,\mathrm{e}^{-\mathrm{i}\nu[\sin(aq')-\sin(aq)]/2}. \tag{48}$$

In the Wannier function basis, the calculation is a little longer but does not present any serious difficulty. Expressing the Wannier functions in terms

of the Bloch waves, we arrive at

$$\langle w_{j'}|\hat{U}(t)|w_j\rangle = \mathrm{e}^{\mathrm{i}(j+j')\omega_{\mathrm{B}}t/2}\mathcal{J}_{j'-j}[\nu\sin(\omega_{\mathrm{B}}t/2)]. \tag{49}$$

The periodicity of the Bloch oscillations is obvious for both expressions.

We can take advantage of the explicit expression (49) to study the motion of a wave packet in real space. We will review the two limiting cases of a very localized initial wave packet and of a wave packet spreading over many sites.

In the case of an initial state occupying only one site, for example the state $|w_0\rangle$, the motion corresponds to a breathing of the wave packet, symmetrically with respect to the starting point. The probability $P(j)$ to find the particle on the site $|w_j\rangle$ at time t is obtained directly from (49):

$$P(j) = |\mathcal{J}_j[\nu\sin(\omega_{\mathrm{B}}t/2)]|^2 \tag{50}$$

The extension of the wave packet is maximal after half an oscillation ($\sin(\omega_{\mathrm{B}}t/2) = \pm 1$) and it is typically of the order of $\Delta j \sim \nu$ sites.

Let us now take the case of an initial wave packet of large extension, and choose a Gaussian distribution for the occupation probability amplitude of site $|w_j\rangle$:

$$\langle w_j|\Psi(0)\rangle \propto \mathrm{e}^{-j^2/4\sigma^2}, \qquad \sigma \gg 1. \tag{51}$$

We can then show that the extension of the wave packet remains approximately constant in time, and that its center $j_c(t)$ evolves periodically

$$|\langle w_j|\Psi(t)\rangle|^2 \propto \mathrm{e}^{-[j-j_c(t)|^2/2\sigma^2}, \quad j_c(t) = \nu\sin^2(\omega_{\mathrm{B}}t/2). \tag{52}$$

The total amplitude (peak to peak) of the oscillation is thus ν sites, as we had foreseen when defining ν from Zener's argument. We show on figure 14 two numerical results obtained by Hartmann, Keck, et al. (2004) in these two limiting cases.

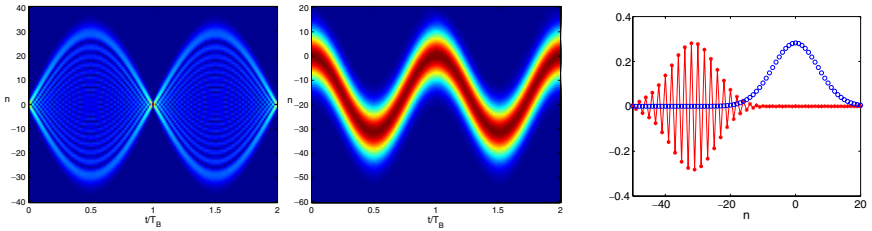

Figure 14. *Bloch oscillations in the tight-binding limit. Left and middle: evolution in real space of a wave packet during two Bloch periods for $\nu = -31.6$ (negative force). For the left figure, the initial state is the Wannier function $j = 0$. The motion is then a breathing motion symmetric with respect to $j = 0$. In the central figure, the initial state is a Gaussian packet of width $\sigma = 5$ and the subsequent evolution is essentially an oscillation of the center of the wave packet, with no noticeable deformation. The figure on the right shows the real part of $\langle w_n|\Psi(t)\rangle$, at $t = 0$ (blue points) and at $t = \pi/\omega_{\mathrm{B}}$ in red [figures taken from Hartmann, Keck, et al. (2004)].*

5 Wannier–Stark ladders

Insofar as the Hamiltonian considered in this chapter is time-independent, at least in the version (2) that we give here:

$$\hat{H} = \frac{\hat{p}^2}{2m} + V(\hat{x}) - F\,\hat{x}, \tag{53}$$

a natural approach to the problem of Bloch oscillations is to look for the eigenstates of this Hamiltonian, in order to deduce the different aspects of the dynamics (Wannier 1960). We immediately note that if $\psi(x)$ is an eigenstate with energy E, then $\psi(x+a)$ is an eigenstate for energy $E+Fa = E + \hbar\omega_{\mathrm{B}}$. To each eigenstate is thus associated a ladder of energies, called *Wannier-Stark ladder*, and the rungs of this ladder have a spacing of $\hbar\omega_{\mathrm{B}}$.

This search for eigenstates has non-trivial mathematical aspects: (i) The spectrum of the Hamiltonian is a continuum extending from $-\infty$ to $+\infty$, since for any energy E, one can find an asymptotically free state for $x \to \infty$. The Wannier–Stark ladders are in this context resonances which appear as poles of a scattering matrix (Gluck, Kolovsky, et al. 2002). (ii) However, restricting the search to a single band (or a finite number of bands) radi-

cally changes the nature of this spectrum, which becomes entirely discrete (Avron, Zak, et al. 1977; Nenciu 1991).

It is this second point of view that we will adopt in the following. Strictly speaking, the Wannier–Stark states we will find have a finite lifetime, which is related to the width of the resonances of the exact problem. This finite lifetime is itself the signature of the Landau-Zener transitions, which cause a leakage of the Bloch oscillation due to transitions to higher bands. But it can be neglected if the validity criteria of the adiabatic approximation are verified.

Let us restrict ourselves to the one-band tight-binding model, with the Hamiltonian given in (42). It is immediate to verify[3] that the state

$$|\Phi_j\rangle = \sum_{j' \in \mathbb{Z}} \mathcal{J}_{j'-j}(\nu/2)\, |w_{j'}\rangle \tag{55}$$

is an eigenstate of $\hat{H}$ with eigenvalue $-j\,Fa$ (Gluck, Kolovsky, et al. 2002; Hartmann, Keck, et al. 2004). This state $|\Phi_j\rangle$ is centered on site j and it spreads on both sides over a number of sites $\sim \nu/2$. Indeed, if $|n| \gg x$, the Bessel function $\mathcal{J}_n(x)$ decreases as $(x/2)^n/n!$. The spread of the Wannier–Stark state thus roughly determines the extent of the Bloch oscillation. We can see on this simple example the particular mathematical character of this problem: a force F, even infinitesimal, radically changes the spectrum of the Hamiltonian: it goes from a bounded continuum between $-2J$ and $2J$ to a completely discrete set, extending from $-\infty$ to $+\infty$.

Wannier–Stark state spectroscopy is done by applying on the atoms a time–dependent perturbation with frequency ω: $\hat{W}(x,t) = \hat{W}^{(+)}(x)\,\mathrm{e}^{-\mathrm{i}\omega t} +$ c.c.. This probe induces a transition from $|\Phi_j\rangle$ to $|\Phi_{j'}\rangle$, a resonance occurring each time $\omega = (j'-j)\omega_{\mathrm{B}}$, provided of course that the matrix element $\langle\Phi_{j'}|\hat{W}^{(\pm)}(x)|\Phi_j\rangle$ is nonzero. We obtain an a priori symmetric spectrum, since the Wannier–Stark scales extend to positive as well as negative energies. One can refer to the article by Mendez & Bastard (1993) to find examples of Wannier–Stark scale spectroscopy for electrons in superlattices.

[3] We recall that the Bessel functions verify the relation

$$x\,(\mathcal{J}_{n+1}(x) + \mathcal{J}_{n-1}(x)) = 2n\,\mathcal{J}_n(x). \tag{54}$$

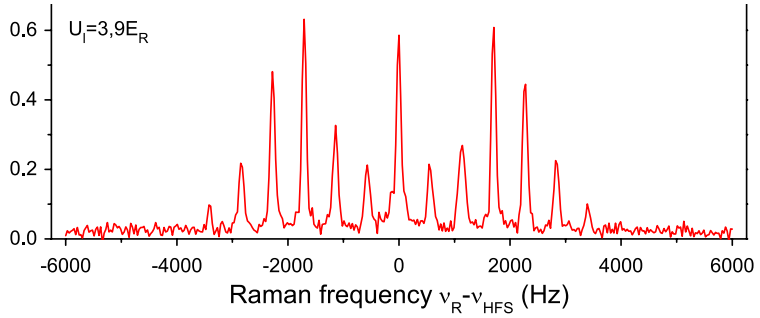

Figure 15. *Raman spectroscopy of Wannier–Stark states of rubidium atoms in an optical lattice in the presence of gravity. We observe transitions $|\Phi_j\rangle \to |\Phi'_j\rangle$ up to $|j'-j| = 6$ for this value of the lattice depth. The frequency of the Bloch oscillations is $\omega_{\mathrm{B}}/(2\pi) = 569\,\mathrm{Hz}$ for the wavelength of the light chosen for the lattice (532 nm) [figure extracted from Beaufils, Tackmann, et al. (2011)].*

This spectroscopic method is another way of looking at the same physical phenomenon: Bloch oscillations like those in figure 1 are the impulse response of the system placed out of equilibrium, whereas this Wannier–Stark spectroscopy studies the response of the system at equilibrium when driven by a low-amplitude probe. During the first demonstrations of Bloch oscillations with cold atoms, Christophe Salomon's group at ENS favored the impulse method while Mark Raizen's group in Austin emphasized the spectroscopic approach (Niu, Zhao, et al. 1996; Wilkinson, Bharucha, et al. 1996).

We show in Figure 15 a result obtained by Beaufils, Tackmann, et al. (2011) at SYRTE [see also Tackmann, Pelle, et al. (2011), Pelle, Hilico, et al. (2013)]. This result is obtained for rubidium 87 atoms in a vertical lattice, and the force F is gravity. The lattice is formed by a standing wave with wavelength 532 nm, corresponding to a Bloch frequency $\omega_{\mathrm{B}}/(2\pi) = 569\,\mathrm{Hz}$. The depth of the lattice is about $4\,E_{\mathrm{r}}$, which corresponds to a bandwidth of $0.5\,E_{\mathrm{r}} \approx 4\,\mathrm{kHz}$. The parameter ν characterizing the number of sites visited during an oscillation as well as the extension of each Wannier–Stark state is $\nu \approx 7$. The Wannier–Stark ladder is measured by inducing a Raman transition between two internal states of the rubidium atom $|g_1, \Phi_j\rangle \to |g_2, \Phi_{j'}\rangle$, with $|g_F\rangle = |F, m_F = 0\rangle$, separated by the

hyperfine splitting $\approx 6.8\,\mathrm{GHz}$.

Recently the SYRTE group used this type of transitions to build a Ramsey interferometer and obtain an accurate measurement of ω_B, hence of g. The relative precision is 0.9×10^{-5} in one second (Pelle, Hilico, et al. 2013), a value comparable to that obtained in Florence (1.5×10^{-7} in one hour), also with Wannier–Stark scale spectroscopy (Poli, Wang, et al. 2011). For comparison, the combination of Bloch oscillations and a Ramsey–Bordé interferometer allowed a team at ONERA to obtain a better accuracy (2×10^{-7} in only 300 s) (Charrière, Cadoret, et al. 2012), and a pure Ramsey–Bordé interferometer at SYRTE provided a sensitivity of $0.6 \times 10^{-9}\,g$ in 3000 s (Louchet-Chauvet, Farah, et al. 2011), but at the cost of a fall of atoms of 0.8 mm in the first case and of about ten cm in the second. In the Wannier–Stark spectroscopy method, the atoms remain trapped and the distance they explore is on the order of a few microns only: this method is thus well adapted to the measurement of local forces, such as those of Casimir–Polder type.

6 Perspectives and applications

Bloch oscillations have become an important tool in quantum optics and atomic physics, used in multiple applications ranging from metrology to the study of collective phenomena. To conclude this chapter, we will briefly discuss two of them.

Measurement of h/m. The first application discussed here concerns the measurement of the constant h/m, where m is the mass of an atom of a given species. This constant is the "weak link" in the determination of the fine structure constant α by a method that does not rely on quantum electrodynamics (independent of $g-2$ of the electron for example):

$$\alpha^2 = \frac{2R_\infty}{c}\,\frac{m}{m_\mathrm{e}}\,\frac{h}{m}, \tag{56}$$

where R_∞ is the Rydberg constant and m_e is the mass of the electron, the precision on the other terms (R_∞/c and m/m_e) being notably better than 10^{-9}.

The method used by Biraben's group at LKB to measure h/m takes advantage of Bloch oscillations to transfer a momentum $2N\hbar k$ to some atoms, where N is a very large integer (between 500 and 1000). The initial momentum of the atoms is almost zero, and defined with a precision much better than $\hbar k$. The velocity of the atoms is measured by a Raman transition which transfers the atoms from a hyperfine state g_1 to another hyperfine state g_2, by a process "absorption of a photon of wave number k_1 – emission of a photon of wave number k_2". If the atoms have a momentum p before the Raman transfer, the transition will be resonant if the energy difference $\hbar\omega$ between the two beams creating the Raman transition verifies:

$$\hbar\omega(p) = \Delta E_\mathrm{hf} + \frac{\left[p+\hbar(k_1+k_2)\right]^2}{2m} - \frac{p^2}{2m}, \tag{57}$$

where all momenta are supposed to be collinear and $\boldsymbol{k}_1$, $\boldsymbol{k}_2$ have opposite directions. The difference between $\hbar\omega(p_\mathrm{init})$ and $\hbar\omega(p_\mathrm{final})$, with $p_\mathrm{final} = p_\mathrm{init} + 2N\hbar k$ leads to:

$$\omega(p_\mathrm{final}) - \omega(p_\mathrm{init}) = 2N\frac{\hbar k(k_1+k_2)}{m}, \tag{58}$$

or by inverting this relation

$$\frac{\hbar}{m} = \frac{\omega(p_\mathrm{final}) - \omega(p_\mathrm{init})}{2Nk(k_1+k_2)}. \tag{59}$$

In the first version of this experiment, the transferred momentum was horizontal and $N \sim 50$ (Battesti, Cladé, et al. 2004). The LKB group then switched to a vertical geometry that allows larger values of N, by eliminating the effect of gravity by equating the upward and downward acceleration (Cladé, Mirandes, et al. 2006). Moreover, for a better accuracy on the determination of the initial and final momenta, the Bloch oscillation has been placed between two pairs of $\pi/2$ pulses linking g_1 and g_2, thus realizing a Ramsey–Bordé interferometer (Cadoret, Mirandes, et al. 2008; Bouchendira, Cladé, et al. 2011). The precision obtained on h/m is now $\sim 10^{-9}$ (systematic + statistical), at a level comparable to that of the other factors entering the expression (56) for α.

Note that these measurements are made with extremely deep lattices, $V_0 \sim 100\,E_\mathrm{r}$, for which the measured efficiency of the Bloch oscillation

reaches 99.97% per period. At this lattice depth, tunnelling between adjacent sites is completely negligible: the asymptotic formula seen in chapter 3 gives a bandwidth of $10^{-6}\,E_{\mathrm{r}}$, i.e. a tunnelling time of several hundred seconds. For the acceleration used in the experiment, of the order of $2000\,\mathrm{ms}^{-2}$, the parameter $\nu = 4J/Fa$ is of the order of 10^{-8}. The Wannier–Stark states are then almost identical to the Wannier functions in each well. The atoms are trapped at the bottom of the potential wells created by the standing wave and they follow adiabatically these wells when the lattice is set in motion.

Measurement of weak forces. Bloch oscillations allows one to directly link the force felt by the atoms to a frequency. This point led several authors to propose to use this phenomenon to measure weak forces, the Casimir–Polder force in the vicinity of a surface for example, or even to search for more exotic forces corresponding to a modification of gravity at short distances. A first experiment in this direction is presented by Sorrentino, Alberti, et al. (2009). Moreover, the study of Bloch oscillations in a Fabry-Perot cavity has also been studied in depth (Prasanna Venkatesh, Trupke, et al. 2009).

We briefly discuss here the results obtained by Carusotto, Pitaevskii, et al. (2005), who studied the value of ω_{B} in the vicinity of a surface, and compared it to the value it would take for a vertical lattice in free space. Carusotto, Pitaevskii, et al. (2005) propose to use a gas of polarized fermions, thus without interaction, to observe only one-particle effects. By a simple analytical study, they show that the relative shift of the Bloch frequency is

$$\frac{\Delta\omega_{\mathrm{B}}}{\omega_{\mathrm{B}}} = -\frac{0.17}{D^4}\,(\mu\mathrm{m})^4, \tag{60}$$

where D is the distance between the atom and the surface. For $D = 10\,$microns, the Casimir force (including thermal effects at 300 K) is about 10^5 times weaker than gravity, which should be detectable since we have seen that the accuracy on the measurement of g with Bloch oscillations could reach 10^{-7} after one hour of integration. In the article by Carusotto, Pitaevskii, et al. (2005), a more thorough numerical study takes into account the averaging of the potential due to the initial extension of the cloud and the region explored during the oscillation (of the order of a micron), but the corrections are minor. Note that the damping of the oscillations due to the inhomogeneity of ω_{B} is small and should not compromise this approach.

Wolf, Lemonde, et al. (2007) have proposed a slightly different approach from that of Carusotto, Pitaevskii, et al. (2005), by imagining an interferometer based on the Wannier–Stark states located j, $j \pm 1$,... sites away from the wall, in two different internal states g_1 and g_2. The expected sensitivity for this type of experiment is a shift of $10^{-4}\,$Hz between two neighbouring sites, whereas gravity creates a typical kHz shift for strontium atoms and a lattice wavelength around 700 nm. A discussion of the possibilities of this device for the search of forces corresponding to a deviation from Newton's law, both in terms of intensity and range of this hypothetic force, can be found in Wolf, Lemonde, et al. (2007). The conclusion is that there is a rather large range of parameters that this type of experiment could address in a more precise way than existing devices.

Chapter VI

Topology in a lattice: the example of Dirac points

Dirac points play a central role in many phenomena of condensed matter. They can be found in graphene, where they give ultra-relativistic properties to the motion of the conduction electrons. They also appear in topological insulators, where they are the origin of the conducting edge states.

A Dirac point is characterized by a contact between two bands with a linear dispersion relation, which allows to illustrate several well-known features of the Dirac equation for massless particles, such as the Klein paradox or the *Zitterbewegung*. This dispersion relation, which is very different from the minimum of a usual band (where $E \propto q^2$), also manifests itself when a magnetic field is added and gives rise to an "anomalous" integer quantum Hall effect.

The existence of Dirac points is a consequence of the geometry, or rather the topology (in the sense defined below) of the band structure. The flexibility of optical lattices has led several authors to imagine configurations of light beams that allow to obtain such points in the band structure (Zhu, Wang, et al. 2007; Wunsch, Guinea, et al. 2008; Lee, Grémaud, et al. 2009). In this chapter, we will first identify the characteristics of a periodic lattice that lead to Dirac points. We will then describe the first demonstration of these Dirac points with cold atoms, made in the group of T. Esslinger in Zürich (Tarruell, Greif, et al. 2012).

1 Dirac points in a Brillouin zone

1-1 Linear dispersion relation

In general, a Dirac point is defined as a point $\boldsymbol{q}_\mathrm{D}$ in the Brillouin zone where two bands touch in a linear way (figure 1). In the particular case where the two bands touch isotropically, the dispersion relation in the neighbourhood of $\boldsymbol{q}_\mathrm{D}$ is written

$$E(\boldsymbol{q}) = \pm\hbar c|\boldsymbol{q} - \boldsymbol{q}_\mathrm{D}| + \epsilon_0, \tag{1}$$

where c has the dimension of a velocity and ϵ_0 is the energy at the point of contact.

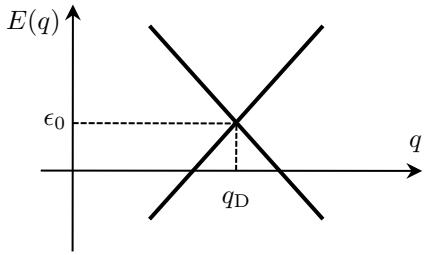

Figure 1. *A Dirac point*

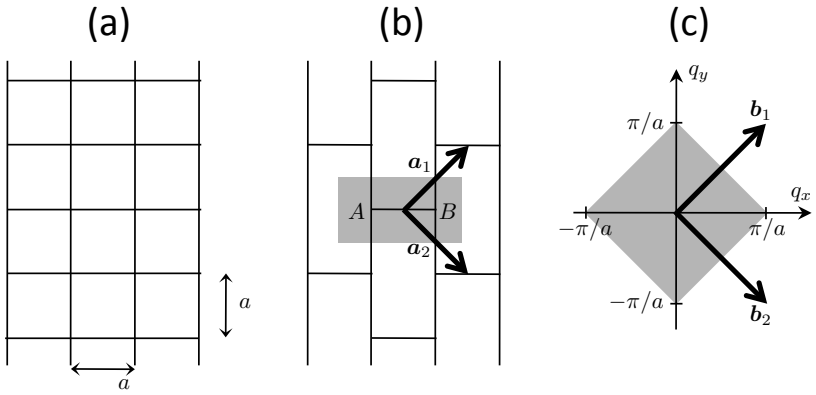

Figure 2. *Brick wall lattice. (a) Square lattice of side a. (b) The brick wall lattice is obtained by deleting every second link along the horizontal direction. (c) Reciprocal space and Brillouin zone.*

In graphene, the chemical potential is equal to ϵ_0 so that the behaviour of the conduction electrons simulates the quantum electrodynamics of massless fermions. The group velocity c at the Dirac points is about $1/300$ of the speed of light.

The dispersion relation (1) can already be found in dimension 1. However, the two-dimensional aspect of graphene adds a second essential feature, the chirality of these Dirac points, which we will now describe.

1-2 Chirality of Dirac points

To give an intuition of the origin of this chirality, let us consider a lattice in a tight-binding model, such that the unit cell of the lattice has two sites A and B. Let us further assume that a particle on a site A (resp. B) can only jump to a site of type B (resp. A), and this site belongs either to the same cell, or to an adjacent cell (see figures 2 and 4).

If the on-site energy is the same for A and B ($E_A = E_B \equiv \epsilon_0$), we know (see Chapter 3) that the Hubbard Hamiltonian in the reciprocal space $\hat{\mathcal{H}}(\boldsymbol{q})$ is a 2×2 matrix of the type :

$$\hat{\mathcal{H}}(\boldsymbol{q}) = \begin{pmatrix} \epsilon_0 & f^*(\boldsymbol{q}) \\ f(\boldsymbol{q}) & \epsilon_0 \end{pmatrix}, \tag{2}$$

whose eigenenergies are

$$E_\pm(\boldsymbol{q}) = \epsilon_0 \pm |f(\boldsymbol{q})|. \tag{3}$$

We will determine later the explicit value of the function $f(\boldsymbol{q})$ for two types of lattices, the brick wall lattice and the hexagonal lattice of graphene.

We consider the two dimensional case, so that $\boldsymbol{q}$ is a vector (q_x, q_y). A Dirac point $\boldsymbol{q}_{\rm D}$ is a point in the Brillouin zone for which

$$f(\boldsymbol{q}_{\rm D}) = 0, \tag{4}$$

so that both eigenenergies (3) are degenerate. We define in the vicinity of $\boldsymbol{q}_{\rm D}$

$$\boldsymbol{\delta q} = \boldsymbol{q} - \boldsymbol{q}_{\rm D} = \delta q \, (\cos\varphi \; \boldsymbol{u}_x + \sin\varphi \; \boldsymbol{u}_y) \tag{5}$$

and we suppose that close to the Dirac point, we have the expansion

$$f(\boldsymbol{q}) = \hbar c(\delta q_x \pm \mathrm{i}\delta q_y) = \hbar c \, \delta q \, \mathrm{e}^{\pm \mathrm{i}\varphi}, \tag{6}$$

We will see later that this expansion in the vicinity of a zero is, with a very simple generalization, natural for the complex function $f(q_x, q_y)$. In the neighborhood of $\boldsymbol{q}_{\rm D}$, the Hamiltonian (2) is thus written

$$f(\boldsymbol{q}) = \hbar c(\delta q_x + \mathrm{i}\delta q_y) : \qquad \hat{\mathcal{H}}(\boldsymbol{q}) = \epsilon_0 \hat{1} \; + \; \hbar c \; \hat{\boldsymbol{\sigma}} \cdot \boldsymbol{\delta q} \, , \tag{7}$$

$$f(\boldsymbol{q}) = \hbar c(\delta q_x - \mathrm{i}\delta q_y) : \qquad \hat{\mathcal{H}}(\boldsymbol{q}) = \epsilon_0 \hat{1} \; + \; \hbar c \; \hat{\boldsymbol{\sigma}} \cdot \boldsymbol{\delta q}^* \, , \tag{8}$$

where $\hat{\sigma}_j$ ($j = x, y$) are the Pauli matrices

$$\hat{\sigma}_x = \begin{pmatrix} 0 & 1 \\ 1 & 0 \end{pmatrix}, \qquad \hat{\sigma}_y = \begin{pmatrix} 0 & -\mathrm{i} \\ \mathrm{i} & 0 \end{pmatrix}. \tag{9}$$

The Hamiltonian (7–8) is formally identical to that of a spin $1/2$ particle in the vicinity of the zero of a magnetic field. In the basis $|+\rangle_z, \; |-\rangle_z$ of $\hat{\sigma}_z$, i.e. the basis of the Wannier functions $|w_A\rangle, \; |w_B\rangle$ centered on sites A and

B, the eigenstates $|\chi_\pm\rangle$ of (7–8) associated with the energies $E_\pm(\boldsymbol{q})$ given in (3) are :

$$f(\boldsymbol{q}) = \hbar c(\delta q_x + \mathrm{i}\delta q_y) : \qquad |\chi_\pm\rangle = \frac{1}{\sqrt{2}}\begin{pmatrix} 1 \\ \pm\,\mathrm{e}^{\mathrm{i}\varphi}\end{pmatrix} \tag{10}$$

$$f(\boldsymbol{q}) = \hbar c(\delta q_x - \mathrm{i}\delta q_y) : \qquad |\chi_\pm\rangle = \frac{1}{\sqrt{2}}\begin{pmatrix} 1 \\ \pm\,\mathrm{e}^{-\mathrm{i}\varphi}\end{pmatrix} \tag{11}$$

The chirality due to the term $\mathrm{e}^{\pm\mathrm{i}\varphi}$ appears clearly on these expressions. More precisely, if we consider a circle centered on the Dirac point and if we adiabatically follow one of the two eigenstates $|\chi_\pm\rangle$ on this circle, the accumulated geometric phase is $\pm\pi$, corresponding to the well-known change of sign of a spin $1/2$ when it performs a 2π rotation.

2 The brick wall lattice

Before presenting the case of graphene, with its regular hexagonal lattice, let us consider the brick wall lattice represented on figure 2b, which is slightly simpler to deal with mathematically and which was implemented by the Zurich group. This lattice is obtained by starting from a square lattice of constant a (fig. 2a), deleting every second horizontal link, and keeping all the vertical links[1]. Note that we can go from this brick wall to graphene by a continuous deformation.

2-1 Hubbard Hamiltonian

The unit cell of this lattice, represented in grey on figure 2b, has two sites noted A and B. We generate the lattice by copying the unit cell according to the square Bravais lattice

$$\mathcal{B} \equiv \{\boldsymbol{r_j} = j_1\boldsymbol{a}_1 + j_2\boldsymbol{a}_2,\ j_1, j_2 \in \mathbb{Z}\} \tag{12}$$

with the two vectors in the Cartesian basis $\boldsymbol{u}_x, \boldsymbol{u}_y$:

$$\boldsymbol{a}_1 = a\begin{pmatrix}1\\1\end{pmatrix}, \qquad \boldsymbol{a}_2 = a\begin{pmatrix}1\\-1\end{pmatrix}. \tag{13}$$

[1] A bricklayer would tell us that for a real brick wall, one would have to swap horizontal and vertical lines, but we take here the convention used by Tarruell, Greif, et al. (2012).

The Bravais lattice of the reciprocal space is also a square, generated by the two vectors

$$\boldsymbol{b}_1 = \frac{\pi}{a}\begin{pmatrix}1\\1\end{pmatrix}, \qquad \boldsymbol{b}_2 = \frac{\pi}{a}\begin{pmatrix}1\\-1\end{pmatrix}. \tag{14}$$

The vectors $\boldsymbol{b}_1, \boldsymbol{b}_2$ verify the general relation

$$\boldsymbol{a}_i \cdot \boldsymbol{b}_j = 2\pi\ \delta_{i,j}. \tag{15}$$

The corresponding Brillouin zone is represented in grey on figure 2c.

We consider the tight-binding regime and note $-J_x$, $-J_y$ the matrix elements along the horizontal and vertical directions of figure 2b. Let us recall the rules to write the Hubbard Hamiltonian, already seen in Chapter 4. We know in general that the eigenfunctions of the Hamiltonian are the Bloch functions $\psi_{\boldsymbol{q}}(\boldsymbol{r}) = \mathrm{e}^{\mathrm{i}\boldsymbol{q}\cdot\boldsymbol{r}}u_{\boldsymbol{q}}(\boldsymbol{r})$. The vector $\boldsymbol{q}$ can be chosen in the Brillouin zone and $u_{\boldsymbol{q}}(\boldsymbol{r})$ is a periodic function on the lattice. In the tight-binding limit restricted to the lowest band, the set of periodic functions on the lattice is a vector space of dimension 2, each function being characterized by two coefficients (α, β):

$$|u_{\boldsymbol{q}}\rangle = \alpha_{\boldsymbol{q}}\left(\sum_{\boldsymbol{j}}|w_{A,\boldsymbol{j}}\rangle\right) + \beta_{\boldsymbol{q}}\left(\sum_{\boldsymbol{j}}|w_{B,\boldsymbol{j}}\rangle\right), \tag{16}$$

where $|w_{A/B,\boldsymbol{j}}\rangle$ are the Wannier functions centered on the A/B site of the $\boldsymbol{j}$ cell. The corresponding Bloch function is written as

$$|\psi_{\boldsymbol{q}}\rangle = \sum_{\boldsymbol{j}}\mathrm{e}^{\mathrm{i}\boldsymbol{r_j}\cdot\boldsymbol{q}}\left(\alpha_{\boldsymbol{q}}|w_{A,\boldsymbol{j}}\rangle + \beta_{\boldsymbol{q}}|w_{B,\boldsymbol{j}}\rangle\right), \tag{17}$$

and our goal is to find the values $(\alpha_{\boldsymbol{q}}, \beta_{\boldsymbol{q}})$ so that $|\psi_{\boldsymbol{q}}\rangle$ is an eigenstate of the Hubbard Hamiltonian.

Let us write explicitly this Hamiltonian. The energies of the particle on a site A and on a site B are equal, and noted E_0. The Hubbard Hamiltonian contains by hypothesis only the hopping terms between nearest neighbours. When a particle is on a B site, it can only hop to an A site, which can belong to the same cell ($\boldsymbol{j}$, horizontal jump) or to one of the two adjacent cells ($\boldsymbol{j}+\boldsymbol{a}_1$ or $\boldsymbol{j}+\boldsymbol{a}_2$, vertical jumps). It is the same for a particle on site A of the cell $\boldsymbol{j}$, which can jump to $(B, \boldsymbol{j})$, $(B, \boldsymbol{j}-\boldsymbol{a}_1)$ and $(B, \boldsymbol{j}-\boldsymbol{a}_2)$.

Let us assume that $|\psi_{\boldsymbol{q}}\rangle$ defined by (17) is an eigenstate of this Hubbard Hamiltonian with eigenvalue $E(\boldsymbol{q})$, and let us project this eigenvalue equation onto a given cell $\boldsymbol{j}$. We obtain the 2×2 system for the coefficients $(\alpha_{\boldsymbol{q}}, \beta_{\boldsymbol{q}})$:

$$\hat{\mathcal{H}}(\boldsymbol{q}) \begin{pmatrix} \alpha_{\boldsymbol{q}} \\ \beta_{\boldsymbol{q}} \end{pmatrix} = E(\boldsymbol{q}) \begin{pmatrix} \alpha_{\boldsymbol{q}} \\ \beta_{\boldsymbol{q}} \end{pmatrix}, \tag{18}$$

where the Hubbard Hamiltonian in the reciprocal space has the structure proposed in (2). In particular the coefficient $f(\boldsymbol{q})$ corresponds to the coupling of a given site B (j_x, j_y) with its three neighbours of type A: one of its neighbours belongs to the same unit cell (horizontal link J_x), the second to the cell $(j_x + 1, j_y)$ and the third to the cell $(j_x, j_y + 1)$ (vertical links J_y). So we have

$$f(\boldsymbol{q}) = -J_x - J_y \left(\mathrm{e}^{\mathrm{i}\boldsymbol{a}_1 \cdot \boldsymbol{q}} + \mathrm{e}^{\mathrm{i}\boldsymbol{a}_2 \cdot \boldsymbol{q}} \right) = -J_x - 2J_y \, \mathrm{e}^{\mathrm{i}aq_x} \, \cos(aq_y). \tag{19}$$

The Dirac points, if they exist, correspond to the zeros of this function and are thus obtained for

$$\sin(aq_x) = 0 \qquad \Rightarrow \qquad q_x = 0 \mod \pi/a \tag{20}$$

$$\cos(aq_x) \cos(aq_y) = -\frac{J_x}{2J_y}. \tag{21}$$

2-2 Pairs of Dirac points

The existence of possible solutions to the system of equations (20-21) depends on the value of the ratio $J_x/(2J_y)$:

- If $J_x > 2J_y$, this system has no solution. The function $f(q)$ does not cancel in the Brillouin zone and there are no Dirac points. The two sub-bands $E_0 \pm |f(\boldsymbol{q})|$ are separated by a non zero gap.
- If $J_x = 2J_y$, the function $f(\boldsymbol{q})$ cancels at the four corners of the Brillouin zone. This is a second-order zero in the y direction, so it is not strictly speaking a Dirac point.
- If $J_x < 2J_y$, the function $f(\boldsymbol{q})$ cancels at two Dirac points located symmetrically on the vertical axis $q_x = 0$, at points such that $\cos(aq_y) = -J_x/(2J_y)$ (figure 3). When J_x becomes very small compared to J_y, these points approach $q_y = \pm\pi/(2a)$.

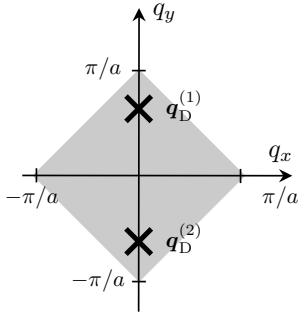

Figure 3. *Positions of the two Dirac points for the brick wall lattice, in the case $J_x < 2J_y$.*

We consider the case $J_x < 2J_y$ and expand the function $f(\boldsymbol{q})$ in the neighbourhood of a Dirac point $\boldsymbol{q}_{\mathrm{D}}$. We find:

$$f(\boldsymbol{q}) \approx \mathrm{i}aJ_x \left[\delta q_x + \mathrm{i}\, \delta q_y \, \tan(aq_{\mathrm{D},y}) \right], \tag{22}$$

which is close to the particular form assumed in (6). More precisely, since $\tan(aq_{\mathrm{D},y})$ does not have the same sign for the two Dirac points (it is negative for the point located in the upper part of the Brillouin zone, positive for the other), the two Dirac points have an opposite chirality. We note that the function $f(\boldsymbol{q})$ is generally not isotropic around the Dirac points, unless $\tan(aq_{\mathrm{D},y}) = 1$, which is obtained for $J_x = \sqrt{2}\, J_y$.

The fact that the Dirac points appear in pairs is a direct consequence of the time reversal invariance of the considered problem. We have seen in Chapter 2 that this invariance implies that if $\psi_{\boldsymbol{q}}$ is an eigenstate for the eigenvalue $E(\boldsymbol{q})$, then $\psi_{-\boldsymbol{q}} \propto \psi_{\boldsymbol{q}}^*$ is an eigenstate for the same eigenvalue. We deduce that if $\boldsymbol{q}_{\mathrm{D}}^{(1)}$ is a Dirac point associated to a certain chirality, then $\boldsymbol{q}_{\mathrm{D}}^{(2)} = -\boldsymbol{q}_{\mathrm{D}}^{(1)}$ is also a Dirac point, with an opposite chirality because of the complex conjugation involved in the relation $\psi_{-\boldsymbol{q}} \propto \psi_{\boldsymbol{q}}^*$.

When we continuously decrease the parameter J_x/J_y and cross the value 2, the Dirac points are superimposed in a corner of the Brillouin zone, which is still compatible with $\boldsymbol{q}_{\mathrm{D}}^{(2)} = -\boldsymbol{q}_{\mathrm{D}}^{(1)}$, since $\boldsymbol{q}_D^{(2)}$ and $\boldsymbol{q}_D^{(1)}$ then differ by one vector of the reciprocal lattice (Montambaux, Piéchon, et al. 2009).

3 The graphene lattice

The study of the Dirac points in graphene is done in a very similar way to what we have done above for the brick wall lattice, and we will therefore limit ourselves to presenting the main lines of the approach providing these points.

3-1 Unit cell and reciprocal lattice

Graphene is obtained by placing one carbon atom per site of a hexagonal structure of side a. The unit cell of this structure has two sites, noted A and B on figure 4. We generate the hexagonal lattice by copying this unit cell (represented in grey on the figure) on all the nodes of the triangular Bravais lattice

$$\mathcal{B} \equiv \{\boldsymbol{r_j} = j_1\boldsymbol{a}_1 + j_2\boldsymbol{a}_2,\ j_1, j_2 \in \mathbb{Z}\} \tag{23}$$

where the vectors $\boldsymbol{a}_1$, $\boldsymbol{a}_2$ are defined by:

$$\boldsymbol{a}_1 = \frac{\sqrt{3}\,a}{2}\begin{pmatrix}\sqrt{3}\\1\end{pmatrix}, \qquad \boldsymbol{a}_2 = \frac{\sqrt{3}}{2}\begin{pmatrix}\sqrt{3}\\-1\end{pmatrix}. \tag{24}$$

The reciprocal lattice $\mathcal{B}' \equiv \{\boldsymbol{Q_j} = j_1\boldsymbol{b}_1 + j_2\boldsymbol{b}_2,\ j_1, j_2 \in \mathbb{Z}\}$ is generated by the vectors

$$\boldsymbol{b}_1 = \frac{2\pi}{3a}\begin{pmatrix}1\\\sqrt{3}\end{pmatrix}, \qquad \boldsymbol{b}_2 = \frac{2\pi}{3a}\begin{pmatrix}1\\-\sqrt{3}\end{pmatrix}. \tag{25}$$

The reciprocal lattice is therefore triangular.

Brillouin zone. Recall that the Bloch functions $|\psi_{\boldsymbol{q}}\rangle$ are eigenstates of the Hamiltonian and of the translation operators $\hat{T}_{\boldsymbol{a}_1}$ and $\hat{T}_{\boldsymbol{a}_2}$ that leave the lattice invariant. The eigenvalues associated to the translation operations are noted $\mathrm{e}^{\mathrm{i}\theta_1} = \mathrm{e}^{\mathrm{i}\boldsymbol{a}_1\cdot\boldsymbol{q}}$ and $\mathrm{e}^{\mathrm{i}\theta_2} = \mathrm{e}^{\mathrm{i}\boldsymbol{a}_2\cdot\boldsymbol{q}}$. The Brillouin zone is a domain[2] centered at $\boldsymbol{q} = 0$, in which one and only one vector $\boldsymbol{q}$ corresponds to a pair (θ_1, θ_2). It is a hexagon of side $4\pi/(3\sqrt{3}a)$, whose orientation is rotated by 30° with respect to the hexagons of the lattice in real space (figure 4).

[2]More precisely, it is defined as the Wigner–Seitz cell centered at $\boldsymbol{q} = 0$ of the reciprocal lattice

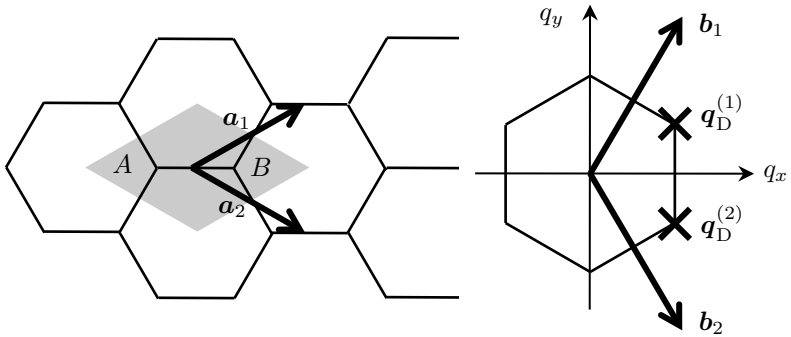

Figure 4. *Left: hexagonal structure of graphene. This structure is composed of a unit cell with two sites A and B, which is repeated by placing it on the nodes of a triangular lattice $j_1\boldsymbol{a}_1 + j_2\boldsymbol{a}_2,\ j_1, j_2 \in \mathbb{Z}$. A unit cell is represented in grey. Right: reciprocal lattice for graphene, $j_1\boldsymbol{b}_1 + j_2\boldsymbol{b}_2,\ j_1, j_2 \in \mathbb{Z}$. The Brillouin zone is hexagonal and the Dirac points are the corners of this hexagon.*

3-2 Dirac points for graphene

With the same reasoning as for the brick wall lattice, we find that the Hubbard Hamiltonian in reciprocal space has the form anticipated in (2) (Wallace 1947)

$$\hat{\mathcal{H}}(\boldsymbol{q}) = \begin{pmatrix} E_0 & f^*(\boldsymbol{q}) \\ f(\boldsymbol{q}) & E_0 \end{pmatrix}, \tag{26}$$

with the function $f(\boldsymbol{q})$ defined by

$$f(\boldsymbol{q}) = -J\left(1 + \mathrm{e}^{\mathrm{i}\boldsymbol{q}\cdot\boldsymbol{a}_1} + \mathrm{e}^{\mathrm{i}\boldsymbol{q}\cdot\boldsymbol{a}_2}\right). \tag{27}$$

Let us look for the zeros of $f(\boldsymbol{k})$, by cancelling both the real part f_r and the imaginary part f_i:

$$\begin{aligned} \text{Cancellation of } f_r(\boldsymbol{q}): &\quad 1 + \cos(\boldsymbol{q}\cdot\boldsymbol{a}_1) + \cos(\boldsymbol{q}\cdot\boldsymbol{a}_2) = 0, \\ \text{Cancellation of } f_i(\boldsymbol{q}): &\quad \sin(\boldsymbol{q}\cdot\boldsymbol{a}_1) + \sin(\boldsymbol{q}\cdot\boldsymbol{a}_2) = 0. \end{aligned} \tag{28}$$

Two types of zeros appear. The first one corresponds to

$$\begin{aligned} \cos(\boldsymbol{q}\cdot\boldsymbol{a}_1) &= \cos(\boldsymbol{q}\cdot\boldsymbol{a}_2) = -\frac{1}{2}, \\ \sin(\boldsymbol{q}\cdot\boldsymbol{a}_1) &= -\sin(\boldsymbol{q}\cdot\boldsymbol{a}_2) = -\frac{\sqrt{3}}{2} \end{aligned} \tag{29}$$

i.e.

$$\boldsymbol{q}\cdot\boldsymbol{a}_1 = \frac{4\pi}{3} \bmod 2\pi, \qquad \boldsymbol{q}\cdot\boldsymbol{a}_2 = \frac{2\pi}{3} \bmod 2\pi. \tag{30}$$

The second type of zero is given by

$$\boldsymbol{q}\cdot\boldsymbol{a}_1 = \frac{2\pi}{3} \bmod 2\pi, \qquad \boldsymbol{q}\cdot\boldsymbol{a}_2 = \frac{4\pi}{3} \bmod 2\pi. \tag{31}$$

By writing the solution $\boldsymbol{q}$ under the form $\boldsymbol{q} = \alpha_1\boldsymbol{b}_1 + \alpha_2\boldsymbol{b}_2$, we immediately deduce the coordinates (α_1, α_2) of these Dirac points in the reciprocal space. There are two Dirac points (one of each chirality) in the Brillouin zone, and these points are located in

$$\boldsymbol{q}_{\rm D}^{(1)} = \frac{1}{3}\,(2\boldsymbol{b}_1 + \boldsymbol{b}_2) = \frac{2\pi}{3\sqrt{3}\,a}\left(\sqrt{3}\;\boldsymbol{u}_x + \boldsymbol{u}_y\right), \tag{32}$$

$$\boldsymbol{q}_{\rm D}^{(2)} = \frac{1}{3}\,(\boldsymbol{b}_1 + 2\boldsymbol{b}_2) = \frac{2\pi}{3\sqrt{3}\,a}\left(\sqrt{3}\;\boldsymbol{u}_x - \boldsymbol{u}_y\right). \tag{33}$$

These points are located at the edge of the Brillouin zone, at the vertices of the hexagon limiting this zone (figure 4). Note that each of the six vertices of the hexagonal Brillouin zone is a Dirac point. However, one must be careful with double counting. A vector $\boldsymbol{q}$ and a vector $\boldsymbol{q}'$ that differ by a vector of the reciprocal lattice correspond to the same Bloch state. This is the case for the four other vertices of the hexagonal Brillouin zone: they are deduced from the two marked on the figure by subtracting $\boldsymbol{b}_1$, $\boldsymbol{b}_2$ and $\boldsymbol{b}_1 + \boldsymbol{b}_2$. Moreover, we can verify that the function $f(\boldsymbol{q})$ is at first order isotropic around these two zeros, with

$$f(\boldsymbol{q}) \approx \mathrm{i}\frac{3Ja}{2}\,(\delta q_x \;\pm\; \mathrm{i}\,\delta q_y)\,, \tag{34}$$

which corresponds (up to the global factor i) to the form announced in (6). The velocity c is given here by $c = 3\,Ja/2$ and it is of the order of 10^6 m/s for graphene (Castro Neto, Guinea, et al. 2009).

3-3 Additional comments

The chirality of the zeros of $f(\boldsymbol{q})$. We have seen in the previous examples that the search for Dirac points is similar to the search for the zeros of a function $f(\boldsymbol{q})$ with two real variables, q_x and q_y, with values in the complex plane. The zeros of such a function generally have a vortex structure, with a positive or negative phase winding. This is the phase winding that gives its chirality to a Dirac point.

Let us specify the origin of this winding in a very qualitative way. Depending on the value of $\boldsymbol{q}$, the real part $f_r(\boldsymbol{q})$ of $f(\boldsymbol{q})$ can be positive or negative. The domains of the plane (q_x, q_y) corresponding to a positive value of f_r and those corresponding to a negative value of f_r are separated by lines (open or closed) along which f_r cancels. The same is true for the imaginary part f_i, which cancels along other lines of the plane (q_x, q_y). A zero $\boldsymbol{q}_{\rm D}$ of the complex function $f(\boldsymbol{q})$ corresponds to a point where two lines of zeros, one for f_r, the other for f_i, intersect. This crossing generally defines[3] four quadrants that correspond to the four possible choices for the signs of the pair (f_r, f_i): $(+,+)$, $(+,-)$, $(-,-)$, $(-,+)$. Depending on whether we find this order by turning around the zero clockwise or anti-clockwise, we have one chirality or its opposite for the Dirac point.

Anomalous quantum Hall effect. The chirality of Dirac points has important consequences. Let us mention only one of them here. When such a material is placed in a magnetic field, the energy levels (Landau levels) are labelled with an integer n and vary as $E_n \propto \sqrt{n}$. In particular, there is a zero energy level, which is very different from the ordinary case where we find $E_n \propto (n + 1/2)$. The appearance of this zero energy state can be interpreted semi-classically by evaluating the action on a cyclotron orbit in the reciprocal space encircling the Dirac point. In addition to the usual action, the Berry phase associated to the chirality of the Dirac point replaces $n + 1/2$ by $n + 1/2 \pm 1/2$ (Mikitik & Sharlai 1999); this allows in particular the appearance of a zero-energy state, which plays an important role in the anomalous quantum Hall effect observed on graphene (Zhang, Tan, et al. 2005; Novoselov, Geim, et al. 2005).

[3] One can imagine more exotic solutions where the zero of f_r or f_i is of order 2, but we describe here only the "standard" situation.

Robustness of the Dirac points. Suppose that the lattice parameters are chosen such that the function $f(\boldsymbol{q})$ has 2 (or 4, 6,...) zeros in the Brillouin zone. When the lattice parameters are modified while keeping the same energy for both sites, only the function $f(\boldsymbol{q})$ changes. But the zeros of $f(\boldsymbol{q})$ are topologically protected by their chirality: in other words, the two curves defining $f_r(\boldsymbol{q}) = 0$ and $f_i(\boldsymbol{q}) = 0$ will continue to cross each other (at another location) if we slightly modify these curves. The only way to make the crossings disappear in this context is to merge two zeros, one of positive chirality and the other of negative chirality, by realizing a situation where the two curves $f_r(\boldsymbol{q}) = 0$ and $f_i(\boldsymbol{q}) = 0$ become tangent one to the other. For a graphene-like state filling, this particular case of two Dirac points merging corresponds to a topological transition between a semi-metallic phase and a band insulator, and it is studied in detail by Montambaux, Piéchon, et al. (2009).

On-site energies. While the Dirac points can stand a (slight) modification of the function $f(\boldsymbol{k})$, it is not the same with respect to a dissymmetry between the two sites A and B. If we modify the Hubbard Hamiltonian by giving an energy $E_0 + \Delta$ (resp. $E_0 - \Delta$) to sites A (resp. B), then the eigenvalues of

$$\hat{\mathcal{H}}(\boldsymbol{q}) = \begin{pmatrix} E_0 + \Delta & f^*(\boldsymbol{q}) \\ f(\boldsymbol{q}) & E_0 - \Delta \end{pmatrix}, \tag{35}$$

become

$$E_\pm(\boldsymbol{q}) = E_0 \pm \left[|f(\boldsymbol{q})|^2 + \Delta^2\right]^{1/2} \tag{36}$$

and we find two ordinary sub-bands, separated by a gap $2\,\Delta$ and without any remarkable topological property. While such a dissymmetry is difficult to create on real graphene (see for example Montambaux, Piéchon, et al. (2009) and the references therein), it is on the other hand easy in optical lattices, as we will see below.

4 The cold atoms version of graphene

The Zurich group has recently realized an optical lattice of the brick wall type, in which they were able to highlight Dirac points and show that their positions were controllable with the parameter J_x/J_y. The existence of these Dirac points was shown thanks to Bloch oscillations: the particles are transferred with a high probability from the lower band to the upper band when they pass in the vicinity of these contact points.

4-1 Realization of the brick wall lattice

The light potential that was used results from the superposition of several standing light waves. The most intense wave is a standing wave in the x direction creating the potential

$$V_1(\boldsymbol{r}) = -V_{\bar{X}} \cos^2(kx + \theta/2) \tag{37}$$

where θ is a parameter that can be adjusted by slightly varying the frequency of this wave. We superimpose an optical lattice in the xy plane formed by two standing light waves along the x and y directions, phase-locked to each other[4]:

$$V_2(\boldsymbol{r}) = -V_Y \cos^2(ky) \;-\; 2\sqrt{V_X V_Y}\, \cos(kx)\, \cos(ky) \;-\; V_X \cos^2(kx). \tag{38}$$

The intensities of these waves are chosen such that

$$V_X \ll \sqrt{V_X V_Y} \ll V_Y < V_{\bar{X}}. \tag{39}$$

In practice, only the three terms with the largest amplitudes are relevant to the formation of the desired lattice and we will neglect the fourth term, $-V_X \cos^2(kx)$, in our discussion.

Let us start with $\theta = \pi$, so that $V_1(\boldsymbol{r}) = -V_{\bar{X}} \sin^2(kx)$; this parameter will be varied later, in particular to obtain the results of figure 8. With only the terms V_1 and $V_2^{(a)} = -V_Y \cos^2(ky)$, we make a square lattice whose sites are the points

$$kx = \pi/2 \;[\text{mod. } \pi], \qquad ky = 0 \;[\text{mod. } \pi]. \tag{40}$$

Note that the tunnel effect is weaker along x than along y since $V_{\bar{X}} > V_Y$. The term in $V_2^{(b)}(\boldsymbol{r}) = -2\sqrt{V_X V_Y}\, \cos(kx)\, \cos(ky)$ modulates some tunnelling coefficients (figure 5):

[4] In the article by Tarruell, Greif, et al. (2012), the term in $\sqrt{V_X V_Y}$ is reduced by a multiplicative factor $\alpha \approx 0.9$ which characterizes the visibility of the interference between the standing wave along y and that along x. We will omit this coefficient here as it does not play a role in our semi-quantitative description.

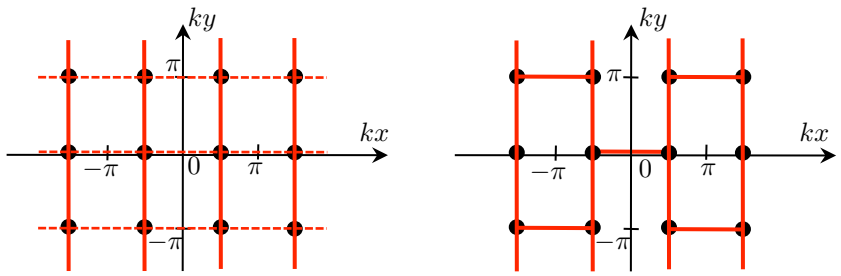

Figure 5. *Construction of a brick wall lattice (Tarruell, Greif, et al. 2012). Left: square lattice obtained by superimposing* $V_1(\boldsymbol{r}) = -V_{\bar{X}} \sin^2(kx)$ *and* $V_2^{(a)} = -V_Y \cos^2(ky)$*. Right: increase or decrease of the horizontal tunneling coefficients with the term* $V_2^{(b)}(\boldsymbol{r}) = -2\sqrt{V_X V_Y}\, \cos(kx)\, \cos(ky)$*. Typical values are (in units of* E_r*):* $V_{\bar{X}} = 4.0$*,* $V_Y = 2.0$*,* $V_X = 0.3$*.*

- The vertical links are centered on points such that $kx = \pi/2$ modulo π and $ky = \pi/2$ modulo π. The tunneling matrix elements of these links are little affected by $V_2^{(b)}$ since $V_2^{(b)}(\boldsymbol{r}) \propto \cos(kx)$ is zero along these links.
- The horizontal links are centered on points such that $kx = 0$ modulo π and $ky = 0$ modulo π. At the center of these links, we have $\cos(kx) = \pm 1$ and $\cos(ky) = \pm 1$. The potential $V_2^{(b)}$ takes a significant value there and modifies the tunneling matrix elements. Two cases are possible:
  - A horizontal link centered on a point such that $\cos(kx)$ and $\cos(ky)$ have the same sign (equal to ± 1) corresponds to a negative value of $V_2^{(b)}$ which lowers the tunnel barrier between the two sites concerned by this link: the tunnel effect between these two sites is increased.
  - A horizontal link centered on a point such that $\cos(kx)$ and $\cos(ky)$ have opposite sign corresponds to a positive value of $V_2^{(b)}$ and the corresponding tunnel effect (already weak without $V_2^{(b)}$) is further decreased.

In the end, the brick wall lattice is effectively realized.

4-2 Bloch oscillations and Dirac points

To probe the position of the Dirac points, the Zurich group observed the result of Bloch oscillations. These oscillations occur in the x direction under the effect of a constant force caused by a magnetic field gradient. When the trajectory in $\boldsymbol{q}$ space passes in the vicinity of a Dirac point, the atom can be transferred with a high probability to the upper band (for a detailed study of this transition, see Lim, Fuchs, et al. (2012)). The transition to the excited band can then be detected by the *band mapping* technique presented in chapter 2 of this lecture: one adiabatically ramps down the lattice (duration 0.5 ms) so that an atom remains in the band it occupied at the beginning of the ramp, and then performs a time-of-flight which thus reveals the population of each band.

The atomic gas that is used is an ensemble of polarized fermions without interactions (^{40}K). The atoms initially occupy the center of the Brillouin zone and do not meet the Dirac points which are located close to the edge of the band (figure 3). On the other hand, the second part of the Bloch oscillation (after Bragg reflection at the boundary of the Brillouin zone) can bring them to the vicinity of the Dirac points and the transition can then occur (figure 6).

The position of the peaks that have been transferred to the upper band provides direct information on the position of the Dirac points. We recall that this position is a function of the ratio J_x/J_y, and the points disappear when this ratio becomes too high. The Zurich group studied the position of the Dirac points by varying the potential $V_{\bar{X}}$. The result, shown on figure 7, is in good agreement with the predictions. Note that the tight-binding model is not quantitatively valid in this parameter domain and that a numerical diagonalization of the lattice Hamiltonian must be used to determine precisely the position of the Dirac points.

It is also possible in this experiment to break the symmetry between the two sites A and B of the lattice. For that, one can take a value of θ in (37) different from π. We have seen in (36) that this amounts to opening a gap between the two sub-bands; the Bloch oscillation should then no longer cause a transition between these two sub-bands, at least if the force is not too large. This reduction is indeed observed experimentally (figure 8).

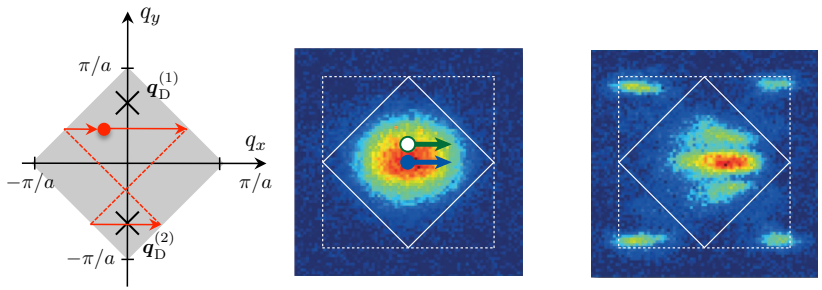

Figure 6. *Left: Bloch oscillations along the x axis. Middle: initial distribution in $\boldsymbol{q}$ space. Right: distribution in $\boldsymbol{q}$ space after a Bloch oscillation (period τ_{B}). One can clearly distinguish the atoms which passed in the vicinity of a Dirac point during the oscillation and which were then transferred to the upper band [figure extracted from Tarruell, Greif, et al. (2012)].*

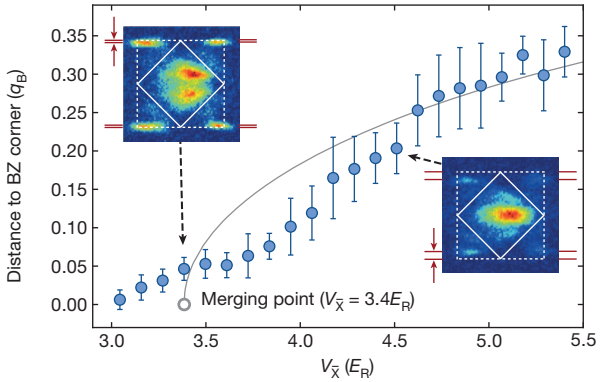

Figure 7. *Variation of the position of Dirac points on the axis $q_x = 0$ as a function of the potential depth $V_{\bar{X}}$. For this figure, $V_Y = 1.8$ and $V_X = 0.28$. The two Dirac points are expected to merge in the corner of the Brillouin zone for $V_{\bar{X}} = 3.4$, which is in good agreement with the observations [figure taken from Tarruell, Greif, et al. (2012)].*

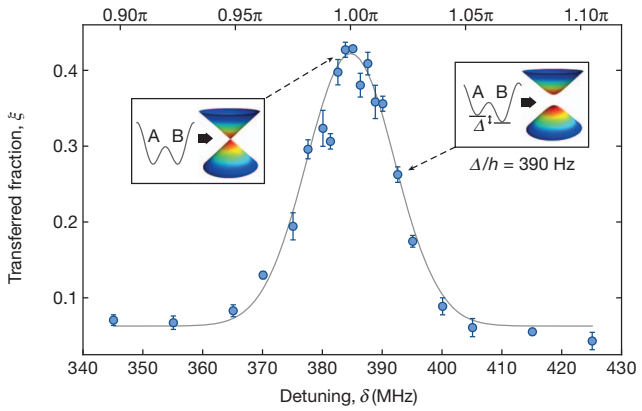

Figure 8. *Disappearance of the Dirac points when the symmetry between the A and B sites is broken. Transition probability to the upper band as a function of the angle θ entering the definition of $V_1(\boldsymbol{r})$ (37). This angle is indicated on the upper horizontal scale and is controlled by the detuning of the beam creating the standing wave (lower horizontal scale) [figure extracted from Tarruell, Greif, et al. (2012)].*

4-3 Perspectives

The Zurich experiment has thus demonstrated the existence of Dirac points in an optical lattice. The flexibility offered by these lattices is illustrated on figure 7, where one can control the position of these points, make them merge and then disappear. This experiment is probably only a starting point in this cold atom simulation of graphene. Many aspects of the ultra-relativistic physics encountered in the vicinity of Dirac points could be addressed with these systems, such as Klein's paradox, i.e. the quasi-total transmission of a wave packet through a very high barrier (Katsnelson, Novoselov, et al. 2006). Let us recall that this paradox plays an important role in real graphene because it prevents the backscattering of conduction electrons; Dirac electrons are insensitive to the localization effects observed for ordinary electrons and thus propagate ballistically over long distances (micrometers). Moreover, the implementation of artificial magnetic fields on this lattice should allow the study of the anomalous quantum Hall effect with cold atoms.

References

Ashcroft, N. W. & N. D. Mermin (1976), *Solid State Physics*, New York: Holt, Rinehardt and Winston.

Avron, JE, J Zak, A Grossman & L Gunther (1977), "Instability of continuous spectrum – N-band Stark Ladder", in *Journal of Mathematical Physics* **18**, 918–921.

Battesti, R., P. Cladé, S. Guellati-Khélifa, C. Schwob, B. Grémaud, F. Nez, L. Julien & F. Biraben (2004), "Bloch Oscillations of Ultracold Atoms: A Tool for a Metrological Determination of h/m_{Rb}", in *Phys. Rev. Lett.* **92** (25), p. 253001.

Beaufils, Q., G. Tackmann, X. Wang, B. Pelle, S. Pelisson, P. Wolf & F. Pereira dos Santos (2011), "Laser Controlled Tunneling in a Vertical Optical Lattice", in *Phys. Rev. Lett.* **106** (21), p. 213002.

Becker, C, P Soltan-Panahi, J Kronjäger, S Dörscher, K Bongs & K Sengstock (2010), "Ultracold quantum gases in triangular optical lattices", in *New Journal of Physics* **12**, p. 065025.

Ben Dahan, Maxime, Ekkehard Peik, Jakob Reichel, Yvan Castin & Christophe Salomon (1996), "Bloch Oscillations of Atoms in an Optical Potential", in *Phys. Rev. Lett.* **76** (24), pp. 4508–4511.

Bloch, F. (July 1929), "Über die Quantenmechanik der Elektronen in Kristallgittern", in *Zeitschrift fur Physik* **52**, pp. 555–600.

Bouchendira, R., P. Cladé, S. Guellati-Khélifa, F. Nez & F. Biraben (2011), "New Determination of the Fine Structure Constant and Test of the Quantum Electrodynamics", in *Phys. Rev. Lett.* **106** (8), p. 080801.

Browaeys, A., H. Häffner, C. McKenzie, S. L. Rolston, K. Helmerson & W. D. Phillips (2005), "Transport of atoms in a quantum conveyor belt", in *Phys. Rev. A* **72** (5), p. 053605.

Cadoret, M., E. de Mirandes, P. Cladé, S. Guellati-Khélifa, C. Schwob, F. Nez, L. Julien & F. Biraben (2008), "Combination of Bloch Oscillations with a Ramsey-Bordé Interferometer: New Determination of the Fine Structure Constant", in *Phys. Rev. Lett.* **101** (23), p. 230801.

Campbell, R. (1955), *Théorie générale de l'équation de Mathieu*, Masson et Cie.

Carusotto, I., L. Pitaevskii, S. Stringari, G. Modugno & M. Inguscio (2005), "Sensitive Measurement of Forces at the Micron Scale Using Bloch Oscillations of Ultracold Atoms", in *Phys. Rev. Lett.* **95** (9), p. 093202.

Castro Neto, A. H., F. Guinea, N. M. R. Peres, K. S. Novoselov & A. K. Geim (2009), "The electronic properties of graphene", in *Rev. Mod. Phys.* **81** (1), pp. 109–162.

Champenois, C, M Buchner, R Dehuille, R Mathevet, C Robilliard, C Rizzo & J Vigue (2001), "Atomic diffraction by a laser standing wave: Analysis using Bloch states", in *European Physical Journal D* **13**, 271–278.

Charrière, Renée, Malo Cadoret, Nassim Zahzam, Yannick Bidel & Alexandre Bresson (2012), "Local gravity measurement with the combination of atom interferometry and Bloch oscillations", in *Phys. Rev. A* **85** (1), p. 013639.

Cladé, P., S. Guellati-Khélifa, F. Nez & F. Biraben (2009), "Large Momentum Beam Splitter Using Bloch Oscillations", in *Phys. Rev. Lett.* **102** (24), p. 240402.

Cladé, P., E. de Mirandes, M. Cadoret, S. Guellati-Khélifa, C. Schwob, F. Nez, L. Julien & F. Biraben (2006), "Determination of the Fine Structure Constant Based on Bloch Oscillations of Ultracold Atoms in a Vertical Optical Lattice", in *Phys. Rev. Lett.* **96** (3), p. 033001.

Cohen-Tannoudji, C. (1992), "Atomic motion in laser light", in *Fundamental Systems in Quantum Optics*, ed. by J. Dalibard, J.-M. Raimond & J. Zinn-Justin, North-Holland Amsterdam, , pp. 1–164.

Cohen-Tannoudji, C. & J. Dupont-Roc (1972), "Experimental Study of Zeeman Light Shifts in Weak Magnetic Fields", in *Phys. Rev. A* **5**, pp. 968–984.

Cohen-Tannoudji, C., J. Dupont-Roc & G. Grynberg (1989), *Photons and Atoms–Introduction to Quantum Electrodynamics*, New-York: Wiley.

– (1992), *Atom-Photon Interactions*, New York: Wiley.

Creffield, C. E., F. Sols, D. Ciampini, O. Morsch & E. Arimondo (2010), "Expansion of matter waves in static and driven periodic potentials", in *Phys. Rev. A* **82** (3), p. 035601.

Dahan, Maxime (1997), "Transport et relaxation d'atomes de césium : oscillations de Bloch et résonance de diffusion", PhD thesis, Université Paris 6.

Dalibard, J & C Cohen-Tannoudji (1985), "Dressed atom approach to atomic motion in laser light – the dipole force revisited ", in *Journal of the Optical Society of America B-Optical Physics* **2**, 1707–1720.

Denschlag, J Hecker, J E Simsarian, H Häffner, C McKenzie, A Browaeys, D Cho, K Helmerson, S L Rolston & W D Phillips (2002), "A Bose-Einstein condensate in an optical lattice", in *Journal of Physics B: Atomic, Molecular and Optical Physics* **35**, p. 3095.

Deutsch, Ivan H. & Poul S. Jessen (1998), "Quantum-state control in optical lattices", in *Phys. Rev. A* **57** (3), pp. 1972–1986.

Dunlap, D. H. & V. M. Kenkre (1986), "Dynamic localization of a charged particle moving under the influence of an electric field", in *Phys. Rev. B* **34** (6), pp. 3625–3633.

Durfee, D. S., Y. K. Shaham & M. A. Kasevich (2006), "Long-Term Stability of an Area-Reversible Atom-Interferometer Sagnac Gyroscope", in *Phys. Rev. Lett.* **97** (24), p. 240801.

Eckardt, André, Martin Holthaus, Hans Lignier, Alessandro Zenesini, Donatella Ciampini, Oliver Morsch & Ennio Arimondo (2009), "Exploring dynamic localization with a Bose-Einstein condensate", in *Phys. Rev. A* **79** (1), p. 013611.

Eckardt, Andre, Christoph Weiss & Martin Holthaus (2005), "Superfluid-Insulator Transition in a Periodically Driven Optical Lattice", in *Phys. Rev. Lett.* **95**, p. 260404.

Fisher, M. P. A., P. B. Weichman, G. Grinstein & D. S. Fisher (1989), "Boson localization and the superfluid-insulator transition", in *Phys. Rev. B* **40**, p. 546.

Floquet, Gaston (1883), "Sur les équations différentielles linéaires à coefficients périodiques", in *Annales de l'École Normale Supérieure*, pp. 47–88.

Fölling, S., S. Trotzky, P. Cheinet, M. Feld, R. Saers, A. Widera, T. Muller & I. Bloch (2007), "Direct observation of second-order atom tunnelling", in *Nature* **448**, p. 1029.

Gauguet, A., B. Canuel, T. Lévèque, W. Chaibi & A. Landragin (2009), "Characterization and limits of a cold-atom Sagnac interferometer", in *Phys. Rev. A* **80** (6), p. 063604.

Gerbier, Fabrice & Jean Dalibard (2010), "Gauge fields for ultracold atoms in optical superlattices", in *New Journal of Physics* **12**, p. 033007.

Gluck, M, AR Kolovsky & HJ Korsch (2002), "Wannier-Stark resonances in optical and semiconductor superlattices", in *PHYSICS REPORTS-REVIEW SECTION OF PHYSICS LETTERS* **366**, 103–182.

Gordon, J. P. & A. Ashkin (1980), "Motion of atoms in a radiation trap", in *Phys. Rev. A* **21**, pp. 1606–1617.

Greiner, M., M. O. Mandel, T. Esslinger, T. Hänsch & I. Bloch (2002), "Quantum Phase Transition from a Superfluid to a Mott Insulator in a Gas of Ultracold Atoms", in *Nature* **415**, p. 39.

Greiner, Markus, Immanuel Bloch, Olaf Mandel, Theodor W. Hänsch & Tilman Esslinger (2001), "Exploring Phase Coherence in a 2D Lattice of Bose-Einstein Condensates", in *Phys. Rev. Lett.* **87**, p. 160405.

Grifoni, Milena & Peter Hänggi (1998), "Driven quantum tunneling", in *Physics Reports* **304**, pp. 229 –354.

Grimm, R, M Weidemüller & YB Ovchinnikov (2000), "Optical dipole traps for neutral atoms", in *Advances in Atomic, Molecular, and Optical Physics*, vol. 42, , 95–170.

Grossmann, F., T. Dittrich, P. Jung & P. Hänggi (1991), "Coherent destruction of tunneling", in *Phys. Rev. Lett.* **67** (4), pp. 516–519.

Grynberg, G., B. Lounis, P. Verkerk, J.-Y. Courtois & C. Salomon (1993), "Quantized motion of cold cesium atoms in two- and three-dimensional optical potentials", in *Phys. Rev. Lett.* **70** (15), pp. 2249–2252.

Grynberg, G & C Robilliard (2001), "Cold atoms in dissipative optical lattices", in *Physics Reports* **355**, 335–451.

Guidoni, L., C. Triché, P. Verkerk & G. Grynberg (1997), "Quasiperiodic Optical Lattices", in *Phys. Rev. Lett.* **79** (18), pp. 3363–3366.

Haroche, S., C. Cohen-Tannoudji, C. Audoin & J. P. Schermann (1970), "Modified Zeeman Hyperfine Spectra Observed in H^1 and Rb^{87} Ground States Interacting with a Nonresonant rf Field", in *Phys. Rev. Lett.* **24** (16), pp. 861–864.

Hartmann, T, F Keck, H J Korsch & S Mossmann (2004), "Dynamics of Bloch oscillations", in *New Journal of Physics* **6**, p. 2.

Hemmerich, A. & T. W. Hänsch (1993), "Two-dimensional atomic crystal bound by light", in *Phys. Rev. Lett.* **70**, p. 410.

Holthaus, Martin (1992), "Collapse of minibands in far-infrared irradiated superlattices", in *Phys. Rev. Lett.* **69** (2), pp. 351–354.

– (2000), "Bloch oscillations and Zener breakdown in an optical lattice", in *Journal of Optics B: Quantum and Semiclassical Optics* **2**, p. 589.

Horne, M., I. Jex & A. Zeilinger (1999), "Schrödinger wave functions in strong periodic potentials with applications to atom optics", in *Phys. Rev. A* **59** (3), pp. 2190–2202.

Huber, Sebastian D. & Ehud Altman (2010), "Bose condensation in flat bands", in *Phys. Rev. B* **82** (18), p. 184502.

Jaksch, D., C. Bruder, J. I. Cirac, C. W. Gardiner & P. Zoller (1998), "Cold Bosonic Atoms in Optical Lattices", in *Phys. Rev. Lett.* **81** (15), pp. 3108–3111.

Jo, Gyu-Boong, Jennie Guzman, Claire K. Thomas, Pavan Hosur, Ashvin Vishwanath & Dan M. Stamper-Kurn (2012), "Ultracold Atoms in a Tunable Optical Kagome Lattice", in *Phys. Rev. Lett.* **108** (4), p. 045305.

Kasevich, Mark & Steven Chu (1991), "Atomic interferometry using stimulated Raman transitions", in *Phys. Rev. Lett.* **67** (2), pp. 181–184.

Katsnelson, M. I., K. S. Novoselov & A. K. Geim (2006), "Chiral tunnelling and the Klein paradox in graphene", in *Nature Physics* **2**, pp. 620–625.

Keller, C, J Schmiedmayer, A Zeilinger, T Nonn, S Durr & G Rempe (1999), "Adiabatic following in standing-wave diffraction of atoms", in *Applied Physics B - Lasers and Optics* **69**, 303–309.

Kierig, E., U. Schnorrberger, A. Schietinger, J. Tomkovic & M. K. Oberthaler (2008), "Single-Particle Tunneling in Strongly Driven Double-Well Potentials", in *Phys. Rev. Lett.* **100** (19), p. 190405.

Kittel, Charles (1987), *Quantum Theory of Solids*, John Wiley & Sons Inc..

Kling, Sebastian, Tobias Salger, Christopher Grossert & Martin Weitz (2010), "Atomic Bloch-Zener Oscillations and Stückelberg Interferometry in Optical Lattices", in *Phys. Rev. Lett.* **105** (21), p. 215301.

Köhl, Michael, Henning Moritz, Thilo Stöferle, Kenneth Günter & Tilman Esslinger (2005), "Fermionic Atoms in a Three Dimensional Optical Lattice: Observing Fermi Surfaces, Dynamics, and Interactions", in *Phys. Rev. Lett.* **94** (8), p. 080403.

Kohn, W. (1959), "Analytic Properties of Bloch Waves and Wannier Functions", in *Phys. Rev.* **115** (4), pp. 809–821.

Kollath, C., A. Iucci, T. Giamarchi, W. Hofstetter & U. Schollwöck (2006), "Spectroscopy of Ultracold Atoms by Periodic Lattice Modulations", in *Phys. Rev. Lett.* **97** (5), p. 050402.

Kovachy, Tim, Sheng-wey Chiow & Mark A. Kasevich (2012), "Adiabatic-rapid-passage multiphoton Bragg atom optics", in *Phys. Rev. A* **86** (1), p. 011606.

Kozuma, M., L. Deng, E. W. Hagley, J. Wen, R. Lutwak, K. Helmerson, S. L. Rolston & W. D. Phillips (1999), "Coherent Splitting of Bose-Einstein Condensed Atoms with Optically Induced Bragg Diffraction", in *Phys. Rev. Lett.* **82** (5), pp. 871–875.

Lee, Kean Loon, Benoit Grémaud, Rui Han, Berthold-Georg Englert & Christian Miniatura (2009), "Ultracold fermions in a graphene-type optical lattice", in *Phys. Rev. A* **80** (4), p. 043411.

Lee, P. J., M. Anderlini, B. L. Brown, J. Sebby-Strabley, W. D. Phillips & J. V. Porto (2007), "Sublattice Addressing and Spin-Dependent Motion of Atoms in a Double-Well Lattice", in *Phys. Rev. Lett.* **99**, p. 020402.

Lepoutre, S., A. Gauguet, G. Trénec, M. Büchner & J. Vigué (2012), "He–McKellar–Wilkens Topological Phase in Atom Interferometry", in *Phys. Rev. Lett.* **109** (12), p. 120404.

Lignier, H., C. Sias, D. Ciampini, Y. Singh, A. Zenesini, O. Morsch & E. Arimondo (2007), "Dynamical Control of Matter-Wave Tunneling in Periodic Potentials", in *Phys. Rev. Lett.* **99** (22), p. 220403.

Lim, Lih-King, Jean-Noël Fuchs & Gilles Montambaux (2012), "Bloch-Zener Oscillations across a Merging Transition of Dirac Points", in *Phys. Rev. Lett.* **108** (17), p. 175303.

Lopez, Matthias, Jean-François Clément, Pascal Szriftgiser, Jean Claude Garreau & Dominique Delande (2012), "Experimental Test of Universality of the Anderson Transition", in *Phys. Rev. Lett.* **108** (9), p. 095701.

Louchet-Chauvet, Anne, Tristan Farah, Quentin Bodart, André Clairon, Arnaud Landragin, Sébastien Merlet & Franck Pereira Dos Santos (2011), "The influence of transverse motion within an atomic gravimeter", in *New Journal of Physics* **13**, p. 065025.

Madison, K. W., M. C. Fischer, R. B. Diener, Qian Niu & M. G. Raizen (1998), "Dynamical Bloch Band Suppression in an Optical Lattice", in *Phys. Rev. Lett.* **81** (23), pp. 5093–5096.

Martin, Peter J., Bruce G. Oldaker, Andrew H. Miklich & David E. Pritchard (1988), "Bragg scattering of atoms from a standing light wave", in *Phys. Rev. Lett.* **60** (6), pp. 515–518.

Marzari, Nicola, Arash A. Mostofi, Jonathan R. Yates, Ivo Souza & David Vanderbilt (2012), "Maximally localized Wannier functions: Theory and applications", in *Rev. Mod. Phys.* **84** (4), pp. 1419–1475.

Mendez, Emilio E. & Gérald Bastard (1993), "Wannier-Stark Ladders and Bloch Oscillations in Superlattices", in *Physics Today* **46**, pp. 34–42.

Messiah, A. (2003), *Mécanique quantique*, vol. II, Paris: Dunod.

Mikitik, G. P. & Yu. V. Sharlai (1999), "Manifestation of Berry's Phase in Metal Physics", in *Phys. Rev. Lett.* **82**, pp. 2147–2150.

Montambaux, G., F. Piéchon, J.-N. Fuchs & M. O. Goerbig (2009), "Merging of Dirac points in a two-dimensional crystal", in *Phys. Rev. B* **80** (15), p. 153412.

Müller, Holger, Sheng-wey Chiow, Sven Herrmann & Steven Chu (2009), "Atom Interferometers with Scalable Enclosed Area", in *Phys. Rev. Lett.* **102** (24), p. 240403.

Murr, K., P. Maunz, P. W. H. Pinkse, T. Puppe, I. Schuster, D. Vitali & G. Rempe (2006), "Momentum diffusion for coupled atom-cavity oscillators", in *Phys. Rev. A* **74** (4), p. 043412.

Nenciu, G. (1991), "Dynamics of band electrons in electric and magnetic fields: rigorous justification of the effective Hamiltonians", in *Rev. Mod. Phys.* **63** (1), pp. 91–127.

Niu, Q., X. G. Zhao, G. A. Georgakis & M. G. Raizen (1996), "Atomic Landau-Zener Tunneling and Wannier-Stark Ladders in Optical Potentials", in *Phys. Rev. Lett.* **76**, p. 4504.

Niu, Qian & M. G. Raizen (1998), "How Landau-Zener Tunneling Takes Time", in *Phys. Rev. Lett.* **80** (16), pp. 3491–3494.

Novoselov, KS, AK Geim, SV Morozov, D Jiang, MI Katsnelson, IV Grigorieva, SV Dubonos & AA Firsov (2005), "Two-dimensional gas of massless Dirac fermions in graphene", in *NATURE* **438**, 197–200.

Peik, Ekkehard, Maxime Ben Dahan, Isabelle Bouchoule, Yvan Castin & Christophe Salomon (1997), "Bloch oscillations of atoms, adiabatic rapid passage, and monokinetic atomic beams", in *Phys. Rev. A* **55** (4), pp. 2989–3001.

Pelle, B., A. Hilico, G. Tackmann, Q. Beaufils & F. Pereira dos Santos (2013), "State-labeling Wannier-Stark atomic interferometers", in *Phys. Rev. A* **87** (2), p. 023601.

Poli, N., F.-Y. Wang, M. G. Tarallo, A. Alberti, M. Prevedelli & G. M. Tino (2011), "Precision Measurement of Gravity with Cold Atoms in an Optical Lattice and Comparison with a Classical Gravimeter", in *Phys. Rev. Lett.* **106** (3), p. 038501.

Prasanna Venkatesh, B., M. Trupke, E. A. Hinds & D. H. J. O'Dell (2009), "Atomic Bloch-Zener oscillations for sensitive force measurements in a cavity", in *Phys. Rev. A* **80** (6), p. 063834.

Raizen, Mark, Christophe Salomon & Qian Niu (1997), "New Light on Quantum Transport", in *Physics Today* **50**, pp. 30–34.

Roati, G., E. de Mirandes, F. Ferlaino, H. Ott, G. Modugno & M. Inguscio (2004), "Atom Interferometry with Trapped Fermi Gases", in *Phys. Rev. Lett.* **92** (23), p. 230402.

Sebby-Strabley, J., B.L. Brown, M. Anderlini, P.J. Lee, P.R. Johnson, W.D. Phillips & J.V. Porto (2007), "Preparing and probing atomic number states with an atom interferometer", in *Phys. Rev. Lett.* **98**, p. 200405.

Sorrentino, F., A. Alberti, G. Ferrari, V. V. Ivanov, N. Poli, M. Schioppo & G. M. Tino (2009), "Quantum sensor for atom-surface interactions below 10 μm", in *Phys. Rev. A* **79** (1), p. 013409.

Steinhauer, J., R. Ozeri, N. Katz & N. Davidson (2002), "Excitation spectrum of a Bose–Einstein condensate", in *Phys. Phys. Lett.* **88**, p. 120407.

Stenger, J., S. Inouye, A. P. Chikkatur, D. M. Stamper-Kurn, D. E. Pritchard & W. Ketterle (1999), "Bragg Spectroscopy of a Bose-Einstein Condensate", in *Phys. Rev. Lett.* **82** (23), pp. 4569–4573.

Struck, J., C. Oelschlaeger, R. Le Targat, P. Soltan-Panahi, A. Eckardt, M. Lewenstein, P. Windpassinger & K. Sengstock (2011), "Quantum Simulation of Frustrated Classical Magnetism in Triangular Optical Lattices", in *SCIENCE* **333**, 996–999.

Struck, J., C. Ölschläger, M. Weinberg, P. Hauke, J. Simonet, A. Eckardt, M. Lewenstein, K. Sengstock & P. Windpassinger (2012), "Tunable Gauge Potential for Neutral and Spinless Particles in Driven Optical Lattices", in *Phys. Rev. Lett.* **108** (22), p. 225304.

Tackmann, G., B. Pelle, A. Hilico, Q. Beaufils & F. Pereira dos Santos (2011), "Raman-laser spectroscopy of Wannier-Stark states", in *Phys. Rev. A* **84** (6), p. 063422.

Tarruell, Leticia, Daniel Greif, Thomas Uehlinger, Gregor Jotzu & Tilman Esslinger (2012), "Creating, moving and merging Dirac points with a Fermi gas in a tunable honeycomb lattice", in *Nature* **483**, p. 302.

Wallace, P. R. (1947), "The Band Theory of Graphite", in *Phys. Rev.* **71** (9), pp. 622–634.

Wannier, Gregory H. (1937), "The Structure of Electronic Excitation Levels in Insulating Crystals", in *Phys. Rev.* **52** (3), pp. 191–197.

– (1960), "Wave Functions and Effective Hamiltonian for Bloch Electrons in an Electric Field", in *Phys. Rev.* **117** (2), pp. 432–439.

Wilkinson, S. R., C. F. Bharucha, K. W. Madison, Qian Niu & M. G. Raizen (1996), "Observation of Atomic Wannier-Stark Ladders in an Accelerating Optical Potential", in *Phys. Rev. Lett.* **76** (24), pp. 4512–4515.

Wilkinson, SR, CF Bharucha, MC Fischer, KW Madison, PR Morrow, Q Niu, B Sundaram & MG Raizen (1997), "Experimental evidence for non-exponential decay in quantum tunnelling", in *NATURE* **387**, 575–577.

Winkler, K., G. Thalhammer, F. Lang, R. Grimm, J. Hecker-Denschlag, A. J. Daley, A. Kantian, H. P. Büchler & P. Zoller (2006), "Repulsively bound atom pairs in an optical lattice", in *Nature* **441**, p. 853.

Wolf, Peter, Pierre Lemonde, Astrid Lambrecht, Sébastien Bize, Arnaud Landragin & André Clairon (2007), "From optical lattice clocks to the measurement of forces in the Casimir regime", in *Phys. Rev. A* **75** (6), p. 063608.

Wunsch, B, F Guinea & F Sols (2008), "Dirac-point engineering and topological phase transitions in honeycomb optical lattices", in *New Journal of Physics* **10**, p. 103027.

Zak, J. (1989), "Berry's phase for energy bands in solids", in *Phys. Rev. Lett.* **62** (23), pp. 2747–2750.

Zener, C (1934), "A Theory of the Electrical Breakdown of Solid Dielectrics", in *Proc. R. Soc. Lond. A* **145**, 523.

Zenesini, A., D. Ciampini, O. Morsch & E. Arimondo (2010), "Observation of Stückelberg oscillations in accelerated optical lattices", in *Phys. Rev. A* **82** (6), p. 065601.

Zenesini, A., H. Lignier, G. Tayebirad, J. Radogostowicz, D. Ciampini, R. Mannella, S. Wimberger, O. Morsch & E. Arimondo (2009), "Time-Resolved Measurement of Landau-Zener Tunneling in Periodic Potentials", in *Phys. Rev. Lett.* **103** (9), p. 090403.

Zhang, YB, YW Tan, HL Stormer & P Kim (2005), "Experimental observation of the quantum Hall effect and Berry's phase in graphene", in *NATURE* **438**, 201–204.

Zhu, Shi-Liang, Baigeng Wang & L.-M. Duan (2007), "Simulation and Detection of Dirac Fermions with Cold Atoms in an Optical Lattice", in *Phys. Rev. Lett.* **98** (26), p. 260402.